Centre of Mathematics and Physics in the Life Sciences and Experimental Biology
&
Centre of Nanotechnology and Regenerative Medicine

Design and Development of a Prosthetic Implant for Cardiovascular Reconstructions

To be submitted for the degree of Doctor of Philosophy (Ph.D) by

Maqsood Ahmed

Division of Surgery and Interventional Science
University College London

October 2011

I, Maqsood Ahmed, confirm that the work presented in this thesis is my own. Where information has been derived from other sources, I confirm that this has been indicated in the thesis.

- -

Acknowledgements

In the completion of this work, I received invaluable assistance from many gracious people, without whom, I would still be toiling away on this project. First and foremost, I am grateful to my supervisors, Prof Alex Seifalian and Prof George Hamilton, for there constant encouragement, support and guidance throughout my PhD.

Thereafter, I would like to thank all other collaborators who have helped me over the years which includes Dr Laurent Bozec, Eastman Dental Institute, for assistance with AFM and Dr Marianne Odlyha, Birkbeck College, and Sue Stephens, TARRC, for help with materials characterisation, and DSC and GPC in particular. I'd also like to thank the Northwick Park Institute for Medical Research and Sandra Shurey for assisting with the *in vivo* work and carrying out animal surgery. Finally, I'd like to thank John Lennard, Isotron, for helping with gamma irradiation and sterilisation work.

I would also like to express my sincerest gratitude to the staff in the Division of Surgery and Interventional Science for their help and encouragement. In particular, Noreen Farooqui and Geoff Punshon for teaching me the finer points of cell culture. Arnold Darbyshire and Dr Brian Cousins for their advice, technical support and practical assistance; and many, many useful conversations on a wide range of topics. Further, I'd like to thank Dr Kevin Sales and Dr Marilena Loizidou for the unique brand of encouragement that they provided! I would also like to extend my gratitude to the other students in the lab, particularly Adelola Oseni and Claire Crowley, for the endless discussions, debates and gossip; and for making coming to work in the morning a more enticing prospect.

I would also like to take this opportunity to thank CoMPLEX for funding and supporting my research for the past 4 years and the other members of CoMPLEX for providing such an amicable environment to conduct research in.

Finally, no set of acknowledgements would be complete without mentioning Kevin Lau, Gwenan Knight, Charles Mullon and Dorothy Kuipers for sharing in all the highs and lows of the past 4 years with me - I really could not have done this without you all. Your mere presence helped me to keep my research in perspective and made the past 4 years of my life far more enjoyable. For that I am eternally grateful.

Abstract

There is a significant worldwide demand for a small calibre vascular graft for use as a bypass or replacement conduit. Our lab has developed a novel nanocomposite polymer based on polyhedral oligomeric silsesquioxane and poly(carbonate-urea)urethane (POSS-PCU) which has displayed promising properties *in vitro*. In this thesis, POSS-PCU has been utilised to fabricate prosthetic small calibre conduits for use as arterial replacements. An important feature in determining the success of a graft is the wall structure which includes porosity, pore size and pore interconnectivity, which play a crucial role not only in determining the extent of graft healing but also on mechanical behaviour. A novel extrusion/phase inversion method was investigated and optimised to produce grafts with a range of pore sizes (0-30 μm) and porosities (up to 90%). With mismatches in mechanical properties implicated in the aetiology of intimal hyperplasia, the dynamic mechanical behaviour of grafts was investigated. Grafts could be engineered with compliance values ranging from 5 to 12 per mmHg $\times$ 10^{-2} compared to an average value of 5.9 per mmHg $\times$ 10^{-2} for the native artery. Biocompatibility is largely dependent on surface properties which were extensively characterised for each of the porous grafts. Grafts were found to readily endothelialise *in vitro* and were resistant to platelet activation. An external graft reinforcement method was developed in order to minimise graft kinking. Finally, the grafts were evaluated in vivo in an ovine model following GLP protocols for a period of 9 months. A patency rate of 70% was achieved (n=10). The positive in vitro results and successful conclusion to the large animal trial suggest that POSS-PCU small calibre grafts are a promising candidate for cardiovascular reconstructions.

Contents

List of Figures

List of Tables

Abbreviations

ADP	Adenosine diphosphate
AFM	Atomic force microscopy
ANOVA	Analysis of Variance
ASC	Amniotic stem cell
ATR-FTIR	Attenuated total reflectance fourier transform infrared
bFGF	Basic fibroblast growth factor
CABG	Coronary artery bypass graft
CVD	Cardiovascular disease
DMAc	Dimethyl acetamide
DMF	Dimethyl formamide
DSC	Differential scanning calorimetry
EC	Endothelial Cells
ECM	Extracellular matrix
ELISA	Enzyme linked immunosorbent assay
EPC	Endothelial progenitor cells
ePTFE	Expanded polytetrafluoroethylene
ESC	Embryonic stem cells
FACS	Fluorescence activated cell sorter
FAP	Femoral artery pseudoaneurysm
FBGC	Foreign body giant cells
FBS	Fetal bovine serum
FGF	Fibroblast growth factor
GCMS	Gas chromatography mass spectroscopy
GCSF	Granulocyte colony-stimulating factor
GPC	Gell permeation chromatography
GSV	Great saphenous vein
HBSS	Hanks balanced salt solution
HDL	High density lipoprotein
HUVEC	Human umbilical vein endothelial cells
ICP-OES	Inductively coupled plasma optical emission spectroscopy
IPN	Interpenetrating polymer network
IH	Intimal hyperplasia
iPSC	Induced pluripotent stem cells
IVC	Inferior vena cava

LCA	Left carotid artery
LDL	Low density lipoproteins
MDI	Methylene diphenyl diisocyanate
MI	Myocardial infarction
MMP	Matrix metalloproteinase
Mn	Number average molecular weight
MRI	Magnetic resonance imaging
MSC	Mesenchymal stem cells
Mw	Weight average molecular weight
$NaHCO_3$	Sodium bicarbonate
NO	Nitric oxide
OSI	Oscillatory shear index
P4HB	Poly-4-hydroxybutyrate
PAD	Peripheral arterial disease
Pd	Polydispersity index
PDGF	Platelet derived growth factor
PBMC	Peripheral blood mononuclear cells
PF4	Platelet factor 4
PCU	Poly(carbonate) urethane
PDMS	Polydimethylsiloxane
PET	Polyethylene terephthalate
PGA	Polyglycolic acid
PGS	Poly(glycerol-sebacate)
PLGA	Poly(lactic-co-glycolic acid)
POSS	Polyhedral oligomeric silsesquioxane
PPP	Platelet poor plasma
PRP	Platelet rich plasma
PTA	Percutaneous transmural angioplasty
PU	Polyurethane
RBC	Red blood cells
RCA	Right carotid artery
REDV	Arginine-glutamic acid-aspartic acid-valine
RGD	Argininegly cineaspartic acid
SEM	Scanning electron microscopy
SIMS	Secondary ion mass spectroscopy
SIS	Small intestinal submucosa
SMC	Smooth muscle cells
TCP	Tissue culture plastic
TEBV	Tissue engineered blood vessel

tPA	tissue-type plasminogen activator
TF	Tissue Factor
THY	Fluid Thioglycollate medium
TNFα	Tumour necrosis factor α
TSB	Tryptone soya broth
TGFb	Transforming growth factor b
uPA	urokinase-type plasminogen activator
UTS	Ultimate tensile strength
VEGF	Vascular endothelial growth factor
vWF	von Willebrand Factor
WBC	White blood cells
WSS	wall shear stress
WSSG	wall shear stress gradients
YIGSR	Tyrosine-isoleucine-glycine-serine-arginine

1

Cardiovascular Disease and Treatments

Cardiovascular diseases (CVD), such as myocardial infarction (MI) and peripheral arterial disease (PAD), are the principle cause of death globally. In 2006, nearly 200,000 deaths were attributed to CVD in the UK alone [1]. In addition to the morbidity and mortality associated with CVD, there is also a significant economic burden, estimated to be over $30.7bn annually. CVDs are often associated with occlusion of the blood vessels resulting in ischaemia and damage to the surrounding tissue. Current therapies aim to relieve ischaemia, by restoring vascular perfusion, through surgical interventions, which include balloon angioplasty, with or without stenting, and bypass surgery. Unfortunately, 40% of surgical interventions fail within the first year due, principally, to thrombosis, restenosis and graft stenosis resulting in graft occlusion. This problem is particularly acute in the treatment of low flow, small calibre – less than 6mm in diameter – vessels such as the coronary, carotid and peripheral arteries. With minimal alternative treatment options available, there is a considerable clinical demand for improvements in invasive therapies and surgical techniques for revascularisation. Therapies include the development of improved implants such as stents and prosthetic grafts.

1.1 Blood Vessel Anatomy

The circulatory system is the largest organ in the human body and is comprised of arteries, arterioles, capillaries, venules and veins. Arteries and arterioles are designed to withstand high blood pressures and consist of 3 layers (fig 1.1): the tunica intima, tunica media and tunica adventitia. The tunica intima is the innermost layer, in direct contact with blood, consisting of longitudinally arranged squamous endothelial cells (EC). The endothelium acts as a protective barrier regulating vascular permeability, inflammation, coagulation and fibrinolysis [2–4]. The middle layer, tunica media,

is composed primarily of concentrically arranged smooth muscle cells (SMC). The medial layer is responsible for vascular tone through the contraction and dilation of the muscular and elastic components in response to mechanical stimuli or nervous innervations [5]. The outermost layer, tunica adventitia, is a collagen rich connective tissue layer consisting of fibroblasts, nerves, lymph vessels and capillaries known as the vaso vasorum. The vaso vasorum is responsible for supplying the advenititia and the outer part of the media with oxygen and nutrients [6]. It also provides the blood vessel with the mechanical strength to cope with high blood pressures [7].

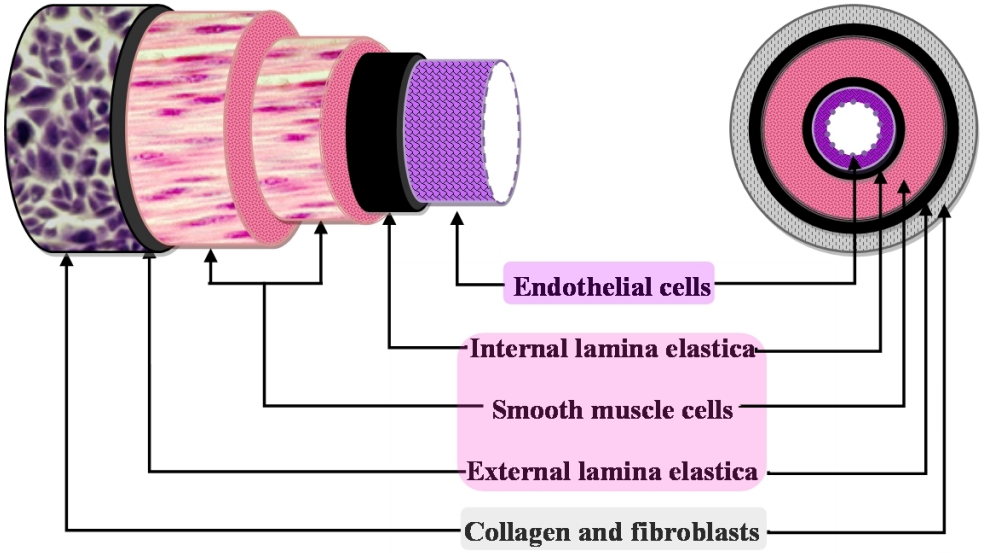

Figure 1.1: Blood vessel anatomy. The structure consists of 3 distinct layers: the outermost tunica adventitia, primarily composed of fibroblasts and collagen, which provides mechanical strength to the vessel. The tunica media which consists of smooth muscle cells inbetween the elastic lamina. The tunica media is responsible for controlling vasomotor tone. The innermost tunica intima regulating coagulation, inflammation and fibrinolysis and is composed of a thin layer of endothelial cells.

1.2 Atherosclerosis

Principle amongst the causes of ischaemia and CVD is atherosclerosis – a condition in which the artery wall thickens due to the build up of fatty materials such as cholesterol. Atherosclerosis can lead to the narrowing and blockage of the arteries to the brain, heart, legs, arms, stomach or kidneys and can lead to stroke, myocardial infarction (MI), amputation and even death. Atherosclerosis is characterised as a chronic inflammatory response in the arteries due to the accumulation of macrophages pro-

moted by low density lipoproteins (LDL), without the adequate removal of fats and cholesterol from the macrophages by functional high density lipoproteins (HDL) [8]. Lesions tend to develop at arterial bifurcations or major curvatures, areas which show an increased permeability to macromolecules like LDL [9]. An endothelial dysfunction, possibly due to chemical or mechanical injury, shear stress or the presence of elevated levels of modified LDL, leads to an increase in permeability allowing LDL into the intima [10]. Leukocytes and monocytes then migrate into the intima and transform into macrophages, which take up the LDL creating lipid rich foam cells; characterising a general state of inflammation. Activated platelets, EC and macrophages all release platelet derived growth factor (PDGF) which induces the migration of SMC into the intima. The proliferating SMC form a fibrous cap surrounding a lipid core, consisting of the foam cells, forming a focal intimal thickening known as a plaque. In advanced stages of the disease, a narrowing of the arterial lumen develops with a high risk for the formation of superimposed thrombosis leading to acute ischemia of the end organ. Detection is difficult as atherosclerosis tends to be quite advanced, having progressed for decades, before it manifests itself clinically. Known risk factors include lifestyle choices such as smoking and drinking as well as diabetes, hypertension and hyperlipidemia.

1.3 Treatment Options

Treatment options for atherosclerosis can be roughly divided into three main categories: lifestyle changes, medicines or surgical intervention. A change in lifestyle is usually the first step in treating atherosclerosis with regular exercise, change in diet, reduction in alcohol intake and a cessation of smoking encouraged. However, if that has a limited impact the next stage is for medication. Statins, a class of drugs used to lower cholesterol levels, have been shown to be effective in reducing incidences of intermittent claudication and angina pectoris [11]. Described as the most important contribution to clinical medicine and pharmacology of the 20th century, beta blockers have been shown to lower blood pressure which reduces the hearts workload and incidences of MI [12, 13]. Anti-platelet therapy can be administered to reduce the proclivity for blood clots. Aspirin, clopidogrel and abciximab have all been shown to be efficacious in reducing thrombotic complications in CVD [14, 15].

When medical intervention fails and blockage of an artery has progressed to the point where there is a severe reduction in blood flow, surgery needs to be considered. In occlusions smaller than 70%, a minimally invasive procedure known as a percutaneous transluminal angioplasty (PTA), or balloon angioplasty, can be carried out. PTA is

a procedure in which a small balloon at the tip of a catheter is inserted through the blocked or narrowed area of the artery. The balloon is inflated to a pre-determined diameter to dilate the artery and push the plaque back to open the diseased blood vessel. When the balloon is inflated, the fatty plaque or blockage is compressed against the artery walls and the diameter of the blood vessel is widened to increase blood flow. In some cases, balloon angioplasty is performed in combination with a stenting procedure. A stent is a small metal mesh tube that acts as a scaffold to provide support inside the artery. A catheter, placed over a guide wire, is used to insert the stent into the narrowed artery. Once in place, the stent is deployed and expands to the size of the artery and holds it open. A balloon may be used to insert the stent or the stent may have an outward force itself that allows it to expand independently. If a balloon is used to deliver and deploy or expand the stent, it is deflated and removed, and the stent stays in place permanently. Since the inception of stents, the number of people opting for the minimally invasive procedure has grown steadily. However, question marks have been raised more recently over the efficacy of stenting patients with stable coronary artery disease [16].

In more serious occlusions, 70% or more, or in cases where stenosis is multi-focal or when multiple vessels are involved; invasive bypass surgery is recommended. Bypass surgery involves circumventing blocked arteries with an alternative conduit restoring blood flow distal to the blockage. To bypass the blockage, the surgeon makes a small opening in the diseased artery and places a graft above and below the blockage to allow blood flow around the blockage. Whilst bypass surgery is considerably more costly and involves extended hospital stays; survival rates in the coronary and carotid position are significantly greater compared to PTA, suggesting bypass surgery still has a considerable role to play despite the growing popularity of minimally invasive procedures [17, 18].

The conduit of choice for bypass surgery is still autologous vessels. Arterial grafts – such as the left or right internal thoracic artery, radial artery and more rarely the right gastroepiploic artery or inferior epigastric arteries – are the favoured options for coronary grafting demonstrating patency rates in excess of 90% at 15 years [19]. Despite their remarkable patency rates, only 30% of surgeons use arterial grafts in over 90% of their operations with the majority of surgeons often avoiding using arterial grafts [20]. Reasons for not using arterial grafts include the time taken for mobilisation, especially during emergency revascularisation, and restricted dimensions especially in the elderly population [21]. However, the major disadvantage to the use of arterial grafts is insufficient material for multiple grafting. For these rea-

sons the great saphenous vein (GSV) remains the most popular conduit for bypass surgery. Patency rates for the GSV are not as impressive as arterial grafts – 50% after 10 years – with thrombosis, intimal hyperplasia (IH), and the onset of progressive atheroscelrosis principle factors in vein graft failure [22]. The harvesting of the GSV still requires a second, invasive procedure, with potential concomitant morbidities, and the problem of insufficient material still exists. This is particularly problematic as the number patients requiring repeat operations is steadily increasing [23]. This has led to 30% of patients requiring surgery not having suitable or sufficient blood vessels to be used for transplantation [24]. As a result, synthetic grafts have been developed to try and meet the pressing clinical need.

1.4 Prosthetic Grafts

Synthetic grafts, made from polyethylene terephthalate (PET) and expanded polytetrafluoroethylene (ePTFE), have offered viable alternative prostheses for vascular reconstructions. PET is a polyester fibre that can be woven or knitted into a fabric resulting in prosthesis with two distinct structures. Woven grafts tend to be minimally permeable to liquids with high bursting strengths and a limited tendency to deform under stress. Knitted grafts, on the other hand, tend to contain large voids, allowing tissue ingrowth, but also requiring preclotting or coating with a thin layer of blood proteins to prevent blood leakage through the walls. ePTFE, better known as teflon, is a synthetic, semi-crystalline, thermosetting fluoropolymer patented by Gore for use as a vascular prosthesis. ePTFE is strong, chemically inert, durable and biocompatible making it an ideal vascular graft material. Clinical trials suggest there is little difference in patency between the two grafts – both function adequately in the replacement of large arteries yet disappoint in the replacement of small diameter or under low flow conditions. Patency rates were a rather impressive 90% at 5 years and 80% at 8 years at the aortoilliac position [25, 26]. However, when it came to the above knee femoropopliteal bypass, patency rates dropped to 63% at 3 years and decreasing further to 36% after 5 years [27, 28]. Graft failure is primarily due to the acute thrombogenicity of the graft material in the short term and anastomotic IH in the long term [29].

In addition to PET and ePTFE, polyurethanes (PU) have been heavily investigated for use as vascular grafts. PU are a chain of organic units linked together by a urethane bond. They are composed of hard and soft segments which offers a degree of versatility in the characteristics of the final material through fine tuning the properties of the individual components. PU were initially greeted with enthusiasm as they had

two significant advantages over PET and ePTFE: elasticity, meaning they were more compliant, and ease of handling. The hard segment provided the tensile strength and rigidity whilst the soft segment provided the flexibility. This initial enthusiasm was dampened due to the lack of long term durability, with polyester based soft segments suffering from hydrolysis, whilst polyether based PUs susceptible to oxidative attack [30]. The next generation of PU were carbonate-based which were resistant to degradation [31]. Poly(carbonate-urea)urethane grafts were implanted into the aorto-iliac artery of eight dogs and were found to be patent at 36 months. Currently a PU graft is available for use for haemodialysis access having been approved by the Food and Drug Administration (FDA).

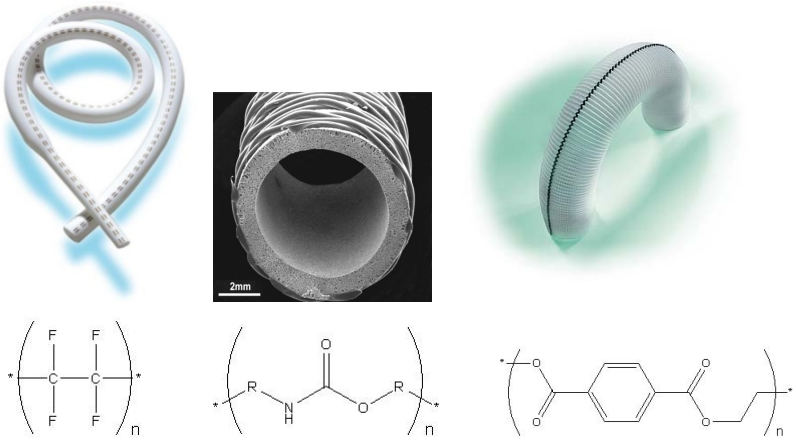

(a) ePTFE (b) PU (c) PET

Figure 1.2: Commercially available synthetic grafts and the chemical structure of synthetic graft materials

1.5 Failure Mechanisms of Prosthetic Grafts

Graft failure can often be attributed to two primary causes: thrombosis and IH. Early failure is often due to poor surgical technique, thrombosis or infection. Infection can be as a result of contamination during surgery or inefficient sterilisation process. Midterm failure – 3 months to 2 years – is often associated with cellular infiltration or IH whereas late failure is often due to the development of atherosclerotic lesions in the graft.

Thrombosis

In the native vessel, blood is in contact with the endothelium, a thin layer of cells forming an interface with circulating blood in the lumen and the rest of the vessel. Endothelial cells form a barrier against the blood through the entirety of the circulatory system from the smallest capillary to the heart. The endothelium provides a non-thrombogenic surface as it contains a variety of anti-thrombogenic and fibrinolytic factors including heparan sulphate, which acts as a cofactor for activating antithrombin III, a protease that cleaves several factors in the coagulation cascade [32].

On the implantation of a synthetic graft, an exogenous material with a distinct lack of an endothelium is introduced into the circulation resulting in the adsorption of various plasma proteins and activation of the coagulation cascade, providing binding sites for integrin receptor mediated adhesion and activation of platelets amongst other cells [33]. The composition and confirmation of proteins adsorbed is determined by the interfacial interactions between polymer surface and proteins and can dictate subsequent reactions including platelet activation, thrombus formation, and complement activation [34]. Platelets are highly sensitive, anuclear, disc shaped fragments of cells circulating throughout the blood stream. Platelets bind to the plasma proteins fibronectin, von Willebrand Factor (vWF), fibrinogen and vitronectin through the surface glycoprotein GP IIb/IIIa and GP Ib [35]. Once bound a series of complex reactions take place often resulting in the secretion of various biologically active compounds such as platelet factor 4 (PF4), adenosine diphosphate (ADP), serotonin and *P*-selectin, a cell-surface glycoprotein. All of these biologically active agents go on to further propagate platelet activation, coagulation and inflammation. This foreign body induced platelet aggregation is felt even more severely in the case of small calibre grafts due to the increased surface to volume ratio and reduced blood flow rates. Further, thrombus formation has a greater impact on the flow of blood in small diameter blood vessels.

In addition to platelet aggregation, the coagulation cascade can lead to the formation of fibrin clots through the chemical cross linking of Factor VIIIa [34]. The coagulation cascade acts via two complementary pathways: the intrinsic and extrinsic pathways (fig 1.3). The extrinsic pathway, or tissue factor (TF) pathway, becomes activated when plasma comes into contact with cells expressing TF. In the presence of Ca^{2+}, TF activates Factor VII forming TF-FVIIa complexes, which then cleave Factor X producing Factor Xa – a common component in both the intrinsic and extrinsic pathways. Thrombin is then generated through the prothrombinase complex which is able to cleave fibrinopeptides, from the plasma protein fibrinogen, forming the

fibrin monomer. Fibrin is then able to cross link with Factor VIIIa forming fibrin clots, which express an RGD tripeptide motif, allowing it to bind to the surface glycoprotein GP IIb/IIIa of activated platelets; further amplifying thrombosis [36]. The intrinsic pathway generates Factor Xa through a cascade of reactions beginning with the activation of Factor XII which goes on to convert prekallikrein into kallikrein resulting in the activation of Factor XI. Factor XIa activates Factor IX, which in conjunction with Ca^{2+} and Factor VIIIa, activates Factor X which proceeds to form stable, fibrin clots, or thrombus.

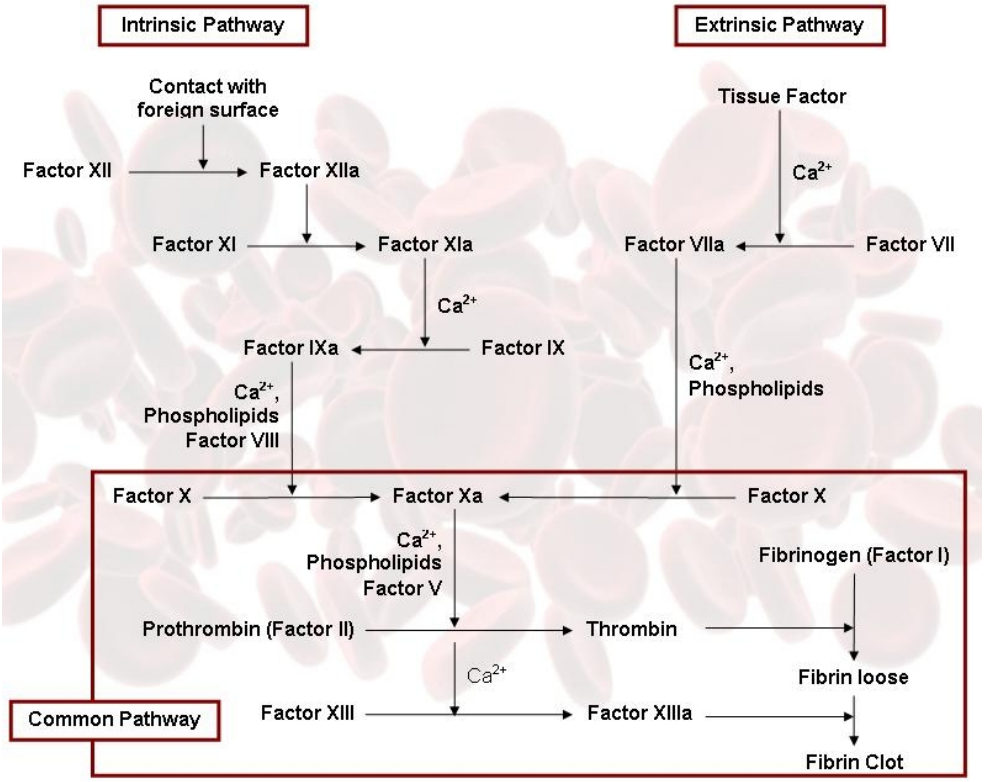

Figure 1.3: The coagulation cascade summarising the role of the intrinsic and extrinsic pathways in forming fibrin clots and stable thrombus

Intimal Hyperplasia

In the long term, tissue IH is the major cause of failure for surgical interventions to treat atheroscelrosis, whether by PTA or bypass grafting. IH causes the narrowing or stenosis of grafts due to the growth and thickening of the tunica intima of the blood vessel and is the result of a series of events involving the invasion and proliferation of

vascular SMC, fibroblasts and extracellular matrix (ECM) deposition [37]. The development of intimal hyperplasia is multifactorial, and its aetiology is not completely understood; however, it always involves some damage to the endothelium. The IH area is usually composed of about 20% of SMC which migrate from the media to the intima where they proliferate and deposit ECM components. The ECM components make up about 60-80% of the IH area. Other components include macrophages and lymphocytes. A multitude of growth factors and signalling molecules have been implicated in the development of IH resulting from damaged EC.

Initially the excessive SMC proliferation takes place in the medial layer. At the site of damaged endothelium, thrombosis forms reducing the capacity of EC to produce nitiric oxide (NO), heparan sulphate and other inhibitors of SMC proliferation. This effect is coupled with damaged EC producing more PDGF, basic fibroblast growth factor (bFGF) and transforming growth factor β (TGFβ); all of which promote SMC proliferation thus shifting the balance towards excessive SMC proliferation [38, 39]. Furthermore, the SMC found at sites of IH appear to be of a synthetic phenotype which have a proliferation rate 10% higher than contractile SMC and produce 4 to 5 times more ECM [40]. The second stage of IH involves the migration of SMC from the medial layer to the intima. This is primarily caused by degradation to the ECM, which prevents SMC migration, by the overexpression of tissue-type plasminogen activator (tPA) and urokinase-type plasminogen activator (uPA) which also activate matrix metalloproteinase (MMP) [41]. SMC migration usually starts 4 days after injury and can continue for up to a month. Finally, the third wave of intimal expansion occurs through a combination of SMC accumulation through proliferation, continued migration, and copious ECM synthesis.

The sequence of events in the development of IH is the same for all forms of IH, PTA or vascular graft induced; however, the events initiating the start of IH and speed of development are different. IH in bypass grafting is commonly found on the arterial floor near the anastomosis and/or at the heel and toe around the anastomosis. After grafting, blood flow patterns tend to change drastically leading to the local anastomotic region experiencing an altered haemodynamic environment (fig1.4) [42]. Turbulence, flow separation and zones of high/low shear stress around the anastomosis can damage EC and lead to platelet activation and adhesion resulting in a release of growth factors mentioned previously promoting SMC proliferation [43, 44]. Wall shear stress (WSS) is the product of the wall shear rate, the radial derivative of axial velocity, and the local blood viscosity. Shear stress can be calculated using Poiseuilles

law:

$$\tau = \frac{4\mu Q}{\pi r^3} \tag{1.1}$$

where μ is blood viscosity, Q is the volume flow rate and r is the internal vessel

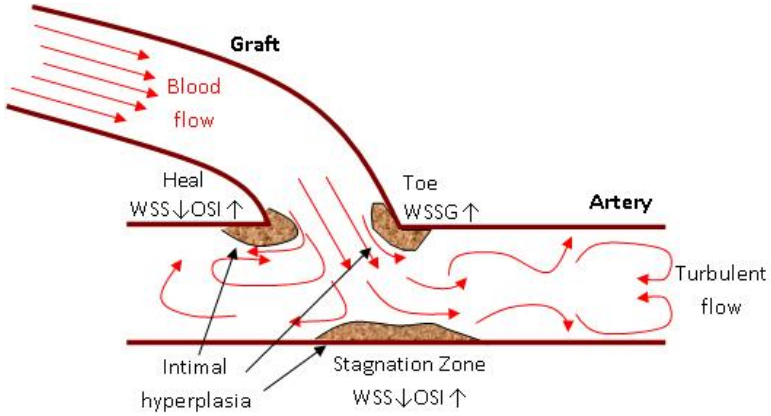

Figure 1.4: Spatial distribution of blood flow patterns and IH in arterial bypass graft anastomosis

radius. WSS has been shown to be an important determinant in the release of several vasoactive molecules from EC [44]. Arteries tend to change their radius in order to maintain a mean WSS value roughly in the range of 1.5Nm^{-2}, with IH readily observed in areas of low WSS, such as bifurcations, wall curves, and the stagnation point on the arterial floor opposite the anastomosis, where flow divides proximally and distally [45, 46]. Normal vessels respond to low WSS levels by constricting – a process not possible with synthetic grafts. Therefore, the correlation between low flow and IH may be an attempt by EC to maintain WSS levels within physiological range. However, low WSS does not explain the formation of IH at the heel and toe regions of anastomosis. Spatial and temporal gradients in WSS have been found at the site of IH and it is the oscillations in WSS that appear to be the major determinants in IH [47, 48]. Furthermore, at the heel of an anastomosis, rapid fluctuations in direction of WSS – shear stress changing from positive to negative – tends to occur during the systolic phase of the flow cycle [49]. Termed the oscillatory shear index (OSI), it was devised to account for the cyclic departure of the WSS vector from its predominantly axial alignment [50]. In a haemodynamic investigation conducted in a canine model, WSS, WSS gradients and OSI were all evaluated and it was found that the exponential function of OSI correlated best with IH formation [48]. This leads to the production of ECM components and an invasion of SMC into the intima – the hallmarks of IH. How the EC transmit these biomechanical signals into a biochemical

response is still unclear with several mechanisms being proposed [48, 51, 52].

1.6 Overview of Thesis

This thesis presents a clinical viable alternative to currently available prosthesis for vascular reconstructions. Given the clear clinical need, the general aim was to design and construct a prosthetic small calibre conduit which can be used as an arterial replacement in bypass surgery. By making use of a nanocomposite biomaterial with improved biostability, mechanical properties and anti-thrombogenicity, it was anticipated that the grafts would have improved mechanical and interfacial properties in an effort to minimise IH and thrombosis, without the need for complex cell therapies. In chapter 4, a novel extrusion-phase separation, fabrication method, to produce small calibre grafts was developed and optimised, which was reproducible and scalable. The resultant grafts were then evaluated for their mechanical behaviour in chapter 5. The interfacial properties of the luminal surface were characterised extensively in chapter 6 in order to better understand the blood-material interactions which were investigated in chapter 7. Chapter 8 dealt with developing a stringent sterilisation process which does not inadvertently harm material properties. Finally, the results of a long term *in vivo* study is presented in chapter 9, which aims to investigate the efficacy of using POSS-PCU grafts as bypass conduits.

2

Replacement Blood Vessels: Concepts, Progress and Future Challenges

Despite the long-standing clinical need, there have been few alternatives to autologous vessels for bypass grafting. The ideal blood vessel substitute must overcome a myriad of difficulties; principle amongst them is that blood vessels contain an interface with blood, and with the exception of a fully functioning endothelium, no other substance known to man is completely anti-thrombogenic. This presents the rather formidable challenge of blood clotting when exposed to alternative surfaces, particularly in the low flow, small diameter positions. The second challenge facing researchers is to develop a conduit with the required radial strength which can withstand the, not insignificant, arterial blood pressures. With mean arterial blood pressures approximately 100 mmHg, any implantable device must be robust enough to withstand the constant pulsatile, shearing forces generated. Common with any other implantable device, any developed graft must be resistant to infection and non-immunogenic. Additionally, any replacement artery would have to be readily mobilisable for use in emergency procedures, easy to handle and suture and available in a range of sizes depending on the clinical need.

With such a challenging design criteria it is easy to see why success in finding alternative prosthetic grafts has been limited. A wide range of strategies have been proposed and investigated, which usually fall into two categories: biological grafts which generally have better healing characteristics, and synthetic grafts with better mechanical and functional properties.

The ideal small calibre bypass graft	
Biocompatible	Safe, nontoxic and resistant to infection; graft does not induce thrombosis or a severe inflammatory response
Healing characteristics	Able to sustain a fully functioning endothelium and integrate into the wider vasculature without a hyperplastic response
Mechanical properties	Viscoelasticity comparable to native vessels so as to minimise the compliance mismatch between graft and vessel; kink resistant
Durable	Resistant to biodegradation, radial dilation and aneurysm formation; bursting pressures in excess of systolic pressures
Handling characteristics	Easy to sterilise safely and suture and readily available in a range of sizes

Table 2.1: Properties for the ideal small bore arterial substitute

2.1 Importance of Compliance Matching

As long ago as the 1960's, it was suggested that the elastic properties of vascular grafts may be an important parameter in determining long term patency of small calibre grafts. However, this was merely an empirical observation as few controlled studies were able to establish a clear correlation between graft performance, as measured by patency rates, and the mismatch in elastic properties between graft and host artery.

The lack of reliable controls is a major problem in investigating the compliance mismatch hypothesis. Studies have sought to compare the patency rates of a variety of conduits with different elastic properties including PET grafts, veins grafts and arterial grafts; however, these studies fail to take into consideration the different surface properties, graft tearing, and wall thicknesses that each conduit exhibits. More recently, the importance of compliance in determining graft patency was investigated in a canine model whereby common carotid artery autografts were treated with gluteraldehyde, in a variable manner to differentially alter compliance, and then implanted end to end with the femoral artery [53]. The compliance of grafts and arteries were either 10% matched or 60% mismatched, resulting in patencies of 85% and 37% at 90 days respectively providing a clear link between graft compliance and patency. These results were corroborated by a separate study where 36 femoropopliteal recon-

structions were performed in 18 sheep with autologous venous grafts [54]. Dacron mesh was used to surround the venous graft to achieve a state of compliance mismatch and lumen adaptation. A clear correlation was found between compliance and thickness of the hyperplastic intima that formed at the distal anastomosis 8 months post-implantation. The study was initiated with autologous grafts and so influences of exogenous materials were discounted; with it being assumed that the mechanisms effecting prosthetic and autologous grafts are the same.

Whilst the mechanism remains elusive, clinical evidence suggests that patency rates of small calibre grafts is significantly improved by matching graft and arterial compliance. For this reason, compliance matching is now thought to be an essential prerequisite for the successful design of a vascular graft. However, combining strength and elasticity is a difficult challenge to meet. Neither of the current industry standard biomaterials, PTFE or PET, displays the elastic properties to be used as conduits in small calibre reconstructions.

2.2 Biological Grafts as Arterial Substitutes

The central aim of biological grafts is to mimic the structure and function of the native vessel (fig 1.1). The intima consists of a confluent layer of EC which is antithrombogenic, nonimmunogenic and resistant to infection. Thereafter, the medial layer, which is also the thickest, consists of SMC, collagen and elastin. The SMC are arranged concentrically around the vessel and are surrounded by ECM proteins. As has been mentioned, the medial layer is primarily responsible for the vessels mechanical strength and maintaining structural integrity, with dilation and constriction the result of SMC response to external stimulus. The re-creation of the properties of the intimal and medial layers is thought to be vital for a functioning arterial graft that is antithrombogenic and maintains structural integrity. A number of paradigms have been proposed to engineer vascular tissue most of which involve a scaffold, cells and a bioreactor. The central hypothesis is that cells are cultured on the scaffold; which, over time, results in the deposition of ECM and spatial reorganisation of cells into continuous tissue formation. Whilst the concept is simple, many decisions are required over cell sourcing, culture conditions and the types of scaffolds. Furthermore, two opposing concepts have been pursued, each yielding promising results; namely, the engineering of arteries *in vitro* or regenerating the artery *in vivo*.

Substrate material	Scaffold fabrication method	Cell type	Comments	Ref
PCL and collagen	Electrospinning	Bovine EC and SMC	Sustain confluent layer of EC on the lumen and SMC on the outer surface. Mechanically robust enough to withstand arterial blood flow in the long term.	[55, 56]
PCL and PU	Wet spinning and electrospinning	Human EC	Stable formation of functional EC monolayer actively releasing bioactive agents.	[57]
PU	Phase separation and electrospinning	Muscle derived stem cells	Efficient cell seeding, maintaining cell viability and high proliferation rates. Mechanically robust with sufficient burst strengths and suture retention	[58–60]
Elastin PCL	Electrospinning	Human umbilical vein EC	Mechanically optimised with reduced platelet adhesion and increased endothelialisation.	[61]
Fibrin and PLA	Electrospinning	EC, EMC, fibroblasts	Mechanically robust autologous graft with remodelling capabilities. Exibited a confluent EC layer	[62, 63]
Silk fibroin from Bombyx mori	Fibres woven and then coated with silk solution	EC, SMC and bone marrow stem cells	85% patency rate following 12 month implantation in rat aorta.	[64, 65]
PGA, PLA and PCL	Electrospinning	Bone marrow derived mononuclear cells	Successfully used in humans and fully patent after 7 years. Mechanically fragile thus used for pulmonary circulation applications.	[66, 67]
PGS	Electrospinning	EC and SMC	Improved haemocompatibility and reduced immunogenic response. Sustain EC and SMC growth.	[68–70]
PU	Phase separation	EC and SMC	Improved cell retention due to preconditioning. Compliant and mechanically robust.	[71]

Table 2.2: Popular strategies for tissue engineering blood vessels. A range of biomaterials and fabrication methods are combined to produce scaffolds which are then populated with cells. The results of these investigations are summarised.

2.2.1 Scaffolds

The primary function of the scaffold is to provide support for the cells to adhere, grow and organise themselves into functional tissue. A range of materials have been exploited including degradable synthetic polymers, decellularised tissue and biopolymers. The basic premise of using synthetic polymers is that they will provide the required mechanical support and stimulus for the cells to grow and remodel. Over time, the synthetic material would then biodegrade leaving behind load bearing, functional tissue. The use of synthetic materials has some distinct advantages; the polymer chemical composition can be carefully controlled to manipulate the microstructure, physical properties and degradation rates of the polymers in effort to optimise tissue formation.

Polyglycolic acid (PGA) is perhaps the most popular synthetic material due to its FDA approval and current widespread use in surgery as sutures. Polyglycolic acid (PGA) degrades through hydrolysis of its ester bonds, with glycolic acid being metabolised and eliminated as water and carbon dioxide. However, PGA is rapidly absorbed and loses its mechanical strength in as little as 4 weeks raising the possibility of a failure of the cells to produce sufficient amount of ECM before polymer degradation. Copolymerising PGA with a range of other polymers, poly-L-lactic acid, polyhydroxyalkanoate and polyethylene glycol (PEG) to name a few, can improve its mechanical properties and adsorption rates [72, 73]. PGA scaffolds were coated with poly-4-hydroxybutyrate (P4HB) to produce a scaffold on which myofibroblasts and EC were seeded and cultured before implantation in the pulmonary artery of a lamb model. By investigating the up-regulation of key enzymes, the authors were able to show matrix remodelling on their grafts [74].

Alternatively, an elastomeric biodegradable polyester, Poly(glycerol-sebacate) (PGS), has also been suggested for vascular tissue engineering [68]. PGS was shown to sustain both EC and SMC growth, with the expression of vWF and alpha-smooth muscle actin, respectively, being confirmed by immuofluorescence. Further, PGS demonstrated considerably improved haemocompatibility with platelet adhesion, IL-1β and TNFα release being considerably less than reference materials [69]. Further, the PGS scaffold was shown to induce SMC characteristics from bone marrow mononuclear cells, in conjunction with platelets and plasma [70].

Whilst the use of biodegradable synthetic polymers, such as PGA, has yielded some promising results there is evidence to suggest that the scaffold degradation products may cause IH [75]. PGA remnants were found to change SMC phenotype from con-

tractile to synthetic, with the latter being associated with IH in intermediate to late graft occlusion [76].

The use of biopolymers is highly appealing as the resultant construct would be a completely biological graft minimising problems associated with exogenous materials. Collagen, an ECM protein and the most abundant mammalian protein, was used in the pioneering work of Weinberg and Bell who demonstrated that dissociated cells can be used to generate functional tissue [77]. Collagen appears to be the best placed biopolymer for successfully TEBV as it is the collagen fibres that limit the high strain deformations of blood vessels that prevent rupture [78]. Due to the ubiquitous nature of collagen it tends to induce a minimal inflammatory and antigenic response from the host [79]. Furthermore, collagen expresses integrin binding receptors on its surface allowing for cellular adhesion and endothelialisation. The major drawback to using collagen is its inadequate mechanical strength. Weinberg and Bell reported nominal burst pressures of 90 mmHg. In recent years that has been improved upon drastically through SMC alignment, cross linking with polysaccharides and proteins and shear preconditioning; however, the mechanical properties of collagen scaffolds still remain inadequate [80–82].

Composites of biopolymers and degradable synthetic materials have been developed in a bid to improve mechanical properties. An elastin/polycaprolactone (PCL) construct was produced via electrospinning resulting in a bilayered graft whereby the luminal side was composed of elastin and the outer layer was a elastin/PCL hybrid. The multilayer construct demonstrated improved mechanical durability and low thrombogenicity, both *in vitro* and *in vivo*, in a small scale rabbit carotid interposition model [61]. Alternatively, autologous fibrin with a biodegradable polylactide mesh support has been fabricated into a vascular graft. Seeded with SMC and fibroblasts and then lined with EC, the construct was attached to a bioreactor and mechanically conditioned for a period of 21 days [62]. The resultant graft appeared to be mechanical robust and capable of sustaining EC growth; it was thus implanted in a carotid artery of a sheep for a period of 6 months [63]. With the exception of one graft, which experienced severe stenosis, the fibrin/polylactide constructs were fully patent with the complete absence of thrombus formation on the luminal surface of grafts and no evidence of aneurysm formation or calcification.

The use of decellularised tissue has some distinct advantages as it is almost entirely composed of ECM giving it numerous advantages in terms of biocompatibility. The critical step in decellularised tissue is the removal of the cellular components with

detergents, enzyme inhibitors, and buffers whilst keeping the biological scaffold intact [83]. The scaffold can then be implanted into a host without any cells present under the premise that they will provide optimal cell anchoring sites and thus will be recellularised by host cells following implantation. The drawbacks of decellularising are that the mechanical properties, tensile strength and compliance, often suffer severely during the extraction process [84]. Shrinkage, possibly due to the loss of proteoglycans, is often observed as well as aneurysm, infection and thrombosis [85]. The residual antigenicity is also problematic as it can impair endothelialisation [86]. The tissue used for decellularising can be vascular in origin or non-vascular. Small intestinal submucosa (SIS) has been successfully decellularised resulting in a scaffold composed primarily of collagen (type I), fibronectin, growth factors, glycosaminoglycans, proteoglycans, and glycoproteins [87]. Patency rates, in a canine model, of SIS grafts are comparable with saphenous vein with cellular infiltration being observed at the midportion of the graft [88]. Alternatively, human umbilical arteries were decellularised using the detergent CHAPS and sodium dodecyl sulfate buffers followed by incubation in endothelial growth media-2. The decellularised umbilical arteries supported EC growth and remained functional following an 8 week implantation in a rat model [89]. Xenogenic tissue has also been investigated for decellularisation. An ovine carotid artery was decellularised and seeded with mesenchymal stem cell (MSC) derived smooth muscle and endothelial like cells and interposed into the carotid arteries in an ovine host model [90]. The authors report the constructs to be patent, anti-thrombogenic, and mechanically stable for 5 months *in vivo*.

2.2.2 Cells

All biological grafts require a cell source. The cells used have to be non-immunogenic, easy to harvest and expand, and have the ability to differentiate into specific cell types. Autologous cells obtained from the patient tend to be difficult to retrieve in any great number, have limited proliferative capacity or require excessive time periods for expansion. Stem cells possess some distinct advantages which include excellent proliferative and growth potential; and current technologies mean they are easily accessible. Table 2.3 lists provides a brief summary of some of the different stem cells which have been used for tissue engineering a blood vessel.

Embryonic stem cells (ESC) offer the potential for unlimited expansion: ideal for tissue engineering. Further, their pluripotent nature makes them amenable to any number of applications, including vascular. ESC have been shown to differentiate into both EC and mural cells, and can contribute to developing vasculature *in vivo* [91]. The use of VEGF aides in promoting EC whilst PDGF induces mural cells. ESC

have been shown to integrate into the circulatory system, grow on synthetic materials, and the mechanical cues regulating their behaviour are beginning to be understood [92–94]. Whilst the differentiation of ESC down vascular lineages has been described, the precise conditions by which this is achieved have not been discovered. So far, it has not been possible to differentiate ESC down a single cell line. A variety of culturing conditions have been investigated with no clear consensus arising as to the optimum method for differentiation and purification [95, 96]. Before ESC can become a clinical reality, a robust culturing protocol must be elucidated.

Induced pluripotent stem cells (iPSC) are a type of pluripotent stem cell derived from non-pluripotent sources through the 'forced' expression of specific genes. In many ways iPSC are similar to ESC and offer the opportunity to generate donor specific pluripotent cells without the controversial use of embryos. iPSC generated from mouse fibroblasts and juvenescent cells from cord blood have been shown to different down cardiovascular lineages [97, 98]. iPSC can mitigate any immunogenic side complications of cell therapy, patient specific iPSC were prepared for the treatment of limb ischaemia, thus offering an 'off the shelf' treatment option for the treatment of limb ischaemia [99]. iPSc have also been successfully combined with polymeric scaffolds [100]. In subcutaneous implantation of the iPSC seeded polylactide scaffold, the cells maintained a SMC phenotype, offering up the possibility of personalised tissue engineering applications.

Mesenchymal stem cells (MSC) are primarily derived from bone marrow or adipose tissue. They are easy to isolate, expand, have low immunogenicity and are multipotent; a combination of properties making them promising for use in TE. MSC have already found use in a clinical setting for orthopaedic applications [101]. The ability of MSC to differentiate down a vascular lineage has been demonstrated on a number of occasions [102]. MSC have also been seeded on PU grafts and implanted in Wistar male rats. It was found that MSC restored the medial like thick wall and enhanced endothelialisation of grafts [103]. Further, a bioreactor system was utilised to engineer a blood vessel *in vitro* from bone marrow MSC and was found to be substantially similar to a native vessel [104].

Amniotic stem cells (ASC) have also been demonstrated to be pluripotent and can give rise to multiple lineages of all three embryonic germ layers. Further, they are easy to isolate and expand. Their suitability for cardiovascular applications, amongst others, has been demonstrated many times over [105, 106]. In addition to inducing angiogenesis, ASC have been used to stimulate arteriogenesis through the secretion

of mediators which are responsible for the stimulation and/or recruitment of host reparative cells [107, 108].

Endothelial progenitor cells (EPC) are a type of circulating CD34+ mononuclear cell capable of attaining endothelial characteristics. Residing in the bone marrow and circulating in low concentrations in peripheral blood, growth factors such as granulocyte colony-stimulating factor (GCSF) and VEGF as well as tissue ischemia and vascular injury can mobilise EPC which proceed to stimulate re-endothelialisation of injured blood vessel and repair function of ischemic organs [109, 110]. EPC extracted from human peripheral blood by the density gradient method have been cultured *in vitro* and seeded onto vascular grafts [111, 112]. Studies indicate exceptional growth characteristics suggesting they are a highly promising candidate for tissue engineering purposes.

2.2.3 Bioreactors

Vascular cells, such as EC and SMC, are in a highly dynamic environment *in vivo*; they are exposed to a range of mechanical forces which have been shown to influence cell morphology, function and gene expression [113]. Indeed, mechanical forces have been implicated as being critical to the tissue formation process [114]. In the tissue engineering paradigm, ensuring proliferating cells adopt the correct phenotype is a non-trivial task. In the vasculature, four distinct forces are known to regulate cellular function, both in synergy and independently [115–117]:

1. Shear stresses: tangential frictional forces acting on EC and SMC due to blood flow and transmural interstitial flow
2. Luminal pressure: cyclic normal force exerted by blood pressure
3. Mechanical stretch: cyclic circumferential strain also attributable to blood pressure
4. Tension in the longitudinal direction

EC proliferation was shown to be shear dependant, with peak proliferative states at $\sim$5dynecm^{-2} (0.5 Pa) [118]. Both cyclic stretch and pulsatile hydrostatic pressure further increased EC proliferation, with the proliferation rate being dependant on both frequency of pressure and mean pressure [119, 120]. In the case of SMC, as they are not in direct contact with shearing forces, pulsatile distension is the dominant mechanical stimuli. Cultured statically, SMC dedifferentiated and proliferated rapidly displaying a synthetic phenotype characterised by the production of large quantities of ECM [121]. SMC with a contractile phenotype tend to have a cytoplasm rich in

Cell type	Cell source	Comments	Ref
Embryonic stem cells	Derived from the inner cell mass of the blastocyst	Pluripotent and unlimited differentiation capacity, highly controversial	[91–96]
Induced pluripotent stem cells	artificially derived from a non-pluripotent cell	Pluripotent and similar to ESC. Potential to avoid immunogenic side effects, reprogramming could pose significant risk.	[97–100]
Mesenchymal stem cells	Derived from bone marrow and adipose tissue	Multipotent, relatively easy isolation and expansion, low immunogenicity. Widely used with a number of clinical applications.	[101–104]
Amniotic stem cells	Amniotic fluid	Multipotent, non-controversial, easy to isolate and expand.	[107, 108]
Endothelial progenitor cells	Derived from bone marrow	Can differentiate into EC, easy to isolate and expand, low numbers in circulation.	[109–112]

Table 2.3: Summary of cells available for tissue engineering a blood vessel

myofilaments. The change from contractile – present in the medial layer of healthy arteries – to synthetic phenotype is seen in atherosclerosis and IH lesions. An important parameter in ensuring a contractile phenotype is the exposure to pulsatile stretch; this is borne out by numerous studies suggesting mechanical preconditioning is vital, prior to implantation, for the correct functioning of vascular cells cultured *in vitro* [71].

To expose cells to the necessary mechanical stimuli, a range of bioreactors have been developed. Bioreactors are laboratory tissue culture devices that aim to provide a controllable, mechanically active environment for tissue culture. Whereas some bioreactors expose only one aspect of the cardiovascular environment, such as shear force

or cyclic distension; other more intricate systems, mimic the entire vascular environment [122, 123]. All such systems have demonstrated their ability to improve cell proliferation, ECM synthesis and tissue growth. In addition to transmitting, mechanical stimuli, bioreactors have been developed to improve the cell seeding density and homogeneity by making use of convective mixing and flow [124, 125].

2.2.4 Tissue Engineering a Blood Vessel

Tissue engineering a blood vessel refers to the complete engineering of a functional vessel *in vitro* before implantation. This concept usually involves the culture of cells on an appropriate scaffold in a bioreactor which provides the necessary perfusion of nutrients and mechanical stimulus.

Perhaps the most impressive demonstration of tissue engineering a blood vessel *in vitro* is the cell sheet approach, whereby no scaffold or any other exogenous material was used to produce a fully functioning blood vessel [126]. Sheets of SMC were cultured in the presence of elevated levels of ascorbic acid to induce collagen production, which was then wrapped around a tubular support to produce the media of the vessel. In the same manner, a sheet of fibroblasts were grown and wrapped round the media to produce the adventitia. After several weeks of maturation the construct was placed in a bioreactor designed to provide both luminal flow of culture medium and mechanical support. Finally, EC were seeded by cannulating the ends of the constructs and filling with EC solution and rotating slowly overnight.

Whilst the constructs were antithrombogenic and the mechanical properties were impressive, the SMC did not exhibit circumferential alignment which is believed to confer the artery with its unique mechanical properties [127]. The engineered blood vessel was more compliant than ePTFE but not as compliant as the arteries it aims to replace. Additionally, the production period took a total of 3 months, making it unsuitable for emergency revascularisation purposes. The extended periods of cell culture increase the chance of contamination and malignant dedifferentiation of the cells. The TEBVs have been used for haemodialysis access on 10 patients with the 6 months results not wholly encouraging [128]. 3 grafts failed in the safety phase, one patient died due to unrelated reasons, and another patient was withdrawn from the study due to severe gastrointestinal bleeding. Of the remaining 5 patients, a further surgical intervention was required on one patient to maintain secondary patency.

2.2.5 A Regenerative Medicine Approach

The regenerative medicine approach has found favour amongst some researchers as it eliminates the need for complex culturing conditions and bioreactors. Here the cell seeded scaffold is directly implanted into the patient, where the body is allowed to act as a natural bioreactor to induce tissue formation, with the scaffold gradually degrading over time. In this strategy, the role of the scaffold is critical as it must be mechanically robust enough to transport blood, and withstand systolic arterial pressures, before tissue formation. Further, the scaffold should guide and support continuous tissue formation in a homogeneous manner providing the necessary chemical and mechanical stimuli for the cells to produce proteins, remodel the tissue and organise their environment.

The *in vivo* approach has probably yielded the clinically most successful TEBV. A scaffold composed of polyglycolic acid fibres coated with a 50:50 copolymer of polylactic acid and polycaprolactone was seeded with autologous bone marrow derived mononuclear cells and inserted as an intrathoracic inferior vena cava (IVF) interposition graft in a juvenile lamb model [66]. The graft was monitored using magnetic resonance imaging (MRI) and remained patent whilst increasing in size over time, in a symmetrical manner, proportional to the increase in size of the surrounding vasculature, indicating growth and remodelling as opposed to aneurysmal dilation. The TEBV was then used to repair an occluded pulmonary artery in a 4 year old girl – the first successful clinical application of a tissue engineered graft [129]. Based on the successful results in both animals and humans a clinical trial took place whereby the TEBV was implanted into 25 patients who underwent extracardiac total cavopulmonary connection modified Fontan surgery [67]. 1 year after implantation there were no graft related deaths, with only one complication reported – a partial mural thrombosis, which was successfully treated with coumadin. 5 to 7 years after implantation and all grafts were patent and intact; however, 4 grafts developed stenosis requiring angioplasty.

Whilst the progress in tissue engineering vascular grafts is encouraging and has helped to elucidate some of the fundamental remodelling mechanisms at play; it should be noted, however, that the grafts were implanted in the low-pressure pulmonary circulation where pressures are approximately 20-30 mmHg during systole, which is considerably less demanding than systemic or coronary circulation where pressures reach 100-140 mmHg during systole. The arterial circulation is far more demanding and requires constructs with considerable radial strength to prevent rupture and/or aneurysm formation. Currently, tissue engineered constructs, after scaffold degrada-

tion, do not have the necessary mechanical strength to survive in the arterial circulation.

2.3 Synthetic Grafts as Arterial Substitutes

Whilst there is no doubt that there has been significant progress in the field of tissue engineering a blood vessel since the pioneering work of Weinberg and Bell 25 years ago, there is still no clinically viable conduit for arterial replacements. The lack of radial strength to withstand systolic pressures coupled with practical drawbacks, such as insufficient length of conduit produced by current bioreactor technologies, and expensive and time consuming cell culture protocols have meant that no TE substitute has been translated to clinical practice. At the same time, the need for small calibre grafts is increasing at an alarming rate. To meet this clinical need, improvements to synthetic grafts have been sought. A range of strategies have been explored to counteract the problems of thrombosis and IH; the two primary causes of small calibre graft failure. These include the development of novel biomaterials, surface modifications and functionalisation with either anti-coagulant bioactive agents or molecules which promote spontaneous endothelialisation; and optimising graft mechanical properties in a bid to produce more elastic grafts thus minimising the compliance mismatch between graft and artery.

2.3.1 Cell seeding

The most common problem in tissue engineered blood vessels tends to be insufficient radial strength resulting in excessive dilation and aneurysmal formation, and in severe cases construct failure under systolic pressures. With this in mind, the idea of a biologically active 'hybrid' graft was mooted whereby a fully functioning endothelium would be seeded onto the luminal surface of synthetic vascular grafts. The endothelium would alleviate many of the problems associated with exogenous materials coming into contact with blood; namely, thrombosis and, to a degree, IH. The synthetic graft, meanwhile, would provide the mechanical support and radial strength that fully tissue engineered constructs lack.

Initially, EC were isolated from a subcutaneous vein segment, or usually from venipuncture, and were immediately seeded onto the graft lumen. Clinical results, however were largely disappointing with a lack of a confluent endothelium reported 14 weeks after bypass surgery [130]. A further trial revealed that after 30 months the patency

of a EC seeded ePTFE graft was significantly worse compared to a vein graft – 38% vs 92% [131]. These disappointing results were put down to insufficient initial cell density, poor adhesion under flow, and failure to achieve a confluent EC monolayer.

Undeterred by the poor clinical results, an improved cell seeding procedure was developed which involved EC being extracted from the vein or artery of a patient and cultured *ex vivo* before seeding, resulting in an increase in cell density upon a 3-4 week cell culture period [132]. Clinical results with the two stage procedure are a lot more encouraging with 9 year patency rates of 65% for EC seeded ePTFE grafts in the femoropopliteal position [133]. Furthermore, 14 patients received autologous EC seeded, 4mm ePTFE grafts as conduits for coronary artery bypass grafting of which 91% were patent at 28 months [134]. Mechanical preconditioning further enhanced cell retention by inducing structural changes and adaptation of EC cultured on synthetic vascular grafts [71].

Whilst conceptually promising, care must be taken when seeding grafts with cells. EC grown on prosthetic surfaces may alter phenotype and display a pro-coagulant phenotype promoting thrombosis rather than inhibiting it. Activated EC may increase growth factor production, encouraging SMC proliferation leading to IH. Cell sourcing, attachment and retention during pulsatile flow continues to be a problem. Possible solutions continue to be found with new cell sources, such as peripheral blood, bone marrow, omentum and subcutaneous fat being reported [135–137]. Adhesive proteins including fibronectin, collagen and RGD (Arg-Gly-Glu) have been investigated with the aim to improve cell adhesiveness [138]. Whilst the clinical results for the 2 stage seeding of grafts are very promising; it is highly time consuming and can not be used in acute cases. The cell culture process is very costly, highly specialised, labour intensive and carries the risk of infection.

2.3.2 Biofunctionalised materials

Considerable research effort is taking place in modifying current, commercially available, vascular grafts. One way in which patency rates can be increased is through coating or binding commonly used anticoagulants, such as heparin and hirudin, to the lumenal surface of the graft. Modified ePTFE and PET grafts are both commercially available. The Gore-Tex Propaten graft, an ePTFE graft with heparin anchored to the luminal surface via a proprietary end-point attachment mechanism, underwent a prospective non-randomized clinical trial to evaluate its efficacy [139]. The one year patency rate was 82%; 84% in the above knee position, 81% below the knee and 74% for the femorocrural position. This would suggest an improvement in the overall

patency of the heparin anchored graft; however, it should be noted that there was no control arm in the study and a prospective randomized controlled trial is really needed to determine the exact effectiveness of this treatment.

An alternative method to enhance the anti-thrombogenicity of biomaterials is the introduction of nitric oxide (NO) releasing molecules. NO has been shown to be a powerful inhibitor of platelet activation and adhesion, bacterial cell adhesion and SMC proliferation associated with restenosis and intimal hyperplasia [140]. A number of NO donors have been investigated from the exogenous diazeniumdiolates to the endogenous S-nitrosoglutathione and S-nitrosocysteine (fig 2.1). Diazeniumdiolates are NO donors formed by the reaction of secondary amine structures with NO under high pressure. The major advantage of using diazeniumdiolates is that they are stable solids, the half-life of NO release can be tailored to the specific need and NO release can be easily triggered in an aqueous environment [141]. A number of NO releasing grafts have been developed: NO releasing polyethylene-amine , PU and ePTFE grafts [142–144]. All grafts displayed NO releasing characteristics for a period of time ranging from one week to two months. Platelet deposition and SMC proliferation was seen to be diminished and EC growth was enhanced *in vitro*. Patency rates of NO releasing grafts, in arteriovenous shunt models, was much improved. However, there were some significant drawbacks. The incorporation of an NO donor into the graft impacted on the mechanical properties of the graft changing the compliance profile and thus compromising the medium to long term graft patency [142]. Even more worryingly, it was shown that some of the diazeniumdiolate leaches out of the polymer matrixes and form measurable levels of nitrosamines, a well-known carcinogen [143]. Further, the finite nature of the released NO calls into question their ability to coat long-term implants [145]. Liberating NO from endogenous sources may be a more fruitful approach. By immobilising L-cysteine on graft surfaces, NO can be released through the free thiol group undergoing NO exchange reactions [146]. The major advantage of this type of material is the unlimited source of NO which can be generated locally when blood comes into contact with the implant.

With the success of drug eluting stents in mind, sirolimus and paclitaxel (two commonly prescribed antiproliferative drugs) coated ePTFE grafts have been examined *in vivo* in a bid to minimise the proliferative capacity of SMC in IH. A porcine iliac artery bypass model was used to test the sirolimus coated ePTFE graft with the authors reporting a statistically significant reduction in cross-sectional narrowing compared with the untreated and adhesive treated graft [147]. Paclitaxel was examined in a porcine arteriovenous model, and whilst the haemodynamic environment is

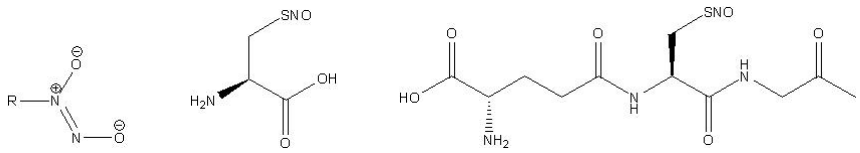

(a) diazeniumdiolate (b) S-nitroso-L-glutathione (c) S-nitroso-L-cysteine

Figure 2.1: The structure of NO donors

very different from an arterial bypass, stenosis was greatly reduced compared to the control [148].

We have discussed the presence of cells with endothelial characteristics circulating in peripheral blood already. A large body of work in developing synthetic grafts for small calibre applications is concerned with the capture and adherence of these cells to the lumen of the graft in an effort to endothelialise *in vivo*, thus providing a non-thrombogenic interface with circulating blood. The principle strategy for synthetic vascular grafts to capture EPC from circulating blood has been the immobilisation of capture molecules on the graft surface [149]. As there is a low concentration of EPC in peripheral blood, the ideal capture molecule must have a high affinity, selectivity and specificity to EPC. Even a weak affinity for other cell types present in blood can be fatal, as the cells or proteins present in higher concentrations, will compete for the binding site and cover the graft surface preventing the adhesion of EPC. Numerous peptides, derived from the ECM, have been postulated as effective EPC capture molecules including YIGSR, REDV and RGD [144, 150]. RGD is a binding sequence found on integrins present on the surface of cells. It is implicated in signal transduction events regulating numerous cell functions such as proliferation and migration and is responsible for connecting cells to themselves and the ECM. RGD functionalised grafts not only displayed an improved endothelialisation potential, but also improved cell retention when exposed to shearing forces [151, 152]. However, the long term safety and efficacy of RGD coated surfaces, and their effect on cell phenotype, is unclear. It should also be noted that RGD is not exclusively found on EPC but is a rather common binding integrin found on numerous plasma proteins including fibronectin, fibrinogen, vWF, collagen, laminin and vitronectin. Of these proteins, only vWF is synthesised in any great quantity by EPC whilst all the other proteins can be found on a multitude of leukocytes and platelets. The non-specificity of RGD has the potential to cause a thrombogenic or inflammatory response and should therefore be viewed critically.

Much more specific capture molecules are antibodies. EPC express a number of cell specific surface markers, including CD34, VEGFR-2, CD31 and VE-cadherin, which can be identified using labelled monoclonal antibodies. Anti-human CD34 monoclonal antibodies were attached to ePTFE grafts and evaluated in a porcine model of arteriovenous graft failure [153]. Histological examination appeared to demonstrate complete endothelialisation of the graft with 95% coverage after day 3 compared to less than 5% of the bare ePTFE graft. However, in spite of the rather impressive and rapid endothelialisation, significantly increased levels of IH at the venous anastomosis was observed. A number of explanations have been proposed for the increase in IH. CD34 is a haematopoietic stem cell marker, with CD34+ cells capable of differentiating into a number of different cell types including SMC. Therefore, it is possible that the CD34+ cells adhered to the graft still had the potential to differentiate into cell types other than EC including SMC. Alternatively, the differentiated EC on the graft could have adopted an alternate phenotype resulting in the secretion of pro-SMC growth factors and cytokines. The lack of compliance of an ePTFE graft could have contributed. It is difficult to draw any significant conclusions from this study as the adhered cells were insufficiently characterised – lectin, a surface antigen common in many blood borne cells including monocytes, was used to characterise EC.

The major drawback in this strategy is the low concentration of EPC in the circulation. Strategies to boost the mobilisation of EPC from the bone marrow and into the circulation are required. Furthermore, a deeper understanding of the factors controlling EPC differentiation on synthetic materials is required to get a firmer grasp of factors influencing cell phenotype, growth factor and cytokine release.

2.3.3 Biomimetic materials

By utilising advances in nanotechnology, a new generation of biomaterials are being developed that can mimic the structure and biological functions of the natural ECM. The cellular microenvironment largely dictates its fate; the natural ECM is not a smooth structure but rather it contains nanostructured grooves, ridges, pits and pores and fibrillar networks composed mostly of collagen and elastin fibres, with diameters ranging from 10-300nm, providing topographical cues to regulate cell behaviour. Nanopatterning of the luminal surface of a vascular graft can increase its cellular adhesiveness. Poly(lactic-co-glycolic) acid (PLGA) was chemically etched with sodium hydroxide to produce a nano-scale surface that exhibited an increased affinity for endothelial cells [154]. Cellular function was also shown to improve as cells

grown on nano-structured surfaces were observed to have long filopodia protruding from the cell body allowing the cell to sense the surrounding area and interact with the nanometre structures [155]. Furthermore, an increase in matrix metalloproteinases, enzymes linked to cell movement and adhesion to substrata was observed from the supernatant of EC cultured on nano-structured surfaces.

A highly versatile and inexpensive method of mimicking the native ECM fibrous network is through electrospinning [156, 157]. In this method (Fig 2.2), an electrostatic force is applied between the positively charged polymer solution and the substrate. When the electrostatic charge overcomes the surface tension of the droplet, a polymer jet is formed (Fig 2.2A), which then elongates and thins. As the solvent evaporates from the jet, an electrically charged polymer is left behind. These solidified fibres are then collected on a grounded surface (Fig 2.2B). Due to the simplicity of this method, electrospinning has been widely used by a variety of research groups. A range of materials - biodegradable and non-biodegradable, synthetic and natural polymers - can be electrospun, ranging from silk fibroin and collagen to PU and polyesters. This technique allows for the control of thickness, composition and porosity of nanofibre meshes with a relatively simple experimental set up. Fibres with a diameter of a few micrometers down to as small as 3nm can be developed, resulting in significantly larger surface areas [158]. Porosities in excess of 90% and pore sizes ranging from a few microns to tens of microns can be produced resulting in effective cellular infiltration and allowing mass transport of nutrient and waste products to and from cells [159, 160]. Blends of different materials can be used to augment the mechanical and/or biological behaviour of the scaffold. Furthermore, the fibres can be functionalised with a wide range of ECM proteins and bioactive agents resulting in a scaffold which has ECM like physical and biochemical properties. Through providing a more biomimitec environment for cells to grow upon; cell adhesion, proliferation, migration and differentiation were all shown to improve on electrospun fibres [161]. Cells orientate in the direction of the fibres, which is particularly pertinent for EC as it mimics the morphology of EC *in vivo* under blood flow.

A number of vascular grafts have been manufactured through electrospinning hoping to benefit from the improved substrate topography; however, these constructs are often limited by the size in which they can be manufactured leading to poor burst strengths [162]. By aligning the nanofibres, greater mechanical strength and modulus of nanofibre can be achieved and some degree of control over direction of cell growth can be administered [163, 164]. Further functionalization of the graft with ECM proteins such as gelatin and collagen, appeared to improve EC and SMC ad-

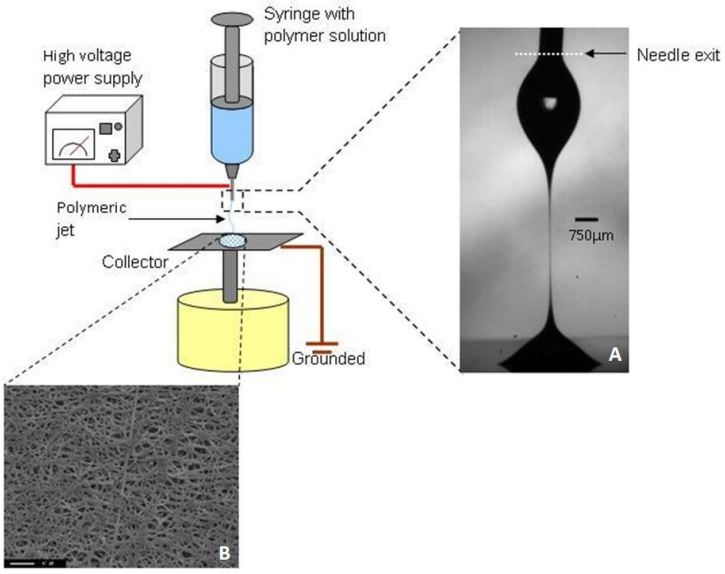

Figure 2.2: Schematic diagram of the electrospinning process for the production of polymeric nanofibres. A polymer solution is held in a syringe and pumped through a metal needle. A high voltage supply is connected to the needle, producing a fine jet of polymer solution (A). This dries out in transit, resulting in fine fibres which are collected on an earthed target (B)

hesion, growth and functionality [165]. The expression of EC specific markers such as vWF, CD31, CD54 and CD106 indicate normal cell function is maintained *in vitro* [166]. Electrospinning can be further utilised to overcome the inherent problem of cellular infiltration into scaffold pores, by concurrently electrospraying cells whilst electrospinning the polymer [167]. SMCs were uniformly integrated into the graft both radially and circumferentially using this technique. The graft appeared to be strong and flexible with reasonable dynamic compliance and burst strength values.

An alternative method to achieve the ECM like morphology is through self assembly of peptides. Molecular self-assembly is unique in its simplicity and ability to form a wide range of diverse nanostructures. It involves the spontaneous organisation of molecules into more energetically stable conformations favoured by hydrophobic, Van der Waal and electrostatic interactions, as well as hydrogen bonding, resulting in a final supramolecular structure ordered on multiple length scales [168–170]. This technique allows for the molecular control of the materials whilst fabricating three dimensional (3D) scaffolds providing the potential to mimic the complex signalling machinery of the ECM. An elegant example of collagen, a key component

of the native ECM, self-assembly was demonstrated using peptide amphiphiles held together in a staggered array by disulfide bonds [171]. The hydrophobic head of the peptide amphiphiles formed the triple helical structure whilst the hydrophilic tail reorganises and stabilises the self-assembled three dimensional structure of the scaffold. Scaffolds can be functionalised with self-assembled peptide amphiphiles which act as cell adhesive ligands such as Tyr-Ile-Gly-Ser-Arg (YIGSR) and Val-Ala-Pro-Gly (VAPG) [172]. The attachment of these peptides can significantly increase the adhesion, spreading and proliferation of EC. It was also found that these particular ligands reduced platelet adhesion compared to collagen controls, which for vascular applications, is highly desirable.

The mechanical behaviour of the graft is important not only in terms of compliance and improving graft patency, but recent evidence also suggests that substrate mechanics play a pivotal role in cell behaviour [173]. Substrate stiffness, in terms of compressibility, has been shown to affect the mechanical properties of the cell itself with EC cultured on stiff collagen gels being twice as rigid [174]. Further, in recent studies with SMC, substrate stiffness was the determining factor in dictating cell shape rather than the density of adhesive ligand to which the cell binds [175]. Whilst EC attach to substrates with a modulus less than 1000 Pa, they do not spread and there is a lack of stress fibres and other actin bindles [176]. When cultured on substrates with a modulus of 3200 Pa or more, stress fibres were abundant. Cytoskeletal tension and cell shape have been implicated as critical in determining stem cell fate [177].

2.3.4 Polyhedral oligomeric silsesquioxane

Polyhedral oligomeric silsesquioxanes (POSS) is a caged silsesquioxane molecule (fig 2.3). Silsesquioxanes are structures with the stoichiometric formula $R_nSi_nO_{1.5n}$ with the inner inorganic framework made of silicone and oxygen, whereas the outer organic covering consists of substituent groups that can range from purely hydrocarbon to an alkyl, alkene, aryl or arylene group. The molecular architecture of silsesquioxanes can be classified into two categories: caged and non-caged. A closed cage silsesquioxanes results in POSS molecules with the formula of $(RSiO_{1.5})_n$ where n=8,10,12. A typical POSS molecule with the silica-like core (0.53 nm in diameter), externally covered by eight organic corner group with the general sizes ranging from 1 to 3 nm in diameter, can be thought of as the smallest possible particles of silica [178]. The hybrid organic-inorganic framework renders POSS thermally and chemically robust; so much so, that it has been shown to be resistant to atomic oxygen oxidation resulting in POSS based polymers being used in orbiting space vehicles [179, 180]. Further, the

inner framework of POSS, consisting of Si-O and Si-C bonds is analogous to silicone, a favoured option in biomaterials due to its inert nature and low inflammatory response.

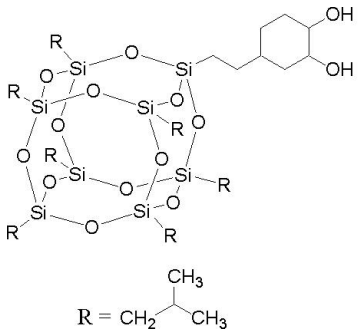

Figure 2.3: Molecular structure of POSS

Despite the promising mechanical properties, the drawback of conventional PU as implantable biomaterials has been discussed previously; namely, degradation due to oxidation and hydrolysis. With POSS known to be chemically robust and non-inflammatory, combining the beneficial effects of POSS with PU would yield a highly promising biomaterial. When used as filler, POSS tends to aggregate into larger agglomerates due to its small size and to minimise its high surface energy [178]. Therefore, the Seifalian lab aimed to covalently attach the POSS molecule to the 4,4-methylenebis(phenylisocyanate) (MDI), PU hard segment; which was then reacted with poly(1,6-hexamethylene carbonate) diol, the soft segment in the PU. This resulted in a pre-polymer which was chain extended with ethylenediamine in dimethylacetamide (DMAc) forming the end polymer – polyhedral oligomeric silsesquioxane poly(carbonate-urea) urethane (POSS-PCU, fig 2.4) [181].

POSS-PCU was shown to be more resistant to degradation and biostable, both *in vitro* and *in vivo* [182, 183]. No changes in strength, toughness or elasticity were detected after incubation with a range of degradative solutions for a period of 10 weeks; thereby preserving the compliant properties of the parent PU. Following implantation in a sheep model for 3 years, no signs of degradation or inflammation were noted.

The POSS moiety is known to migrate to the surface of the polymer matrix, this coupled with its high surface area, allows minimal quantities of POSS to be added to the polymer whilst still exerting a significant influence over the material surface and bulk properties. The amphiphilic, lipid-like, nature of the POSS-PCU nanocomposite resulted in it having anti-thrombogenic properties by both repelling platelet surface

adsorption and lowering the binding strength of platelets to the nanocomposite polymer. Coupled with its potential to support EC growth, it is a promising candidate for cardiovascular applications [184, 185]. POSS-PCU has already been used in the development of heart valves and for stent coating applications; and its feasibility for use in developing vascular grafts has been explored [186–188].

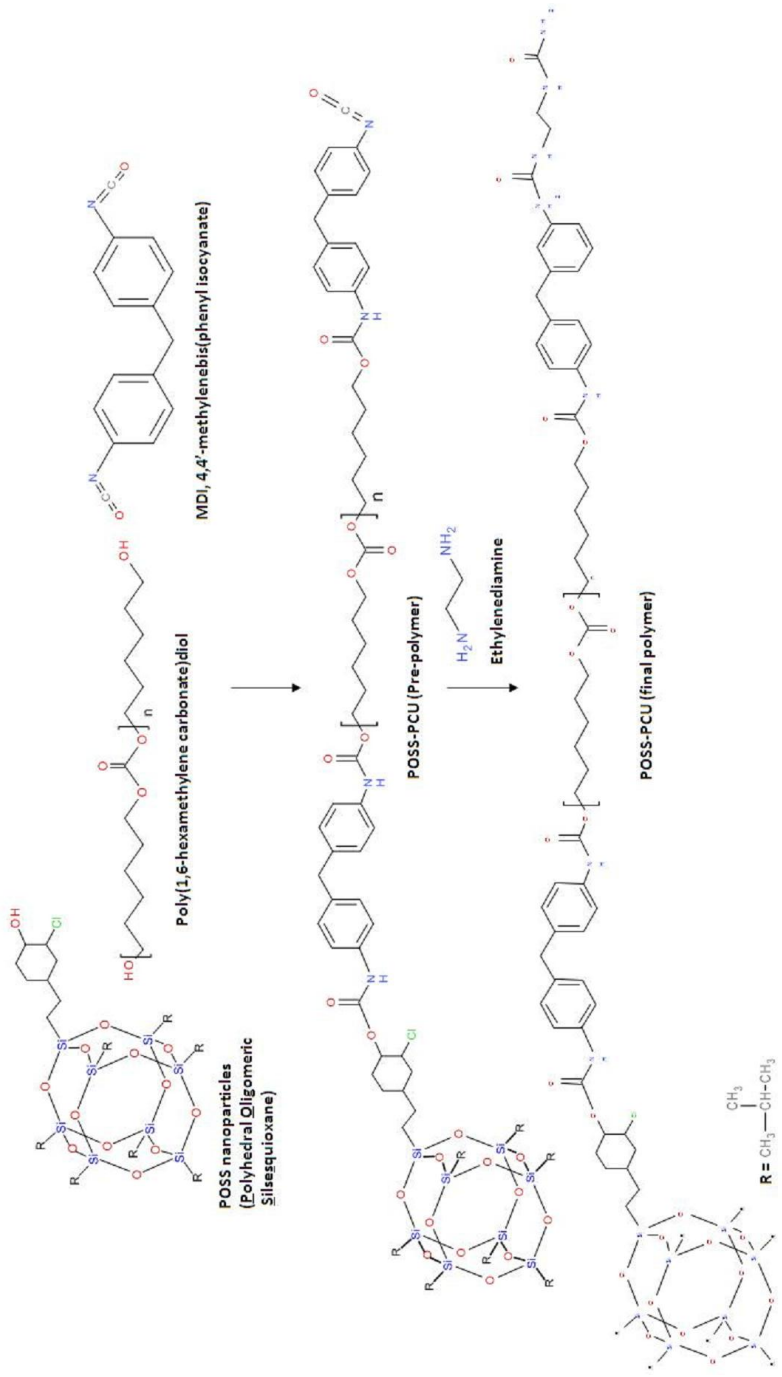

Figure 2.4: Reaction scheme detailing the synthesis of the novel nanocomposite polymer POSS-PCU used in this thesis

3

Aims of Thesis

Previously, the Seifalian lab has developed a novel nanocomposite biomaterial which displayed improved anti-thrombogenic and mechanical properties; making it a promising material for cardiovascular applications. It has already been used to develop range of medical devices including stents and heart valves. The central aim of this thesis is to develop a clinically viable, small calibre prosthetic graft for bypass surgery.

Multiple challenges need to be overcome in the creation of small calibre vascular graft. A method to fabricate conduits, in a scalable and reproducible manner, to a clinical standard with acceptable handling characteristics needs to be developed. Thereafter, the functional behaviour of the grafts needs to be characterised and the biocompatibility assessed. Before the graft can be considered for human use, it must undergo a pre-clinical trial in vivo in a suitable animal model.

Therefore, the work in this thesis can be further broken down into four specific aims as follows:

1. **Develop and optimise a reproducible and scalable method for the fabrication of POSS-PCU vascular grafts.**
   A novel extrusion-phase inversion method was developed and evaluated through a qualitative assessment of handling characteristics and a quantitative assessment of graft geometry and porosity. An automated extrusion machine was commissioned to assist in the manufacturing and the scalability of the process. The addition of a porogen to control graft pore size and porosity was investigated. The method was iteratively improved to manufacture fully scalable grafts in a range of dimensions.

2. **Achieve biomechanical properties similar to the native artery**

The tensile strength was evaluated as a measure of graft strength and its ability to withstand systolic pressures in the circulation. Handling characteristics such as suture retention were characterised to ensure that graft was clinically viable. A flow circuit was developed to mimic the circulatory system to examine the dynamic mechanical properties, such as compliance and viscoelasticity, of the vascular grafts at physiologically relevant arterial pressures.

3. **Characterise the biocompatibility of the grafts, in terms of the thrombogenic and immunogenic response as well as the potential for endothelial cell growth to these surfaces *in vitro***
   Biocompatibility was assessed through measuring the release of a range of cytokines including PF4, IL-1β, IL-6. IL-10 and TNF-α. The presence of proteins critical in the coagulation cascade was assessed as was platelet and mononuclear cell adhesion. The expression of surface of markers (CD14, CD69 and CD86) were examined and the ability to sustain endothelial cell growth evaluated. Surface properties of the grafts were characterised in order to get a more complete understanding of graft surface structure and functional properties especially with regards to interface with blood.

4. **Investigate healing and functional properties of POSS-PCU grafts *in vivo* in a large animal model**
   Implant POSS-PCU vascular grafts for an extended period of time in a large animal model following GLP protocols as per FDA guidelines. Monitor implanted grafts for their perfusion efficiency. Upon explantation histologically evaluate grafts to get an idea on the healing characteristics upon prolonged implantation.

4

Fabrication of Vascular Grafts Using an Extrusion-Phase Inversion Method

Developing a facile method that is able to meet the numerous structural requirements for a small calibre vascular graft is a non-trivial task with multiple design considerations to take into account. A major challenge in developing any load-bearing device is balancing the conflicting interests between material porosity and mechanical strength. The graft must be mechanically robust to withstand systolic arterial blood pressures whilst having a porous graft wall. Porosity has been deemed an essential prerequisite for the successful healing of a vascular graft [189]. It is essential to anchor the neointima in position and for the mass transport of nutrients and the removal of metabolic waste products. Further, porous graft walls have been demonstrated to improve endothelialisation of the constructs [190]. The challenge is further complicated as there are no clearly defined criteria for the porosity of vascular substitutes or, indeed, mechanical properties of arterial replacements.

Any fabrication process for the manufacture of vascular grafts must also be able to produce grafts in a range of dimensions. For the treatment of coronary or carotid occlusions, grafts rarely require a length of more than 150 mm; however, for the treatment of PAD, particularly from the above knee femoral position to the dorsalis pedis or posterior tibial artery, requires grafts of approximately 1 m in length. Furthermore, there should be a uniform wall thickness throughout the prosthesis and it should be defect free as any imperfection could be fatal. Finally the fabrication method must be fully reproducible and scalable. The ability to control the structural elements of graft design is important as it is these properties which will essentially dictate the mechanical and, along with the nature of the material, the biological properties of the graft.

A number of different techniques have been proposed and utilised which range from electrospinning and salt leaching to excimer laser ablation [191]. In this work, an extrusion phase inversion method was developed with the aim to produce grafts in a reproducible manner in a range of dimensions. Phase inversion involves the immersion of a thin layer of polymer solution in to a liquid non-solvent in which the polymer is immiscible. The exchange of solvent from the polymer solution with the non-solvent from the coagulation bath produces thermodynamic instabilities which are resolved by the separation into polymer-rich and polymer-lean phases. The polymer-rich phase forms a solid membrane matrix while the polymer-lean phase leaves a porous structure by leaching out of the system. The rates of solvent/non-solvent demixing and polymer precipitation during phase separation are two primary influencers of the membrane morphology [192]. Fine tuning factors which influence these twin properties provide a means with which grafts with a range of structural properties can be produced. Additionally, a porogen can be added to the system which is then leached out during the phase inversion step. The addition of the porogen allows greater control over macropore formation with the porosity effectively controlled by the quantity of porogen added, and the pore size of the structure can be adjusted independently of the porosity by using particles of different sizes.

In this study, we developed and optimised a phase inversion method to produce vascular grafts in a range of dimensions from the previously discussed POSS-PCU biomaterial. An automated extrusion machine was designed to produce grafts to a clinically viable standard. The influence of manufacturing parameters on the graft structure were investigated in order to get a fuller understanding of the phase separation process.

4.1 Materials and Methods

4.1.1 Polymer preparation

POSS-PCU synthesis

The reaction scheme for the synthesis of POSS-PCU is shown in fig 2.4. Polycarbonate polyol, 2000 MWt,(Bayer MaterialScience GmbH) and trans cyclohexanechloroydrinisobutyl silsesquioxane (Hybrid Plastics Inc) were placed in a 250 ml reaction flask equipped with mechanical stirrer and nitrogen inlet. The mixture was heated to 135°C to dissolve the POSS cage into the polyol and then cooled to 70°C. Flake MDI was added to the polyol blend and then reacted, under nitrogen, at 75°C-85°C

for 90 minutes to form a pre-polymer. DMAc was added slowly to the pre-polymer to form a solution; the solution was cooled to 40°C. Chain extension of the pre-polymer was carried out by the drop wise addition of a mixture of ethylenediamine and diethylamine in DMAc to form a solution of POSS-PCU in DMAc. Unless otherwise stated, all chemicals and reagents were purchased from Aldrich Limited, Gillingham, UK.

POSS-PCU/$NaHCO_3$ preparation

Sodium bicarbonate ($NaHCO_3$, 40μm particle size, Bruner Mond, Cheshire, UK) was dispersed into an 18% (w/w) solution of POSS-PCU in DMAc containing Tween 80 surfactant. The mixture was dispersed and degassed in one process using a Thinky ARE 250 mixer (Intertonics, Oxfordshire, UK) resulting in a viscous slurry. The quantity of $NaHCO_3$ used was altered to manufacture graft of varying porosities.

Polymer rheology

Rheological evaluation of POSS-PCU and POSS-PCU/$NaHCO_3$ was undertaken using a Bohlin CVO Rheometer (Malvern Instruments, Malvern, United Kingdom) at ambient temperatures of 25°C. The viscosity of the samples was obtained over a shear rate range of 0-250 s^{-1} using a cone and plate geometry configuration for samples.

4.1.2 Graft fabrication

Design of automated extrusion machine

Previously, we have developed a bench top extrusion machine capable of producing grafts with a maximum 10 cm length (fig 4.1). A mechanical arm descended vertically through a stainless steel chamber. The stainless steel chamber contains the polymer solution, so that when the mechanical arm was driven through it, it would be coated with a layer of polymer. A column of distilled water was placed directly below the chamber into which the mechanical arm would be driven into and left undisturbed for a period of 20 minutes. The formed tube was then removed from the mechanical arm by gentle agitation. Whilst this experimental set-up worked reasonably well and allowed the optimisation of the phase separation method, the grafts produced were neither reproducible nor scalable. Further problems with the eccentricity of the grafts led to inconsistent mechanical properties due to the unevenness of the graft walls. Further, the addition of the polymer to the chamber via a syringe led to copious trapped air bubbles which would cause inconsistencies and mechanical weak points

in the graft wall structure.

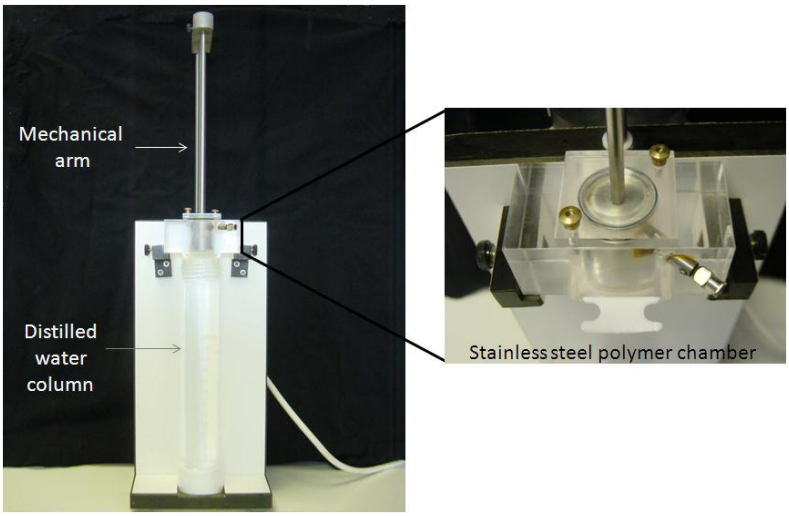

Figure 4.1: Digital images of bench top extrusion used for manufacturing vascular grafts.

An improved extrusion machine was designed and manufactured in conjunction with industrial partners (W. Bibby Ltd, Neston) with the aim of eradicating the drawbacks of the previous machine (fig 4.2). The principles behind the extrusion machine is the same; a mandrel is driven through a polymer chamber and die and into a water bath. The mandrel and die are interchangeable and have a range of dimensions allowing the fabrication of grafts with a range of wall thicknesses and internal diameters. The internal diameter of the graft is governed by the diameter of the mandrel whilst the wall thickness is principally controlled by the size of extrusion die. Horizontal extrusion was preferred to minimise the effects of gravity in distorting the polymer coating vertically and both the mandrel and die rotate to prevent any eccentricity forming in the polymer coating. The mandrel is pulled through the polymer chamber by a second distal die which also acts to stabilise the 1 m long mandrel ensuring a smooth coat of polymer is applied. The polymer is placed in a piston pump and is dispensed onto the mandrel at controlled rates. A bleed valve just proximal to the die helps to dissipate any trapped air bubbles which may cause imperfections in the graft wall. Following extrusion, the mandrel is left in the water bath for a period of 30 mins whereupon solvent exchange with distilled water takes place and the polymer crystallises. Thereafter, the grafts are removed from the mandrel and placed in de-ionised water for a period of 48 hrs followed by air drying for a further 48 hours.

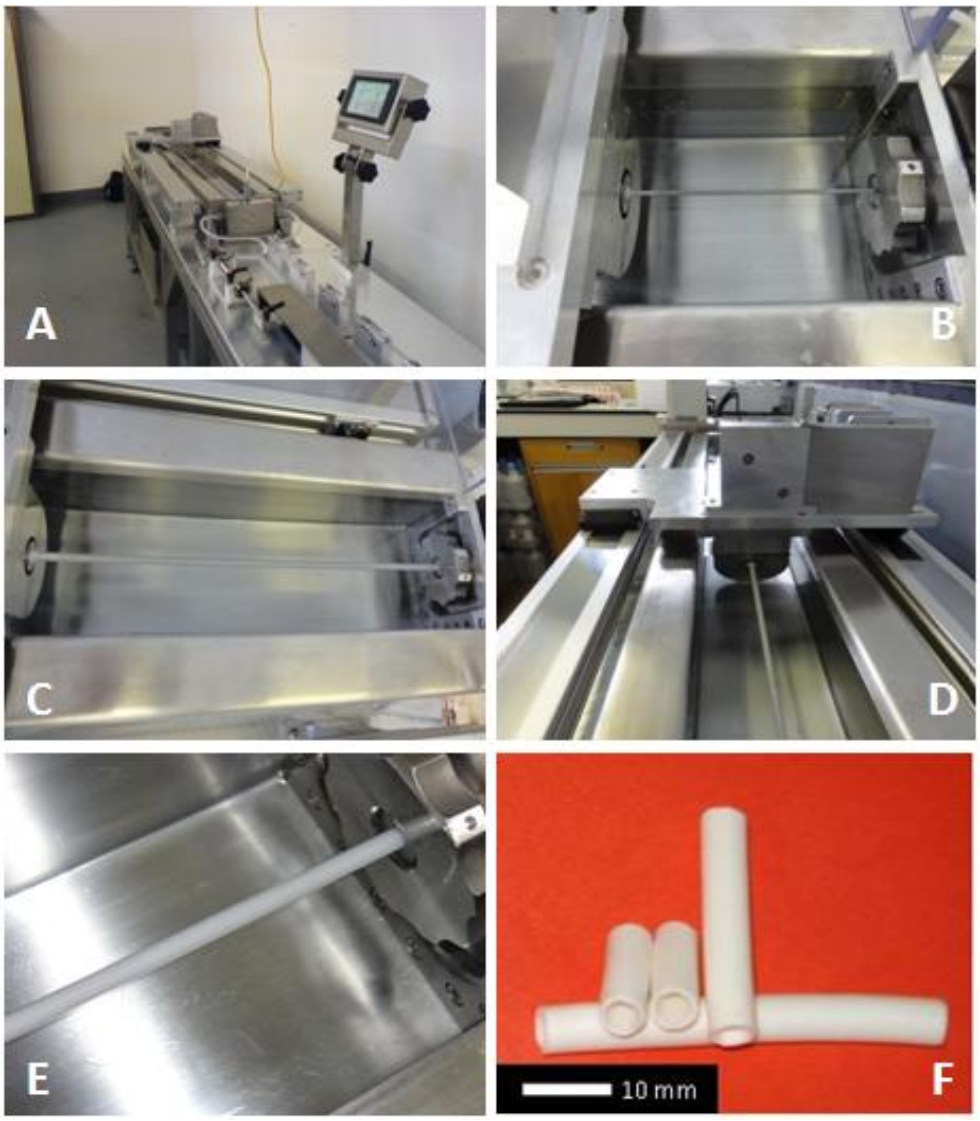

Figure 4.2: (a) Novel extrusion machine designed to manufacture grafts. (b) Proximal and distal die showing the early stages of graft extrusion (c) The latter stages of graft extrusion with phase separation taking place and the graft becoming more opaque (d) Distal die at the latter stages of graft extrusion (e) A closer image of the proximal die, which determines the wall thickness of the graft, and of a fully phase separated graft (f) Digital images of vascular grafts following p complete phase separation and removal from mandrels

Manufacture of vascular grafts

Vascular grafts were manufactured using the modified extrusion machine previously discussed. An 18% solution of POSS-PCU in DMAc was placed in the piston pump

and dispensed at a speed of 0.07 mms^{-1}. A mandrel with diameter 5 mm was used to extrude grafts through a 7 mm die, at a speed of 3 mms^{-1}, applying a 1 mm thick wet coating of polymer. Both the extrusion die and mandrel rotate at a speed of 3rpm. The graft is extruded into a water bath at room temperature and left undisturbed for a period of 30 minutes. A number of variations were made in order to optimise the extrusion conditions which included:

Temperature The temperature of the coagulant water bath was adjusted from a minimum of 0°C to a maximum of 50°C in 10°C increments. The remaining conditions were kept constant. The effect of temperature on the morphology of the phase separated membrane was evaluated.

Mandrel and die size Mandrels size was varied in an effort to produce graft with a range of internal diameters. Mandrels of diameter 2, 3 and 4 mm were utilised in addition to the standard 5mm mandrel. Mandrels were extruded through die's with diameters of 4, 5 and 6 mm respectively ensuring that the wet coating was of the same thickness.

Use of porogen $NaHCO_3$ was utilised as a porogen and combined with POSS-PCU as detailed above. The concentrations of $NaHCO_3$ used are described in table 4.1. Additionally, POSS-PCU/$NaHCO_3$ composite was extruded through die's of 8 mm and 9 mm diameter in order to form wet film coatings 1.5 and 2 mm thick.

POSS-PCU/%	**$NaHCO_3$/%**	**Tween 80/%**
63	35	2
53	45	2
43	55	2

Table 4.1: Porogen:polymer formulations used to manufacture grafts. Values are displayed as percentages of the total weight. POSS-PCU is an 18% solution in DMAc

4.1.3 Graft evaluation

DMAc liberation

The exchange of solvent during the phase separation process was monitored via gas chromatography–mass spectroscopy (GCMS) (i2 Analytical services, Watford, UK). Samples from the water bath were taken after 1, 12, 24, 36 and 48 hours and analysed via GCMS for DMAc.

$NaHCO_3$ leaching

Inductively coupled plasma optical emission spectrometry (ICP-OES) (Warwick Analytical Services, Coventry, UK) was utilised to ensure all the $NaHCO_3$ was leached out of the grafts. Samples of grafts produced from POSS-PCU/$NaHCO_3$ were taken at 0, 1, 6, 12, 24, 36 and 48 hours after extrusion and exposed to inductively coupled plasma detecting for electromagnetic radiation characteristic of Na^+ as an indicator of the presence of $NaHCO_3$. The intensity of the emission is indicative of the concentration of the element within the sample.

Differential scanning calorimetry

DSC analysis was undertaken to investigate whether the phase separation process effects the crystallinity of the sample. 3 by 3mm samples of POSS-PCU and the phase separated POSS-PCU were subjected to heat-flux DSC (Shimadzu DSC Ltd, Japan) at a heating rate of $10°Cmin^{-1}$. All samples were weighed pre and post-test to confirm that there was no change in mass after melting. Analysis was done in duplicates.

Gel permeation chromatography

GPC was carried out on POSS-PCU before and after phase separation to in order to ensure that the phase separation process does not alter the molecular weight of the material. Solutions of both samples were prepared by adding 15 mL of DMF to 30 mg of sample and left to dissolve on a roller mixer over night. The samples were analysed using a PL-GPC 50 system equipped with PLGel column guard and 3 PLGel 5m mixed bed-C columns (300×7.5mm). The measurement was carried out at 50^oC in DMF and the eluent was pumped at the constant flow rate of 1.0 mL/min. The system was calibrated by performing Universal Calibration with single PL-polystyrene standard and a set of PL-EasyVial PS-H polystyrene standards of known molecular weights. The detection was done using PL-BV 400RT viscometer and PL-RI differential refractometer. The data has been collected and analysed using Varian 'Cirrus Multi detector' software. Analysis was done in duplicates.

Wall thickness

Digital images were taken and image analysis software (Carl Zeiss KS 400 version 3.0) was used to measure the uniformity of wall thickness at 72 points distributed equally around the circumference.

Tensile Strength

Samples were cut longitudinally into a dogbone shaped specimen, 20 × 4 mm, using a sharp cutter and mechanical press ensuring a clean cut with no flaws or stress aggregation. However, due to the random nature of pore size and porosity in the coagulated samples, variability is to be expected. Sample thickness was recorded using an electric micrometer. Stress-strain profiles were characterised using a uniaxial load testing machine (Instron 5565, UK) and the ultimate tensile strength (UTS) recorded (n=6).

Porosity

The porosity of foams was calculated on the basis of their apparent density (ρ) and bulk density (ρ_o) according to the following equation:

$$Porosity(\%) = \left(1 - \frac{\rho_o}{\rho}\right) \times 100 \tag{4.1}$$

ρ values were measured gravimetrically on the basis of their dimensions and weights and ρ_0 is equal to 1.15 gcm^{-3} for non-porous virgin POSS-PCU (n=3).

Pore size and surface area

Mercury porosimetry was performed on the grafts to evaluate pore size and surface area using a Poremaster automated mercury porosimeter (Quantachrome UK). Grafts (n=3) were weighed, sealed in penetrometers and subjected to porosimetry analysis. For the purposes of data analysis, the surface tension of mercury and the intrinsic contact angle with polymer, regardless of the sample, was taken to be $\gamma_{Hg} = 480\text{Nm}^{-1}$ and $\theta = 140°$ respectively.

Scanning electron microscope

Graft samples (n=6) were washed with several changes of phosphate buffered saline (Oxoid) and post fixed using 1% osmium tetroxide/1.5% potassium ferricyanide for 1 hour. The samples were then washed with distilled water and dehydrated through a degrading acetone series (30%, 50%, 70%, 90% and 100% HPLC grade) washing twice for 15 mins each. After dehydration the samples were transferred to tetramethylsilane for 10 mins and then allowed to air dry. Finally, the samples were attached to aluminium stubs with double sided sticky tabs (TAAB) and coated with gold using an SC500 (EMScope) sputter coater for electrical conductance. The stubs were examined and photographed using a Philips 501 scanning electron microscope. Images were captured from random areas and were representative of the entire surface.

4.2 Results

4.2.1 Graft fabrication

Empirical observations of the manufacturing process suggest that altering the temperature or mandrel/die sizes did not significantly affect the extrusion or phase separation process: grafts were successfully manufactured with internal diameters of 2,3,4 and 5mm (fig 4.3). However, upon storage and drying the grafts produced via phase separation were found to be structurally unstable resulting in them shrivelling up and collapsing (fig 4.4).

Figure 4.3: Digital image of POSS-PCU vascular grafts fabricated via extrusion-phase separation method in a range of internal diameters.

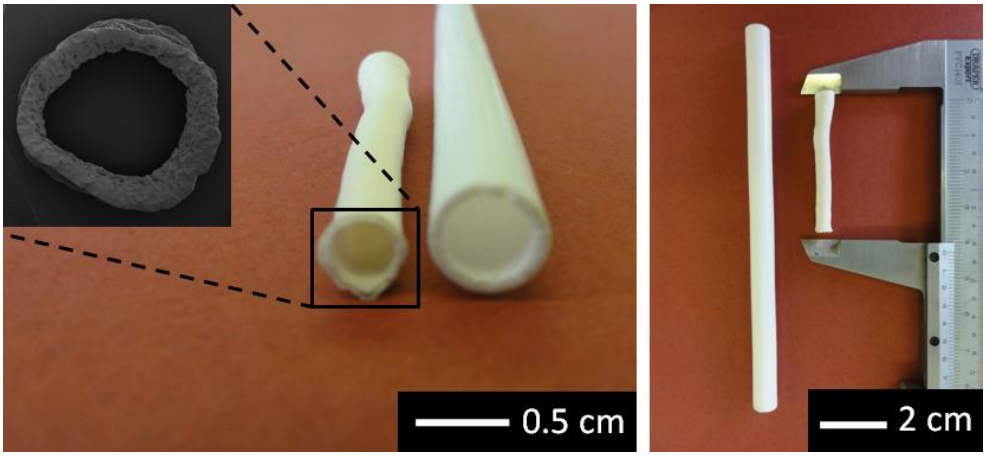

Figure 4.4: Digital image of POSS-PCU vascular grafts before and after dehydration. Graft is unable to maintain structural integrity resulting in deformation and shrinkage.

$NaHCO_3$ was introduced to the system as a porogen which would be leached out

in the phase separation process. Preparing the POSS-PCU/$NaHCO_3$ dispersions became increasingly more challenging as the quantity of $NaHCO_3$ was increased. There were minimal differences in viscosity for up to 45% $NaHCO_3$ (fig 4.5); however, concentrations in excess of 55% were highly viscous and were difficult to handle and extrude therefore, it was not possible to manufacture grafts. Using 55% of $NaHCO_3$ resulted in a viscous slurry however it was still possible to extrude and manufacture grafts. The extrusions of the dispersions were successful and upon the drying the grafts were found to be stable and maintain their shape and size.

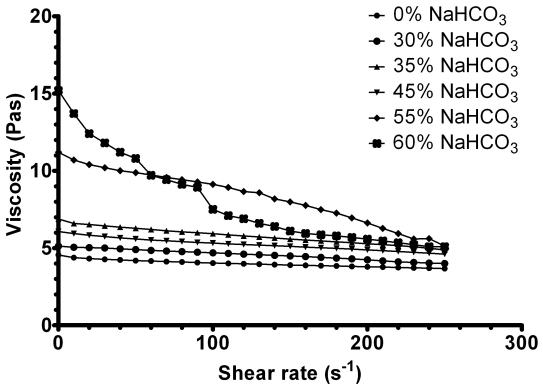

Figure 4.5: Viscosity of POSS-PCU/$NaHCO_3$ dispersions. There were minimal changes in viscosity following the addition of $NaHCO_3$ up to 45%. 55% $NaHCO_3$ was significantly more viscous but still extrudable whereas 60% $NaHCO_3$ was difficult to handle and not possible to extrude.

4.2.2 Graft evaluation

DMAc liberation

The concentration of DMAc in the water bath was evaluated with GCMS over a period of 48 hours. The complete removal of DMAc was confirmed after 24 hours as no further DMAc was liberated from the graft (fig 4.6a).

$NaHCO_3$ leaching

The complete removal of $NaHCO_3$ was confirmed via ICP–OES. After 24 hours only trace amounts of Na^+, 0.08%(wt/wt), was detected (fig 4.6b).

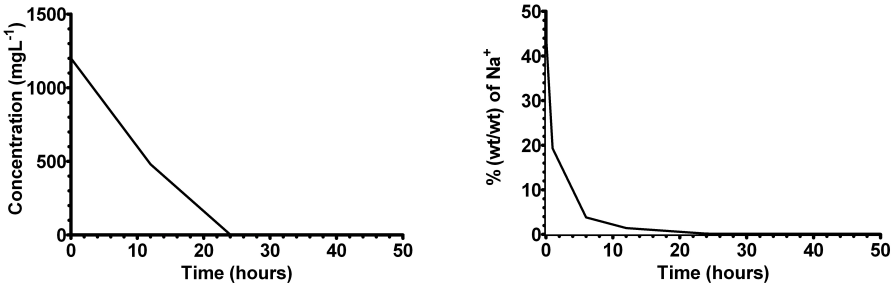

(a) DMAc released into the water bath

(b) Na^+ remaining in the graft

Figure 4.6: GCMS and ICP–OES analysis confirming that all solvent and porogen are removed from the graft.

DSC

The thermal properties of the graft assessed following phase separation to ensure no change in polymer crystallinity. Phase separation induced no changes in glass transition temperature (Tg), which remained at -30°C, suggesting polymer crystallinity is not effected by phase separation.

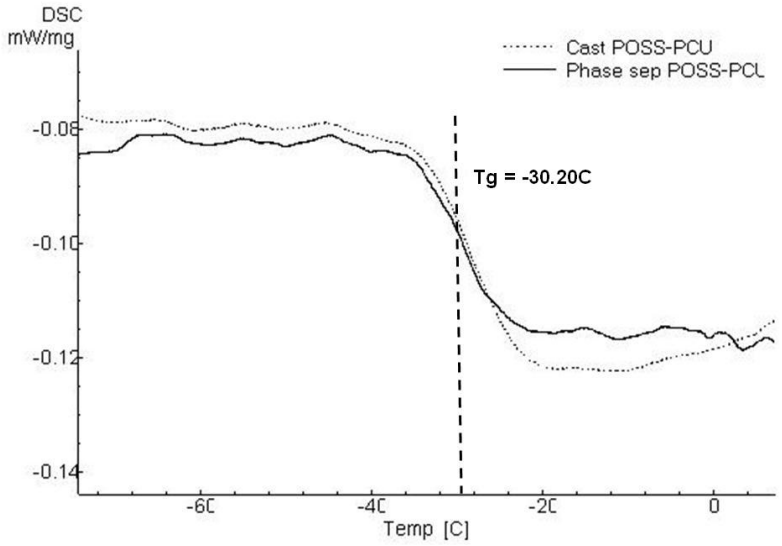

Figure 4.7: Glass transition temperature (Tg) of cast and phase separated POSS-PCU indicating no significant difference in the thermal properties of the polymer following phase separation.

GPC

GPC analysis of both POSS-PCU and the POSS-PCU graft formed through phase separation was conducted to investigate whether any change in molecular weight took place during the phase separation process. No significant changes were observed in the number average molecular weight (Mn), weight average molecular weight (Mw) or indeed the polydispersity (Pd) suggesting that phase separation does not adversely affect the polymer chain structure (fig 4.8).

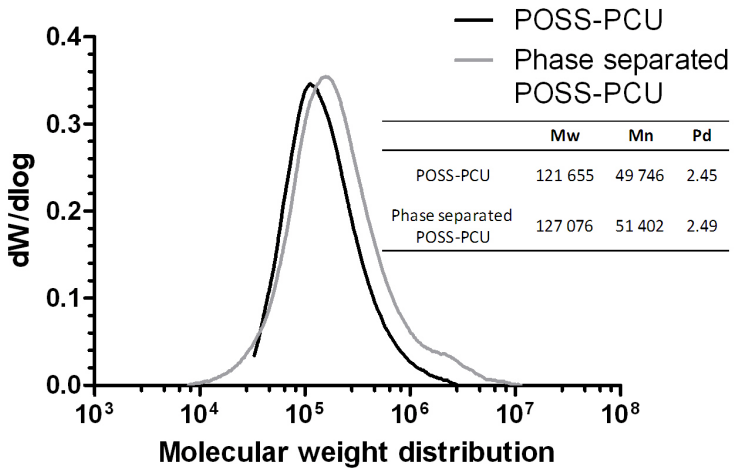

	Mw	Mn	Pd
POSS-PCU	121 655	49 746	2.45
Phase separated POSS-PCU	127 076	51 402	2.49

Figure 4.8: Molecular weight distributions of POSS-PCU and phase separated POSS-PCU with the Mn, Mw and Pd values inset.

Wall thickness

Whilst the thickness of the wet polymer coating was the same in each case, the phase separation process results in a contraction of the polymeric coating leading to a reduction in wall thickness. Both the temperature and the addition of $NaHCO_3$ all had a significant impact on the degree of contraction. At an extrusion temperature of 0°C the wall thickness was found to be 0.95 ± 0.04 mm which decreased significantly ($p < 0.001$, n=5) to 0.81 ± 0.02 mm at 10°C. The reductions in wall thickness continued with each incremental increase in temperature with the wall thickness being 0.56 ± 0.03 mm at 50^{o}C. However, the severity of reduction decreased as temperature increased with no significant difference detected between grafts formed at 30 and 40°C or 40 and 50°C (fig 4.9a).

With the extrusion temperature held constant at 25°C, the addition of $NaHCO_3$ significantly impacted the wall thickness of the grafts (fig 4.9b). The introduction of 35% $NaHCO_3$ resulted in a contraction twice the size of the $NaHCO_3$ free graft. Further addition of $NaHCO_3$ resulted in a wall thickness of 0.42 ± 0.01 mm at 55% $NaHCO_3$.

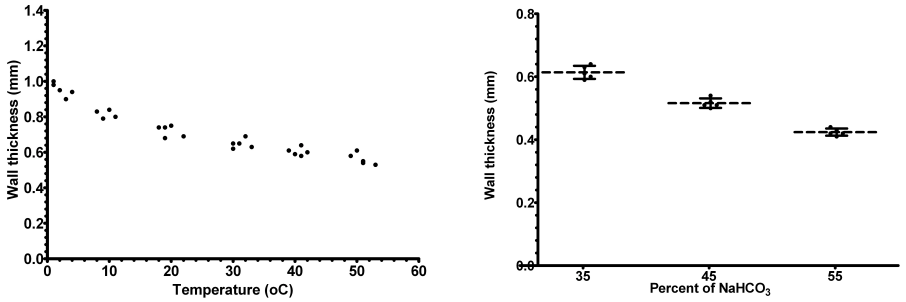

(a) Effect of coagulant temperature on graft wall thickness

(b) Effect of adding $NaHCO_3$ on graft wall thickness at a coagulant temperature of 25°C

Figure 4.9: The impact of manufacturing conditions on the wall thickness of grafts extruded via phase separation

Tensile strength

Figure 4.10 summarises the tensile properties of the vascular grafts produced via phase separation. A gradual increase in UTS is seen for grafts as the coagulant temperature is increased. Whilst no significant difference is observed between the grafts produced between 0 and 30°C there was a significant ($p < 0.001$) increase in UTS for the grafts produced at 40 and 50°C (fig 4.10a). The addition of 35% $NaHCO_3$, at a coagulant temperature of 25°C, significantly ($p < 0.001$) increased the UTS to 3.21 ± 0.20 MPa. However, the further addition of $NaHCO_3$ led to a reduction in UTS with 45% $NaHCO_3$ yielding a UTS of 2.38 ± 0.20 MPa and 55% $NaHCO_3$ exhibiting UTS values of 1.66 ± 0.30 MPa the latter being insignificantly different to the graft produced with no $NaHCO_3$ (fig 4.10b).

Porosity

SEM images of the cross sections of vascular grafts clearly indicate a porous structure (fig 4.11). Phase separation of POSS-PCU produced large isolated pores sandwiched between two skin layers. There appears to be a correlation between temperature and cross section morphology of grafts. Phase separating at low temperatures produces

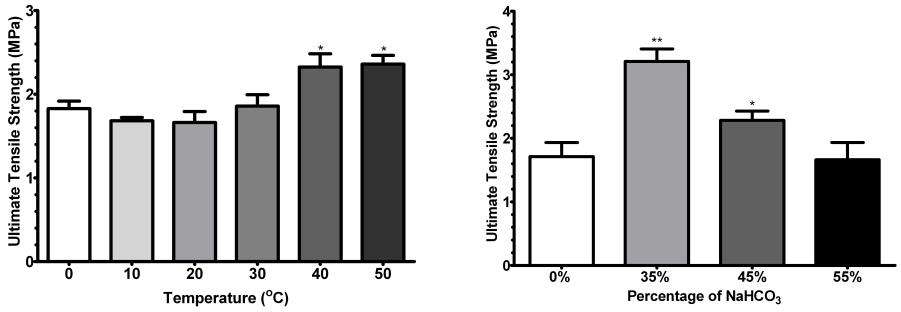

(a) (b)

Figure 4.10: Ultimate tensile strength of POSS-PCU vascular grafts produced via phase separation over (a) temperature range of 0 to 50° and (b) with or without $NaHCO_3$ (*=p<0.001)

a highly porous graft with large isolated macrovoids. Increasing the temperature of the water bath led to a, less porous, more compact membrane with smaller pore size. This fact is borne out by the bulk density and porosity calculations (table 4.2) which demonstrate that the bulk density doubles as you increase the temperature of the water bath from 0°C to 50°C which manifests itself into a 20% reduction in porosity.

The introduction of $NaHCO_3$ further dramatically altered the graft cross-sectional morphology. The POSS-PCU/$NaHCO_3$ grafts displayed a far more homogenous structure composed of smaller, more evenly distributed, interconnected pores, interdispersed amongst a fibrous network of polymer (fig 4.12). SEM images did not display a visual difference between graft structure and concentration of $NaHCO_3$; a result which was confirmed with the bulk density and porosity calculations. The addition of $NaHCO_3$ did not alter the bulk density or porosity of the grafts significantly, compared to the grafts produced with no porogen and produced at room temperature. Increasing the concentration of $NaHCO_3$ did result in a slight increase in porosity; however, a significant variation was only detected when 55% of $NaCHO_3$ was used suggesting that the density and porosity ratio is relatively insensitive to the concentration of $NaHCO_3$ used.

Pore size

In order to obtain a more quantitative measure of graft pore size, mercury intrusion porosimetry in the axial direction was conducted. Table 4.2 provides the modal pore

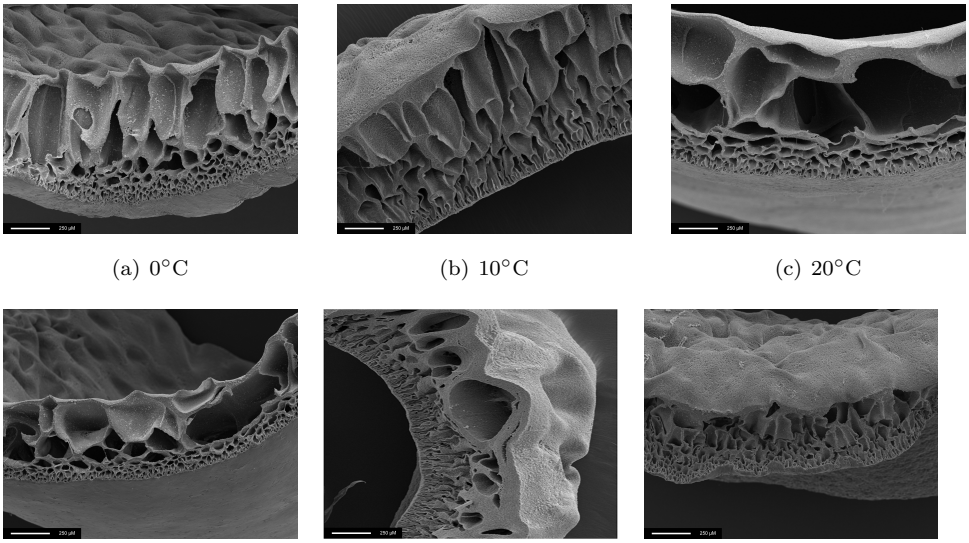

(a) 0°C (b) 10°C (c) 20°C

(d) 30°C (e) 40°C (f) 50°C

Figure 4.11: SEM images of the cross section of grafts produced at a range of temperatures between 0 and 50°C. Magnification is ×80. Pore size and wall thickness reduce in size as temperature increases.

Temp (°C)	**$NaHCO_3$ (%)**	**Bulk denisty (gcm^{-3})**	**Porosity (%)**	**Pore size (μm)**	**Surface area(m^2g^{-1})**
0	0	0.13 ± 0.02	88.70 ± 2.38	n/a	n/a
10	0	0.16 ± 0.03	86.09 ± 3.19	n/a	n/a
20	0	0.18 ± 0.05	84.35 ± 1.56	n/a	n/a
30	0	0.19 ± 0.03	83.48 ± 2.78	n/a	n/a
40	0	0.23 ± 0.05	80.02 ± 3.57	n/a	n/a
50	0	0.27 ± 0.04	76.52 ± 3.39	n/a	n/a
RT	35	0.15 ± 0.03	86.96 ± 2.19	15.21 ± 1.48	0.22 ± 0.04
RT	45	0.14 ± 0.03	87.83 ± 1.81	20.87 ± 1.87	0.50 ± 0.02
RT	55	0.11 ± 0.02	90.43 ± 1.33	30.75 ± 2.64	0.65 ± 0.04

Table 4.2: Mercury porosimetry and density measurements of grafts phase separated over a temperature range of 0-50^{o}C or fabricated with $NaHCO_3$. Porosity is calculated from equation 4.1. Mercury porosimetry and was not possible on the grafts produced with no porogen. RT = room temperature.

diameters for the grafts produced with $NaHCO_3$ with figure 4.12 displaying the pore size distribution. Unfortunately, intrusion porosimetry could not be carried out on

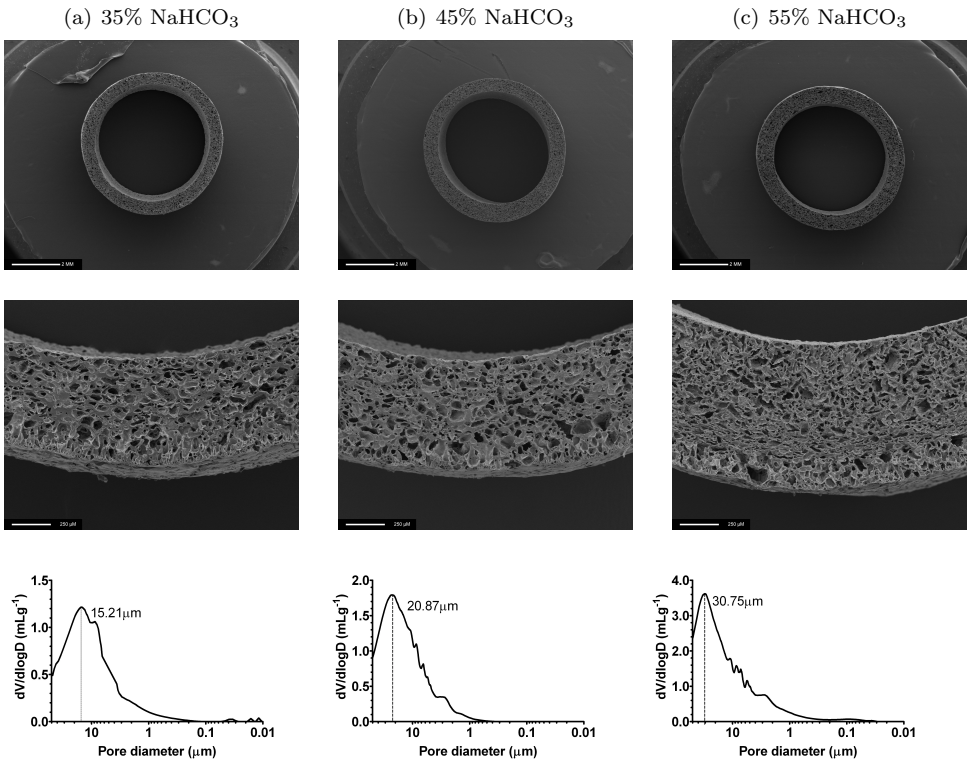

Figure 4.12: SEM images of graft cross sections at ×10 magnification (top), ×160 magnification (middle), and a distribution of pore sizes as obtained from mercury porosimetry analysis (bottom).

grafts produced without $NaHCO_3$ due to their closed-pore nature leading to excessive torsion and compression of the sample. A significant ($p < 0.001$) increase in pore size is evident with increasing concentration of $NaHCO_3$. Whereas using 35% $NaHCO_3$ results in a modal pore size of 15.21 ± 1.48 μm, 45% $NaHCO_3$ yields a pore size of 20.87 ± 1.87 μm which further increases to 30.75 ± 2.64 μm with 55% $NaHCO_3$. The increase in pore size further manifested itself in an increase in surface area. The total surface area of the graft produced with 55% $NaHCO_3$ is significantly higher ($p < 0.001$) than the graft produced with 35% $NaHCO_3$.

4.3 Discussion

The work in this chapter aimed at developing a facile method for the fabrication of small diameter bypass grafts in a range of dimensions. An extrusion machine capable of extruding 18% (w/w) POSS-PCU in DMAc was developed. Grafts with a range of internal diameters, wall thicknesses and lengths can be fabricated in a reproducible

manner. The versatility, simplicity and reproducibility of this production method are major advantages.

In any extrusion process, viscosity of material is an important parameter. In this instance the polymers behaviour was almost Newtonian with negligible variation in viscosity over the shear rate range (fig 4.5) ensuring that the viscosity of the polymer remains constant irrespective of the extrusion rate. Upon extrusion, a porous structure trapped between two skin layers was formed. SEM images of the cross section (fig 4.11) suggested that the pores were isolated and large in size. This is likely due to the almost instantaneous demixing when POSS-PCU is exposed to water. The ratio of solvent outflow far exceeds that of non-solvent inflow resulting in large concentration gradients which leads to the diffusion process dominating polymer precipitation initiating the formation of isolated macrovoids [193].

There appears to be a correlation between porosity and temperature of the water bath (table 4.2). Increasing the temperature reduced the prominence of the large tear shaped macrovoids; however, SEM images still display isolated and unconnected pores. The lack of large pores and macrovoids translates itself into a reduction in the overall porosity of grafts from approximately 90% to 75%. The principle effect of an increase in the temperature of the water bath is an increase in the thermal motion of the non-solvent and a reduction in surface tension of the water bath. The combined effect of the two properties is likely to be an increase in diffusion of the non-solvent through the skin, leading to an increase in the polymer crystallisation rate resulting in fewer large macrovoids [194]. The combined effect of the two processes is likely to prevent the development of the tear-shaped macroviods at an early stage. This is also reflected by the high dimensional shrinkage with water bath temperature.

The closed pore structure is impermeable to water, solutes and cells and thus is likely to inhibit the healing process by frustrating cellular attempt at successful integration of the graft into its surrounding tissues due to the smooth surface providing no tethering points which can result in the formation of a florid capsule around the graft. The large pores also create structural weak points which can lead to excessive localised dilation and even mechanical failure under pressure. Further, the grafts produced were structurally unstable upon drying resulting in them shrivelling and collapsing. It was postulated that the structural instability originated from the isolated nature of the pores. Introducing solvents such as EtOH in the water bath have been shown to produce graft with an interconnected pore morphology, however, in this instance, the augmentation of the water bath rendered the graft unstable at the phase separation

stage [194]. Therefore, in a bid to increase the interconnectivity of the pore structure, a porogen ($NaHCO_3$) was introduced into the system.

The introduction of $NaHCO_3$ resulted in a minor increase in viscosity and led to the suspension displaying pseudoplastic behaviour whereby the viscosity began to reduce with increased shear rate. However, as the range of shear rates tested far exceeds those applied by the extrusion machine, this reduction in viscosity is not likely to be a problem. A maximum concentration of 55% (w/w) of $NaHCO_3$ was used as anymore porogen and the viscosity of the mixture became too great making extrusion very difficult.

The addition of $NaHCO_3$ resulted in a dramatic alterations in graft structure; the graft wall became more homogenous with an interconnected pore structure (fig 4.12), with a high level of pore interconnectivity been shown to improve cell viability [195]. It's thought the increased interconnectivity is primarily due to the leaching of the $NaHCO_3$ out of the polymer matrix. However, $NaHCO_3$ particle size is 40 μm whereas the pore size, as determined by mercury porosimetry and visually via SEM, is considerable smaller than 40 μm. The pore size also varies with concentration of $NaHCO_3$ used indicating that $NaHCO_3$ not only acts as a pore former, or leaching agent, but also effects the phase separation process itself. The introduction of a fourth element to the system ($NaHCO_3$, POSS-PCU, DMAc and H_2O) is likely to slow down the overall membrane formation process favouring the precipitation of the polymer into a porous membrane packed by arrays of interlinked crystallites [196]. The introduction of $NaHCO_3$ resulted in a viscous suspension, which is likely to cause a kinetic barrier to the diffusion process, thus slowing down the overall membrane formation process which is likely to favour coagulation of the polymer rich phase [197]. Further, the rate of demixing of the solvent and non-solvent is also likely to be reduced with the introduction of an inorganic filler, which has been shown to also favour polymer crystallisation [198].

The introduction of $NaHCO_3$ appeared to stabilise the structure of the graft with no distortions seen when dried. No chemical differences between the grafts were detected despite the addition of $NaHCO_3$ and surfactant. Graft morphology and wall structure differ significantly with the addition of $NaHCO_3$. Whether the stabilisation of the graft structure is the direct consequence of the change in pore structure is difficult to ascertain and requires additional study. However, it is possible more in-depth chemical characterisation is required to confirm that the grafts produced with $NaHCO_3$ are not chemically modified as even a small concentration of surfactants have been

known to stabilise pore structures [199, 200].

Increasing the concentration of $NaHCO_3$ led to an increase in the modal pore size (fig 4.12) possibly due to the agglomeration of porogen resulting in a larger particle size. Pore size plays a critical role in the successful healing of vascular grafts. In a previous study, successful endothelialisation was demonstrated on grafts with pores 30 μm in diameter within 8 weeks [201]. It is reported that the ideal pore size is between 10 and 45 μm as larger pores could result in excessive fibrous tissue infiltration resulting in a profound loss of compliance and inadequate endothelial coverage [202]. The modal pore size of the grafts produced with $NaHCO_3$ for this study ranged from 15-30 μm obtained via mercury porosimetry. It was not possible to evaluate the porogen free samples via porosimetry due to their closed-pore nature leading to excessive torsion and compression of the sample. Whilst porosimetry provides an indication of the pore size, it should be noted that the values expressed here should not be thought of as exact pore diameters. The Washburn equation used to convert intrusion pressures into diameters assumes pores off a cylindrical geometry whereas SEM observations clearly indicate that the pores are not cylindrical but are polygonal and interconnected. The values are also likely to be slightly lower than the actual pore size due to porosimetry mainly detecting the smaller contractions within the interconnections between larger pores.

Whereas the pore size increased with increasing $NaHCO_3$ concentration, there was no significant change in the overall bulk density and thus porosity of the grafts which remained between 85-90%. Porosity is defined as the percentage of void space in a solid and can be measured as a ratio of bulk density of graft and density of material. The negligible variation of porosity over the $NaHCO_3$ concentration range is likely due to the greater contraction of the grafts during the phase separation process. Despite a constant 1mm thick coating of POSS-PCU/$NaHCO_3$ slurry being applied to the mandrel for the manufacture of all grafts, the wall thicknesses varied significantly (fig 4.9b) between each sample. The reduction in mass, due to additional void space, would be negated by a reduction in volume leading to a near constant bulk density and thus porosity of 85-90%. A bulk density of 0.1 gcm^{-3} and porosity in the range of 85-90% may be the saturation point for low density polyurethane foams.

Whilst a high level of porosity encourages tissue ingrowth; it diminishes mechanical properties thereby setting an upper limit for pore size and porosity. A slight increase in tensile properties was detected for grafts produced at 40 and 50°C which is likely to be an effect of a significantly denser membrane. The bulk density of grafts pro-

duced between 0 and 30°C did not vary in any significant manner which corresponds to no significant variations in UTS. The addition of $NaHCO_3$ improved the UTS of the graft samples significantly; however, subsequent increases in the concentration of $NaHCO_3$ reduced the UTS. The increase in UTS is most likely a consequence of the more homogenous wall structure of the graft and fewer large macrovoids in the cross-section (fig 4.12). As the bulk density and thus the overall porosity does not vary significantly between the samples produced with $NaHCO_3$, the increase in pore size may be responsible for the observed reduction in UTS. Larger pores would result in a smaller apparent cross sectional area upon which force is applied compared to the measurable cross sectional area resulting in lower UTS values. It should be noted however, that due to the extraordinarily high UTS of the virgin POSS-PCU material (approx 60MPa) the UTS of all the grafts produced exceed those of a number of porcine and human arteries [203, 204].

The phase separation process was able to produce porous membranes with suitable mechanical strength to be used as vascular grafts. The complete removal of solvent (DMAc) and porogen ($NaHCO_3$), for those grafts produced with a porogen, was confirmed via GCMS and ICP-OES ensuring a contaminant free graft is produced. A combination of GPC and DSC analysis was conducted to investigate whether the polymer processing affects any of the bulk material properties. GPC analysis was utilised to investigate changes in molecular weight distributions to determine any physical damage to the polymer via either the extrusion or phase separation process. No change in molecular weight distributions between the grafts and virgin POSS-PCU were detected, thus confirming that the manufacturing process does not damage the polymer. Similarly no difference was detected in the thermal properties of phase separated POSS-PCU as determined via DSC. Molecular weight and thermal properties are important in determining many physical properties which determine the performance, end use and processability of materials. With no change in bulk properties being detected, it can be concluded that phase separation does not adversely effect the biomaterial.

4.4 Conclusions

Graft properties are primarily dependant on the nature of the biomaterial and the fabrication process. In this chapter, an extrusion phase separation fabrication method is described for the production of vascular grafts from POSS-PCU polymer. The phase separation method does not adversely affect material properties. The porosity,

pore size and pore interconnectivity are evaluated and optimised for tissue ingrowth and graft healing. Finally, the UTS was assessed to ensure the grafts are mechanical robust enough to endure the harsh conditions of the vasculature.

5

Mechanical Optimisation of Small Calibre Vascular Grafts

Poor long term patency has, in part, been attributed to physical determinants in biomechanical design of grafts [205]. The ideal graft should have viscoelastic properties comparable to those of the native vessel, circumferential strength capable of withstanding arterial pressures, tensile and shear strength to withstand fraying and tearing out of sutures and a degree of flexibility and kink resistance. Currently available biomaterials meet many of these requirements which has led to the development of a range of large calibre grafts; however, for the treatment of small calibre vessels, viscoelasticity, and more specifically, compliance is critical [53, 54]. The currently available grafts, namely PTFE and PET, fail to meet this crucial requirement resulting in poor functional patency rates when used for small calibre (<6 mm) reconstructions [206].

The mismatch in compliance and its role in the progression of IH, the principal cause of small calibre graft failure, has been discussed in detail previously. Additionally, if one considers the Hagen-Poiseuille equation whereby the pressure drop (ΔP) is proportional to the length of tube (L), flow rate (Q), viscosity (η) and inversely proportional to the fourth power of the internal radius (r^4) and π is the mathematical constant (equation 5.1); and substituting the Ohm's law (P=QR) analogy where R is impedance, then the impedance to flow is drastically increased with any reduction in graft calibre (equation 5.2). The increase in impedance results in a decrease in flow rate which is highly likely to cause an increase in the probability of stasis thus promoting thrombogenicity.

$$\Delta P = \frac{8\eta LQ}{\pi r^4} \tag{5.1}$$

$$R = \frac{8L\eta}{\pi r^4} \tag{5.2}$$

A number of assumptions are present in the equation, namely that flow is laminar, viscous and incompressible and flow is through a constant circular cross section. However, blood vessels are not rigid pipes, they display complex compliant behaviour with intrinsic and extrinsic mechanisms to vary compliance and shape. The distension of the vessel wall in response to pulsatile flow and pressure is viscoelastic in nature. That is to say that whilst vessels return to their original shape upon removal of an external force, the response to force is not instantaneous but is time dependant. The purpose of the viscoelasticity is to convert the pulsatile ejection of blood from the heart into continuous flow [207]. Energy is stored in the vessel wall during systolic distension, which is then responsible for the elastic recoil during diastole ensuring continuous anterograde blood flow. Additionally, the elastic component is responsible for minimising the arterial systolic pressure whilst increasing the diastolic pressure ensuring that the mean arterial pressure remains high and the pulsatility low.

Meanwhile, the viscous component of the vessel wall is responsible for dissipating energy due to the highest frequency components of the incident pressure and flow waves and the amplitude of any reflected waves. Further, mechanical damage to the vessel wall can be reduced by eliminating high frequencies that could cause early fatigue. Plotting pressure against diameter during one cardiac cycle results in a hysteresis being observed with the area of the loop being equal to the energy lost in each cycle. Additionally, the phase angle (δ) between the diameter and pressure wave can be calculated, as a quantitative measurement of the viscous component of the vessel wall, using equation 5.3 [208].

$$sin(\delta) = \frac{a}{\Delta F} \tag{5.3}$$

Where a is the separation between the ascending and descending limbs of the hysteresis at mid-cycle and ΔF is the total excursion of hysteresis (fig 5.1).

For practical purposes, when measuring the viscoelastic properties of vessel walls and vascular grafts, it is convenient to use a single parameter which expresses the mechanical behaviour under living conditions, rather than the well established formulations and constitutive equations, which increase dramatically in complexity as the number of dimensions increases (1D to 3D), and anisotropy and non-linearity is introduced. Several parameters have been suggested and are often used which includes the pressure-strain elastic modulus (Ep) and compliance (C); both of which give a measure of the functional stiffness of the vessel wall i.e. its effectiveness as an

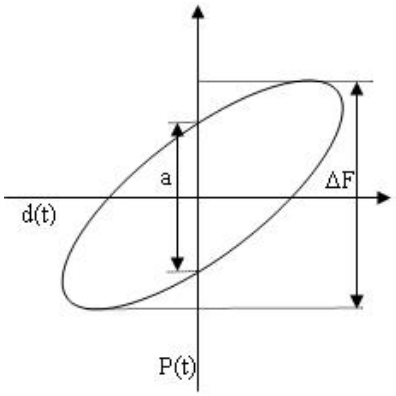

Figure 5.1: Lissajous plot of pressure (P(t)) and diameter (d(t)) resulting in a hysteresis from which the phase angle can be calculated using equation 5.3

elastic reservoir.

$$Ep = \frac{\Delta P D_d}{\Delta D} \tag{5.4}$$

$$C = \frac{\Delta D}{\Delta P D_d} \times 10^4 \tag{5.5}$$

Where P is pressure and D_d is equal to the diastolic diameter. A significant advantage of these models is that measurements can be made non-invasively and routinely; only the pressure-diameter data at a specific pressure level is required. However, these parameters are structural and express the stiffness or distensibility of a blood vessel or graft but do not represent the inherent elastic properties of the wall material, which is still calculated from the elastic modulus.

In addition to the viscoelasticity and inherent graft mechanical properties, a clinically viable graft must meet a number of handling characteristics such as suture retention and kink resistance. The graft wall must be strong enough to withstand tearing of sutures. Sutures tend to apply stress on the graft wall over small areas resulting in the graft being exposed to high levels of localised force which could lead to graft failure [209]. Graft kinking is where bending the graft results in a dramatic reduction in its diameter resulting in stenosis (fig 5.9). The formation of kinks in the arterial circulation has been known to lead to a range of ischaemia related incidences including angina and stroke [210]. Treatment of kinking grafts is rather limited, and can include angioplasty, stenting or a repeat of invasive bypass surgery.

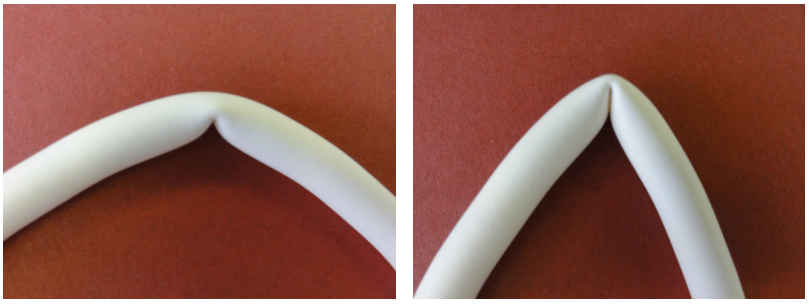

Figure 5.2: Digital images of kink formation in a graft.

In this chapter the inherent mechanical properties (ultimate tensile strength, elongation to break and Youngs modulus) of the graft material were characterised through uniaxial tensiometry. This was followed by investigating the functional dynamic mechanical behaviour of the grafts. A bespoke physiological flow circuit was constructed which allowed the simultaneous collection of pressure and diameter, thus allowing the calculation of compliance over an arterial pressure range, and the phase angle at one reference pressure. Results were directly compared with previously published data for a range of arteries *in vivo*. Three different wall thicknesses (0.5, 0.7, 0.9 mm) and three concentrations of $NaHCO_3$ (35, 45, 55%) were evaluated in an effort to elucidate the influence of wall thickness and porosity on the functional mechanical properties of the grafts. Further, handling properties such as suture retention and kink resistance were characterised using methods outlined in the British Standard ISO 7198:1998. A method for externally reinforcing vascular grafts as a measure against kinking was also developed and assessed for compliance.

5.1 Materials and Methods

Graft fabrication

Grafts were produced as outlined in chapter 4. POSS-PCU grafts with no porogen were produced, with an internal diameter of 5 mm, at three different wall thicknesses: 0.5, 0.7 and 0.9 mm. Additionally, grafts with 35, 45, 55% $NaHCO_3$ were also produced with wall thicknesses of 0.7 mm. This allowed the comparison of both the wall thickness and the effect of porosity on the mechanical behaviour of grafts. All grafts were manufactured at room temperature using the extrusion phase separation method outlined extensively in the previous chapter.

Tensiometry

Grafts were cut open longitudinally and a dogbone shaped specimen, 20 × 4 mm, prepared using a sharp cutter and mechanical press ensuring a clean cut with no flaws or stress aggregation. However, due to the random nature of pore size and porosity, variability between samples is to be expected. Specimens were cut in both the longitudinal and circumferential direction to test for isotropy. Stress-strain profiles were characterised using a uniaxial load testing machine (Instron 5565, UK). The maximum tensile strength, initial Youngs modulus (between strains of 0 and 25%) and elongation at break were obtained (n=6).

Suture retention

Test pieces, 30 mm in length, were prepared from grafts using a scalpel, and a suture (6.0 Prolene) was passed through the graft wall 2mm from the end. The graft was placed in the top grip of the uniaxial load machine (Instron 5565) and the free end of the suture was placed in the bottom grip. The specimen was pulled at a speed of 50 mmmin^{-1} until either the suture ripped or the graft failed. The force required to pull the suture through the prosthesis or cause the wall of the prosthesis to fail was recorded (n=6).

External reinforcement

An external reinforcement of PCU fibres was incorporated onto the grafts using textile braiding techniques. A 1/1 maypole braiding method (Cobra 250, Cheshire, UK) was used to braid POSS-PCU grafts (0.7 mm wall thickness, 0% $NaHCO_3$, n=3). Three different gear ratios were used (0.4, 0.6, 1) to produce three different braiding angles (45, 50, and 60°) (fig 5.3).

Thereafter, an isocyanate prepolymer bioadhesive was sprayed onto the surface of the grafts using an ultrasonic atomisation spray machine (Sono-Tek, USA) in an effort to attach the braiding to the surface of the graft. Grafts were placed on a mandrel rotating at 115 rpm and driven laterally at a speed of 25 mms^{-1} with the prepolymer being sprayed at a rate of 0.3 mLmin^{-1} and atomised at a power setting of 1.20 W. Two layers of the bioadhesive were applied after which the grafts were placed in distilled H_2O.

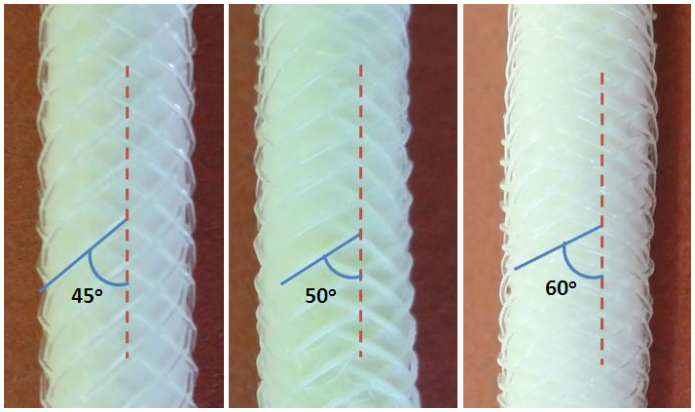

Figure 5.3: Digital image of POSS-PCU vascular grafts following external reinforcement with PCU fibres. Three different braiding angles were evaluated ranging from 45-60°.

Kink resistance

The purpose of this test is to determine the length of curvature required for the grafts to kink. The ends of the vascular grafts, 100 mm in length, are slowly brought into contact with each other until the graft buckles and begins to kink. The distance that separates the two ends of the graft is then recorded as the distance required for kink formation. The smaller the separation distance, the more resistant the graft is to kinking. Tests are conducted at ambient pressure.

Pressure-diameter analysis

A physiological flow circuit was constructed to accurately recreate the haemodynamic environment of pulsatile arterial blood flow *in vitro* (fig 5.4). 10 cm lengths of graft (n=8) were prepared and individually connected with a 10% longitudinal stretch to a phantom pulse generator (Harvard Apparatus Model 1421) set at a frequency of 1 Hz and a pulse pressure of 60 mmHg. Clinically expired human blood was collected from the Royal Free blood bank and held in a reservoir at 37°C, with the mean pressure of the circuit determined by the height of the reservoir, and pumped using the previously mentioned pulse generator. A size 2F Millar Mikro-tip catheter transducer (model SPC-320, Millar Instruments Inc, Houston, USA) was placed within the graft and connected to pressure transducer control unit. A 50 mm 7.5 MHz linear array probe connected to a Doppler ultrasound machine (Picus, Pye Medical) was clamped perpendicular to each graft along its longitudinal axis. Wall tracking software (Pie Medical Wall Track System II) was used to monitor the distension of the inner wall for 20 mmHg increments of mean pressures in the physiological range (30-100 mmHg)

by sampling the radiofrequency signal generated by the vessel wall over a 4 second period (fig 5.4c). This set-up allowed the simultaneous recording of the real time wall distension and pressure (fig 5.4d).

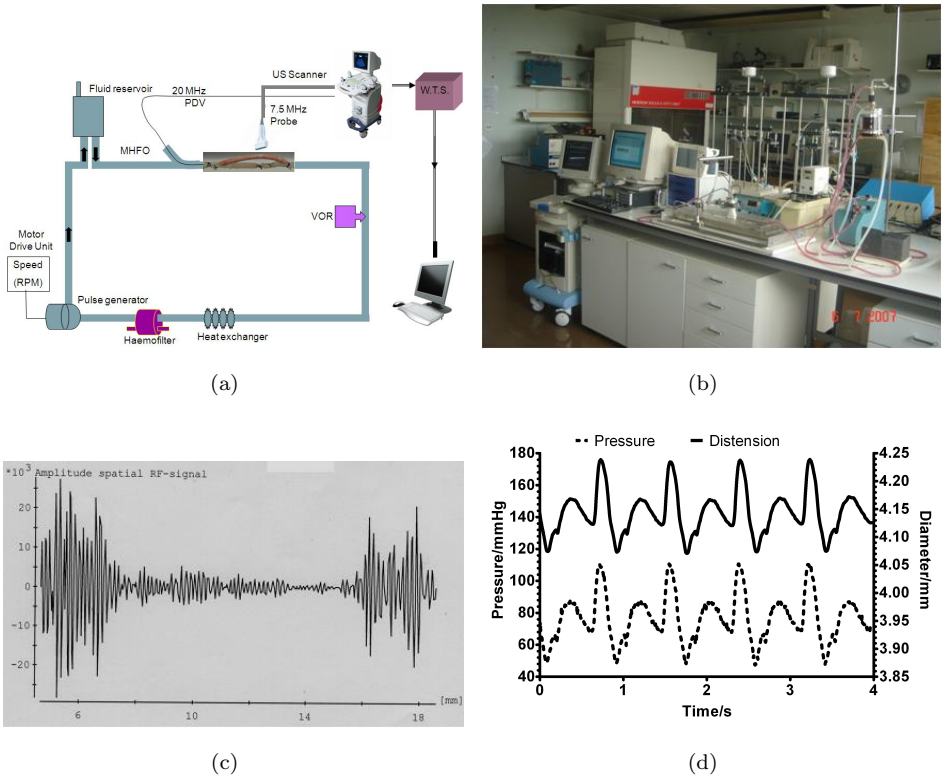

Figure 5.4: Diagramatic representation (a) and digital image (b) of the physiological flow circuit constructed to characterise the dynamic functional behaviour of small calibre vascular grafts. An example of radiofrequency signal generated by vessel wall (c) and the corresponding pressure and diameter waveform (d) generated over a period of 4 seconds.

5.2 Results

Tensiometry

The inherent tensile properties of the grafts wall were evaluated using a uniaxial tensiometer. The effect of porosity, through varying the concentration of porogen, wall thickness and the anistropy were all assessed, the results of which are presented in table 5.1.

Figure 5.5 displays the stress strain curve of grafts produced with varying concentration of $NaHCO_3$. There is a significant reduction ($p < 0.001$) in the tensile strength and elongation at break as the concentration of $NaHCO_3$ is increased. However, the stiffness of the graft wall was not so sensitive, with no significant differences detected in the Youngs Moduli between samples produced with 45 and 55% $NaHCO_3$. However, both had significantly reduced Youngs moduli than the graft produced with 35% $NaHCO_3$.

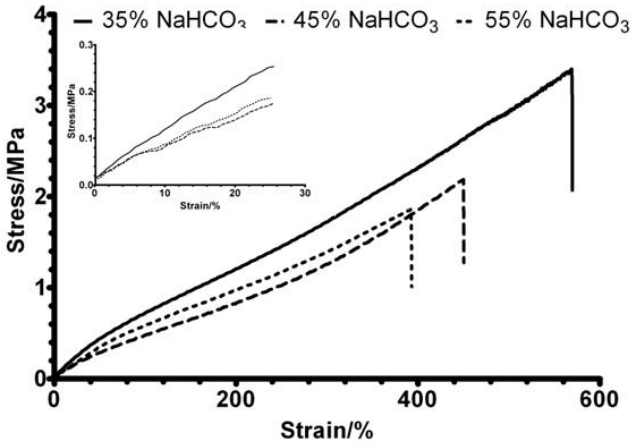

Figure 5.5: Effect of porogen concentration on tensile properties of POSS-PCU grafts. Inset is the region over which the Youngs modulus was calculated, 0-25% strain.

No significant differences were detected in the tensile properties (tensile strength, elongation at break or Youngs Moduli) of grafts with wall thicknesses of 0.5 mm, 0.7 mm or 0.9mm (fig 5.6). Further the tensile properties were found to be isotropic with no significant difference in tensile properties detected in the longitudinal and circumferential direction (fig 5.7).

Suture retention

Suture retention is a critical factor in the design of a vascular graft as it directly relates to the success of the implant. With the continued addition of $NaHCO_3$, the suture retention strength systematically decreases from 4.46 ± 0.32 N for 35% $NaHCO_3$ to 2.33 ± 0.23 N for grafts produced with 55% $NaHCO_3$ (fig 5.8a). Reductions in wall thickness had a similar effect; grafts with walls 0.9 mm thick exhibited significantly higher ($p < 0.01$) suture retention strengths than those with walls 0.7 or 0.5 mm

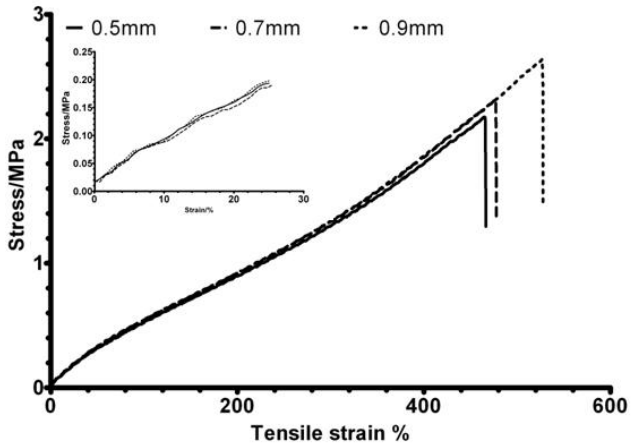

Figure 5.6: Effect of graft wall thickness on tensile properties. Inset is the region over which the Youngs modulus was calculated, 0-25% strain.

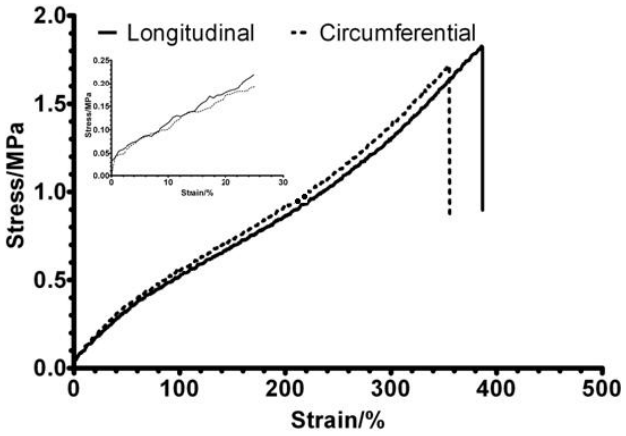

Figure 5.7: Tensile tests in the longitudinal and circumferential direction of POSS-PCU grafts. Inset is the region over which the Youngs modulus was calculated, 0-25% strain.

thick (fig 5.8b).

Kink resistance

The distance at which a kink forms in 100 mm long grafts, at ambient pressure's, was examined. Figure 5.9 displays the relationship between $NaHCO_3$ concentration, wall thickness and graft kinking. Additionally, the effect of adding an external reinforcement, in the form of PCU braiding, is examined for its efficacy in preventing

Sample	Tensile strength/MPa	Elongation/%	Youngs Modulus/MPa
cast	59.67 ± 5.48	856 ± 53	17.03 ± 0.30
35% $NaHCO_3$	3.21 ± 0.20	547 ± 18	0.99 ± 0.05
45% $NaHCO_3$	2.38 ± 0.20	450 ± 27	0.69 ± 0.09
55% $NaHCO_3$	1.66 ± 0.25	416 ± 20	0.66 ± 0.04
0.5mm	2.27 ± 0.23	459 ± 22	0.70 ± 0.08
0.7mm	2.32 ± 0.32	473 ± 19	0.67 ± 0.07
0.9mm	2.67 ± 0.29	528 ± 17	0.70 ± 0.08
Longitudinal	1.92 ± 0.35	397 ± 18	0.77 ± 0.08
Circumferential	1.84 ± 0.32	382 ± 21	0.79 ± 0.08

Table 5.1: A summary of the inherent tensile properties of phase separated POSS-PCU. The tensile strength, elongation at break and Youngs Modulus are presented for samples comparing porosity, wall thickness and anistropy.

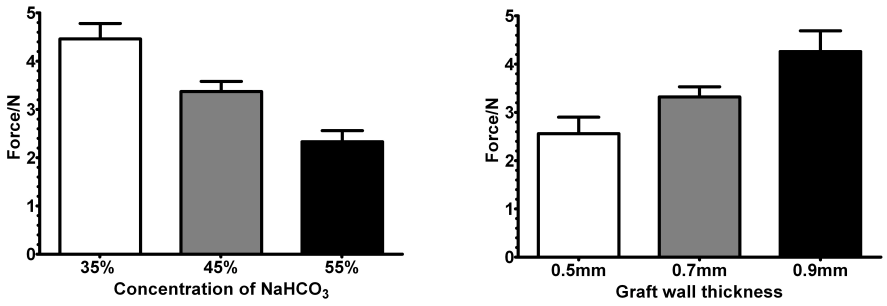

(a) (b)

Figure 5.8: The effect of $NaHCO_3$ concentration (a) and wall thickness (b) on suture retension strength

kink formation. Increasing wall thickness appears to significantly ($p < 0.01$) improve the kink resistance of the vascular grafts with the distance separating the two ends of the graft smallest for the 0.9 mm thick graft. Neither the addition of $NaHCO_3$, nor the concentration, had any significant impact on kink resistance. By applying an external reinforcement, there is a significant initial improvement in kink resistance of

the grafts irrespective of braiding angle. However, at extreme curvatures (very short distances between graft ends) the braiding came apart from the graft which resulted in the graft kinking.

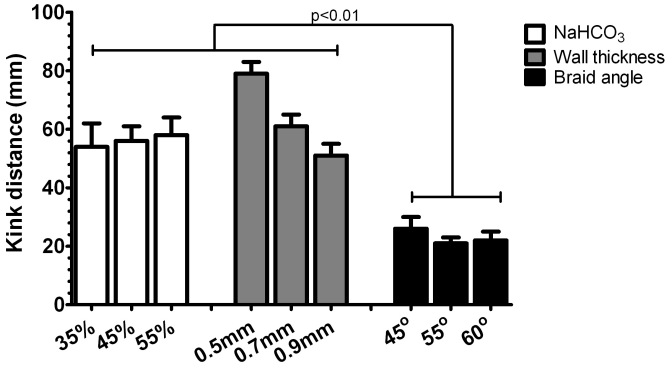

Figure 5.9: Separation distance resulting in kink formation. The shorter the distance separating the two ends of the graft, the more resistant the graft is to kinking. Wall thickness appears to be an important determinant in kink formation as an increase in wall thickness results in significantly improved kink resistance. The addition of $NaHCO_3$ appears to have a negligible effect on kinking whilst the addition of an external reinforcement caused a significant improvement irrespective of braiding angle. n=3, $p<0.01$.

Pressure-diameter analysis

The pressure-diameter plots of POSS-PCU vascular grafts were plotted as shown in fig 5.10, and the phase angle between pressure and distension was calculated from equation 5.3. No significant difference was recorded between the phase angle of thick and thin grafts demonstrating that the viscous component of the graft wall was independant of wall thickness (fig 5.11a). Similarly, $NaHCO_3$ concentration had a negligible effect on the phase angle which remained a constant $16 \pm 1°$ (fig 5.11b).

Compliance, on the other hand, was heavily dependant on both the wall thickness and concentration of $NaHCO_3$. The thin walled graft (0.5 mm) was significantly ($p < 0.001$) more compliant than the thick walled grafts (0.7 and 0.9 mm, fig 5.12). There was no significant difference between the compliance of grafts at 0.7 and 0.9 mm. Further, whereas the compliance of thick grafts was independent of the mean arterial pressure at a near constant value of 5.9 ± 0.4 $\%mmHg^{-1} \times 10^{-2}$; the thin walled graft displayed behaviour that was heavily pressure dependant. At a pressure of approximately 30 mmHg the compliance of the thin walled graft was 6.6 ± 0.3

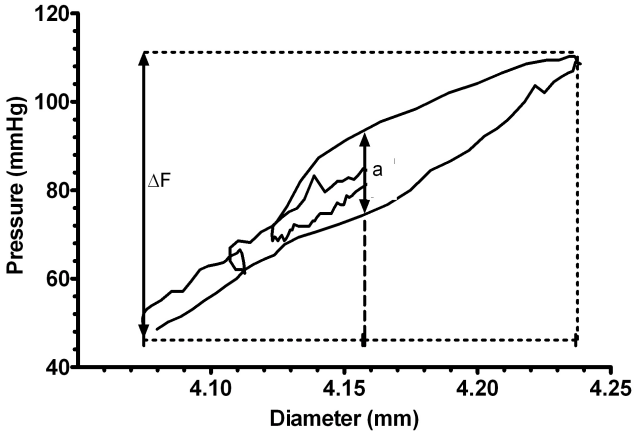

Figure 5.10: Representative pressure diameter plot for POSS-PCU vascular graft displaying a hysteresis due to the viscoelastic nature of the graft.

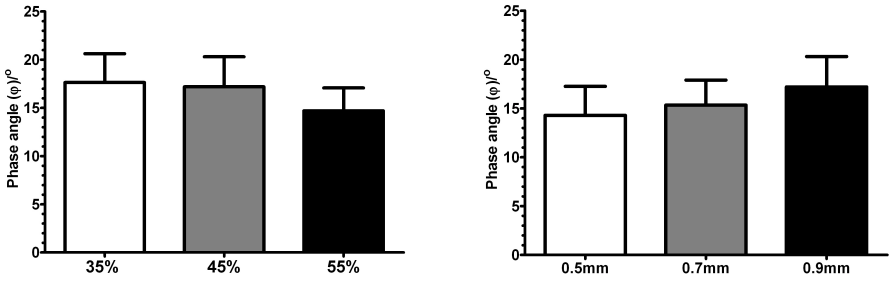

(a) (b)

Figure 5.11: Phase angle between the pressure and distension waveforms of vascular grafts as a function of (a) wall thickness and (b) $NaHCO_3$ concentration.

$\%mmHg^{-1} \times 10^{-2}$ which increased to 12.5 ± 0.6 $\%mmHg^{-1} \times 10^{-2}$ at a pressure of 100 mmHg.

The grafts produced with $NaHCO_3$ were fabricated with walls 0.7 mm thick. The addition of 35% of $NaHCO_3$ does not appear to have significantly altered the compliance averaged over the pressure range compared to grafts with no $NaHCO_3$ (6.1 ± 0.9 v 5.9 ± 0.4 $\%mmHg^{-1} \times 10^{-2}$); however, it is now dependant on the pressure with significant differences between the compliance at 30 mmHg and 100 mmHg (fig 5.13). The continued addition of $NaHCO_3$ not only increased the absolute compliance values but also increased the pressure dependence with the slope of the best fit line

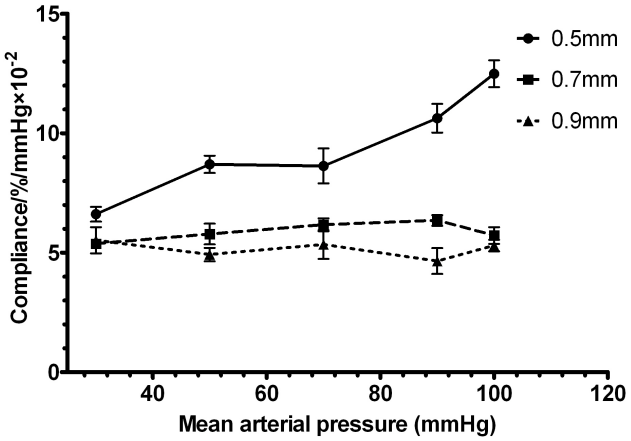

Figure 5.12: Effect of wall thickness on POSS-PCU vascular graft compliance over the mean arterial pressure range. The compliance of thin walled grafts appears to be higher and pressure dependant compared to the two thicker grafts which do not differ significantly (n=8, p<0.001).

of the graft produced with 55% $NaHCO_3$ significantly higher than that of the graft produced with 45% (0.04 v 0.06).

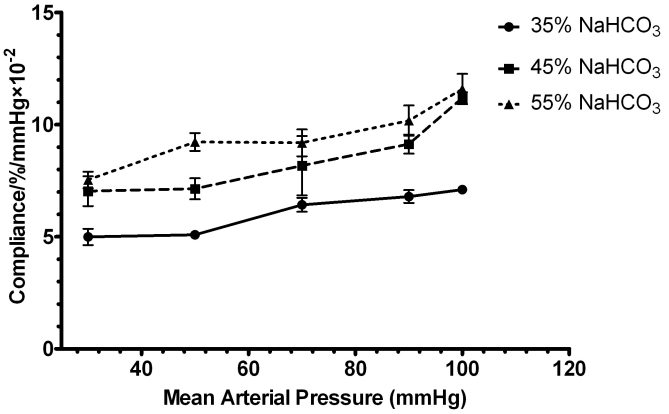

Figure 5.13: Effect of $NaHCO_3$ concentration on compliance over the mean arterial pressure range of POSS-PCU vascular grafts with 0.7 mm wall thickness. An increase in $NaHCO_3$ concentration results in an increase in compliance with the compliance values further dependant on the pressure (n=8, p<0.001.

Through the addition of an external reinforcement for anti-kinking purposes, the

compliance of the grafts suffered a significant decrease. A braiding angle of 45° produced grafts with the tightest braid resulting in the most severe loss of compliance compared to equivalent graft without braiding (0.8 ± 0.3 v 5.9 ± 0.4 %mmHg^{-1} $\times$ 10^{-2}, fig 5.14). The subsequent loosening of the braid through a reduction in the braiding angle at higher gear ratios, resulted in a minor increase in compliance to an average value of 1.4 ± 0.2 %mmHg^{-1} $\times$ 10^{-2}. The braiding at 60° resulted in the loosest reinforcement, and whilst the compliance of the graft was severely compromised at low mean arterial pressures (1.1 ± 0.3 %mmHg^{-1} $\times$ 10^{-2} at 30 mmHg), it was found to significantly increase ($p < 0.001$) as the pressure was also incresed (3.2 ± 0.2 %mmHg^{-1} $\times$ 10^{-2} at 100 mmHg).

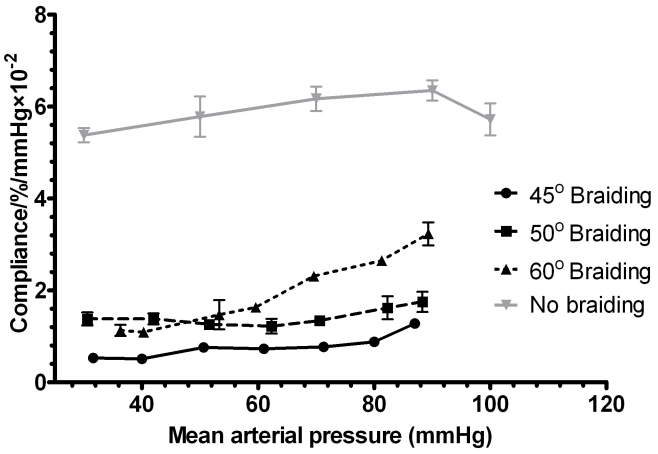

Figure 5.14: Effect of external reinforcement on vascular graft compliance (n=3).

5.3 Discussion

Blood vessels are constantly under continuous and intermittent mechanical stress which includes pulsatile shearing forces, cyclic stretching, longitudinal tension and compression. Any successful vascular substitute must be able to withstand the harsh mechanical environment that it is exposed to in the vasculature. In contrast to many other tissue engineering applications, such as cartilage, liver etc, the function of the scaffold is not merely to support and direct cell proliferation but the scaffold must also successfully fulfil its primary role as a conduit for the transportation of blood round the body. A great number of tissue engineering paradigms rely on mechanically weak biodegradable scaffolds, which may successfully support cellular activity, but do not have the required radial strength to be used in the arterial circulation.

This thesis has examined the use of POSS-PCU for the fabrication of vascular substitutes as it has excellent mechanical properties which include UTS in excess of 60 MPa. A phase separation method was developed in chapter 4 to produce cylindrical conduits with the required UTS and a degree of radial elasticity to be used in the arterial circulation. The use of $NaHCO_3$ as a porogen was investigated to impart a greater degree of porosity to the grafts. In this chapter the functional mechanical behaviour of the grafts is examined through tensiometry to evaluate graft wall behaviour, suture retention, kink resistance and viscoelasticity. The influence of wall thickness and pore size was elucidated. Three different wall thicknesses (0.5, 0.7 and 0.9 mm) and three different concentrations of $NaHCO_3$ (35, 45, 55%) were examined.

Whilst porosity is a necessary prerequisite for the successful healing and tissue ingrowth of vascular grafts, it diminishes mechanical properties thereby setting an upper limit for pore size and porosity. This was seen with the POSS-PCU grafts whereby UTS decreased as the percentage of $NaHCO_3$ increased (fig 5.5). It was interesting to note, however, that the addition of 35% $NaHCO_3$ improved the UTS considerably compared to the vascular graft produced with no $NaHCO_3$. This is most likely due to the more homogenous wall structure and smaller pore size exhibited by the graft produced via porogen leeching. The stiffness of the graft wall suffered a slight reduction with the addition of 45% or more $NaHCO_3$. Whilst a degree of elasticity in the graft wall is vital, there is a considerable risk of excessive dilation and aneurysmal formation if the graft wall is not stiff enough. Wall thickness appears to have a negligible effect on the mechanical properties of the graft wall. This should come as no surprise as stress is calculated as force per unit area, therefore, measurements taken are suitably adjusted for dimensional changes. Similarly, the graft walls were found to be isotropic with no significant change in the mechanical properties in the circumferential or longitudinal direction, therefore there is no directional dependence on the strength of POSS-PCU. Irrespective of the porosity or wall thickness of graft, the UTS of the grafts is well in excess of native human arteries [203, 204].

Similarly, the suture retention values were well in excess of the generally accepted value of 2N for all the grafts tested. As expected, the increase in $NaHCO_3$ concentration results in a decrease in the amount of force required for the graft to fail. This is likely to be a direct consequence of the diminishing mechanical properties of the graft wall as porosity is increased. In contrast to the tensiometry testing, suture retention was dependant on graft wall thickness. The sequential increase in graft wall thickness manifested itself in significantly improved suture retention forces. As suture reten-

tion measures the load at failure (N), as opposed to stress (Nmm^{-2}), suture retention is heavily dependent on graft wall thickness – with thicker grafts more resistant to failure.

Thicker grafts also appeared to be more kink-resistant. Kink formation in vascular grafts is a major problem particularly for below-knee bypasses. Upon knee flexion resulting in bending of the graft, the outer convex wall is under tension resulting in lengthening of the graft wall which, at its maximum, can cause the graft cross section to take on an oval form. Meanwhile the inner concave wall is compressed and shortened resulting in deformations and creating folds which then protrude into the lumen. Whilst minor graft kinks can result in acute ischemia, lumen encroachment of 50% or more results in graft occlusion and requires immediate treatment [211]. Graft wall thickness appears to be a critical parameter in determining the propensity of grafts to kink. Whilst it is clear that thin grafts are prone to kinking, the addition of $NaHCO_3$ does not have any impact on kink formation with no significant changes detected between the different concentrations of $NaHCO_3$ or the equivalent grafts produced with and without $NaHCO_3$.

An external radial support is one method by which kink prevention can be achieved. By utilising commercially available braiding techniques, an external support consisting of PCU fibres was applied to the POSS-PCU grafts. Three different braiding angles were evaluated with the highest angle, 60°, producing the tightest braid whilst a braiding angle of 45° produced a loose braiding. Thereafter, an isocyanate based pre-polymer was sprayed onto the surface of the grafts in an effort to adhere the external reinforcement to the surface of the vascular grafts. The pendant isocyanate groups of the pre-polymer are activated by residual moisture, resulting in the formation of reactive amines. After which the amines react with remaining isocyanate groups resulting in the curing of the pre-polymer and fixation of the braid to the graft. Whilst the external reinforcement improved the kink resistance of the grafts significantly, the braiding appeared to detach itself from the body of the graft at extreme curvatures. This is likely due to the extreme localised stress placed on both walls of the graft, but in particular the concave wall. The driving force behind kink formation was greater than the adhesive force of the isocyanate pre-polymer resulting in the localised detachment of the braiding from the graft, which then led to kink formation. However, the principle behind the external reinforcement appears to be sound with no kink being observed whilst the braiding remains attached to the graft.

The role of the artery is more than just to transport blood from one part of the circu-

lation to another. The complex viscoelastic nature of the vessel wall is responsible for the energy efficient transmission of pulsatile blood flow whilst simultaneously damping excessive pressure fluctuations [207]. Additionally, viscoelasticity has also been shown to reduce the wall stress and strain during a sudden increase in mechanical loading, such as in acute hypertension [212]. The introduction of a stiff prosthetic graft introduces a degree of impedance into the circulation diminishing flow pulsatility and perfusion efficiency, and in small calibre, low flow, situations may lead to flow stagnation and graft thrombosis.

The viscous component of the vessel wall, which results in a force-deformation hysteresis loop, is thought to be important in filtering out instantaneous changes in loading which may lead to mechanical failure. Previously, it has been demonstrated that the phase angle between stress and strain is approximately $12.6 \pm 4.4^{\circ}$ for an iliac artery [213]. Whilst POSS-PCU vascular grafts exhibited generally higher phase angle's (fig 5.11), there is no significant difference between the grafts or iliac artery. It is worth noting, however, that the standard errors in the measurements are approaching 30% in some cases, therefore, any meaningful comparison is negated by the large errors in data collection.

In the native vessel (fig 1.1), the medial layer is primarily responsible for maintaining vasomotor tone in response to pressure. At low pressures elastin is the primary load bearer, responsible for imparting a degree of elasticity to the vessel, allowing it to stretch during systole and resuming its normal shape once load is removed in diastole. However with increasing pressure, the stiffer collagen becomes the dominant load bearer resulting in a stiffer artery and imparting a degree of non-linearity to the vessel wall. The distension and constriction in response to pressure is termed compliance. A mismatch in compliance has been implicated in the aetiology of IH [53]. A stiff graft causes pulsatile stretching at the site of anastomosis damaging EC and stimulating SMC proliferation [214]. Variations in cyclic stretching forces can alter the SMC phenotype producing SMC with an increased proliferation rate which produce four to five times the amount of ECM components as regular SMC, resulting in the increased proliferation and deposition of ECM components in the intima [215]. There is also evidence to suggest that a compliance mismatch can indirectly lead to IH, and even contribute to thrombosis, through impeding the flow of blood causing stagnation and resulting in an increase in residence times of chemotactic factors and platelets [216, 217]. Furthermore, flow patterns are directly affected by the compliance of the graft with inelastic grafts leading to flow reversal, vortex formation and wall shear stress fluctuations which have been implicated in IH progression [218, 219].

POSS-PCU vascular grafts were found to be significantly more compliant than the industry standard PET or PTFE grafts currently available [206]. Both wall thickness and porosity had significant bearing on the compliance properties of the grafts. Whereas grafts with walls 0.7 and 0.9 mm thick had compliance profiles independent of pressure, grafts with walls 0.5 mm thick were heavily pressure dependant with the compliance value more than doubling as the mean arterial pressure increased from 30 to 100 mmHg. Excessively compliant grafts would raise serious concerns over the long-term mechanical robustness as they are likely to be prone to aneurysmal formation and dilation. The addition of 35% of $NaHCO_3$ did not significantly alter the average compliance over the mean pressure range, compared to grafts produced with no $NaHCO_3$ and equivalent wall thicknesses. However, the compliance profile was no longer independent of pressure with significant differences being observed between compliance at 30 mmHg and 100 mmHg. The pressure dependence of compliance increased with the continued addition of $NaHCO_3$. The compliance pressure dependence as a result of thinner graft walls or increased graft porosity is likely due to a reduction in the mass of polymer that pressure is exerted against. Thinner graft walls are unable to resist strain, particularly at high mean arterial pressures. Whereas an increase in $NaHCO_3$ concentration results in a reduction in apparent bulk density of graft which transpires into a less stiff graft wall characterised by a significant reduction in Youngs modulus between grafts produced with 35% $NaHCO_3$ and 45+%. The reduction in stiffness manifests itself in the form of a more compliant graft at high pressures.

By introducing an external reinforcement, the possibility of compromising the radial expansion of grafts is always likely. Whilst the external reinforcement was successful in administrating an additional degree of kink resistance to the grafts, they dramatically reduced the compliance properties of the graft, irrespective of braiding angle. The relatively loose braiding, produced with a braiding angle of 60°, can be seen to be expanding at increased pressures; however, the braiding produced at angles of 45 and 50°, which are tighter in nature, compromises the compliance properties of the graft throughout the pressure range. The PCU fibres are considerably stiffer than the phase separated graft walls therefore it is no surprise to see them impacting on the compliance properties of the grafts.

5.4 Conclusions

The biomechanical properties of any vascular substitute play a decisive role in determining it's patency. In this chapter, the functional mechanical properties of POSS-PCU grafts were evaluated. The role of wall thickness and porosity was evaluated and the feasibility of an external reinforcement explored. POSS-PCU grafts were found to be viscoelastic in nature with tensile strengths and suture retention forces that are able to withstand the harsh conditions found in the arterial circulation. A physiological flow circuit was developed to assess the dynamical mechanical properties whereupon grafts were found to be compliant and able to propagate the flow waveform.

6

Surface Characterisation of POSS-PCU Vascular Grafts

For all implanted biomaterials and devices, the central characteristics are biofunctionality and biocompatibility. Whereas the previous chapter discussed at length the mechanical behaviour of POSS-PCU grafts, the aim of this chapter is to investigate the parameters which influence biocompatibility. Whilst there are differing opinions on the precise definition of biocompatibility, it usually refers to the safety, and lack of adverse interactions of the implant, over its intended lifetime in the body [220]. For blood contacting devices, such as stents, heart valves and vascular grafts, blood compatibility is effectively the tolerance of blood to the implant. As the surface of the biomaterial is the first component of the device that comes into contact with blood, it is the surface properties, such as wettability, flexibility, morphology and the surface chemical composition, which determine the degree of biocompatibility [221].

The chemical composition of a material often dictates many of its properties; however, surface chemistry tends to be rather complex with the exact nature of the chemical constituent interacting with blood difficult to ascertain. It is widely recognised that surface polarity and energy influence cell-substrate interactions [222]. Polar, hydrophilic surfaces, with a greater degree of surface wetting, are thought to improve cellular adhesion. The wettability of a liquid refers to the ease with which a fluid spreads across a solid surface and can be measured quantitatively by determining the contact angle of a droplet of liquid, usually water, in thermal equilibrium on a horizontal surface. Contact angle, θ, is defined as the angle formed by the liquid at the three phase boundary where the liquid, gas and solid intersect (fig 6.1).

Whilst wettability is an example of surface chemistry and the role of intermolecular

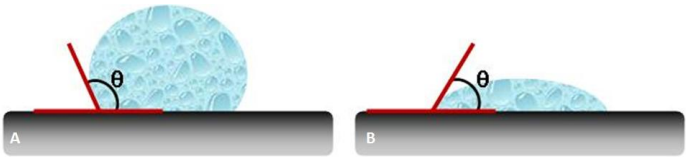

Figure 6.1: Diagrammatic representation of liquid wetting on horizontal surfaces. A high contact angle, θ>90°, signifies poor wetting ability of the surface indicative of a hydrophobic surface (A). Low values of contact angle, θ<90°, indicates a hydrophilic surface on which the liquid spreads well (B).

forces in influencing bioadhesion; physical determinant such as surface topography and surface morphology have been of great interest recently, as factors which influence cellular behaviour. As discussed in section 2.3, cells in their native microenvironment interact with a complex milieu of topographic cues which range from the nano- to the micro-scale [223]. Whereas the underlying molecular mechanisms controlling these interactions have yet to be elucidated, their role in influencing biocompatibility is beyond doubt. Factors such as porosity and surface roughness have proven to be influential parameters to consider in the design of biomaterials [224]. For example, it has been consistently demonstrated that a number of different cell types tend to align and elongate over grooved substrates [225]. The dimensions of the features are critical with cells responding to grooves with depth as little as 35 nm with the effect diminishing when the feature size becomes negligible (<35 nm). Neonatal rat ventricular myocytes cultured on grooves 50 nm in depth led to highly anisotropic cell arrays guided by the underlying nanoridges [226]. Filopodial extension in the groove results in adhesion proteins and actin filaments becoming aligned parallel to the groove direction; with the organisation of actin filaments or microtubules being identified as the first step in contact guided cell alignment. In a similar manner; pits, pores and protrusions have been shown to influence cell behaviour [227].

Topograpahy and surface chemistry are well established factors which influence cell behaviour and have been systematically investigated. More recently, substrate mechanics have emerged as another important factor worth considering in the design of biomaterials [173]. The underlying substrate stiffness is known to influence the cell contractile forces and related cellular functions, such as motility, cytoskeletal organization, and differentiation regardless of whether the substrate is autologous tissue or a synthetic substrate [173, 228, 229]. For example, substrate mechanics have been found to play an important role in determining cell phenotype during the process of wound healing [230]. Fibroblasts are known to differentiate into myofibroblasts in

response to injury, and are responsible for replacing and repairing damaged ECM. As ECM is deposited, the elastic modulus of the cell microenvironment increases, with the myofibroblast deactivating and undergoing apoptosis when the desired modulus is achieved [230]. If de-activation is misregulated and the myofibroblast phenotype persists, ECM secretion would continue and the increasing modulus would affect fibrosis [231].

To be able to investigate the biocompatibility and cellular behaviour of the POSS-PCU vascular grafts, a careful assessment of the vascular graft surface is required. Whilst the surface properties of POSS-PCU have been investigated previously; the aim of this chapter is to evaluate the surface properties of the phase separated membranes from which the vascular grafts are fabricated from. The surface chemical, topographical and mechanical properties were characterised and any differences following phase separation was assessed. The influence of adding a porogen, $NaHCO_3$, on the interfacial properties was evaluated.

6.1 Materials and Methods

Sample preparation

A cast sheet of POSS-PCU which would serve as a control to compare the surface properties of the phase separated membranes was produced by casting a 18%(w/w) solution of POSS-PCU in DMAc onto a glass petri dishes and left in an oven at 60°C overnight. The solvent would evaporate resulting in a solid sheet of polymer for future experiments.

The phase separated membranes were produced in a similar manner to the vascular grafts in chapter 4; however, flat membranes were produced as opposed to cylindrical conduits for ease of analysis. POSS-PCU solution and POSS-PCU/$NaHCO_3$ suspension was cast on to a stainless steel sheet and placed in distilled water at room temperature. The polymer sheets were left immersed in distilled water for a period of 48 hours to ensure complete removal of solvent and $NaHCO_3$. The membranes were then removed from the steel support and air dried for a further 48 hrs before use in downstream experiments. The POSS-PCU/$NaHCO_3$ suspension was prepared as previously stated in chapter 4: 35, 45 and 55% of $NaHCO_3$ was used as per chapter 4. Analysis took place on the luminal surface which is expected to be in contact with blood.

SIMS

Secondary ion mass spectroscopy (SIMS) analysis was undertaken using a Millbrook MiniSIMS instrument (SAI Ltd) equipped with a 5kV gallium ion source in static SIMS mode. Positive and negative ion SIMS spectra were obtained from sample discs 16 mm in diameter. Fragments detected were ascribed chemical species and their relative intensities referenced against the common organic fragments m/z =41 ($C_3H_5^+$) and m/z = 13 (CH^-) in positive and negative spectra respectively. Images of principal ions were collected from areas of approximately 2mm × 2mm of the sample and over-laid as three colour maps.

ATR-FTIR

Samples were subjected to attenuated total reflectance Fourier transform infer-red (ATR-FTIR) spectroscopy (JASCO FT/IR 4200) to evaluate any alterations in the surface chemical functional groups. A total of 30 scans were taken for each sample between 600 and 4000 cm^{-1} (n=6).

Contact angle

Contact angle analysis was carried out using a goniometer (DSA100E, Kruss, Hamburg, Germany) equipped with a high speed framing video recording system with a CCD camera. A 3 μL Milli-Q water drop was placed on the surface of each sample, in air, at room temperature. Manufacturer provided drop shape analysis software was used to determine the air-water contact angles over a period of 10 seconds. A minimum of 10 droplets were examined for each sample (n=6).

SEM

Graft samples (n=3) were washed with several changes of phosphate buffered saline (Oxoid) and post fixed using 1% osmium tetroxide/1.5% potassium ferricyanide for 1 hour. The samples were then washed with distilled water and dehydrated through a degrading acetone series (30%, 50%, 70%, 90% and 100% HPLC grade) washing twice for 15 mins each. After dehydration the samples were transferred to tetramethylsilane for 10 mins and then allowed to air dry. Finally, the samples were attached to aluminium stubs with double sided sticky tabs (TAAB) and coated with gold using an SC500 (EMScope) sputter coater for electrical conductance. The stubs were examined and photographed using a Philips 501 scanning electron microscope. Representative images of the surface were captured at random.

For the purposes of surface porosity analysis, ImageJ software was used to measure the surface pore size distributions. 50 measurements were taken for each image and a total of four images were analysed for each sample.

AFM

Samples (n=6) were examined using a commercial atomic force microscope (XE 100, Park Systems) operating in contact mode. Discs (16mm in diameter) were positioned on a metallic disc and magnetically mounted in the AFM chamber. Surface images for quantitative analysis were obtained from 5×5 μm scans at a scan rate of 0.8Hz. Roughness was quantified by the deviation of the real surface from its ideal form. Two different indices were evaluated (equations 6.1, 6.2): the arithmetic average of absolute values (S_a) and the root mean squared (S_{RMS}).

$$S_a = \frac{1}{n}\sum_{i=1}^{n}|y_i| \tag{6.1}$$

$$S_{RMS} = \sqrt{\frac{1}{n}\sum_{i=1}^{n}|y_i^2|} \tag{6.2}$$

Where n is the number of points and y_i is the vertical distance from the mean plane to the i^{th} data point. The area surface roughness values of the scans were calculated using XEI analysis programme (Park Systems Corp).

Substrate stiffness

Nanoindentation tests were carried out using an AFM in force-displacement mode to measure the substrate stiffness (S) and reduced modulus (Er) of the samples (n=6). An aluminium-coated, silicon AFM tip of 150 kHz resonance frequency and 4.5 Nm^{-1} nominal spring constant(NSC12 tip-C; MikroMasch, Tallinn, Estonia) was driven into the sample at a rate (dz/dt) of 0.25 μms^{-1} and the sample deformation measured by piezo displacement. Multiple points, typically 12, on each sample were measured and the results averaged to ensure reliability and the load versus the specimen deformation for each indentation was plotted and used for data analysis. All measurements were conducted at room temperatures.

The S and Er were determined from force-displacement curves using the Oliver and Pharr model [232]. Stiffness was defined as the resistance of the material to indentation by an externally applied force and was determined from the slope of the unloading force-displacement curve ($S = dF/dh$) where F is force and h displacement.

The stiffness is then related to Er through equation 6.3

$$S = Er\beta 2\sqrt{A/\pi} \tag{6.3}$$

where A is the cross-sectional contact area, and β is a variable, which takes into account non-axisymmetry of the indenter and large strains. Being close to unity, β has only a small influence compared to the overall experimental inaccuracy, and is therefore neglected in the present work [232].

6.2 Results

SIMS

Table 6.1 provides a list of the mass to charge ratios and the ascribed chemical species with their relative intensities for each sample provided in figure 6.2. POSS fragments (28, 73) on the positive SIMS fragments are significantly more intense on the cast sample as opposed to the phase separated POSS-PCU. Further, the fragment at 35 on the negative SIMS is also significantly higher on the cast sample than the phase separated. Fragment with a mass to charge ratio of 35 is attributed to chlorine which is present as on the POSS further reinforcing the belief that the POSS moiety is present in greater numbers on the cast sample. Meanwhile, the negative SIMS fragments indicate that oxygen and nitrogen containing heteroatom fragments are far more prevalent in the phase separated sample indicative of far greater presence of the ethylenediamine, MDI and the polycarbonate soft segment on the surface of the membrane. Figure 6.3 provides a spatial distribution of Si and Cl fragments which are indicative of the POSS distribution on the surfaces of the cast and phase separated samples. The images corroborate the quantitative data by clearly displaying a greater abundance of Si and Cl ions on the cast sample.

ATR-FTIR

Attenuated total reflectance fourier transform infrared (ATR-FTIR) spectroscopy was used to analyse surface chemical composition of the different substrates with the results summarised in figure 6.4. The peak assignment was as follows: 1100 cm^{-1} (Si-O-Si), 1240 cm^{-1} (urethane C-O-C), 1400 cm^{-1} (C-C aromatic ring), 1540 cm^{-1} (N-H and C=N), 1589 cm^{-1} (C=C aromatic), 1632 cm^{-1} (NH2), 1736 cm^{-1} (C=O).

The process of phase separation appears to result in a significant reduction in the amplitude of the Si-O-Si peak at 1100 cm^{-1} belonging to POSS, but an increase in intensity of the carbonyl peak at 1736 cm^{-1} due to the carbonate and urethane

Positive SIMS fragments		Negative SIMS fragments	
m/z+	Fragment	m/z-	Fragment
27	C_2H_3	28	CO
28	Si	35	Cl
29	CHO	39	CHCN
39	C_3H_3	42	OCN
43	CONH	43	C_2H_3
45	CHO_2	54	$C_2H_2N_2$
55	C_3H_3O	59	$C_2H_3O_2$
73	$(CH_3)_3Si$	60	SiO_2/CO_3

Table 6.1: Positive and negative ion SIMS fragments and their corresponding mass to charge ratio (m/z).

moiety. However, the addition of $NaHCO_3$ did not result in any significant changes in the peak intensitie of the ATR-FTIR spectra.

Contact angle

The results of static contact angle tests are presented in figure 6.5. The contact angle of the cast sheets of POSS-PCU was found to be 105° and was consistent over the time period. Upon phase separation, the contact angle decreased to 94° and was found to decrease further over time, to 83° after 10 seconds. The addition of $NaHCO_3$ resulted in a significant increase in contact angle to 100°. Whilst the concentration of $NaHCO_3$ did not have any significant effect on the initial contact angle, it was a significant factor in determining the temporal behaviour of the water droplet on the different samples. Contact angle dropped to 80, 72 and 63° for samples produced with 35, 45 and 55% $NaHCO_3$ respectively.

SEM

SEM images of the surfaces of the different POSS-PCU samples are displayed in figure 6.6. The cast sheet of POSS-PCU appears to be a smooth surface with little else observable through SEM. Upon phase separation, the surface becomes very rough and textured, empirically visible from the SEM image; however, no surface pores are detected. A quantitative measure of the surface roughness is provided via AFM. The addition of $NaHCO_3$ resulted in openly visible surface pores on each of the three samples. A histogram of the pore sizes is provided adjacent to each SEM image. The sample produced with 35% $NaHCO_3$ resulted in a mean pore size of 5.3 $\pm$ 2.2 μm.

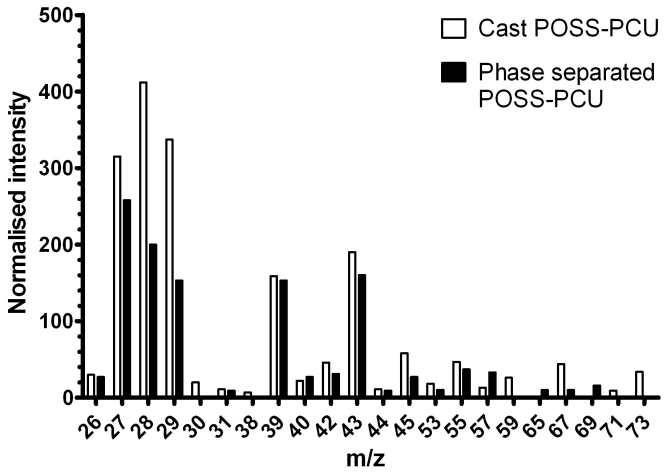

(a) Positive SIMS fragment peak intensities

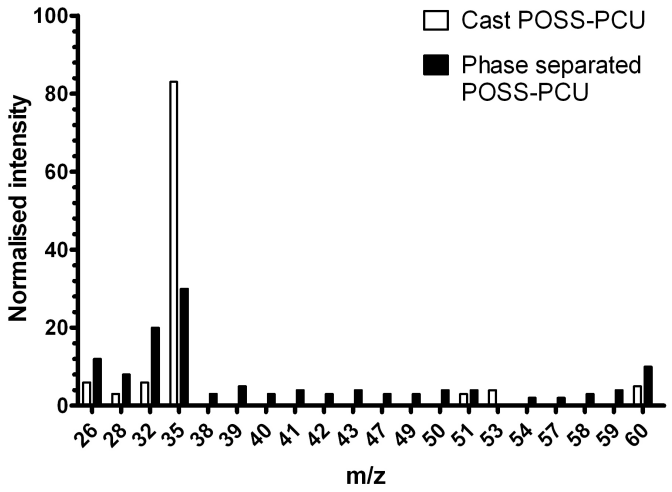

(b) Negative SIMS fragment peak intensities

Figure 6.2: Peak intensities of mass to charge fragments produced by SIMS analysis on cast and phase separated POSS-PCU

Increasing the concentration of $NaHCO_3$ to 45% led to an increase in the mean pore size to 6.1 $\pm$ 2.7 μm, which increased further with 55% $NaHCO_3$ to a mean pore sizes of 7.0 $\pm$ 2.9 μm.

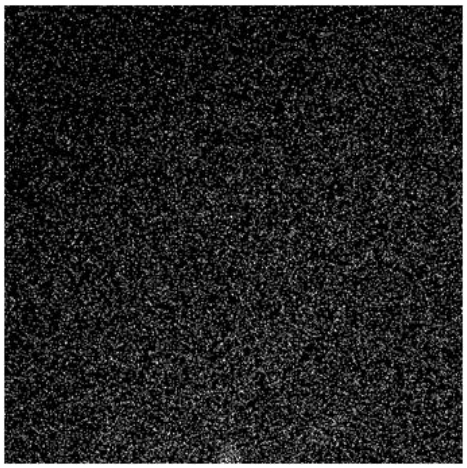

(a) Distribution of Si (m/z 28^+) on cast POSS-PCU

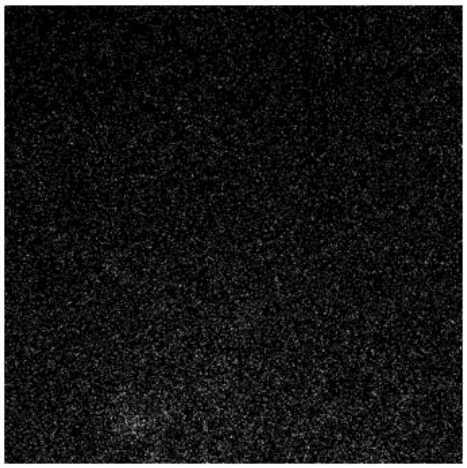

(b) Distribution of Si (m/z 28^+) on phase separated POSS-PCU

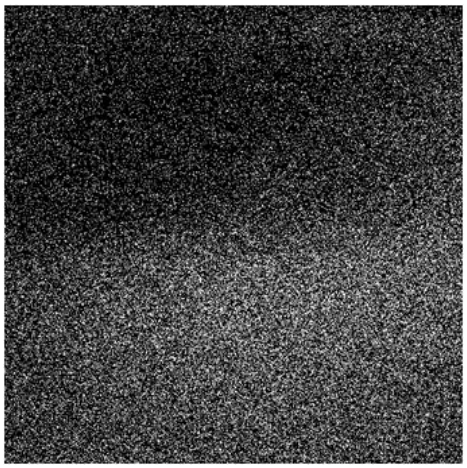

(c) Distribution of Cl (m/z 35^-) on cast POSS-PCU

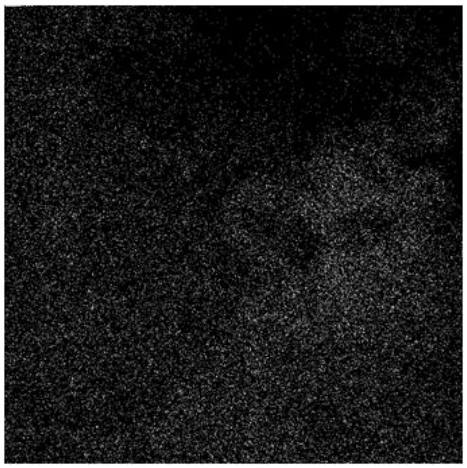

(d) Distribution of Cl (m/z 35^-) on phase separated POSS-PCU

Figure 6.3: SIMS images of cast and phase separated POSS-PCU samples obtained over a 2×2 area. The images display the distribution of Si and Cl ions (white) associated with the POSS moiety. POSS is clearly more abundant on the cast sample as opposed to the phase separated.

AFM

Both 2D and 3D images of the POSS-PCU surface are provided in figure 6.7 and the quantitative roughness measurements are presented in table 6.2. The cast sheet of POSS-PCU has a S_a of 75.3 ± 9.8 nm and a S_{RMS} roughness of 84.2 ± 8.6 nm which

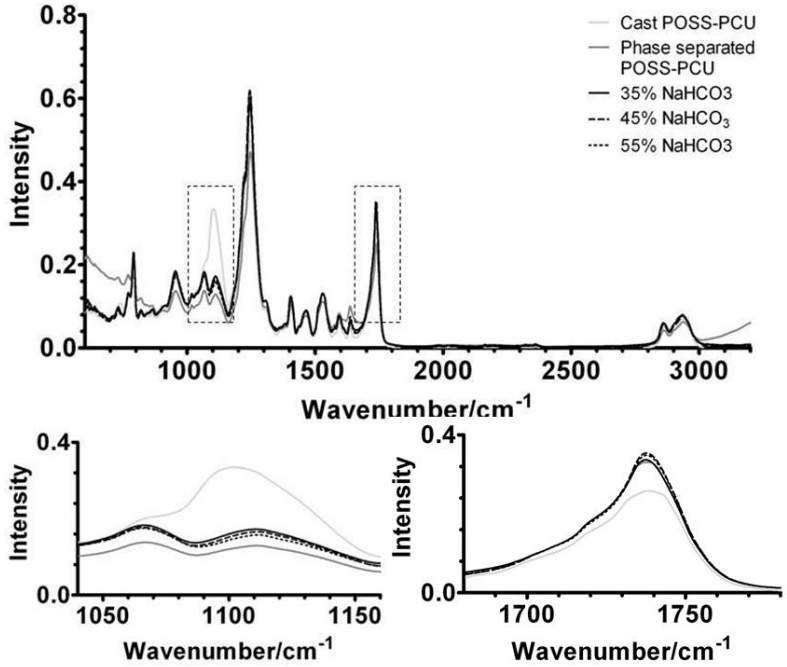

Figure 6.4: ATR-FTIR analysis of surface chemical functional groups on POSS-PCU samples. A magnified image of the changes in the POSS peak at 1100 cm^{-1} and carbonyl peak at 1736 cm^{-1} are also displayed.

increased significantly ($p < 0.01$) to 198.1 ± 7.9 and 215.2 ± 12.8 nm respectively for the phase separated sample. There was a further significant rise in roughness with the addition of 35% $NaHCO_3$ which increased S_a to 278.4 ± 14.2 and S_{RMS} to 294.6 ± 11.2 nm. The subsequent addition of $NaHCO_3$ resulted in further increases in both S_a (45%: 323.9 ± 21.3 nm, 55%: 376.4 ± 28.7 nm) and S_{RMS} (45%: 376.4 ± 28.7 nm, 55%: 404.2 ± 29.8 nm).

Sample	S_a (nm)	S_{RMS} (nm)
Cast POSS-PCU	75.3 ± 9.8	84.2 ± 8.6
Phase separated POSS-PCU	198.1 ± 7.9	215.2 ± 12.8
35% $NaHCO_3$	278.4 ± 14.2	294.6 ± 11.2
45% $NaHCO_3$	323.9 ± 21.3	361.6 ± 19.8
55% $NaHCO_3$	376.4 ± 28.7	404.2 ± 29.8

Table 6.2: The arithmetic average surface roughness (S_a) and root mean square surface roughness (S_{RMS}) of POSS-PCU samples examined with AFM (n=6, $p<0.05$).

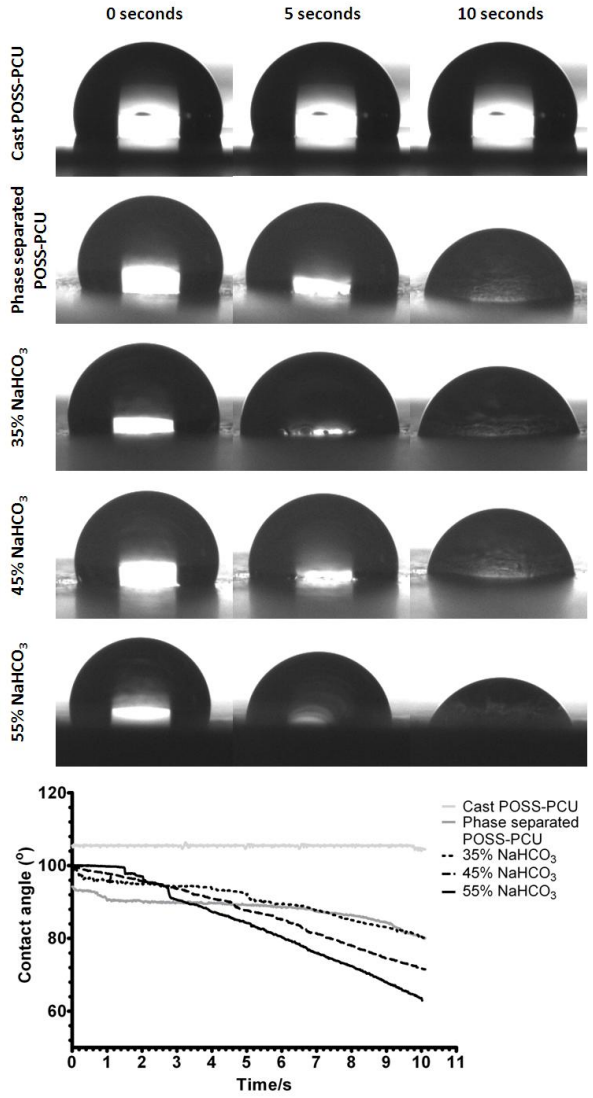

Figure 6.5: Digital images of the water droplet on the different polymer samples over 10 seconds. The static contact angles, determined via the sessile drop method, of the five POSS-PCU samples examined are summarised in the graph.

Substrate stiffness

Figure 6.8 displays a representative force-indentation curve and the reduced modulus of POSS-PCU samples. The cast sheet of POSS-PCU displayed a modulus value of 0.59 ± 0.09 GPa whereas the phase separated samples had stiffness values of 0.55 ± 0.06 GPa. There did not appear to be any significant differences between any of the samples.

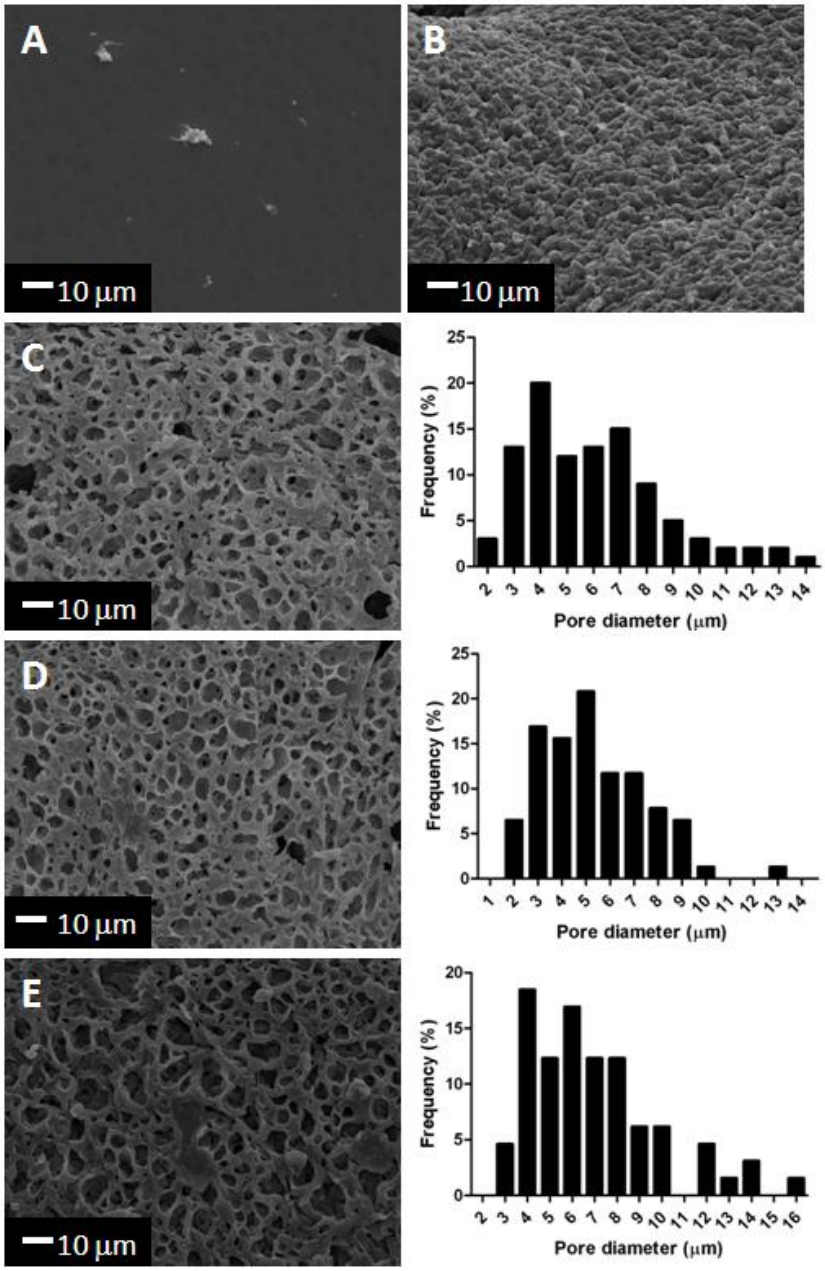

Figure 6.6: SEM images of sample surfaces displaying a smooth surface for the cast sheet of POSS-PCU (A). The phase separated sample appears to be highly textured and rough (B). The addition of $NaHCO_3$ resulted in the formation of surface pores (35% (C), 45% (D) and 55% (E)). The pore size is displayed for each sample in the form of a histogram.

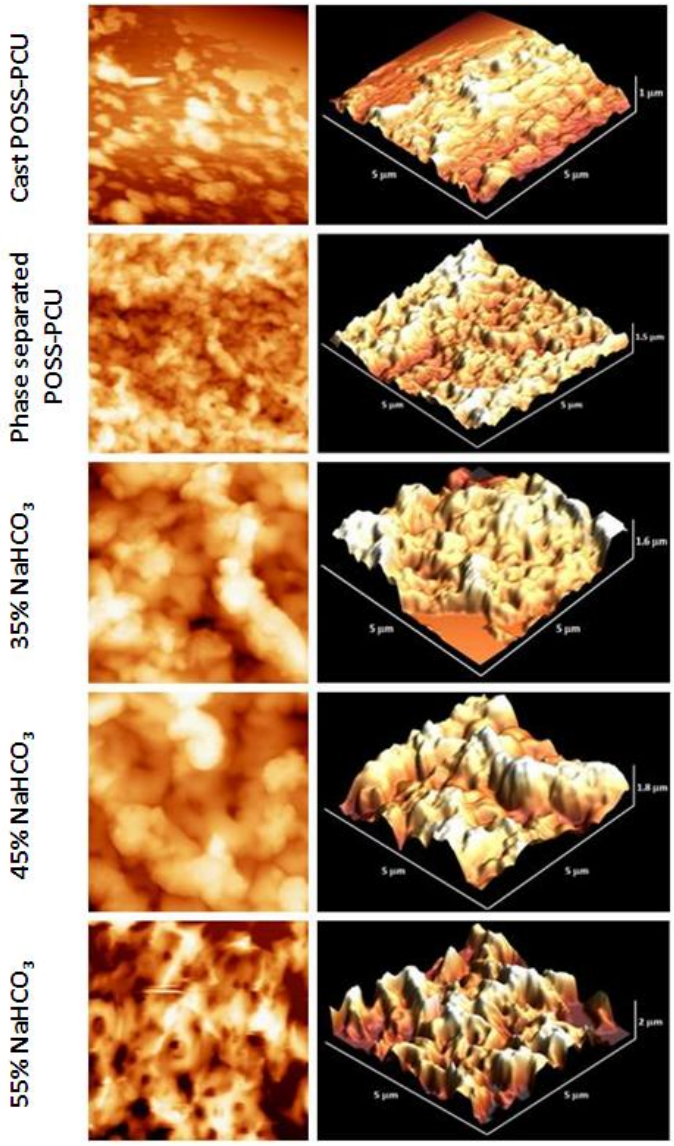

Figure 6.7: AFM images, both 2D and 3D, of the surface of POSS-PCU samples. The arithmetic mean average (S_a and root mean square (S_{RMS}) average surface roughness values are provided in table 6.2

6.3 Discusion

In order to engineer vascular grafts with optimal biocompatibility, a thorough understanding of the surface properties and how such properties affect the response of certain cell types is vital. These surface properties can be ascribed to three main

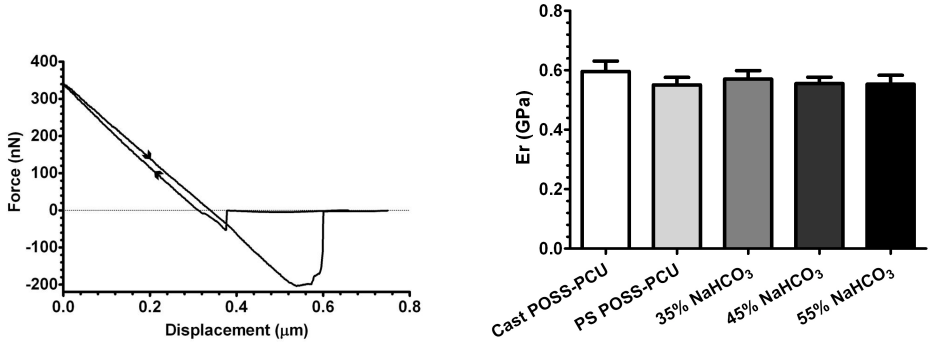

(a) (b)

Figure 6.8: (A) Representative image of the force-displacement curve generated by AFM indentation. (B) Reduced modulus (Er) values generated via AFM and equation 6.3 of the POSS-PCU membranes.

physiochemical categories: chemical, mechanical and structural. All three surface attributes have been demonstrated to modulate interactions between biological matter and biomaterial surfaces. The aim of this chapter was to provide a full characterisation of the surface properties of phase separated substrates, with or without the use of $NaHCO_3$, and compare and contrast with the cast sheet of POSS-PCU which served as a control.

It is clear to see phase separation resulted in significant variations in the chemical, mechanical and structural surface properties of POSS-PCU. Further, the addition of $NaHCO_3$ resulted in significant changes to the surface morphology and topography but did not have any great impact on the chemical or mechanical behaviour of the phase separated membranes.

By utilising SIMS, any differences in surface chemistry, following phase separation were elucidated. SIMS is a surface analytical technique which makes use of a focussed beam of primary ions which induce secondary ions to be released from the top two monolayers (up to 2 nm) of the surface. Secondary ions are analysed by a mass spectrometer to form mass spectra and selected mass images of the surface (fig 6.2 and 6.3). Phase separation appears to reduce the presence of the POSS moiety at the surface. This result is further corroborated by ATR-FTIR analysis which also displayed a reduction in peak intensity at 1100cm^{-1} which is associated with POSS. It is thought that the low surface energy, non-polar, POSS moiety migrates to the surface

in a manner analogous to a number of additives used in the coatings industry [233]. This is validated by the high content of POSS found on the surface of the cast sheet of POSS-PCU via SIMS, and the intensity of the POSS peak on the ATR-FTIR spectra. However, upon phase separation; a highly porous, low density POSS-PCU foam is created which exhibits a dramatically increased surface area. As the surface area is increased but the concentration of POSS remains constant, it is expected that there would be fewer POSS moieties at any given location on the surface of the membranes.

With fewer POSS moieties at the surface of the phase separated membranes, it is expected that the underlying polyurethane would be exposed to a far greater degree. A closer look at the ATR-FTIR results indicate an increase in peak intensity at approximately 1740cm^{-1} which can be attributed to carbonyl peaks associated with the polycarbonate polyol soft segment. Again, SIMS analysis appears to validate these findings. The negative SIMS spectra, which contains many of the nitrogen and oxygen containing heteroatom fragments associated with polyurethanes, is far more abundant for the phase separated sample giving rise to the belief that the first few nanometres of the phase separated sample is predominantly polyurethane in nature.

The reduction in the number of non-polar POSS groups at the surface of the phase separated samples also manifested itself into a significant reduction in surface contact angle (fig 6.5). Contact angle measurements are used to determine the wettability of the substrate with wetting surfaces associated with high surface energy and nonwetting ones with low surface energy. The level of wetting is represented by the contact angle formed at the interface between a solid and a liquid. Whilst phase separation resulted in a significant decrease in the initial contact angle, the addition of $NaHCO_3$ led to a minor increase. This is likely due to the increased surface roughness of the membranes (fig 6.7). In addition to surface chemical constituents, contact angle is known to be highly sensitive to surface heterogeneity and roughness, and an increase in surface roughness is likely to lead to an increase in surface contact angle. Contact angle, however, was not sensitive to the concentration of $NaHCO_3$ as no significant change was noted between samples produced with 35, 45 or 55% $NaHCO_3$.

The wetting behaviour of the samples was noted to change over time. The contact angles formed appear to reduce dramatically on the phase separation samples. Further, the higher the concentration of $NaHCO_3$ the more dramatic the decrease in contact angle. The likely cause of this observation is the increased swelling potential of the porous membranes produced with $NaHCO_3$. As the concentration of $NaHCO_3$ increased to a maximum of 55%, the bulk pore size also expanded to approximately

30 μm (fig4.12). Consequently, the volume of free space for water absorption will also increase resulting in the dramatic reduction in contact angle due to the liquid being swollen by the membranes [234].

Whereas mercury porosimetry reported bulk pore sizes in the range of 15-30 μm, it is clear to see from the surface SEM images (fig 6.6) that the surface pore size is significantly less. Whilst there was a general trend of increasing pore size with an increase in $NaHCO_3$ the differences were not significant and the surface pore size of the membranes produced via phase separation and $NaHCO_3$ ranges from as little as 1 μm to approximately 15 μm. This is in contrast to the membrane via phase separation alone, with no $NaHCO_3$, which does not appear to have a porous surface at all, with a thin skin layer forming at the surface. The fact that the pore size is significantly smaller than the diameter of $NaHCO_3$ would appear to further validate the hypothesis discussed in chapter 4 that the $NaHCO_3$ does not act as a leaching agent, but in fact, fundamentally alters the dynamics of the phase separation process; the result of which, in this case, is to inhibit the formation of a skin. If the $NaHCO_3$ acted as a conventional porogen, one would expect the pore size to be more uniform and correspond to $NaHCO_3$ diameter. As that is not the case, it is likely that the addition of $NaHCO_3$ has a significant influence on the thermodynamic and kinetic properties of the quaternary system. It is likely that the addition of an inorganic filler to the system reduces the build-up of interfacial polymer concentration inhibiting the formation of a dense skin layer.

Recently, the rigidity and roughness of the surface have become important parameters in the design of vascular grafts [235]. Having control over the morphological and mechanical surface properties at the nanoscale could help to aid in the design of more anti-thrombogenic surfaces capable of endothelialisation. The addition of $NaHCO_3$ resulted in a significant increase in the surface roughness of membranes (fig 6.7), reaching a maximum S_{RMS} value of 404.2 $\pm$ 29.8 nm for the membrane produced with 55% of $NaHCO_3$ as measured via AFM.

AFM in indentation mode was utilised to measure the surface stiffness of the membranes. No significant differences were seen between the cast, phase separated or phase separated with $NaHCO_3$ samples. This is in sharp contrast to the bulk stiffness measurements obtained via more conventional means, such as uniaxial tensiometry, whereby there are marked differences in the mechanical properties of the cast and phase separated samples. The Youngs modulus is almost 20 times as stiff as the phase separated membranes [186]. The second surprising feature of the nanoin-

dentation tests was the values of the Youngs relaxation modulus. Whereas tensile testing returned values in the MPa range, AFM produced values in the GPas. However, this is not a unique observation; a number of previous investigations have found significant discrepancies between the bulk stiffness and surface stiffness of polyurethanes [236, 237]. Further, there are several reports of the surface stiffness of polyurethanes, measured via AFM indentation, being in the GPa range [238–241]. Polyurethanes are multiphase samples with complex morphology. The bulk modulus values will be dependent on volume fractions, morphology of phases and interphase crystal connectivity with the tensile characteristics are determined via physical averaging processes. The surface stiffness measured with AFM indentation is a measure of the surface stiffness, at a depth of a few hundred nanometres, in isolated locations. Therefore, surface fractions are the primary determinants of the surface stiffness, with significant variations in stiffness between the hard and soft segments of polyurethanes being reported. Furthermore, in the case of POSS-PCU, POSS is a highly ordered, symmetrical, silica cage which is known to migrate to the surface. Stiffness values of POSS have been measured in the range of tens of GPa, which is likely to further exacerbate the surface stiffness of POSS-PCU, causing a further divergence of bulk and surface stiffness [242].

It should be noted that this chapter dealt with studying the bare surface on the luminal side of the graft - the surface that will be in contact with the blood. However, upon immediate exposure to blood, the surface properties are likely to dramatically alter due the immediate adsorption of proteins. It is this interfacial protein layer that will mediate the cellular adhesion and biocompatibility of any implanted device. Whilst the underlying surface porosity and substrate stiffness are not likely affected, properties such as surface topography, surface energy and contact angle are likely to alter significantly following protein adhesion. Further, the type, concentration and confirmation of the adhered proteins will modulate the downstream cellular behaviour. The adhesion and confirmation of proteins is itself dependent on the surface properties of the biomaterial. Previous studies on POSS-PCU found it to bind fibrinogen irreversibly in a competitive binding assay with albumin [243]. Adsorbed fibrinogen molecules mainly took the dominant trinodular structures in monomeric and dimeric forms [244]. In addition, net positively charged long α chains were prone to being hidden beneath the D domains whilst γ chains predominantly remained exposed. Protein adhesion is a key intermediary process influencing cellular adhesion, gaining further insight on the behavior of proteins on surfaces can help in the design of improved biomaterials.

6.4 Conclusions

Biocompatibility of medical devices and implants is, to a large degree, determined by the interfacial characteristics of the biomaterial. In this chapter, a detailed description of the surface chemical, morphological and mechanical properties of POSS-PCU is provided and discussed. Three quite distinct surfaces were investigated: the virgin POSS-PCU, phase separated POSS-PCU and phase separated with $NaHCO_3$ POSS-PCU. Following phase separation, the surfaces were significantly rougher with fewer POSS moieties at the surface. The addition of $NaHCO_3$ led to a more porous membrane. No differences were found between the surface mechanical properties which is in marked contrast to the bulk mechanical properties which displayed some quite obvious and significant differences. With the exception of surface roughness, the concentration of $NaHCO_3$ did not appear to significantly influence the surface properties of the membranes, which again, is in contrast to the bulk properties which were quite heavily influenced by the concentration of $NaHCO_3$.

7

Blood Material Interactions of POSS-PCU Vascular Grafts

Vascular grafts are, by their very nature, blood contacting devices; and as such, interactions between graft surface and blood are essential in determining graft patency. Blood is a multicomponent fluid, which delivers required substances to the body, such as nutrients and oxygen, whilst simultaneously removing waste products. It is composed of 55% plasma and 45% formed elements. Plasma constitutes approximately 90% water with the other 10% consisting of plasma proteins, electrolytes and nutrients. The formed elements component of blood is composed of a number of cell types which includes red blood cells (RBC), white blood cells (WBC) and platelets. The WBC can be further subdivided into five different and diverse cell types: monocyte, lymphocyte, basophil, eosinophil and neutrophil.

When an exogenous material is exposed to blood, a complex series of events is initiated which begins with protein adsorption resulting in the activation of the coagulation cascade, which regulates thrombosis via the intrinsic pathway (fig 1.3) [34]. Factor XII is activated by adsorption which then goes onto convert prekallikrein into kallikrein initiating a cascade of reactions resulting in prothrombin being cleaved into thrombin. Thrombin converts the soluble plasma protein, fibrinogen, into insoluble strands of fibrin which then forms a mesh resulting in a haemostatic plug or clot in conjunction with platelets. The mesh forms a transient provisional matrix in and around the biomaterial which provides the structural, biochemical and cellular components required for modulating WBC behaviour [245].

The adhesion, survival and phenotype of WBC is dependent on the type, level and surface conformation of adsorbed proteins, which in turn are dependent on the surface

properties of the biomaterial. An inflammatory response results in the migration of monocytes to the biomaterial surface and differentiating into macrophages, expressing various surface markers such as CD14, CD69 and CD86, essential for presenting antigens necessary for T cell activation [245]. Activated macrophages can modulate their behaviour through the release of cytokines, such as IL-1β, IL-6, IL-8, IL-10 and TNF-α, which are chemical messengers mediating the immune response [246]. Eventually macrophages fuse together forming multi-nucleated foreign body giant cells (FBGC) which remain at the tissue-implant interface for the lifetime of the device [247]. If the biomaterial is larger than 10μm, as is the case with vascular grafts, then the FBGC is incapable of undergoing phagocytosis and thus release oxygen free radicals, degradative enzymes and acid in a bid to degrade the foreign body. Ensuring that the biomaterial invokes a minimal macrophage response, and is durable enough to withstand the degradative solutions, is essential for successful long term implants. The release of cytokines, growth factors and chemoattractants provides a rich environment of activating and inhibiting substances capable of regulating the cell populations in the inflammatory and wound healing responses.

Parameters such as chemical composition, electrical charge, surface texture and porosity, discussed extensively in the previous chapter, all modulate the behaviour of implanted device [248]. Hydrophobic head groups such as –CH_3 and –CF_3 were found to be significantly less thrombogenic than more ionic head groups (–COOH and –SO_3H) with the least thrombogenic surface being the hydrophobic silastic tubing which had a water in air contact angle of 108° [249]. In an alternative study conducted on PU catheters, the opposite trend was apparent [250]. The more hydrophilic PU, with increased number of carboxylic groups, led to a decrease in platelet and fibrinogen uptake. Meanwhile, it was reported that a rough, textured surface leads to an increase in the number of adhered platelets and thus poor haemocompatibility [251]. However, this too was contradicted with it being reported that sub-micron texturing of polyurethanes reduce platelet adhesion due to the minimal surface area available for interacting with blood [252]. A similar response was noted on porous substrates where highly porous grafts displayed much improved blood compatibility due to a reduced surface area for platelets to interact with [251].

Human monocytes are equally vulnerable to the material surface affecting their behaviour. When cultured upon hydrophilic and anionic surfaces, monocytes expressed reduced level of the pro-inflammatory cytokine IL-8 and increased levels of the anti-inflammatory cytokine IL-10 compared to monocytes cultured on hydrophobic and cationic surfaces [253]. The same authors also discovered that hydrophilic and anionic

surfaces inhibit monocyte adhesion and IL-4 mediated FBGC formation leading them to conclude that hydrophilic and anionic surfaces promote an anti-inflammatory response by dictating the cytokines produced by adhered monocytes and macrophages. *In vitro* studies, using titanium surfaces with a range of roughnesss, found that the rougher surfaces promoted the secretion of pro-inflammatory cytokines (Il-1β, IL-6 and TNF-α) and chemokines (monocyte chemoattractant protein-1 and macrophage inflammatory protein-1α) from murine macrophage-like cells, in a time dependant manner [254]. Meanwhile, a separate study with polyethylene implants, suggested that a coarse surface induced a lesser tissue reaction compared with the smoother surface [255].

It is clear from the literature that no clear consensus exists on the optimal parameters for blood contacting devices. The contradictory reporting of the effects of biomaterials on the thrombogenic and immunogenic response is indicative of the complex, interwined nature of blood-material interactions. The aim of this chapter is to investigate the biocompatibility of POSS-PCU surfaces by studying the interactions of various components of blood with the phase separated membranes *in vitro*. The activation of plasma proteins, platelet adhesion and activation, mononuclear cell adhesion and activation and the endothelialisation potential were all explored in this study. HUVECs and EPCs were both used to assess endothelialisation with cell viability measured with Alamar Blue assay. The impact of phase separation, with or without $NaHCO_3$, on the biological performance of POSS-PCU was assessed.

7.1 Materials and Methods

7.1.1 Isolation of blood components

Blood samples were collected following consent from healthy adult human volunteers. Samples were collected by venepuncture in citrated blood tubes constituting 3.8% citrated whole blood at 1:10 v/v, pH 7.4 (Sarstedt, UK). Samples were exposed to density gradient centrifugation within an hour of collection (fig 7.1).

Plasma and platelets

Blood was layered onto Ficoll-Paque (GE Health care Bio-science, Sweden) density gradient in a 1:1 ratio and centrifuged at 200g for 15 mins resulting in the red blood cells at the bottom and platelet rich plasma (PRP) at the top separated by the density gradient, Ficoll-Paque. The PRP was separated and further centrifuged at 2000g for

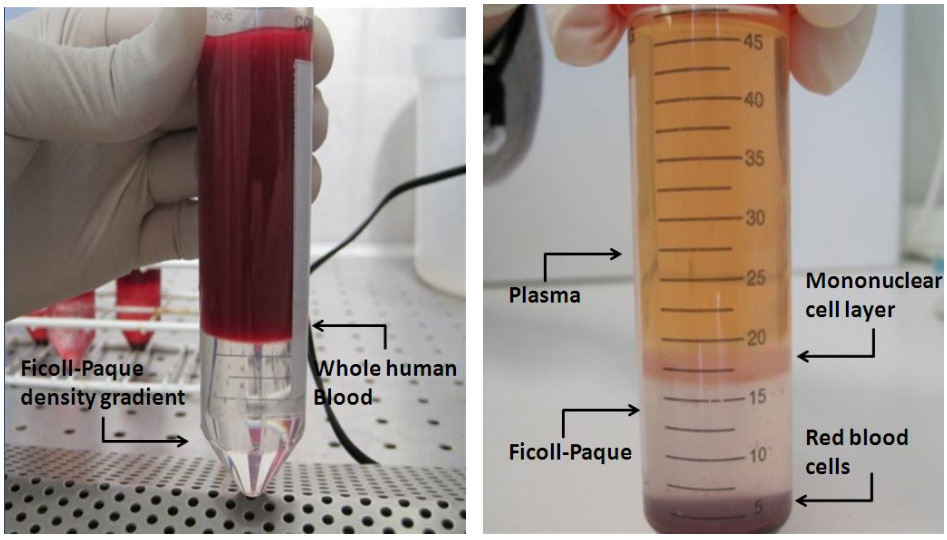

(a) Before centrifugation (b) After centrifugation

Figure 7.1: Images of human blood layered on Ficoll-Paque before and after centrifugation. Centrifuging splits the blood into four layers: plasma, mononuclear cell fraction, Ficoll-Paque and red blood cells.

20 mins resulting in a pellet of platelets at the bottom of the container and a plasma layer. The plasma was collected in a flask and the platelets were resuspended in sterile PBS at a concentration of 1×10^6 per mL.

Mononuclear cells

The mononuclear fraction of the blood was also isolated by centrifugating a 1:1 ratio of blood and Ficoll-Paque at $400g$ for 30 mins at room temperature. The mononuclear fraction was separated from each tube and the samples pooled in 30 mL universal tubes (Falcon, UK). 10 mL of Hanks Balanced Salt Solution (HBSS, Invitrogen, UK) was then added slowly to each tube and the contents mixed and centrifuged at $250g$ for 10 mins at room temperature. The cells were washed three times with HBSS, resuspended in 10% fetal bovine serum (FBS) and counted for downstream experiments.

7.1.2 Thrombogenicity evaluation

Plasma kallikrein assay

Presence of kallikrein in plasma supernatant following incubation with polymer discs was measured spectrophotometrically by a chromogenic kallikrein substrate (H-D-But-CHA-Arg-pNA, Diapharma). Polymer discs (16mm in diameter, n=4) were incubated with 1mL plasma (diluted 1:5 with TrisHCl, pH 7.8) for a period of 60 mins in a 24 well plate. In 96 well plates, 100μL of the incubated plasma was mixed with 200μL of the kallikrein substrate and incubated at 37°C for 30 minutes. 25μL of 50% acetic acid was used to terminate the reaction and optical densities were read at 405nm (Anthos 2010) giving a measure of kallikrein concentration. A calibration curve was constructed following manufacturers instructions using known concentrations of kallikrein diluted in 100μL of sterile PBS.

Platelet adhesion

A 24 well plate was lined with polymer discs (16 mm in diameter, n=4) and incubated in PBS for 1 hour. 1mL of platelet solution was added and incubated at 37°C for 1 hour. The supernatant was then removed and immediately counted using a haemocytometer. The number of attached platelets was calculated from platelet counts before and after incubation with polymer, and expressed as a percentage of platelets adhered (P) using equation 7.1

$$P = \frac{P_i - P_f}{P_i} \times 100 \tag{7.1}$$

where P_i represents the initial platelet concentration and P_f the concentration of platelets in the supernatant after adsorption.

Platelet activation

Platelet activation was determined using direct enzyme linked immunosorbent assay (ELISA). Polymer membrane samples (16mm in diameter, n=4) were incubated in 24 well plates with 1mL platelet solution for a period of 1 hour. The supernatant was removed and the concentration of PF4 in the plasma was determined using an ELISA kit (Human CXCL4/PF4 DuoSet ELISA Kits, R & D Systems, Abingdon, UK) following standard, manufacturer provided protocols (Catalogue Number: BBE6 and human CXCL4/PF4, Catalogue Number: DY795, R&D systems). Platelet adsorption morphology was observed using SEM. Glutaraldehyde solution (2.5% v/v) was used to fix samples which were then dehydrated with ethanol/distilled water (10%

ethanol increments) at 41°C. This was followed by freeze-drying for 48h before subjecting them to SEM observation.

7.1.3 Inflammatory evaluation

PBMC culture and immunostaining

Isolated PBMCs, concentration of 1×10^6 cells/mL, were cultured on 24 well plates coated with polymer samples (n=6). RPMI 1640 (Gibco, UK) supplemented with 2mM glutamine and 10% FBS was used as cell culture medium. The cultured cells were collected from the graft samples for immunostaining after 24 hrs and 7 days. Following washing with sterile PBS, cells were subsequently stained for surface markers including, CD14-PerCP, CD86 Fluorescein, HLA-DR-PE and CD69-APC (all from R&D Systems, Abingdon, UK). The cells were incubated at 4°C for 30 mins then were washed with PBS, re-suspended in 100μL of 4% paraformaldehyde, and were acquired on a FACS Calibur.

Cytokine release

Supernatants were collected from the cells cultured on the different substrates and were freezed and stored at -20°C for quantitative immunoassay. Cytokines, namely Interleukin-1 (IL-1β/IL-1F2), IL-6, IL-10, and Tumour Necrosis Factor (TNFα) were identified using specific ELISA kits (Quantikine, R&D System, Abingdon, UK) following the protocol provided and the optical density of each sample was determined using a microplate reader (Anthos 2010) set to 450nm. Concentrations of each cytokine was determined from calibration curves produced using known quantities of cytokine.

7.1.4 Endothelialisation potential

HUVECs

HUVEC isolation HUVECs were isolated from a fresh human umbilical cord collected from the Royal Free hospital Labour Ward. The cord was inspected for any clamp marks, needle holes or any other damage; clamp marks were cut and the cord was then clamped to allow manipulation. The vein of the cord was cannulated with a 4 cm length sterile nasogastric tubing at both ends and tied firmly in place with sterile silk thread. The clamps were removed from the vein and placed on the tubing. A syringe was then used to flush the vein with sterile PBS until all clotted

blood was removed from the vein. The vein was then filled with collagenase solution (12.5 mg Collagenase A in 25 mL of basic medium) which was filter sterilised before use. The basic medium consisted of 96% M199 medium, 3% $NaHCO_3$, and 1% Penicillin/Streptomycin Solution (Penicillin 10000 U/mL streptomycin 10 mg/mL). The vein was placed in an incubator at 37°C for a period of 10 minutes. Following incubation, the cord was massaged to loosen the EC, and the collagenase solution emptied into a centrifuge tube. The cord was then washed with PBS collecting the washings in a centrifuge tube. The collagenase solution was neutralised with complete medium consisting of basic medium supplemented with FBS and L-glutamine. Cell solutions were centrifuged at $300g$ for 7 minutes, the medium was removed and the cell pellet was resuspended in complete medium and transferred to a culture flask and placed in an incubator. After 24 hrs the RBC were removed by washing with PBS and the cells were fed with fresh complete medium. At confluence, cells were removed using 0.25% trypsin-EDTA and split in a 1:2 ratio. Confluent cultures at passage three were used in all experiments.

HUVEC culture 16 mm discs of polymer samples (n=6) were prepared and sterilised through autoclaving and placed in 24 well plates. Polymer samples were seeded with 2×10^5 cells in 1 mL of medium (M199 supplemented with 20% foetal bovine serum (FBS) and penicillin/streptomycin), and cultured for a period of 14 days. Cells cultured on tissue culture plastic (TCP) served as a positive control.

EPCs

The isolated PBMCs were suspended in cell culture medium (M199 supplemented with 20% fetal bovine serum (FBS) and penicillin/streptomycin) and cultured on polymer discs (n=6) in 24 well plates at a concentration of 5×10^5 cells per well in 1 mL of medium. Cells were cultured for a period of 14 days with TCP cultured cells serving as a control.

Cell viability

Cell metabolism was assessed by AB assay at day 1, 3, 5, 7, 10 and 14 for HUVECs and 5, 7, 10 and 14 for EPCs. Medium was removed from the wells and 1ml 10% AB in cell culture media added. After a 4 hour incubation, AB samples were removed and 0.1 ml was measured on a Fluroskan Ascent FL (Thermo Labsystems, UK) fluorescent plate reader (excitation 530nm, emission at 620nm).

Statistical data analysis

The data is presented as means and standard deviations. One way analysis of variance (ANOVA) with Tukey post hoc test was used to examine the significance between the samples with $p<0.05$ considered to be statistically significant. Two way ANOVA was utilised where indicated for analysing two independent variables.

7.2 Results

Thrombogenicity evaluation

Plasma kallikrein assay The presence of kallikrein in plasma following incubation with the polymer samples was measured spectrophotometrically using a specific kallikrein substrate (H-D-But-CHA-Arg-pNA) and are presented in figure 7.2. Kallikrein activity was lowest on the cast sheet of POSS-PCU polymer rising significantly ($p<0.001$) on the phase separated samples. Samples produced with $NaHCO_3$ induced a greater degree of kallikrein than the sample produced with no $NaHCO_3$; however the concentration of $NaHCO_3$ had no effect on the level of kallikrein production.

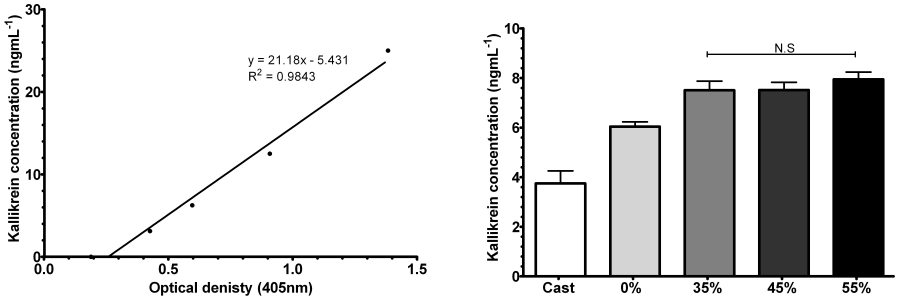

(a) Calibration curve

(b) Kallikrein concentration in supernatant

Figure 7.2: Significant differences in concentration of kallikrein was recorded from plasma supernatant following one hour incubation with the cast, phase separated and phase separated/$NaHCO_3$ samples. No significant differences were detected between the different concentrations of $NaHCO_3$($p<0.001$, N.S = not significant, n=4)

Platelet adhesion Figure 7.3 summarises the percentage of platelets adhered to each polymer sample. The cast sheet of POSS-PCU adhered the least platelets (8.0 $\pm$ 3.8%). Phase separating POSS-PCU resulted in it adhering significantly ($p<0.001$) more platelets compared to the cast sheet (26.3 $\pm$ 3.7%); however, the addition of

$NaHCO_3$ reduced the percentage of platelets adhered to 19.96 ± 3.12%. There was no significant difference between the sample prepared with 35% $NaHCO_3$ and 45% but increasing the concentration of $NaHCO_3$ to 45% reduced the number of platelets adhered to 14.82 ± 2.06%.

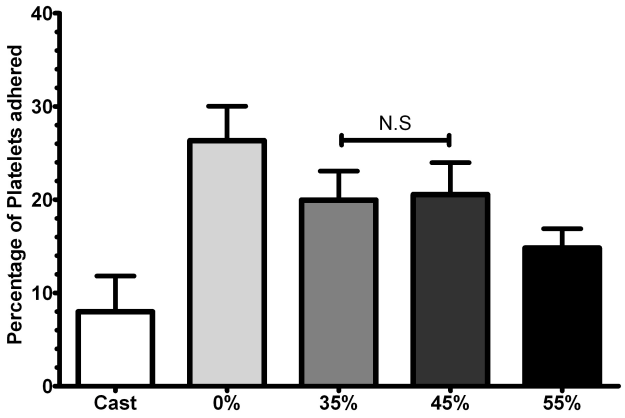

Figure 7.3: Percentage of platelets adhered to polymer samples after incubation with platelets in for 1 hour (N.S = not significant, n=4)

Platelet activation The concentration of PF4 released into the supernatant was used as an indicator of the extent to which the polymer samples activate platelets. No significant differences were detected between any of the samples with the exception of phase separated POSS-PCU produced with no $NaHCO_3$ which induced a significantly ($p<0.001$) greater degree of PF4 release (fig 7.4).

In addition to PF4 concentration, the morphology of the adherent platelets was observed through SEM images (Fig 7.5). On the cast sheet of POSS-PCU, platelets appear spherical in shape and there is no evidence for any pseudopodia emanating from the rounded cells 7.5a. Platelet morphology changes drastically on the phase separated POSS-PCU. Large aggregates of platelets are present on the surface which are flat and highly spread, with protruding pseudopodia, indicative of activated platelets 7.5b. Platelets on the phase separated samples, produced with $NaHCO_3$, are relatively quiescent 7.5c, d, e. There are minor aggregates but little or no evidence of pseudopodia protrusion or flattening and spreading out; the hallmarks of activation.

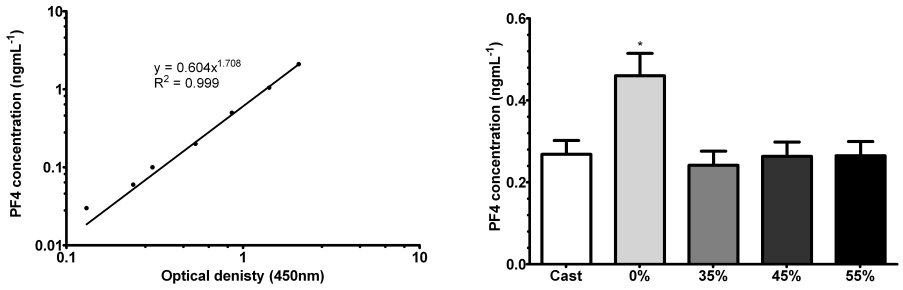

(a) Calibration curve

(b) concentration of PF4 supernatant

Figure 7.4: Concentration of PF4 released into the supernatant by platelets following one hour incubation with polymer samples. * = p<0.001, n=4.

Inflammatory evaluation

PBMC culture and immunostaining PBMC were cultured on the different substrates and labelled with antibodies for four inflammatory cell markers (CD14, CD69, CD86 and HLA-DR) and analysed using a fluorescence activated cell sorter (FACS) at two time points: after 24 hours and 7 days (Fig 7.7). FACS analysis displayed a significantly higher (p<0.001) number of CD14 positive cells on phase separated POSS-PCU; however, after 7 days culture that difference dissipated and all 5 samples exhibited the same number of CD14+ cells. CD86 expression was least on the cast POSS-PCU both after 24 hours and 7 days. In contrast the phase separated POSS-PCU induced the most CD86 expression after 24 hours. Following 7 days of culture, CD86 expression equilibrated between the phase separated samples with no significant differences being detected. No significant difference in CD69 expression was detected between the phase separated samples; however, cast POSS-PCU consistently had fewer CD69+ cells after 24 hours and 7 days. Phase separated POSS-PCU also induced a greater degree of HLA expression, after 24 hrs, than the other 4 samples; however, there was no difference after 7 days of culture. Interestingly, there was no significant change in HLA expression on the cast sample after 24 hours or 7 days.

Cytokine release Commercially available ELISA kits were used to measure the concentration of four cytokines (IL-1β, IL-6, IL-10 and TNFα) released by PBMC into the supernatant (fig 7.8). IL-6 appears to be unaffected by the substrate as no difference was detected in its concentration on any of the samples after 24 hours or 7 days. IL-1β was significantly (p<0.001, marked * or # on figure 7.8) lower on the cast sample than the phase separated; however, there was no difference in IL-1β

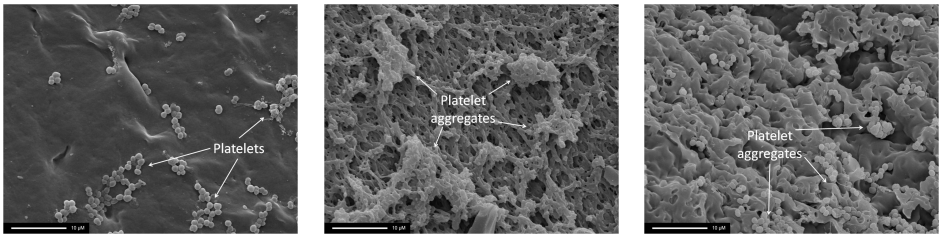

(a) cast POSS-PCU (b) o% $NaHCO_3$ (c) 35% $NaHCO_3$

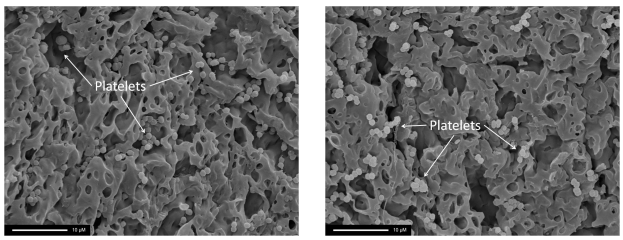

(d) 45% $NaHCO_3$ (e) 55% $NaHCO_3$

Figure 7.5: Representative images of platelets on polymer samples following 1 hour incubation on polymer samples. Platelets on the cast sheet of POSS-PCU are spherical in shape with no aggregates or evidence of pseudopodia protrusions. Large aggregates of platelets with protruding pseudopodia are present on the phase separated sample with no $NaHCO_3$. Evidence of minor platelet aggregation on samples produced with 35% and 45% $NaHCO_3$, but platelets remain relatively spherical in shape. Fewer platelets found on the samples with 55% $NaHCO_3$ with minimal aggregates and no spreading.

release between the different phase separated samples. Further, there were no differences in IL-1β concentration between the two time points on any of the five samples, indicating that cytokine release was at its maximum very quickly after contact with the foreign surface. Both IL-10 and TNFα appear to be heavily surface dependant. There is a significant ($p<0.001$) reduction in IL-10 concentration on the phase separated samples produced with 35 or 45% $NaHCO_3$, compared to the samples with 0 and 55% $NaHCO_3$ after both 24 hours and 7 days (marked * and ## on figure 7.8). IL-10 concentration was at its highest on substrate produced with 55% $NaHCO_3$ after 7 days. TNFα release profile was almost exactly the opposite of IL-10, whereby samples produced with 35 or 45% $NaHCO_3$ produced significantly higher concentrations of TNFα than the samples with 0 and 55% $NaHCO_3$ after 24 hours. The rate of TNFα release over 7 days varied with each substrate. The sample produced with 35% $NaHCO_3$ generated the most TNFα followed by a significant reduction in TNFα on the sample produced with 45% $NaHCO_3$ (marked #). There was no difference between TNFα production on the samples produced with 0 and 55% $NaHCO_3$; how-

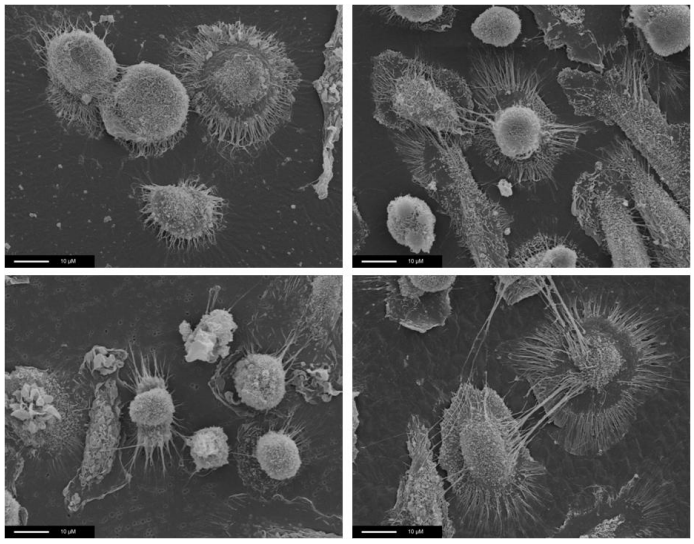

Figure 7.6: Representative SEM images of PBMC cultured on polymeric surfaces.

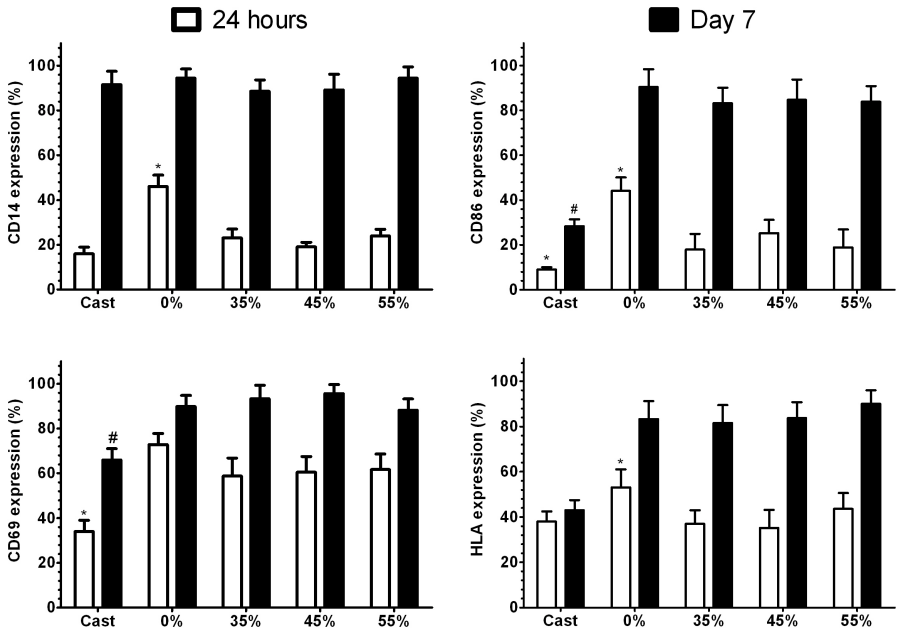

Figure 7.7: Surface receptor expression of PBMC at two time points: 24 hours and 7 days. Surface receptors CD14, CD69, CD86 and HLA-DR were examined. *=p<0.01, # =p <0.01 in second time series, n=6

ever, both produced significantly less than the 35 and 45% samples (marked ##). The cast sample of POSS-PCU consistently had the least concentration of both IL-10 and TNFα after 24 hours and 7 days (marked ** and ###).

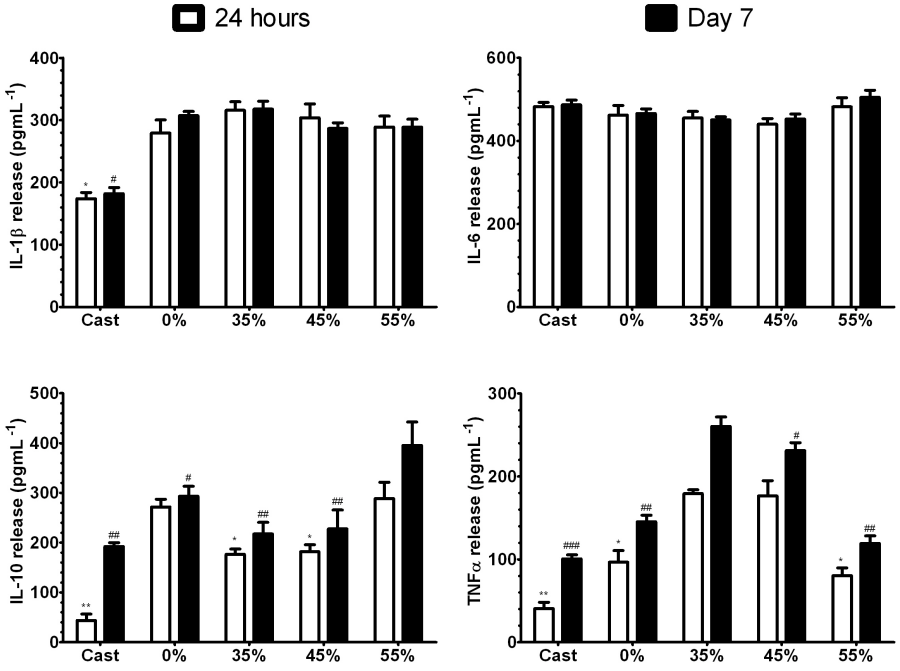

Figure 7.8: Concentration of cytokine release from PBMC supernatants after 24 hours and 7 days. Cytokines IL-1β, IL-6, IL-10 and TNFα were all examined. * indicates significance for the 24 hour time period whereas # indicates significance for 7 days time period. $p<0.01$, n=6)

Endothelialisation potential

HUVEC HUVECs were cultured for a period of 14 days with the results presented in figure 7.9. After 24 hours, no significant difference existed between any of the experimental samples, as determined by one way ANOVA, or indeed the control TCP. After 3 days of culture; the number of viable cell, as determined via Alamar Blue assay, increased however there was still no significant difference between the samples or TCP. A growth in cell numbers was again observed after 5 days; however, HUVECs on the sample with $NaHCO_3$ appear to be growing significantly slower (2 way ANOVA, Bonferroni's post test $p<0.05$). After 7 days, the samples produced with $NaHCO_3$ were still sustaining a significantly lower number of cells compared to TCP. Following 14 days of culture, there were significant differences between the

number of viable cells on TCP and all the test samples with the exception of the substrate produced with 55% $NaHCO_3$.

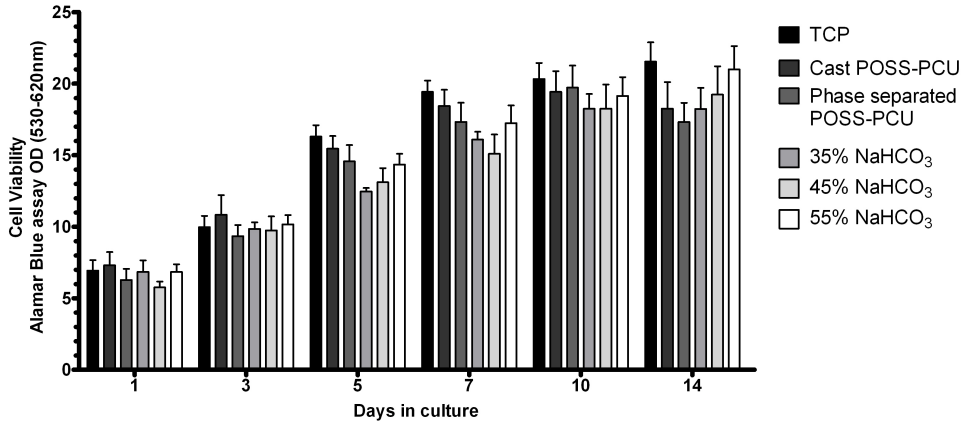

Figure 7.9: HUVEC culture for a period of 14 days. Cell viability is measured at discrete time points via the AB assay. Samples were subjected to 2 way ANOVA to determine significance, n=6)

EPC Results of EPC culture are presented in figure 7.10. Two way ANOVA determined significant differences in cell numbers at different time points. Whilst the initial number of viable cells, after 5 days, is the same on both TCP and cast POSS-PCU; the rates of growth vary significantly so that after 14 days TCP has significantly more viable ECPs than cast POSS-PCU. The phase separated samples, with the exception of the substrate produced with 55% $NaHCO_3$, consistently exhibited a lower nuber of viable cells than TCP. Despite having significantly fewer cells after 5 days, the rate of cell growth on the 55% $NaHCO_3$ sample continued to grow resulting in it sustaining a significantly higher number of cells than the other test samples. The TCP control clearly sustains a significantly higher number of viable cells throughout the 14 days.

7.3 Discussion

The success of any blood contacting, implantable device is based in its ability to resist thrombosis and inflammation. This is particularly pertinent for vascular grafts as thrombosis remains the primary cause of small calibre graft failure [256]. Thrombosis is usually the result when any exogenous material comes into contact with blood. Whilst a truly non-thrombogenic surface does not exist; there have been some successes in reducing protein adsorption and platelet adhesion and elucidating the

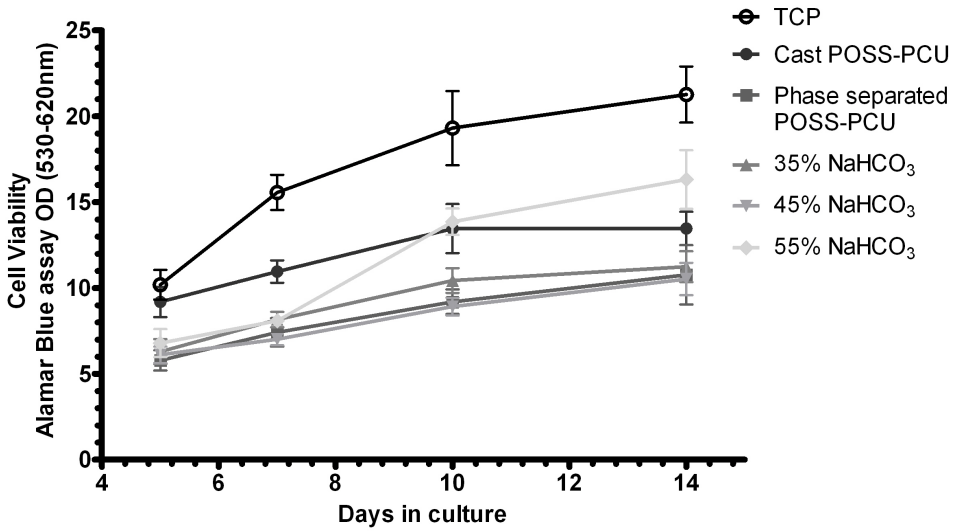

Figure 7.10: EPC growth curves generated over a period of 14 days. The Alamar Blue assay was utilised to measure cell viability. 2 way ANOVA was used to determine statistical significance, n=6)

mechanisms by which exogenous materials activate the coagulation cascade and the cellular components of blood [257, 258].

The concentration of kallikrein present in plasma is a good indicator of the extent of activation of the intrinsic pathway of the coagulation cascade [259]. Kallikrein activation is known to be most prominent on negatively charged or polar, hydrophilic surfaces. Whilst none of the POSS-PCU surfaces are negatively charged, the cast POSS-PCU is the most hydrophobic and was found to induce the least kallikrein activation. Meanwhile, the substrates produced via phase separation with $NaHCO_3$ elicited more kallikrein production than the substrate produced via phase separation alone, despite being more hydrophobic. Whilst there was a modest increase in contact angle between the respective samples, it is unlikely that a small increase in contact angle would translate itself into modulating kallikrein activation. More likely, the increase in activation could be due to the significant increase in surface area. The membranes produced with $NaHCO_3$ are porous surfaces which are significantly rougher translating into a dramatic increase in surface area. The increased surface area would provide more of the polymer for the plasma to interact resulting in plasma activation to a greater extent.

A similar paradigm could be proposed for the interaction of platelets: increased roughness would expose a larger area for platelet adhesion. However, this simplistic view fails to take into consideration the scale of dimensions on the surface [260]. If the dimensions are in excess of 2 μm (the dimension of a platelet) then the increased roughness will simply result in more contact area for platelet surface adhesion, resulting in a more thrombogenic surface. Meanwhile, if surface features are below 75 nm, then the surface structures are even smaller than the pseudopodia of platelets; thus, they can be considered smooth with factors other than surface roughness dominating. However, if the surface roughness dimensions are between 2 μm and 50 nm then the contact area that platelets are in contact with may be reduced as platelets will only be able to adhere to the top of the topographic features.

Accordingly, the smooth, cast POSS-PCU adhered the least platelets. As platelets are insensitive to substrate rigidity and mechanical forces, it is thought the highly hydrophobic nature of the surface repelled platelet adhesion [261]. Thereafter, there appears to be a correlation with surface roughness and platelet adhesion for the phase separated samples. The membrane produced with 55% $NaHCO_3$ had a S_{RMS} equal to 404.2 $\pm$ 29.8 nm (table 6.2) and adhered the least platelets (14.82 $\pm$ 2.06%); whereas the graft produced with 0% $NaHCO_3$ had a S_{RMS} equal to 105.2 $\pm$ 12.8 nm and adhered the most platelets (26.34 $\pm$ 3.69%).

Once adhered, the interaction and activation of formed elements, such as platelets and cells, with a material surface is dependent on the nature of the surface and the adsorbed proteins. Activation is instigated by an extracellular stimulus interacting with the cell surface which usually involves a ligand binding with a specific surface receptor. Various plasma proteins, including thrombin and fibrinogen, can absorb onto material surface and provide the necessary activation. However, for plasma proteins to be able to successfully provide the stimulus needed for activation, they need to be in a suitable orientation and conformation for the correct presentation of an epitope [244]. The orientation and conformation of proteins on material surface is dependent on a number of factors including surface topography, porosity and surface charge with adsorption distorting protein structure.

Platelet activation appeared to be insensitive to surface roughness as no significant difference was detected in PF4 release - a key cytokine released from the α granules of activated platelets - or platelet morphology between the cast POSS-PCU or any of the phase separated with $NaHCO_3$ samples. However, the phase separated membrane with no $NaHCO_3$ did induced a significantly higher level of PF4, after normalisation

for platelet numbers, suggesting a greater extent of activation. SEM images of the platelets on would appear to corroborate these findings with significant aggregation and pseudopodia protrusion, indicative of platelet activation, readily visible on the phase separated with no $NaHCO_3$ sample. This is in sharp contrast to the spherical morphology of platelets on the remaining four samples. The precise mechanism behind this heightened state of activation is difficult to ascertain; however, it may be due to the relative hydrophilicity of the sample, or indeed the surface features may be in the correct size range to induce activation [262].

WBC are produced and derived from haematopoitic stem cells in the bone marrow. Following centrifugation of blood samples, they are often found in the buffy coat, a thin, typically white layer of nucleated cells (fig 7.1). The mononuclear component of these cells includes lymphocytes, monocytes and macrophages. Lymphocytes are primarily responsible for mediating the immune system whereas monocytes and macrophages are concerned with foreign body response. Monocytes tend to migrate from the blood stream and differentiate into macrophages which are then tasked with the engulfment and digestion of exogenous materials. CD14 is a surface receptor commonly expressed by monocytes/macrophages. After 7 days in culture, nearly all the cells on the samples are CD14+.

CD69, CD86 and HLA-DR are all surface markers of activation of macrophages. CD69 is one of the earliest inducible cell surface glycoproteins making it a useful marker for early activation of PBMC [263]. The relatively high level of CD69 expression after 24 hrs ($> 50\%$) suggests the phase separated samples induce early activation of PBMC. Meanwhile, HLA-DR and CD86 are both surface receptors whos primary role is to modulate T cell response [245]. An increased abundance of HLA-DR or CD86 on the cell surface is often in response to stimulation and so can be used as a marker for immune activation. The general trends appears to be slightly increased expression, after 24 hrs, on the substrate prepared with 0% $NaHCO_3$ compared with the other samples. After 7 days culture, the expression levels appear to reach close to 100% on all of the samples.

Cytokine release profiles were measured at two time points - 24 hrs and seven days- in an effort to see if the different surfaces altered the functional behaviour of PBMC. can modulate their behaviour through the release of cytokines, such as IL-1, IL-6, IL-10 and TNFα, which are chemical messengers mediating the immune response [245]. No difference was observed between the release profiles of IL-1β and IL-6 on the different samples after 24 hrs or seven days indicating an initial burst of pro-inflammatory

cytokine release, possibly as a result of the early activation as witnessed by the high levels of CD69 expression.

Despite a higher percentage of CD14, CD86 and HLA-DR positive cells after 24 hrs, the phase separated sample with 0% $NaHCO_3$ induced a lower level of TNFα than the samples produced with 35 and 45% $NaHCO_3$. This may be due to the increased expression of IL-10. IL-10 is an anti-inflammatory cytokine known to inhibit pro-inflammatory cytokine production, such as TNFα, possibly via inhibition of NFκB activation [264]. It would seem the cast sample of POSS-PCU induces a minimal level of cytokine secretion. Thereafter, the phase separated sample with 0% and 55% of $NaHCO_3$ induce the highest level of the anti-inflammatory IL-10 cytokine and the lowest levels of the pro-inflammatory TNFα. The trends remained similar after seven days. Whilst TNFα is potent pro-inflammatory, low levels have been implicated in the healing process by encouraging angiogenesis and increasing macrophage produced growth factors during wound healing [265].

Whilst its clear that the different substrates induced a contrasting immune response; no distinct pattern was observed, suggesting a complex relationship between material surface characteristics and cell behaviour. Recent studies investigating macrophage response to material topography have reported similar findings: no distinct pattern between surface feature size or shape and cell response being detected [266]. This may be a response of the intrinsically dynamic, heterogeneous and complex nature of the macrophage cell system. Further, the chemical composition of the surface and the subsequent changes in surface energy was found to have no impact on macrophage behaviour [267].

Native blood vessels have a thin layer of EC lining the luminal wall which forms an anti-thrombogenic interface with blood. Its postulated that for any prosthetic graft to be successful in the long term, a fully functional endothelium, capable of maintaining vessel integrity, is a necessity. Studies of endothelialising grafts in vitro with cultured EC have shown that a confluent endothelium can improve long term patency of the graft by preventing thrombogenic complications [71, 130, 133, 208]. However, the process of extracting and culturing ECs for in vitro endothelialisation of grafts is labour intensive requiring a great deal of time and expertise making it expensive and restricted to a few specialised clinics. Therefore, material which can sustain and induce in situ endothelialisation are much sought after.

In this study, POSS-PCU was shown to sustain both mature EC and EPC growth

on its surface. Over a period of 14 days, HUVECs appeared to grow best on the highly porous and rough surface of the substrate produced with 55% $NaHCO_3$, compared to the other test substrates; with no significance difference was noted between cell growth on TCP or POSS-PCU. EPC growth was found to be not as robust on POSS-PCU as on TCP; however, the 55% $NaHCO_3$ sample was capable of sustaining significantly higher number of EPC than the remaining test samples. These findings are in agreement with a number of previously published reports which have found EC growth much improved on rough, textured surfaces with pore sizes smaller than 30 μm [154, 155, 202, 224].

7.4 Conclusions

The success of any implantable device is dependent on the biological reactions in the interfacial regions governed by physiochemical properties. In this chapter, the thrombogenic, immunogenic and endothelialisation potential of the different graft surfaces was examined. By studying a wide range of factors which include cytokine release, surface receptor expression on PBMC and the growth of platelets, HUVEC and EPC; the aim of this chapter was to get an understanding of the biological response one can expect upon implantation of a POSS-PCU vascular graft.

In this study, the highly porous and rough surface of the sample produced with 55% $NaHCO_3$ appear to perform better than the substrates produced with 35 and 45% $NaHCO_3$. Whilst the phase separated sample produced with 0% $NaHCO_3$ did suffer in its response to platelets, cytokine release was at a minimum and it did not activate the coagulation pathway as severely as samples produced with $NaHCO_3$.

8

The Impact of Sterilisation on POSS-PCU

Up to 6% of prosthetic grafts can encounter difficulties with infection resulting in approximately $640m in healthcare costs in the USA alone [268]. In addition, there are significant associated morbidity and mortality rates and in 17-40% of patients, graft infection leads to death [268]. A rather common, and completely avoidable, method in which a prosthetic graft can become infected is through directly implanting a graft with microrganisms attached [269]. *Staphylococcus aureus*, the central pathogen responsible for graft infections, and coagulase-negative staphylococci possess virulence factors that facilitate their adherence to the prosthetic materials [270]. The prosthetic device is coated with a biofilm consisting of ECM which contain the infective microbes; protecting it from the hosts immune response.

For these reasons an effective sterilisation protocol is essential when developing biomedical devices. Sterilisation usually involves physical or chemical treatment which results in the deactivation of organic macromolecules and/or microorganisms and can be achieved in a number of ways including steam, gamma irradiation and ethanol. Given the nature of their action, the sterilising techniques can also react with the biomaterial. Steam sterilisation can lead to hydrolysis, softening and degradation of the polymer due to the high temperature, pressure and humidity [271]. Gamma irradiation is known to cause chain scission and cross-linking which can adversely affect material properties [272]. Furthermore, both steam and gamma have been known to deform and yellow the polymeric materials. Immersing in ethanol is a milder technique used *in vitro* to disinfect the polymer sample. It is particularly useful for disinfecting biodegradable tissue engineering scaffolds, such as glycolic acid based materials; which, by their very nature, tend to be fragile [273].

The propensity of PUs to degrade has been discussed often in this thesis. Mean-

while POSS-PCU has been shown to be resistant to biodegradation both *in vivo* and *in vitro* through incubating with a range of oxidation, hydrolysis and enzyme solutions [182]. However, the impact of sterilisation technique on POSS-PCU is as yet unknown. Whilst a range of sterilisation techniques has been used in the past, little thought given to the impact of each method on the material properties. Numerous investigations have characterised microbial activity following sterilisation, as a marker of efficacy, but the impact of sterilisation technique's on the material bulk and surface properties is often ignored; whereas it is often the material bulk and surface properties which determine the effectiveness of the implant/device. The purpose of this study was to evaluate the impact of the sterilisation technique on the bulk and surface properties of POSS-PCU and POSS-PCU vascular grafts. The treatments include 70% ethanol, steam and gamma irradiation. Changes to the molecular weight, mechanical strength, surface chemistry and cytotoxicity were evaluated and the efficacy of sterilisation determined through incubating in bacterial growth broth.

8.1 Materials and Methods

Sample preparation

The 18%(w/w) solution of POSS-PCU in DMAc was cast onto glass petri dishes and left in an oven at 60°C overnight to evaporate the solvent. The resulting solid sheets of polymer were then sterilised accordingly and used for future experiments.

Alternatively, vascular grafts were manufactured as per the instructions in chapter 4 using a formulation consisting of 50% $NaHCO_3$ and 2% Tween 80 surfactant. Following manufacture, the grafts were sterilised for future experiments.

Sterilisation

Gamma irradiation Samples were packed in sterilisation pouches and irradiated with a dose of 28.4 kGy at room temperature, using a 60Co gamma-ray source (Isotron, Berkshire, UK). Samples were exposed to the source on a continuous path for a period of 10 hours.

Autoclave Auotclaving involves exposing the biomaterials to saturated steam at 121°C for a minimum of 15 minutes at pressures of 115 kPa. The samples were autoclaved and then left overnight for cooling.

Ethanol Polymer discs were incubated with 70% (v/v) ethanol and left in a roller mixer for 10 minutes or 24 hours. Samples were then washed (5×) in distilled water,

and stored in distilled water until use.

Material characterisation

Mechanical test Samples were cut longitudinally into a dogbone shaped specimen, 20 × 4 mm, using a sharp cutter and mechanical press ensuring a clean cut with no flaws or stress aggregation. However, due to the random nature of pore size and porosity in the coagulated samples, variability is to be expected. Sample thickness was recorded using an electric micrometer. Stress-strain profiles were characterised using a uniaxial load testing machine (Instron 5565, UK) and the Youngs modulus, ultimate tensile strength and elongation at break obtained (n=6).

ATR-FTIR The chemical structure of the polyurethane samples, following exposure to the various methods of sterilisation, was evaluated via attenuated total reflectance Fourier transform infer-red (ATR-FTIR) spectroscopy (JASCO FT/IR 4200). 30 scans were taken for each sample between 600 and 4000 cm^{-1} (n=6).

Gel permeation chromatography Solutions of both samples were prepared by adding 15 mL of DMF to 30 mg of sample and left to dissolve on a roller mixer over night. The samples were analysed using a PL-GPC 50 system equipped with PLGel column guard and 3 PLGel 5m mixed bed-C columns (300×7.5mm). The measurement was carried out at 50^{o}C in DMF and the eluent was pumped at the constant flow rate of 1.0 mL/min. The system was calibrated by performing Universal Calibration with single PL-polystyrene standard and a set of PL-EasyVial PS-H polystyrene standards of known molecular weights. The detection was done using PL-BV 400RT viscometer and PL-RI differential refractometer. The data has been collected and analysed using Varian 'Cirrus Multi detector' software. Analysis was done in duplicates.

Cytotoxicity

Endothelial Progenitor Cell (EPC) extraction Blood samples were collected following consent from healthy adult human volunteers. 24 ml samples were collected by venepuncture in EDTA blood tubes (Sarstedt, UK). Following collection samples were mixed and used for cell isolation within one hour of collection.

The mononuclear fraction of the blood was isolated using Histopaque 1077 (Sigma-Aldrich, UK). Briefly 3 ml of Histopaque 1077 was added to each of eight 12 ml polystyrene centrifuge tubes (Falcon, UK). 3 ml of blood was carefully layered on top. The tubes were then centrifuged at 400g for 30 minutes at room temperature.

The mononuclear fraction was separated from each tube and the samples pooled in 30 ml universal tubes (Falcon, UK). 10 ml of HBSS (Invitrogen, UK) was then added slowly to each tube and the contents mixed. The tubes were centrifuged at 250g for 10 minutes at room temperature. The cells were washed twice by removing the supernatant, resuspending in 10 ml HBSS and centrifuging at 250g for 10 minutes at room temperature. Finally the isolated cells were resuspended in 5 ml cell culture medium: M199 supplemented with 20% FBS and penicillin/streptomycin (both Invitrogen UK). Cells were then counted using a haemocytometer and seeded onto polymer samples as below.

EPC culture Cells were seeded onto polymer discs (n=4) in a 24 well plate (Falcon, UK) at a seeding density of 5×10^5 cells per well in 1 ml cell culture medium. Cells were then cultured for seven days.

Alamar blue assay Cell metabolism was assessed by Alamar blue^{TM} (AB) assay at day 7. Medium was removed from the wells and 1ml 10% AB in cell culture media added. After a 4 hour incubation, AB samples were removed and measured on a Fluroskan Ascent FL (Thermo Labsystems, UK) fluorescent plate reader (excitation 530nm, emission at 620nm).

Efficacy of sterilisation

All samples were tested for the effectiveness of sterilisation. Samples were immersed in Tryptone soya broth (TSB) and Fluid Thioglycollate medium (THY) for cultivation of microorganisms (Wickham Laboratories, Hampshire) for a period of 14 days at temperatures of 20-25°C for TSB and 30-35°C for THY. Sterile broth was used a negative control and unsterilised samples as positive controls. The broths were examined macroscopically every 1-3 days with clouding of the broth indicative of contamination and inefficient sterilisation whilst a clear broth would indicate no infection and an efficient sterilisation of the samples (n=3).

Statistical analysis

Statistical analysis was conducted using a Students two tailed t test. The difference between the means was deemed to be statistical significant when $p<0.05$.

8.2 Results

Visual inspection

Both POSS-PCU samples appeared to withstand sterilising treatments well with no obvious distortions visible. There was however, some slight discolouring/yellowing of the samples following gamma irradiation.

Material characterisation

Mechanical test Table 8.1 displays the mechanical properties of the materials following exposure to EtOH, autoclaving and gamma irradiation. No significant difference was seen between the Youngs modulus, UTS or elongation at break in any of the samples following incubation with EtOH.

Autoclaving the samples of POSS-PCU did not affect the Youngs modulus or UTS; however, there was a slight significant ($p<0.05$) increase in the elongation at break, for the casted sample, compared to the control. Autoclaving the coagulated sample caused a minor decrease in elongation.

Whereas the coagulated samples withstood the effects of gamma irradiation well, the casted samples suffered a decrease in their mechanical properties. The UTS for POSS-PCU decreased from 62.3 ± 6.7 MPa to 48.9 ± 5.0 MPa ($p<0.001$). The reduction in UTS translated itself to the Youngs modulus which was significantly reduced for the casted samples of POSS-PCU.

ATR-FTIR Attenuated total reflectance fourier transform infrared (ATR-FTIR) spectroscopy was used to analyse surface chemical changes upon sterilisation. Both samples were unaffected by autoclaving or ethanol treatment; however, gamma irradiation led to a reduction in peak intensity at 1245 and 1740 cm^{-1}(table 8.1). In addition, there was a significant increase in the intensity of the peak at 1095 cm^{-1} for the casted POSS-PCU sample.

Gel permeation chromatography GPC results are summarised in figure 8.2. Treatment with EtOH had negligible impact on the number average molecular weight (Mn), weight average molecular weight (Mw) or polydispersity index (Pd), regardless of incubation time, for either of the samples. Autoclaving the cast sheet of POSS-PCU resulted in a slight increase ($p<0.05$) in Mw but no change in Mn, resulting in an increase in Pd, possibly suggesting a degree of cross linking. No changes in

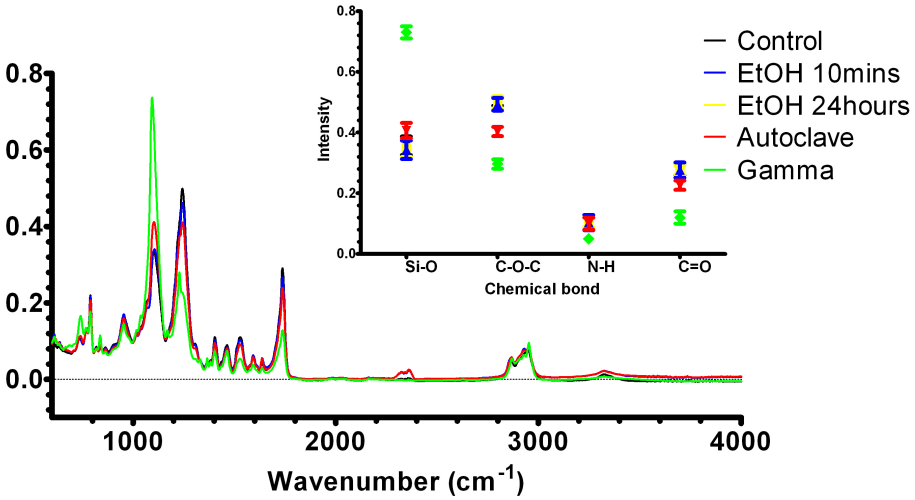

(a) Cast POSS-PCU IR spectra

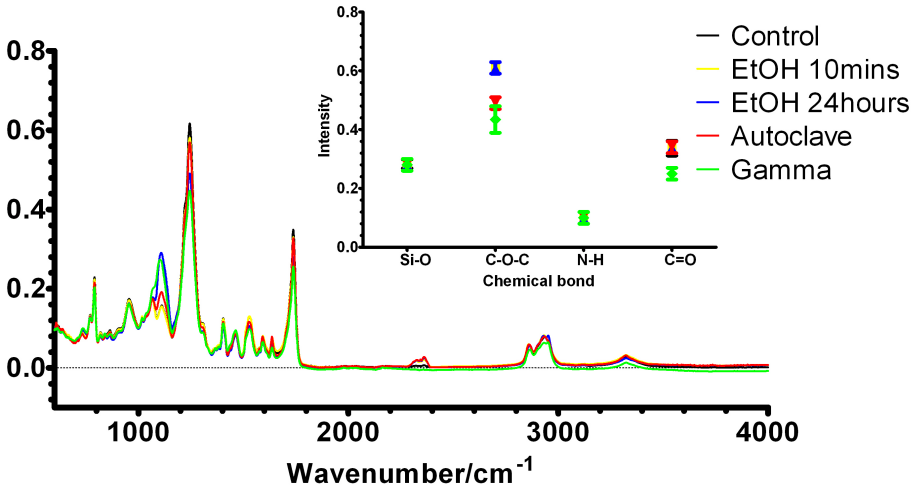

(b) Phase separated POSS-PCU IR spectra

Figure 8.1: ATR-FTIR analysis of cast and coagulated samples of POSS-PCU following sterilisation with EtOH (10 mins and 24 hrs), Autoclave and gamma irradiation. Inset with each spectra is a summary of any changes in key peak intensities (n=6, $p<0.05$). The peak assignment was as follows: 1100 cm^{-1} (Si-O-Si), 1240 cm^{-1} (urethane C-O-C), 1400 cm^{-1} (C-C aromatic ring), 1540 cm^{-1} (N-H and C=N), 1589 cm^{-1} (C=C aromatic), 1632 cm^{-1} (NH2), 1736 cm^{-1} (C=O).

Sample	Sterilisation technique	Youngs Modulus (MPa)	Tensile Strength (MPa)	Elongation (%)
Cast	Control	8.61 ± 0.81	62.35 ± 6.71	823.96 ± 28.03
	EtOH 10mins	7.75 ± 0.47	56.48 ± 2.98	875.36 ± 47.01
	EtOH 24hours	7.75 ± 0.64	66.67 ± 3.73	828.59 ± 29.09
	Autoclave	9.16 ± 0.62	62.39 ± 5.72	904.86 ± 37.40
	Gamma	6.49 ± 0.46	48.87 ± 5.04	853.24 ± 51.02
Coagulated	Control	0.35 ± 0.02	1.08 ± 0.08	440.76 ± 11.66
	EtOH 10mins	0.32 ± 0.03	0.98 ± 0.06	449.33 ± 25.45
	EtOH 24hours	0.32 ± 0.04	1.07 ± 0.07	437.51 ± 31.43
	Autoclave	0.33 ± 0.04	0.97 ± 0.05	382.84 ± 35.46
	Gamma	0.35 ± 0.03	1.22 ± 0.05	407.03 ± 9.87

Table 8.1: Mechanical properties (Youngs modulus, ultimate tensile strength and elongation at break) of POSS-PCU and POSS-PCL samples following sterillisation via a number of different techniques (n=6, $p<0.05$)

molecular weight distributions were detected in coagulated samples of POSS-PCU following autoclaving. Exposure to gamma irradiation had a significant impact on both the samples. The Mn of cast POSS-PCU significantly increased whilst the Mw decreased ($p<0.001$) manifesting itself in a sizeable reduction in Pd. Meanwhile, gamma irradiation increased the Mn and Mw of the coagulated POSS-PCU; however, the degree of increase in Mn was greater than Mw which resulted in a slight decrease in Pd.

Cytotoxicity

The results of the Alamar Blue assay are displayed in figure 8.3 as a percentage of viable cells compared to control cells cultured on tissue culture plastic following seven days of incubation. Whilst no significant differences were detected between cell viability on EtOH treated and autoclaved samples, sterilising via gamma irradiation reduced cell viability by approximately 50%, compared to EtOH treated and autoclaved samples, on both cast and coagulated POSS-PCU samples.

Efficacy of sterilisation

The polymeric materials were incubated in TSB and THY to test the efficiency of sterilisation (table 8.2). THY is a viscous growth medium with reduced oxygen levels, which tests the growth of anaerobic bacteria and other organisms capable of

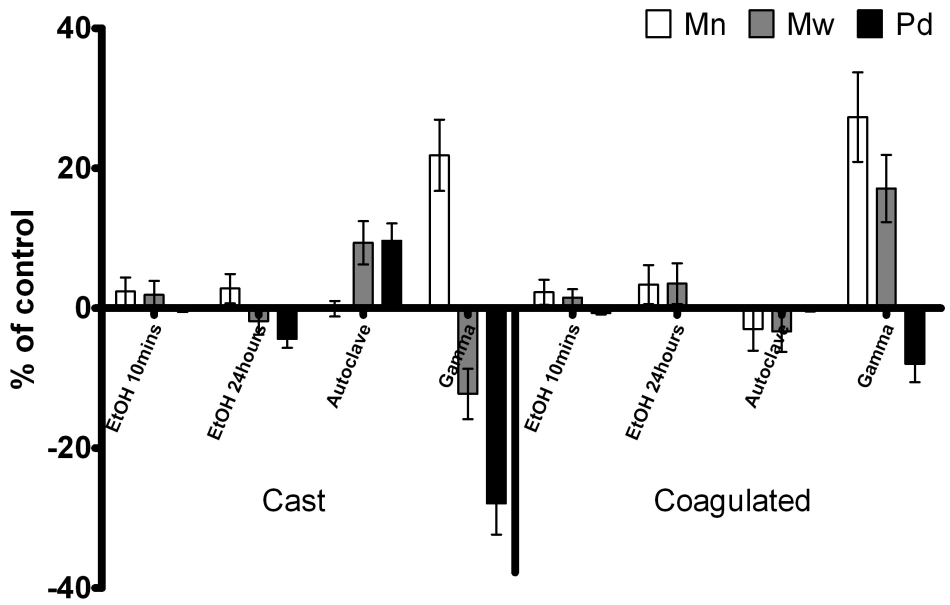

Figure 8.2: Molecular weight (Mn, Mw, polydispersity) of cast and coagulated samples of POSS-PCU following sterilisation via a 10 min incubation in EtOH, 24 hour incubation in EtOH, Autoclaving and gamma irradiation. Data is presented as a percentage variation of the unsterilised controls (mean ± SD, n=3).

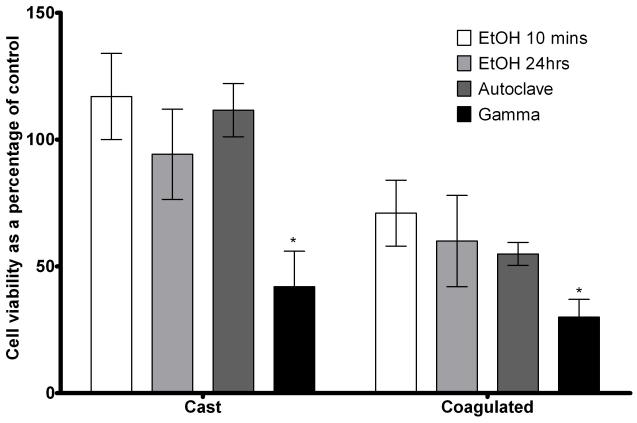

Figure 8.3: viability after 7 day incubation, as determined by Alamar blue assay. Results (mean ± SD) are presented as a percentage of the control cells grown on tissue culture plastic (n=4, * = $p<0.001$). Gamma irradiation appeared to reduce the number of viable cells by approximately 50%.

growing in reduced oxygen tension. No evidence of bacterial growth was observed on any of the materials tested following incubation in THY. TSB however, is a general growth media for aerobic microorganisms and is designed for the growth of aerobic bacteria and yeasts and moulds. The materials sterilised via EtOH incubation were not fully sterile and sustained the growth of bacteria on all three samples tested of each material. Autoclaving and gamma irradiation appear to be far more efficient sterilisation techniques as no evidence of bacterial growth was observed on any of the polymeric materials.

Sample	Sterilisation technique	Growth in TSB	Growth in THY
Cast	EtOH 10mins	3/3	0/3
	EtOH 24hours	2/3	0/3
	Autoclave	0/3	0/3
	Gamma	0/3	0/3
Coagulated	EtOH 10mins	2/3	0/3
	EtOH 24hours	3/3	0/3
	Autoclave	0/3	0/3
	Gamma	0/3	0/3

Table 8.2: Bacterial growth observed on each sample following incubation in Tryptone soya broth (TSB) and Fluid Thioglycollate medium (THY) for cultivation of microorganisms. Samples were tested in triplicates, and no evidence of bacterial growth was found on any of the materials tested which were cultivated in THY. Growth of bacteria was observed on all three samples of both samples sterilised via EtOH incubation and cultivated in TSB. Autoclaved and gamma irradiated materials appeared to be fully sterile and did not support any bacterial growth.

8.3 Discussion

Sterilisation is defined as the complete removal or destruction of viable organisms. More practically, however, it is better defined as a process capable of delivering a certain probability that the device is free from viable microorganisms. The physical or chemical agents capable of achieving sterilisation without adversely affecting the material quality, function and use, are rather limited for healthcare products. Two of the more common sterilisation techniques are moist heat (autoclaving) and ionising irradiation (gamma irradiation). Additional methods capable of inactivating viable organisms exist, but are less effective than terminal sterilisation. These include dis-

infectants such as EtOH incubation.

Depending on the chemical nature of the material and the processing method, sterilisation techniques have been reported to induce changes in material properties. In this study we investigated the effects of sterilisation on POSS-PCU nanocomposites: a non-degradable POSS-PCU with an aromatic hard segment and carbonate based soft segment, and vascular grafts produced from POSS-PCU via phase separation. The properties of the sterilised samples were compared to untreated controls.

The two samples were incubated with 70% ethanol for a period of 10 minutes and 24 hours. ATR-FTIR analysis indicated that no changes in the surface chemical composition took place. Further, there were no significant variations in molecular weight or mechanical properties suggesting that neither surface nor bulk properties were affected by ethanol irrespective of incubation time. Whilst ethanol has been shown to be useful in disinfecting lipophilic viruses and gram-positive, gram-negative, and acid-fast bacteria; hydrophilic viruses and bacterial spores are resistant to the microbial effects of ethanol making it unsuitable for sterilising biomedical devices for *in vivo* applications [274]. Cultivation in TSB broth resulted in microbial growth in both the samples sterilised with EtOH for 10 mins and 24 hours. However, no signs of bacterial infection or cytotxocity were observed in EPC culture with cell growth being in excess of control cells cultured on tissue culture plastic following 7 days of culture for the cast sheets and 75% for the porous samples.

The process of autoclaving requires samples to be exposed to high pressure saturated steam at temperatures of 121^oC or more. The combination of high temperature, humidity and pressure has been shown to be quite detrimental to PUs with decreases in UTS, hydrolysis and oxidation being reported in polyether based PUs [275]. Both of the POSS-PCU samples appeared relatively unaffected by exposure to autoclaving with the cast and coagulated samples retaining their shape and structure. GPC analysis suggested there was a minor increase in Mw of the cast sample which may explain the slight increase in elongation at break experienced by the autoclaved POSS-PCU. The small changes in behaviour may be due to a minimal degree of cross linking experienced by the material. The coagulated sample of POSS-PCU exhibited a small decrease in elongation at break alongside a reduction in ATR-FTIR peak intensity at $1245cm^{-1}$. These results are consistent with chain scission of the hard segment. The porous, coagulated sample has a significantly increased surface area, compared to the cast sample, offering a possible explanation for the difference in behaviour between the cast and coagulated samples. Chain scission may be induced by the moist

environment at the surface of the material as opposed to the high temperatures being experienced by the bulk. No significant changes were recorded in the molecular weight profile of the coagulated POSS-PCU sample further reinforcing the belief that chain scission is a surface effect as opposed to bulk. Autoclaving appears to be an effective sterilisation technique as no sign of microbial growth was detected in either of the broths for both the cast or coagulated samples. Further, no cytotoxic side effects were recorded.

Mixed findings have been reported regarding the effects of gamma irradiation on PUs. Whilst some investigators have found no change in material properties following exposure to gamma irradiation, an equally significant number of publications indicate severe degradation of material [272, 275–277]. Gamma irradiation is advantageous in that it is a rapid and highly effective sterilisation technique; no sign of microbial growth was detected on any of the samples following gamma irradiation. However, in the case of both the POSS samples that were tested it caused severe damage and displayed cytotoxic effects upon the cultured mononuclear cells reducing cell viability by more than half on the cast and coagulated samples. Whilst the exact mechanism behind this observation is unclear, there are reports in the literature of PUs with MDI based hard segments releasing 4,4'–methylene dianiline as a degradation product [272, 278]. Aromatic amines are known to be highly cytotoxic and gamma irradiation has been shown to release 4,4–methylene dianiline previously giving rise to cytotoxic side effects [279–281].

Whilst structurally there were no changes in the POSS-PCU samples, visually they had turned a dull yellow collour. This is likely due to the MDI in the aromatic hard segment of POSS-PCU. Exposure to gamma irradiation may have oxidised the central methylene group of the biphenyl leading to a highly conjugated quinone chromophore (fig 8.4).

Analysis of the surface functional groups of the cast and coagulated samples of POSS-PCU via ATR-FTIR provided further evidence of material degradation. Reductions in peak intensities at 1245 cm^{-1}, 1540 cm^{-1} and 1740 cm^{-1} are all consistent with hydrolysis of the hard segment. The significant reductions in Mw for both samples, as well as Mn for the coagulated sample would appear to corroborate those findings. The Mn for casted samples of POSS-PCU increased suggesting that cross linking is taking place. As Mn is a more sensitive parameter to the lower end of the molecular weight distribution, these results would suggest that chain scission is taking place followed by cross linking of the low molecular weight chains of the casted POSS-PCU.

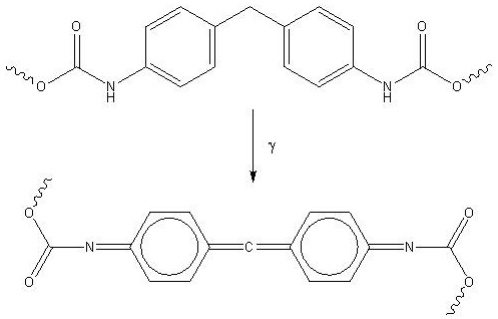

Figure 8.4: Reaction mechanism for the formation of quinone chromophore responsible for yellowing the samples.

An increase in ATR-FTIR peak intensity at 1095 cm^{-1} would reinforce these findings as 1100 cm^{-1} is the region where we would expect to find ether peak as a result of cross linking. However, it is difficult to assign this peak with any certainty as the Si-O-Si of POSS is also expected in this region.

The effect of polymer degradation was seen in the mechanical testing of the samples. The UTS and Youngs modulus decreased significantly for the casted samples of POSS-PCU. The coagulated sample did not display any significant changes in their mechanical properties. This is probably due to the highly porous nature of the coagulated samples meaning that the true cross sectional area upon which force was applied was considerably lower than the measured area resulting in lower than expected values. The force range upon which the samples were examined may not be large enough to determine any detrimental effects on the polymer chains.

8.4 Conclusions

Sterilising POSS modified polyurethanes via EtOH resulted in no observable damage but the sterilisation process was inefficient. On the other hand, both autoclaving and gamma irradiation resulted in effective sterilisation of samples; but gamma irradiation led to significant degradation in both POSS-PCU samples and had a cytotoxic effect upon EPC culture. Both POSS-PCU samples did, however, withstand the effects of autoclaving well with no structural damage observed or polymer degradation noted. The results indicate that autoclaving is the optimal sterilisation procedure for POSS-PCU.

9

Long Term Performance of POSS-PCU Vascular Grafts: An *In Vivo* Assessment

It is currently not possible to predict blood and tissue compatibility from mere *in vitro* assays. Whilst *in vitro* testing is a useful guide which helps to elucidate the response of individual components (e.g. proteins, platelets, cells) to the graft; they fail to capture the complex, multifactorial, emergent behaviour encountered in the physiological environment. This is particularly pertinent for the coagulation, inflammation and wound healing behaviour of the body in response to foreign objects, which involves multiple interconnected networks in a non-linear manner. For these reasons, long-term studies in animals still need to be performed to assess the safety and efficacy of any medical device. This is an essential requirement for the construct to gain CE marking or FDA approval prior to clinical application and commercialisation.

A number of animal models exist to evaluate the performance and safety of vascular grafts. Amongst them, primates resemble humans most closely from an anatomical and physiological point of view. They lack any dramatic growth spurts and thus are ideal for long term studies over several years. A number of investigators have made use of a primate model to evaluate their constructs; however, the ethical considerations tend to restrict their use in a number of countries [282, 283]. Furthermore, primates are expensive to purchase and maintain, compared to other species, making them economically unviable. Whilst porcine models are popular due to the similarities in cardiovascular anatomy and physiology, to that of humans, they are uncooperative without full anaesthetic and are prone to rapid growth. For example, a typical 25 kg pig will grow to approximately 100 kg after 8 weeks. The rapid growth of the animal limits the length of time the *in vivo* assessment can take place due to a size mismatch between the vasculature and the graft and difficulties in animal handling.

A number of further 'small animal' models have been utilised which include rabbits, rodents and mice. These models are inexpensive and easy to anaesthetise and work with; however, when it comes to performing surgery their small size presents quite a technical challenge.

In this study, an ovine model was used to establish the safety and efficacy of POSS-PCU vascular grafts. Their large size, lack of growth and low cost made them the ideal animal model. Further, the vascular tissue of sheep is physiologically and structurally similar to human tissue. The anatomy of this species facilitates easy surgical access to vessels of appropriate size. For these reasons, the carotid artery was chosen as the site to implant the vascular grafts. The long neck of sheep affords easy access for follow up doppler ultrasound and assessment of patency (fig 9.1).

The optimal graft to undergo *in vivo* evaluation was chosen based on the previous *in vitro* assessment. It was decided that the phase separated graft produced with 0% $NaHCO_3$ would be taken forward to the animal trial. With previous PU based grafts failing primarily due to a lack of mechanical robustness leading to dilation and aneurysmal formation, it was thought the mechanically robust phase separated graft, with a compliance profile independent of pressure was best placed to survive an extended period of time in the arterial circulation. The improved biocompatibility compared to the grafts produced with 35 and 45% $NaHCO_3$ was also a contributing factor. Whilst the graft produced with 55% $NaHCO_3$ also performed well in the biocompatibility evaluation, it was mechanically fragile and displaced excessive dilation at elevated pressures during the pressure-diameter evaluation.

9.1 Materials and Methods

Graft preparation

Grafts were prepared from synthesised polymer as described in chapter 4. Briefly, a mandrel 5 mm in diameter was used to extrude an 18% POSS-PCU solution in DMAc, through a 7 mm die, into a water bath at room temperature. The grafts were left in the water bath for a period of 30 mins allowing the phase separation process to take place, after which they were removed from the mandrel and left in distilled water for a period of 48 hrs ensuring complete removal of solvent. The grafts were then sterilised via autoclaving and thoroughly rinsed and stored in sterile distilled water at a temperature of 4°C.

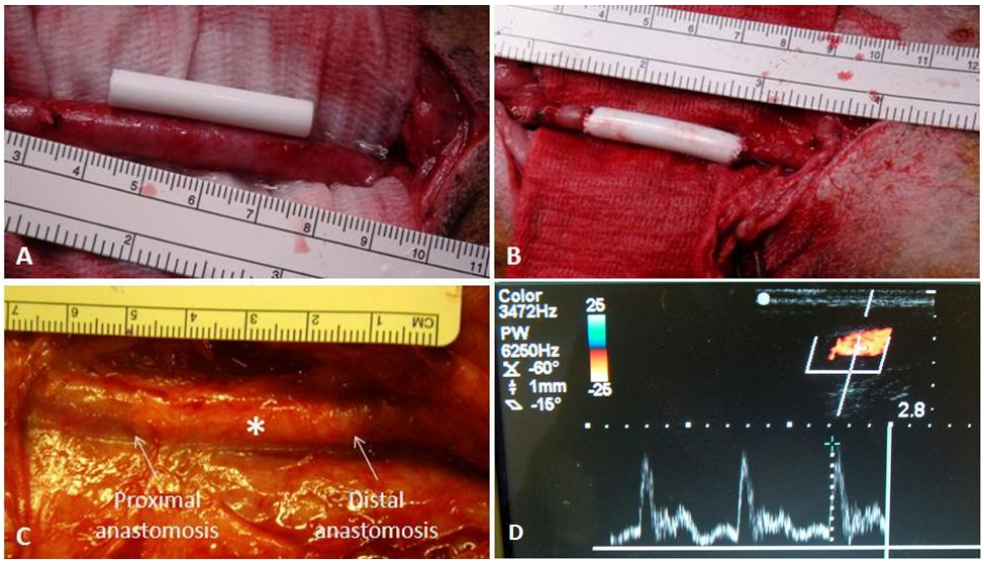

Figure 9.1: Digital images of (A) exposed LCA and soon to be implanted graft (B) POSS-PCU vascular graft anastomosed end-to-end to the LCA (C) Graft after 9 months implantation surrounded by a thin layer of reddish fibrous tissue (D) Ultrasound image demonstrating flow through the graft.

Implantation of grafts

The study was performed in compliance with the Good Laboratory Practice Regulations 1999 (S.I. No. 3106) as amended by the 2004 regulations (S.I. 994) which are based on the principles of Good Laboratory Practice as adopted by the Organisation for Economic Co-operation and Development (OECD), ENV/MC/CHEM (98) 17. They are in conformity with, and implement the requirements of, Directives 2004/09/EC and 2004/10/EC.

Ten adult sheep (animal numbers 1-10) with a body weight ranging from 45-60 kg were used for the study. A day prior to surgery, animal diet was withdrawn and a 75 mg tablet of Aspirin was administered orally.

Animals were administered diazepam (0.3mg/kg) and buprenorphine (0.01mg/kg) intravenously via a cannula positioned in a cephalic vein in the animal holding pen and then transported to the operating theatre. The sedated animals were then more deeply anaesthetised with a further bolus of diazepam (0.3mg/kg) and ketamine (3mg/kg) intravenously along with inhalational nitrous oxide and oxygen over isoflurane via a face-mask. The animals were then transferred to the operating table and

intubated with a cuffed endotracheal tube which was attached to a ventilator to control respiration. General anaesthesia was maintained using nitrous oxide, oxygen and isoflurane as above via the endotracheal tube.

Prior to surgery the animals were administered the analgesic carprofen 'Rimadyl' (1-2mg/kg) subcutaneously; the antibiotic cefuroxime 'Ceporex' (750mg) intravenously; the calcium solution 'Calciject' by subcutaneous injection (50ml) and sodium bicarbonate 8.4% (1 ml/hr) intravenously. A continuous intravenous drip of Hartmanns solution was delivered via a peripheral vein throughout the procedure. At least 20 mL blood was drawn from the right jugular vein for full haematology, clinical chemistry and coagulation screening.

A midline skin incision was made to expose and skeletalise the left carotid artery (LCA). Heparin (500 units/10kg) was administered intravenously via the drip and procaine 2% was applied topically to the artery to provoke dilatation. When fully dilated, the carotid artery was divided, and vascular clamps were applied to the proximal and distal ends of the artery. Animals 1-4 suffered slight spasms which caused a diameter mismatch between the artery and graft. Meanwhile, animal 7 exhibited abnormal physiology with the artery large and tortuous resulting in the diameter of the artery being larger than that of the graft. A 3 cm segment of the artery was removed and the POSS-PCU grafts were trimmed to length. Each end of the graft was anastomosed end-to-end to a cut end of the artery using continuous 6/0 prolene sutures. The *in situ* length of the graft was measured by ruler and recorded. On completion of the anastomoses, the distal vessel clamp was released to allow blood access to the anastomoses and any leakage assessed before release of the proximal clamp.

The muscle was closed with interrupted 2/0 vicryl sutures and the skin with interrupted 2/0 prolene sutures. Animals were administered 1 2 mL doxapram (20 mg/mL) intravenously to improve breathing and the antibiotic oxytetracycline 'Oxytet 20 LA' (1ml/10kg) by deep intramuscular injection and returned to their holding pen for recovery.

The grafts were monitored regularly using Doppler imaging (Sonosite Titan Ultrasound System) on study days 1, 7, 14 and then about once a month for the duration of the study ensuring that they remain fully patent.

Blood flow measurements

Volume blood flow was measured using Transonic Medical flowmeter system (HT207, Transonic Medical System, USA) with a flow probe of appropriate size. The flow probe houses two ultrasonic transducers and a fixed acoustic reflector. The transducers are positioned on one side of the vessel and the reflector midway between the two transducers on the opposite side of the vessel. An electrical excitation causes one of the transducers to emit a plane wave of ultrasound which intersects the vessel and bounces off the reflector before being received by the other transducer and being converted into electrical signals. The signals are then used to calculate the transit time from one transducer to the other. The results may be read from a digital readout and recorded manually.

Compliance measurements

Compliance of the graft determined by assessing the change in vessel wall diameter during each cardiac cycle as described in chapter 5 extensively. The measurements were taken in the sagittal plane at 90 degrees to the long axis of the vessels at three discrete sites along the graft and the artery. Segments of the graft were also imaged with a specially adapted duplex colour Doppler ultrasound scanning system (Easote Picus PRO, Esate Spa, Italy) with signal output to a high resolution, echo-locked wall tracking system (Wall Track; Pie Medical Systems, Maastricht, The Netherlands). Real-time M-mode images of the graft and arterial wall were obtained with a 7.5-MHz linear array probe.

Graft explantation

Animals were anaesthetised and blood samples collected as described previously. The graft implant site was surgically exposed with any observations recorded as a study note. The graft was explanted intact along with at least 1cm of native vessel at each extremity and pinned, fully extended, to an appropriate backing with the proximal end identified with a marker suture. The patency of each harvested graft was assessed by perfusion of physiologic saline and the specimen was placed in 0.9% saline to remove blood but care was taken to avoid dislodging thrombi. A specimen of the un-operated right carotid artery was also collected and treated similarly.

The animal was exsanguinated by implanting a cannula into the right carotid artery and allowing blood to flow to waste. Specimens of the lungs, heart, liver, kidneys, spleen and mesenteric lymph nodes, along with any other tissues considered relevant by the pathologist, were then transferred to 10% neutral buffered formal saline and

stored for later examination.

Histology

Specimens of the graft and other organs, as detailed in the graft explantation section, were fixed in 10% neutral buffered formal saline for a minimum of 48 hrs. The whole graft specimen, including native vessel at each end, was divided transversely at 2.5 mm intervals along its length. Samples of the graft were placed in pairs in processing cassettes in such a way that the proximal surface was presented for microtomy. These and other samples that were then processed by routine automated procedures to wax embedding. From each wax block, two 5 micron sections were cut; one section stained with haematoxylin and eosin and the other with picrosirus red. Sections of the graft were examined for cellular integration of the graft, chronic inflammatory response, healthy cells, apoptotic cells, proliferating cells, macrophages, T cells, intimal hyperplasia and the presence of collagen.

9.2 Results

Gross observation at implantation and explantation

The graft was found to be easy to handle, cut and suture. Upon perfusion, by releasing the proximal and distal clamps, the grafts began to pulsate gently which was visible both to the naked eye and through palpation. The grafts slowly became a reddish colour as blood was continuously flowing through with no leakage or oozing of blood that was apparent. Neither was there any release of blood at the anastomosis as the sponge like structure of the graft was able to self-seal following perforation by the suture needle.

Grafts 1 and 4 were found to be immediately non-patent (within 24 hrs post-implant) and graft 7 was found to be non-patent at day 14. The remaining 7 grafts were fully patent and functioning 9 months post-op at termination. The 7 grafts displayed no signs of infection, scar tissue or adhesions and were found to be pulsating strongly indicative of fully functioning and patent grafts. A layer of reddish fibrinous material appeared to surround the grafts. Upon explantation, the 7 grafts were perfused *ex vivo* with saline solutions, at which point none of the 7 grafts provided any resistance to the flow of liquid through the lumen. Further, there was no change in the dimensions of the graft upon explantation suggesting that the grafts are relatively elastic and can maintain arterial blood flow without dilation and aneurysmal formation.

The patency of the POSS-PCU grafts were compared to the 3 PTFE grafts implanted in the same position. PTFE grafts were found to have occluded within 3 weeks of implantation.

Toxicology screening

Blood samples were collected both on the day of, and prior to, surgery and the day of, and prior to, termination into appropriate tubes. No abnormalities were reported with any of the parameters analysed, which included immune cell count, plasma protein activations markers (prothrombin time and activated partial thromboplastin time) and serum protein counts. The lack of any significant difference in blood clotting time pre- and post implantation was positive as it is indicative of the graft having no significant impact on the thrombogenic response.

Blood flow rates

Blood flow rates were measured both pre- and post grafting at implantation and explantation and are presented in table 9.1 for all the animals with a summary in figure 9.2. The mean blood flow through the LCA, prior to implantation, was found to be 364.55 $\pm$ 87.83 mLmin^{-1}. There was some variation between the different animals with the range of measured blood flow rates being 264 mLmin^{-1}.

Following implantation of the grafts, the mean flow rate reduced slightly to 330.92 $\pm$ 80.63 mLmin^{-1} with the range narrowing a little to 209 mLmin^{-1}. There was no significant difference in the perfusion rates between the native LCA and the replacement POSS-PCU vascular grafts.

Flow rates were re-measured prior to explantation. Having been implanted for a period of 9 months, the mean flow rate through the grafts was found to be 311.8 $\pm$ 62.22 mLmin^{-1} with a range of 270 mLmin^{-1}. Animal 3 was excluded from the measurements as the reading of 32 mLmin^{-1} appeared to be an anomaly, possibly due to inappropriate equipment and/or user error. The flow rates through the RCA were also determined, allowing a comparison between the grafted LCA and RCA. The mean flow rate was 387.5 $\pm$ 177.87 mLmin^{-1} through the RCA which was found to be not significantly different (p=0.2045) to the grafted LCA.

On comparing the blood flow rate through the grafts post-grafting at day 0 (mean 330.92 $\pm$ 80.63 mLmin^{-1}) and just prior to explantation after 9 months (mean 311.8 $\pm$ 62.22 mLmin^{-1}), no significant differences was detected (p=0.3408). From the

blood flow rates, it can be concluded that the perfusion efficiency is not restricted by grafting and nor does it diminish over time.

Animal No	**LCA Pre-grafting ($mLmin^{-1}$)**	**LCA Post-grafting ($mLmin^{-1}$)**	**Graft at termination ($mLmin^{-1}$)**	**RCA at termination ($mLmin^{-1}$)**
1	380	350	Non-patent at termination	
2	480	473	Appropriate probe not available	
3	400	280	32	330
4	340	480	Non-patent at termination	
5	350	230	230	400
6	410	404	320	410
7	Not recorded	310	Non-patent at termination	
8	292	282	400	400
9	494	300	325	670
10	231	298	284	115

Table 9.1: Blood flow rates, as measured using a Transonic flowmeter, of the left carotid artery (LCA) both pre- and post grafting, the graft just prior to explantation after 9 months and the right carotid artery (RCA). Measurements were taken from all 10 animals in the study.

Compliance

Graft compliance was assessed *in vitro* in chapter 5 and was found to be 5.9 ± 0.4 $\%mmHg^{-1} \times 10^{-2}$ through the physiological pressure range. The compliance of the graft *in vivo* was found to be similar at 5.4 ± 1.6 $\%mmHg^{-1} \times 10^{-2}$. The average compliance of the LCA prior to graft implantation was not significantly different at 5.3 ± 2.64 $\%mmHg^{-1} \times 10^{-2}$. Following 9 months implantation, the graft compliance did not significantly alter and remained at 5.62 ± 3.04 $\%mmHg^{-1} \times 10^{-2}$ which compared favourably with the compliance of the RCA which was 5.48 ± 2.45 $\%mmHg^{-1} \times 10^{-2}$. These results would indicate that the compliance properties are not compromised upon implantation either through graft degradation or by the growth of connective tissue which surrounded the graft (fig 9.3).

Histology

Figure 9.4 displays representative histology images of the patent grafts upon explantation after 9 months. There appears to be some significant cellular infiltration from

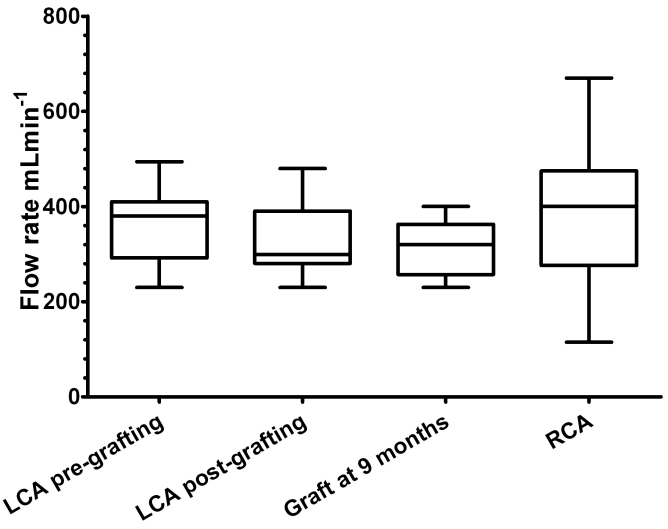

Figure 9.2: Mean blood flow rates through the native carotid arteries and the graft. LCA: left carotid artery, RCA: right carotid artery

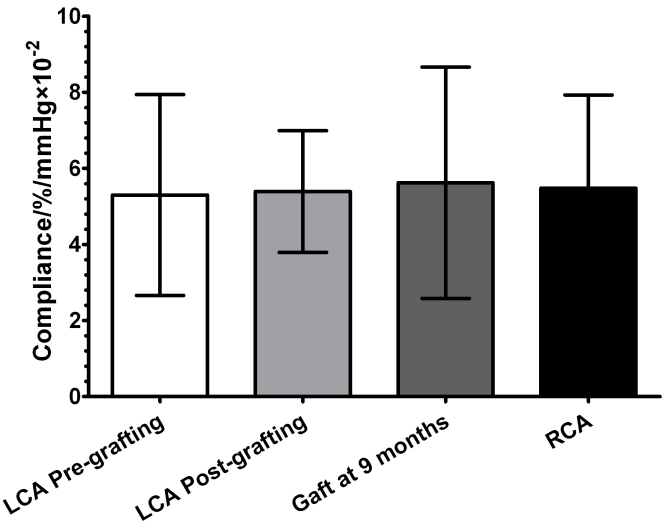

Figure 9.3: Compliance values of the native ovine LCA, RCA and POSS-PCU vascuar grafts on day 0 and after 9 months implantation. No significant differences were detected between the different subjects. Measurements were taken on all 12 animals at the physiological pressure.

the adventitia into the structure of the graft (fig 9.4A, B). However, those cells do not migrate into the lumen of the graft which, with is largely devoid of any great cellularisation (fig 9.4C). There is evidence for minor cell deposition in the lunem but there is no invasion and build up of tissue in the luminal space suggesting that there are no signs of IH formation (fig 9.4D). Picrosirius red stain confirmed these findings as there were no indications of collagen deposition in the luminal space of the graft (fig 9.4E). The adventitial tissue surrounding the graft is collagenous in nature and there is minor deposition of collagen in the structure of the graft.

Histology analysis was also conducted on the animals which were terminated prior to the end of the study (fig 9.4F). All of the non-patent grafts demonstrated similar features, namely, the length of the graft was filled to occlusion with clotted blood. This exists from just proximal of the proximal anastomosis to just distal of the distal anastomosis. Rather curiously, the thrombus and clot appear to be disassociated from the lumen with no cells deposited on the luminal border of the implanted grafts. No integrated adventitial growth is seen on any of these grafts.

9.3 Discussion

There is an acute clinical need for alternative conduits for small calibre vascular bypass grafts. Intense research effort has taken place aimed at developing more suitable grafts, which are not prone to thrombosis and/or IH. Other requirements, such as 'off the shelf' availability and available in a number of sizes further complicate matters. Several tissue engineering paradigms have been proposed, which have been discussed at length in chapter 2; however none of them have been wholly successful. A lack of radial strength in tissue engineered constructs severely limits their use in the arterial circulation [129]. Further, the high costs associated with their production is rather prohibitive to widespread clinical use; as is the complex manufacturing methods which limits them to a few highly specialised clinics [126, 127]. The time period required for their production means tissue engineered constructs cant be used in emergency revascularisation procedures, which invariably, the majority of situations requiring vascular grafting are [126, 127]. Many of the drawbacks are due to a fundamental lack of knowledge in cell biology and cannot be rectified easily. Consequently, no alternative concepts have emerged which could replace or improve the current industry standard Dacron or PTFE grafts.

The approach taken in this thesis has been to develop a prosthetic graft which meets all the functional requirements of a small calibre graft, whilst possessing a

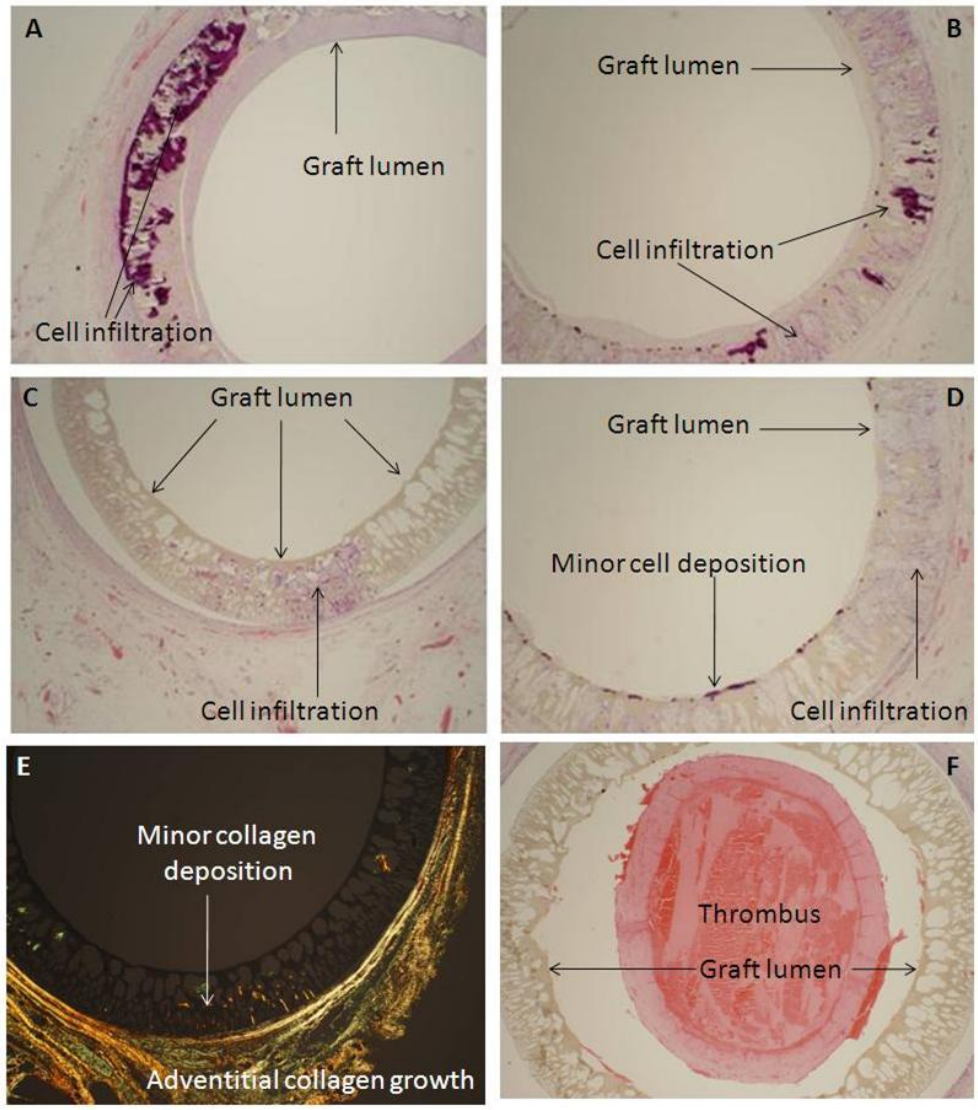

Figure 9.4: Representative histology images of POSS-PCU vascular graft cross-sections. Sections are taken from the proximal anastomosis, the main body of the graft and the distal graft. Images A-D display significant infiltration of cellular material from the adventitia. Image E indicates that whilst the adventitial tissue growth was collagenous in nature, there was no evidence of collagen in the body of the graft. Image F is of a thrombosed graft displaying a solid thrombus in the lumen of the graft. Interestingly, the thrombus is not attached to the graft lumen but has formed in the centre of the conduit.

more thromboresistant surface which is not prone to occlusion on prolonged exposure to blood; thus offering an improved and readily available, viable treatment option.

Whereas the previous chapters have discussed at length the fabrication process, functional mechanical properties and biocompatibility *in vitro*; the purpose of this chapter was to determine the performance and healing of a POSS-PCU vascular graft following long-term implantation in a suitable animal model. A senescent ovine model was selected for implanting POSS-PCU vascular grafts. The long neck region and readily accessible carotid arteries were highly appealing attributes of this model. The coagulation system of sheep has been previously been described as being similar to that of humans and has been used in a number of material evaluation tests [284]. Its use is recommended by the International Regulatory Affairs Offices of the FDA [285]. Further, the adult sheep are easy to handle and do not show further growth, thus there will be minimal disruption due to size mismatch throughout the study time period.

The decision to implant the graft produced with 0% $NaHCO_3$ was taken with the knowledge that mechanical vulnerability upon prolonged implantation is a significant drawback to using PU vascular grafts. PU grafts can be susceptible to dilation, and subsequent aneurysmal formation, in the arterial circulation. Therefore, the more porous grafts produced with $NaHCO_3$ were not implanted. The graft chosen to be implanted displayed a compliance profile of circa 5 %/mmHg $\times 10^{-2}$ throughout the mean arterial pressure range *in vitro*, which was a reasonable match to the compliance of the sheep carotid artery.

Vascular grafts were implanted in the left carotid artery (LCA) of 10 adult sheep, using a double end-to-end anastomosis, and left for a period of 9 months. Doppler sonography was used to periodically examine the grafts to ensure they remained patent. Once implanted, the compliance profile of the grafts was measured *in vivo* to ensure there was no significant mismatch. There was no significant difference between the compliance of the graft *in vitro* or *in vivo*, or indeed between the graft and the LCA pre-operatively indicating excellent initial functionality. To further determine the functional behaviour of the newly implanted grafts, blood flow rates were determined both pre- and post-operatively. Again, there were no significant differences between the flow of blood through the native LCA or the grafted LCA. With no significant difference in compliance or flow of the LCA pre- and post-operatively being observed, the synthetic graft does not cause any impedance or increase vascular resistance upon implantation.

Following implantation, 2 grafts were found to be occluded at day 1 (nos. 1 and 4) whilst a further graft (no. 7) was found to be occluded after day 14. The early or

acute failure (<30 days) of 3 of the grafts is a cause for concern. Rather intriguingly, the histology of the failed grafts (fig 9.4F) displays the thrombus formation being detached from the internal body of the graft. This would suggest that it was not the surface of the graft *per se* that caused the thrombotic occlusion. If the biomaterial itself was responsible for initiating coagulation, one would expect the thrombus to be attached to surface of the graft with adhesion mediated by fibrin. The exact cause of graft failure is difficult to ascertain; however, early graft failure is often associated with technical issues which include surgical technique [286]. A diverse range of factors, including the type of anaesthesia, have been implicated in early graft occlusion [287,288]. Further graft related issues could also have contributed to the sudden thrombus formation. Had any residual solvent (DMAc) not been leeched and was still present in the grafts, then that would cause a rather dramatic and immediate thrombotic response.

The patency rate of POSS-PCU vascular grafts was 70% (7/10). On examining graft compliance after 9 months *in vivo*, no significant changes were detected. The compliance of the RCA was also determined, that too remained circa 5 %/mmHg $\times 10^{-2}$. Previous studies have reported a significant reduction in graft compliance following implantation and wound healing [289]. This is usually a consequence of excessive fibrovascular infiltration in and around the graft. From the histology images (fig 9.4)it is clear that there is no significant infiltration of adventitial tissue which is likely to cause any restrictions in graft compliance.

Blood flow rates after 9 months implantation were also measured through the grafted LCA and compared with flow rates through the pre-grafted LCA and the RCA. Again, no significant changes were seen, suggesting perfusion efficiency is unhindered by grafting with POSS-PCU vascular grafts. As there is no restrictive barrier due to narrowing of the lumen, and the graft-artery mismatch is minimal; one would not expect to see any great reduction in the blood flow rates. With IH being the most common cause of synthetic small calibre graft failure, the lack of narrowing of the lumen is a promising finding.

A closer examination of the histology sections demonstrates that there was little in the way of cellular deposits or mineralisation on the luminal surface of the graft. Previous PU implants have been prone to calcification and mineralisation upon prolonged implantation [290]. A link has been made between graft hydrophilicity and mineralisation rate [291]. It is possible that the hydrophobic nature of POSS-PCU provided a surface resistant to the accumulation of mineral ions.

The lack of EC adhesion is of concern. The conventional paradigm in developing prosthetic grafts is that spontaneous endothelialisation is an absolute necessity. Whilst the POSS-PCU graft has not endothelialised, it was patent and functioning 9 months after implantation. Possible reasons for the lack of endothelialisation may be that the exposed surface lacked an open-pored structure. The lack of pores would mean there would not be any readily available tethering points for cells to adhere and stick to. Considering the luminal surface is exposed to high shearing forces in the arterial circulation, there is a risk that any adhered cellular material will be washed away by the continuous pulsatile flow of blood if adhesion is not strong enough.

Whilst endothelialisation is considered a necessary requirement, interpreting endothelialisation studies in animal models is a challenge task. Despite countless years of research and the development of a great number of grafts which have, to a certain extent, endothelialised in a range of animal models, including sheep; none of them have successfully endothelialised in humans [292]. Even when grafts do form an endothelium, there is no guarantee that the EC are of the correct phenotype. EC have a wide range of functions and can range from the pro-thrombogenic to anti-thrombogenic. Previously, it has been shown that a fully endothelialised PTFE graft resulted in a greater degree of IH compared to the control PTFE graft [153]. This is likely to be a direct consequence of having EC in the wrong phenotype. The successful healing of a vascular graft is a great deal more complex, inflammation-mediated process as opposed to the rather simplistic view of mere endothelialisation [293–295].

9.4 From Lab to Patient

A 26 year old male had developed a right femoral artery pseudoaneurysm (FAP) following continued and repeated intravenous drug use. The repeated puncture wounds had resulted in a haematoma forming outside the artery wall as a result of a leaking hole in the artery. Whereas ligation and excision of the pseudoaneurysm, without revascularisation, is an accepted means of treatment in the majority of patients; in this case, the patient had presented late when complications such as bleeding, sepsis and limb ischaemia had occurred making management of the FAP more difficult. This resulted in the pseudoaneurysm rupturing (fig 9.5A) and acute interruption of femoral artery flow. In these circumstances a high probability of amputation is generally expected.

Once the clinical decision to restore femoral blood flow was made, a suitable conduit for reconstructing the infrainguinal vasculature was required. Although the GSV is the generally favoured conduit for lower extremity arterial reconstructions, its availability is restricted in patients with a history of drug abuse, as the superficial veins are commonly damaged by prolonged direct injections. Autologous arterial grafts were not considered due to the length of the conduit required. Autologous grafts are often severely limited in their use due to insufficient lengths. Consequently, prosthetic grafts are often the only viable option for arterial reconstructions in this subset of patients.

Ethical approval was granted to treat the patient with a POSS-PCU vascular graft, as opposed to the more conventionally used PTFE graft. PTFE grafts are prone to infection and thrombosis. A POSS-PCU graft was fabricated with an internal diameter of 5.1 mm and length of 300 mm. The graft was trimmed to the required length of 180 mm at the on-site and was used for an iliac to femoral reconstruction (fig 9.5).

Following implantation and on future examinations, no evidence of infection or thrombosis was witnessed. Further, the graft was monitored via Duplex Sonography. The Doppler waveform obtained from the reconstructed iliac-femoral artery demonstrated a low resistance profile with a characteristic triphasic Doppler signal throughout the cardiac cycle. An initial fast upstroke to peak systole was followed by reversal of blood flow during early diastole and a forward flow component during late diastole. Flow rates were found to be equivalent, both proximal and distal to the graft, with the peak systolic velocity approximately 60-80 cms^{-1}. The graft was implanted June 2011 and, as yet, appears to be fully patent and fully functioning. The patient is being monitored regularly, every 3 months, via Doppler ultrasound.

9.5 Conclusions

In this chapter, the functional behaviour and tissue compatibility of POSS-PCU vascular grafts was assessed *in vivo*. Grafts were implanted into the left carotid artery of 10 adult sheep for a period of 9 months. Grafts were monitored via Doppler sonography for patency. The compliance and flow rates were measured pre- and post-operatively as well as pre-explanting. Furthermore, the explanted grafts were exposed to histological examination. POSS-PCU vascular grafts exhibited a 70% patency rate whereas the PTFE grafts failed within the first 3 weeks of implantation. Grafts did not compromise the functional properties of the artery with flow rates

Figure 9.5: Digital images of (A) femoral artery pseudoaneurysm (B) exposed iliac artery proximal to pseudoaneurysm (C) POSS-PCU vascular graft (180 mm length) used for reconstruction (D) graft-iliac anastomosis (E) graft-femoral anastomosis and (F) complete reconstruction from the above groin iliac artery to the below groin femoral artery.

and compliance unchanged after grafting and comparable to the native right carotid artery. Despite the lack of a fully functioning endothelium, there was no sign of intimal thickening or hyperplasia even after 9 months implantation.

Following the animal trial, a POSS-PCU graft was used for clinical evaluation in a

human patient. The graft was used to treat an iliac-femoral pseudoaneurysm in a 26 year old male. To date, the graft is fully patent and functioning with no detrimental effects on perfusion efficiency.

10

Summary and Future Outlook

Prosthetic vascular grafts have been an integral tool of vascular surgery for over half a century. In this time, whilst large calibre grafts (>5 mm) have performed impressively, with patency rates in excess of 90% in the aorto-iliac position, the use of synthetic small calibre grafts has been met with failure [25, 26]. Despite continuous research, no clinically viable conduit has been developed which could help to meet the critical need for small calibre arterial replacements. Failure is often attributed to material surface thrombogenicity and the development of anastomotic IH.

A variety of paradigms have been explored, with sophisticated tissue engineering approaches dominating in recent years. However, despite the intensive research effort, little progress has been made in tackling the key drawbacks to using tissue engineering concepts, namely: cost, time, availability and lack of radial strength for exposure to the arterial circulation.

The research in this thesis aimed to develop a synthetic small calibre graft which has the functional properties to be used as an arterial replacement. By using a biomaterial, POSS-PCU, with improved biostability, blood compatibility and viscoelastic properties; it was hoped the two primary modes of graft failure could be alleviated.

The first challenge faced in this thesis was to develop a facile manufacturing method to produce vascular grafts less than 5 mm in diameter. The protocol had to be flexible to allow the production of grafts in a range of dimensions, depending on the clinical need or physiological requirement, with a degree of porosity and with mechanical properties resembling those of soft tissue. Phase separation was exploited as a means to produce porous membranes, and a bespoke extrusion machine was commissioned to produce cylindrical conduits. Key parameters in the extrusion-phase separation

method which affect the final graft dimensions and morphology were optimised. GPC and DSC analysis confirmed that in undergoing phase separation from solution, the POSS-PCU polymer was not damaged or degraded in any way. Furthermore, GCMS and ICP-OES were utilised to confirm that after extrusion, no impurities or additives (DMAc and $NaHCO_3$) remain in the grafts. Chapter 4 also explored changes in graft morphology (wall thickness, pore size and porosity); particularly in response to the addition of an inorganic filler, $NaHCO_3$ and the temperature at which phase separation takes place. The introduction of $NaHCO_3$ into the polymer matrix appeared to have a significant effect on graft morphology following phase separation. More homogenous, porous walls were produced with pore size increasing with the concentration of $NaHCO_3$. Wall thickness was also significantly reduced with the continued addition of $NaHCO_3$. At the completion of chapter 4, cylindrical conduits in a range of dimensions, pore sizes and porosities could be manufactured, in a reproducible and scalable manner, depending on the clinical need.

Following on from chapter 4, the functional properties of the manufactured grafts were assessed. The effect of 3 different wall thicknesses and 3 different porosities (corresponding to 3 different $NaHCO_3$ concentrations) on the dynamic mechanical properties of the grafts was investigated. Blood vessels have numerous complex functions; however, the primary role of any vessel is to transport blood efficiently. The ability of the different vascular grafts to propagate the blood flow was assessed in a physiological flow circuit. The strength of the graft was characterised in terms of suture retention force, an important parameter in the development of any arterial replacement. Finally, the feasibility of incorporating an external reinforcement to minimise graft kinking was evaluated. Phase separated, POSS-PCU grafts had tensile strength in excess of the native artery and suture retentions strengths in excess of the generally accepted value of 2N. The grafts were viscoelastic in nature, and displayed compliance profiles similar to the native iliac artery and were far more compliant than the current industry standard Dacron or PTFE grafts. Whilst the introduction of an external reinforcement did significantly improve the kink resistance of the grafts, the reinforcement eventually delaminated and separated from the graft. However, whilst the kink resistance improved with the introduction of an external reinforcement, the graft compliance suffered a dramatic decrease. The compliance values of externally reinforced grafts were below acceptable levels and closer to values associated with Dacron and PTFE grafts.

The aim of chapter 6 was to provide an extensive characterisation of the surface properties of vascular grafts as a precursor for assessing the biocompatibility of the

grafts. From previous studies, the cast sheet of POSS-PCU, that has not been subjected to phase separation, is known to be biocompatible, illicit a minimal immune response and is conducive to EC growth [183, 185]. The surfaces of phase separated POSS-PCU with 0, 35, 45 55% $NaHCO_3$ were compared and contrasted to the cast sheet. An initial characterisation of the surface chemistry was provided via SIMS and ATR-FTIR analysis. The key finding was that there is significantly less of the POSS moiety on the surface of the phase separated samples. The surface wettability was assessed using a goniometer. POSS-PCU is highly hydrophobic; however, following phase separation, the degree of hydrophobicity is reduced possibly as a consequence of fewer POSS moieties at the surface. The addition of $NaHCO_3$ caused a minor increase in the contact angle which can be attributed to an increase in surface roughness and exposure to an increased surface area which was a consequence on adding $NaHCO_3$. The major difference observed between the surfaces was that phase separating produces a significantly rougher surface and the addition of $NaHCO_3$ resulted in an open-pored surface. A histogram of pore size distribution was constructed which demonstrated that surface pore size was in the region of 5-10 μm. Finally, the substrate stiffness has recently been suggested to be an important mediator of cell function, and as such, it was characterised between the different samples. No significant difference was detected between the samples with all of them having a reduced modulus of circa 0.6 GPa.

Having characterised the surface properties of the grafts, biocompatibility of each surface was investigated using a wide range of assays. Grafts produced with $NaHCO_3$ appeared to activate the coagulation cascade the most as the concentration of kallikrein was most abundant on those surfaces. This is likely to be a result of the increase in surface area of the rougher substrates. Platelets were attached to the phase separated substrates far more so than the cast sample which also translated into the degree of activation. PBMC were culture on the different surfaces to assess the inflammatory potential of the grafts. After 7 days, PBMC were all highly activated and pro-inflammatory. A look at the cytokine release profiles confirmed these findings. However, the graft produced with 0 and 55% $NaHCO_3$ elicited the highest concentration of IL-10, an anti-inflammatory cytokine which can down-regulate the production of other pro-inflammatory cytokines. In looking at the endothelialisation potential of the different grafts, all of the surfaces adhered HUVEC and EPC. There were subtle differences in the rates of growth on the different grafts but cell growth was comparable to TCP control in the case of HUVEC. For EPC, growth was significantly less on the POSS-PCU compared to TCP; however no cytotoxic side effects were detected.

Having completed a thorough *in vitro* assessment of the grafts developed in chapter 4, a pre-clinical study was designed to examine the long term tissue compatibility and performance *in vivo*. Before grafts could be implanted a suitable sterilisation technique was sought which does not damage or degrade the graft material. In chapter 8, grafts were exposed to a very mild disinfectant, 70% EtOH, autoclaving and gamma irradiation. Ethanol did not harm the material properties but neither did it sterilise the grafts to an acceptable level. Gamma irradiation was a very successful steriliser but it caused severe damage to the biomaterial and resulted in cytotoxic side effects. Autoclaving was chosen as the optimal technique to sterilise the grafts as it was efficient in sterilising, maintained cell growth, and did not cause any significant damage to the material.

For the commencement of the animal study, a decision was required on which graft was best placed to withstand a long-term pre-clinical study. The decision was based primarily on the results from chapters 5 and 7. Taking into consideration that previous PU grafts are prone to radial dilation and mechanical fragility upon prolonged implantation *in vivo*, the graft produced with 0% $NaHCO_3$ was chosen for pre-clinical evaluation. It displayed compliant behaviour independent of pressure, so it was thought that it was least likely to enlarge circumferentially compared to the other graft samples. It also had an acceptable immune response and sustained EC growth. The graft was implanted into the left carotid artery of 10 sheep, and on immediate implantation, no significant difference was seen between compliance and blood flow rates in the native artery of the grafted artery. After implantation for 9 months, the compliance and flow rates were assessed again and there still were no significant differences between the grafted and native artery. The patency rate of the grafts were 70% with 3 grafts failing very early in the trial due to thrombus formation. The PTFE grafts used as controls in this study all failed due to thrombosis within 3 weeks. Histology results confirmed tissue ingrowth from the adventitial side of the POSS-PCU grafts, but no cellularisation was seen on the luminal side.

Following on from the results of the pre-clinical trial; an initial clinical evaluation was undertaken by implanting the graft into a 26 year old male, human patient, with a FAP. At the time of writing, the graft is patent and fully functioning.

In the absence of autologous conduits, POSS-PCU grafts offer a viable alternative for vascular surgeons to use in small calibre applications such as the peripheral and coronary circulation. Whilst there is room for improvement we believe the grafts developed in this thesis can be successfully translated to clinical practice. In comparing

POSS-PCU grafts with PTFE, the POSS-PCU grafts performed considerably better.

10.1 Further Work

Having conducted a pre-clinical trial in an ovine model, the next step would be for a clinical trial to test the efficacy of POSS-PCU grafts in humans. Regulatory approval is being sought to commence a clinical trial with POSS-PCU grafts acting as arteriovenous grafts for kidney dialysis. The model is relatively low risk with failure being non-fatal.

Further studies to improve the thrombogenicity of the grafts are also merited. The graft can be functionalised with a range of chemistries to include, amongst other things, NO donors, popular anticoagulants, such as heparin and hirudin, and proteins such as Protein C – an anti-coagulant found on the surface of EC. Further, a robust model should be developed which can assess blood compatibility of the substrates under flow. Flow is an important mediator in blood-material interactions, and to get a better understanding of the performance materials, they should be examined in *ex vivo* conditions.

Similarly, strategies to improve endothelialisation of the graft by functionalising the biomaterial can be developed. A great number of peptides and proteins have been reported to improve endothelialisation ranging from CD34 to RGD. Care should be taken to ensure that the EC grown on the material are of the correct phenotype.

Looking to the future, the work presented in this thesis can be relatively easily translated into tissue engineering paradigms. Tissue engineering a blood vessel initially requires a scaffold which at the time of implantation displays the physical characteristics of an ideal vascular graft. Once implanted, the graft should slowly biodegrade being replaced by regenerated tissue, without compromising the functional properties of the graft. The graft manufacturing and assessment techniques presented in this thesis are all valid for assessing a tissue engineering scaffold. The biomaterial would require re-formulation to include a biodegradable component, ideally without compromising the initial mechanical properties. The degradation rates would have to be carefully characterised and matched with the regeneration rates of vascular tissue.

Publications and Presentations

M. Desai, **M. Ahmed**, Z. You, G. Hamilton, A. Seifalian, "An aortic model for the physiological assessment of endovascular stent-grafts", *Annals of Vascular Surgery*, 2011, 25(4), 530-537

M. Ahmed, H. Ghanbari, B. Cousins, G. Hamilton, A. Seifalian, "Small calibre POSS-nanocomposite cardiovascular grafts: influence of porosity on the structure, haemocompatibility and mechanical properties ", *Acta Biomaterialia*, 2011, 7(11), 3857-67

M. Ahmed, L. Yildrimer, A. Khademhosseini, A. Seifalian, "Nanostructured Materials for Cardiovascular Tissue Engineering", *Journal of Nanoscience and Nanotechnology*, *in press*

M. Ahmed, G. Punshon, A. Seifalian, "Impact of sterilising technique on POSS nanocomposites", *Journal of Biomaterials Applications*, *submitted*

M. Ahmed, L. Bozec, A. Seifalian, "Porous membranes via phase separation: biomimetic surfaces for cell growth", *in preparation*

M. Ahmed, G. Punshon, A. Seifalian, "The long term implantation of a POSS-PCU vascular graft: an *in vivo* study", *in preparation*

M. Ahmed and A. Seifalian, "Organs from Nanomaterials" in *Handbook of Nanophysics: Nanomedicine and Nanorobotics*, CRC Press, **2010**, Chapter 19

M. Ahmed, G. Hamilton and A. Seifalian"Viscoelastic behaviour of a small calibre vascular graft made from a POSS-nanocomposite" *Conf Proc IEEE Eng Med Biol Soc*, **2010**, pp 251-254, Buenos Aires, Argentina

M. Ahmed and A. Seifalian"*In vitro* inflammatory potential of a 3D, porous, POSS/Polyurethane Nanocomposite Scaffold for Vascular Tissue Engineering" EUPOC2011: Biobased polymers and related biomaterials, Lake Gargnano, Italy, **2011**

H. Ghanbari, **M. Ahmed**, B. Cousins, G. Hamilton, A. Seifalian, "Enhanced haemocompatibility of POSS nanocomposite: a material of choice for cardiovascular application", Society of Academic & Research Surgery **2011**

M. Desai, A. Darbyshire, R. Bakhshi, **M. Ahmed**, A. Seifalian, G. Hamilton, "Thermo-Mechanical Resistance of a Nanocomposite Polymer Exposed to Simulated in Vivo Hydrodynamic Fatigue for 10 Years in Development of a Sutureless Endovascular Stent-Graft", Annual Vascular Meeting, **2011**

M. Desai, A. Darbyshire, **M. Ahmed**, R. Bakhshi, A. Seifalian, G. Hamilton, "Development Of An Innovative Endovascular Stent-graft For Aortic Aneurysms Using A Nanocomposite Polymer", International Society for Applied Cardiovascular Biology, **2010**

Bibliography

[1] P. Scarborough, P. Bhatnagar, K. Wickramasinghe, K. Smolina, C. Mitchell, and M. Rayner, "Cardiovascular disease statistics: 2010 update," *BHF Statistics database*, p. www.heartstats.org, 2010.

[2] S. M. Weis and D. A. Cheresh, "Pathophysiological consequences of vegf-induced vascular permeability," *Nature*, vol. 437, pp. 497–504, 2005.

[3] R. M. Rao, L. Yang, G. Garcia-Cardena, and F. W. Luscinskas, "Endothelial-dependent mechanisms of leukocyte recruitment to the vascular wall," *Circ Res*, vol. 101, no. 3, pp. 234–247, 2007.

[4] T. Minami, A. Sugiyama, S. Q. Wu, R. Abid, T. Kodama, and W. C. Aird, "Thrombin and phenotypic modulation of the endothelium," *Arterioscler Thromb Vasc Biol*, vol. 24, no. 1, pp. 41–53, 2004.

[5] G. K. Owens, M. S. Kumar, and B. R. Wamhoff, "Molecular regulation of vascular smooth muscle cell differentiation in development and disease," *Physiol Rev*, vol. 84, no. 3, pp. 767–801, 2004.

[6] D. D. Gutterman, "Adventitia-dependent influences on vascular function," *Am J Physiol*, vol. 277, no. 4, pp. H1265–H1272, 1999.

[7] Z. Teng, D. Tang, J. Zheng, P. K. Woodard, and A. H. Hoffman, "An experimental study on the ultimate strength of the adventitia and media of human atherosclerotic carotid arteries in circumferential and axial directions," *J Biomech*, vol. 42, no. 15, pp. 2535–2539, 2009.

[8] R. R. Ross, "Atherosclerosis: an inflammatory disease," *New Eng J Med*, vol. 340, no. 2, pp. 115–126, 1999.

[9] M. A. Gimbrone, "Vascular endothelium, hemodynamic forces, and atherogenesis," *Am J Physiol*, vol. 155, no. 1, pp. 1–5, 1999.

[10] P. D. Weinberg, "Rate-limiting steps in the development of atherosclerosis: The response-to-influx theory," *J Vasc Res*, vol. 41, pp. 1–17, 2004.

[11] T. R. Pedersen, J. Kjekshus, K. Pyrl, A. G. Olsson, T. J. Cook, T. A. Musliner, J. A. Tobert, and T. Haghfelt, "Effect of simvastatin on ischemic signs and symptoms in the scandinavian simvastatin survival study (4s)," *Am J Cardiol*, vol. 81, no. 3, pp. 333–335, 1998.

[12] A. S. Go, C. Iribarren, M. Chandra, P. V. Lathon, S. P. Fortmann, T. Quertermous, and M. A. Hlatky, "Statin and beta-blocker therapy and the initial presentation of coronary heart disease," *Ann Intern Med*, vol. 44, no. 4, pp. 229–238, 2006.

[13] K. Radack and C. Deck, "Beta-adrenergic blocker therapy does not worsen intermittent claudication in subjects with peripheral arterial disease. a meta-analysis of randomized controlled trials," *Arch Intern Med*, vol. 155, no. 9, pp. 1769–1776, 1991.

[14] J. C. Merritt and D. L. Bhatt, "The efficacy and safety of perioperative antiplatelet therapy," *J Thromb Thrombolysis*, vol. 13, no. 2, pp. 97–103, 2002.

[15] E. Braunwald, D. Angiolillo, E. Bates, P. B. Berger, D. Bhatt, C. P. Cannon, M. I. Furman, P. Gurbel, A. D. Michelson, E. Peterson, and S. Wiviott, "Antiplatelet strategies: Evaluating their current role in the setting of acute coronary syndromes," *Clin Cardiol*, vol. 31, pp. I1–I9, 2008.

[16] W. E. Boden, R. A. O'Rourke, K. K. Teo, and *et al*, "Optimal medical therapy with or without pci for stable coronary disease," *New Eng J Med*, vol. 356, pp. 1503–1516, 2007.

[17] J. Ederle, J. Dobson, R. L. Featherstone, and *et al*, "Carotid artery stenting compared with endarterectomy in patients with symptomatic carotid stenosis (international carotid stenting study): an interim analysis of a randomised controlled trial," *Lancet*, vol. 375, no. 9719, pp. 985–997, 2010.

[18] E. L. Hannan, M. J. Racz, G. Walford, R. H. Jones, T. J. Ryan, E. Bennett, A. T. Culliford, O. W. Isom, J. P. Gold, and E. A. Rose, "Long term outcomes of coronary-artery bypass grafting versus stent implantation," *New Eng J Med*, vol. 352, pp. 2174–2183, 2005.

[19] B. F. Buxton, P. A. R. Hayward, A. E. Newcomb, S. Moten, S. Seevanayagam, and I. Gordon, "Choice of conduits for coronary artery bypass grafting: craft or science?," *Eur J Cardiothorac Surg*, vol. 35, pp. 658–670, 2009.

[20] E. A. Lefrak, "The internal mammary artery bypass graft: Praise versus practice," *Tex Heart Inst J*, vol. 14, no. 2, pp. 139–143, 1987.

[21] G. D. Angelini and A. Newby, "The future of saphenous vein as a coronary artery bypass," *Eur Heart J*, vol. 10, no. 3, pp. 273–280, 1988.

[22] P. J. Shah, I. Gordon, J. Fuller, S. Seevanayagam, A. Rosalion, J. Tatoulis, J. S. Raman, and B. F. Buxton, "Factors affecting saphenous vein graft patency: clinical and angiographic study in 1402 symptomatic patients operated on between 1977 and 1999," *J Thorac Cardiovasc Surg*, vol. 126, pp. 1972–1977, 2003.

[23] T. J. B. Ferguson, B. G. Hammill, E. D. Peterson, E. R. DeLong, and F. L. Grover, "A decade of changing risk profiles and outcomes for isolated coronary artery bypass grafting procedures, 1990–1999: a report from the sts national database committee and the duke clinical research institute," *Ann Thorac Surg*, vol. 73, pp. 480–489, 2002.

[24] R. D. Sayers, S. Raptis, M. Berce, and J. H. Miller, "Long-term results of femorotibial bypass with vein or polytetrafluoroethylene," *Br J Surg*, vol. 85, no. 7, pp. 934–938, 2003.

[25] M. R. Prager, P. Polterauer, H.-J. Bhmig, O. Wagner, A. Fgl, G. Kretschmer, M. Plohner, J. Nanobashvili, and M. Huk, "Collagen versus gelatin-coated dacron versus stretch polytetrafluoroethylene in abdominal aortic bifurcation graft surgery: Results of a seven-year prospective, randomized multicenter trial," *Surgery*, vol. 130, pp. 408–414, 2001.

[26] M. R. Prager, T. Hoblaj, J. Nanobashvili, E. Sporn, P. Polterauer, O. Wagner, H. J. Bhmig, H. Teufelsbauer, M. Ploner, and I. Huk, "Collagen- versus gelatine-coated dacron versus stretch ptfe bifurcation grafts for aortoiliac occlusive disease: Long-term results of a prospective, randomized multicenter trial," *Surgery*, vol. 134, pp. 80–88, 2003.

[27] S. Posta, T. Krausb, U. Mller-Reinartzc, C. Weissd, H. Kortmanne, A. Quentmeierd, M. Winklera, K. J. Husfeldtc, and J. R. Allenberg, "Dacron vs polytetrafluoroethylene grafts for femoropopliteal bypass: a prospective randomised multicentre trial," *Eur J Vasc Endovasc Surg*, vol. 22, no. 3, pp. 226–231, 2001.

[28] R. J. van Det, B. H. Vriens, J. van der Palen, and R. H. Geelkerken, "Dacron or eptfe for femoro-popliteal above-knee bypass grafting: short and long-term results of a multicentre randomised trial," *Eur J Vasc Endovasc Surg*, vol. 37, no. 4, pp. 457–463, 2009.

[29] M. S. Conte, "The ideal small arterial substitute: a search for the holy grail?," *FASEB J*, vol. 12, pp. 43–45, 1998.

[30] K. Stokes, R. McVenes, and J. M. Anderson, "Polyurethane elastomer biostability,," *J Biomater Appl*, vol. 9, no. 4, pp. 321–354,, 1995.

[31] A. M. Seifalian, H. J. Salacinski, A. Tiwari, A. Edwards, S. Bowald, and G. Hamilton, "In vivo biostability of a poly(carbonate-urea)urethane graft," *Biomaterials*, vol. 24, no. 12, pp. 2549–2557, 2003.

[32] H. F. Galley and N. R. Webster, "Physiology of the endothelium," *Br J Anaesth*, vol. 93, no. 1, pp. 105–113, 2004.

[33] B. Furie and B. C. Furie, "Mechanisms of thrombus formation," *N Engl J Med*, vol. 359, no. 9, pp. 938–949, 2008.

[34] M. B. Gorbet and M. V. Sefton, "Biomaterial-associated thrombosis: roles of coagulation factors, complement, platelets and leukocytes," *Biomaterials*, vol. 25, pp. 5681–5703, 2004.

[35] G. Davi and C. Patrono, "Platelet activation and atherothrombosis," *New Eng J Med*, vol. 357, pp. 2482–2494, 2007.

[36] A. Andrieux, G. Hudry-Clergeon, J. J. Ryckewaert, A. Chapel, M. H. Ginsberg, E. F. Plow, and G. Marguerie, "Amino acid sequences in fibrinogen mediating its interaction with its platelet receptor, gpiib/iiia," *J Biol Chem*, vol. 264, pp. 9258–9265, 1989.

[37] A. C. Newby and A. B. Zaltsman, "Molecular mechanisms in intimal hyperplasia," *J Pathol*, vol. 190, no. 3, pp. 300–309, 2000.

[38] M. R. Ward, P. S. Tsao, A. Agrotis, R. J. Dilley, G. L. Jennings, and A. Bobik, "Low blood flow after angioplasty augments mechanisms of restenosis: inward vessel remodeling, cell migration, and activity of genes regulating migration," *Arterioscler Thromb Vasc Biol*, vol. 21, no. 2, pp. 208–213, 2001.

[39] R. Vashisht, M. Sian, and P. J. Franks, "Long-term reduction of intimal hyperoplasia by the selective alpha-1 adrenergic antagonist doxazosin," *Br J Surg*, vol. 792, no. 12, p. 1285, 1992.

[40] L. W. Kraiss and A. W. Clowes, *The Basic Science of Vascular Disease.* Futura Publishing Company Inc, 1997.

[41] G. Murphy and A. J. Docherty, "The matrix metalloproteinases and their inhibitors," *Am J Respir Cell Mol Biol*, vol. 7, no. 2, pp. 120–125, 1992.

[42] H. Haruguchi and S. Teraoka, "Intimal hyperplasia and hemodynamic factors in arterial bypass and arteriovenous grafts: a review," *Journal of Artificial Organs*, vol. 6, no. 4, pp. 227–235, 2003.

[43] A. Dardik, A. Yamashita, F. Aziz, H. Asada, and B. E. Sumpio, "Shear stress-stimulated endothelial cells induce smooth muscle cell chemotaxis via platelet-derived growth factor-bb and interleukin-1alpha," *J Vasc Surg*, vol. 41, no. 2, pp. 321–331, 2005.

[44] R. Palumbo, C. Gaetano, A. Antonini, G. Pompilio, E. Bracco, L. Rnnstrand, C. H. Heldin, and M. C. Capogrossi, "Different effects of high and low shear stress on platelet-derived growth factor isoform release by endothelial cells: consequences for smooth muscle cell migration," *Arterioscler Thromb Vasc Biol*, vol. 22, no. 3, pp. 405–411, 2002.

[45] D. P. Giddens, C. K. Zarins, and S. Glagov, "The role of fluid mechanics in the localization and detection of atherosclerosis," *J Biomech Eng*, vol. 115, pp. 588–594, 1993.

[46] L. W. Kraiss, T. R. Kirkman, T. R. Kohler, B. Zierler, and A. W. Clowes, "Shear stress regulates smooth muscle proliferation and neointimal thickening in porous polytetrafluoroethylene grafts," *Arterioscler Thromb*, vol. 11, pp. 1844–1852, 1991.

[47] S. W. Lee, L. Antiga, and D. A. Steinman, "Correlations among indicators of disturbed flow at the normal carotid bifurcation," *J Biomech Eng*, vol. 131, no. 6, p. 061013, 2009.

[48] R. S. Keynton, M. M. Evancho, R. L. Sims, N. V. Rodway, A. Gobin, and S. E. Rittgers, "Intimal hyperplasia and wall shear in arterial bypass graft distal anastomoses: an in vivo model study," *J Biomech Eng*, vol. 123, pp. 464–473, 2001.

[49] H. S. Bassiouny, S. White, S. Glagov, E. Choi, D. P. Giddens, and C. K. Zarins, "Anastomotic intimal hyperplasia: Mechanical injury or flow induced," *J Vasc Surg*, vol. 15, pp. 708–716, 1992.

[50] D. N. Ku, D. P. Giddens, C. K. Zarins, and S. Glagov, "Pulsatile flow and atherosclerosis in the human carotid bifurcation. positive correlation between plaque location and low oscillating shear stress," *Arteriosclerosis*, vol. 5, pp. 293–302, 1985.

[51] K. A. Barbee, T. Mundel, R. Lal, and P. F. Davies, "Subcellular distribution of shear stress at the surface of flow-aligned and nonaligned endothelial monolayers," *A J Physiol*, vol. 268, pp. H1765–H1772,, 1995.

[52] M. A. Gimbrone, T. Nagle, and J. N. Topper, "Biomechanical activation: an emerging paradigm in endothelial adhesion biology," *J Clin Invest*, vol. 99, pp. 1809–1813, 1997.

[53] W. M, Abbott, J. Megerman, J. E. Hasson, G. L'Italien, and D. F. Warnock, "Effect of compliance mismatch on vascular graft patency," *J Vasc Surg*, vol. 5, no. 2, pp. 376–382, 1987.

[54] W. Trubel, H. Schima, A. Moritz, F. Raderer, A. Windisch, R. Ullrich, U. Windberger, U. Losert, and P. Polterauer, "Compliance mismatch and formation of distal anastomotic intimal hyperplasia in externally stiffened and lumen-adapted venous grafts," *Eur J Vasc Endovasc Surg*, vol. 10, no. 4, pp. 415–423, 1995.

[55] S. J. Lee, J. Liu, S. H. Oh, S. Soker, A. Atala, and J. J. Yoo, "Development of a composite vascular scaffolding system that withstands physiological vascular conditions," *Biomaterials*, vol. 29, p. 28912898, 2008.

[56] Y. M. Ju, J. S. Choi, A. Atala, J. J. Yoo, and S. J. Lee, "Bilayered scaffold for engineering cellularized blood vessels," *Biomaterials*, vol. 31, no. 15, pp. 4313–4321, 2010.

[57] M. R. Williamson, R. Black, and C. Kielty, "Pclpu composite vascular scaffold production for vascular tissue engineering: Attachment, proliferation and bioactivity of human vascular endothelial cells," *Biomaterials*, vol. 27, p. 36083616, 2006.

[58] A. Nieponice, L. Soletti, J. Guan, B. M. Deasy, J. Huard, W. R. Wagner, and D. A. Vorp, "Development of a tissue-engineered vascular graft combining a biodegradable scaffold, muscle-derived stem cells and a rotational vacuum seeding technique," *Biomaterials*, vol. 29, no. 7, pp. 825–833, 2008.

[59] L. Soletti, Y. Hong, J. Guan, J. J. Stankus, M. S. El-Kurdi, W. R. Wagner, and D. A. Vorp, "A bilayered elastomeric scaffold for tissue engineering of small diameter vascular grafts," *Acta Biomater*, vol. 6, no. 1, pp. 110–122, 2010.

[60] A. Nieponice, L. Soletti, J. Guan, Y. Hong, B. Gharaibeh, T. M. Maul, J. Huard, W. R. Wagner, and D. A. Vorp, "In vivo assessment of a tissue-engineered vascular graft combining a biodegradable elastomeric scaffold and muscle-derived stem cells in a rat model," *Tissue Eng Part A*, vol. 16, no. 4, pp. 1215–1223, 2010.

[61] S. G. Wise, M. J. Byrom, A. Waterhouse, P. G. Bannon, M. K. Ng, and A. S. Weiss, "A multilayered synthetic human elastin/polycaprolactone hybrid vascular graft with tailored mechanical properties," *Acta Biomater*, vol. 7, no. 1, pp. 295–303, 2011.

[62] B. Tschoeke, T. C. Flanagan, S. Koch, M. S. Harwoko, T. Deichmann, V. Ell, J. S. Sachweh, M. Kellomki, T. Gries, T. Schmitz-Rode, and S. Jockenhoevel, "Tissue-engineered small-caliber vascular graft based on a novel biodegradable composite fibrin-polylactide scaffold," *Tissue Eng Part A*, vol. 15, no. 8, pp. 1909–1918, 2009.

[63] S. Koch, T. C. Flanagan, J. S. Sachweh, F. Tanios, H. Schnoering, T. Deichmann, V. Ell, M. Kellomki, N. Gronloh, T. Gries, R. Tolba, T. Schmitz-Rode, and S. Jockenhoevel, "Fibrin-polylactide-based tissue-engineered vascular graft in the arterial circulation," *Biomaterials*, vol. 31, no. 17, pp. 4731–4739, 2010.

[64] S. Enomoto, M. Sumi, K. Kajimoto, Y. Nakazawa, R. Takahashi, C. Takabayashi, T. Asakura, and M. Sata, "Long-term patency of small-diameter vascular graft made from fibroin, a silk-based biodegradable material," *J Vasc Surg*, vol. 51, no. 1, pp. 155–156, 2010.

[65] Y. Nakazawa, M. Sato, R. Takahashi, D. Aytemiz, C. Takabayashi, T. Tamura, S. Enomoto, M. Sata, and T. Asakura, "Development of small-diameter vascular grafts based on silk fibroin fibers from bombyx mori for vascular regeneration," *J Biomater Sci Polym Ed*, vol. 22, no. 1-3, pp. 195–206, 2011.

[66] M. P. Brennan, A. Dardik, N. Hibino, J. D. Roh, G. N. Nelson, X. Papademitris, T. Shinoka, and C. K. Breuer, "Tissue-engineered vascular grafts demonstrate evidence of growth and development when implanted in a juvenile animal model," *Ann Surg*, vol. 248, no. 3, pp. 370–377, 2008.

[67] N. Hibino, E. McGillicuddy, G. Matsumura, Y. Ichihara, Y. Naito, C. Breuer, and T. Shinoka, "Late-term results of tissue-engineered vascular grafts in humans," *J Thorac Cardiovasc Surg*, vol. 139, no. 2, pp. 431–6, 436.e1–2, 2010.

[68] J. Gao, A. E. Ensley, R. M. Nerem, and Y. Wang, "Poly(glycerol sebacate) supports the proliferation and phenotypic protein expression of primary baboon vascular cells," *J Biomed Mater Res A*, vol. 83, no. 4, pp. 1070–1075, 2007.

[69] D. Motlagh, J. Yang, K. Y. Lui, A. R. Webb, and G. A. Ameer, "Hemocompatibility evaluation of poly(glycerol-sebacate) in vitro for vascular tissue engineering," *Biomaterials. 2006 Aug;27(24):4315-24*, vol. 27, no. 24, pp. 4315–4324, 2006.

[70] W. Wu, R. Allen, J. Gao, and Y. Wang, "Artificial niche combining elastomeric substrate and platelets guides vascular differentiation of bone marrow mononuclear cells," *Tissue Eng Part A*, vol. doi:10.1089/ten.tea.2010.0550, 2011.

[71] S. T. Rashid, B. Fuller, G. Hamilton, and A. M. Seifalian, "Tissue engineering of a hybrid bypass graft for coronary and lower limb bypass surgery," *FASEB J*, vol. 22, no. 6, pp. 2084–2089, 2008.

[72] L. Gui, L. Zhao, R. W. Spencer, A. Burghouwt, M. S. Taylor, S. W. Shalaby, and L. E. Niklason, "Development of novel biodegradable polymer scaffolds for vascular tissue engineering," *Tissue Eng Part A*, vol. 17, no. 9-10, pp. 1191–1200, 2011.

[73] S. P. Hoerstrup, I. Cummings, M. Lachat, F. J. Schoen, R. Jenni, S. Leschka, S. Neuenschwander, D. Schmidt, A. Mol, C. Gnter, M. Gssi, M. Genoni, and G. Zund, "Functional growth in tissue-engineered living, vascular grafts: follow-up at 100 weeks in a large animal model," *Circulation*, vol. 114, no. 1 Suppl, pp. I159–I166, 2006.

[74] I. Cummings, S. George, J. Kelm, D. Schmidt, M. Y. Emmert, B. Weber, G. Znd, and S. P. Hoerstrup, "Tissue-engineered vascular graft remodeling in a growing lamb model: expression of matrix metalloproteinases," *Eur J Cardiothorac Surg*, 2011.

[75] S. P. Higgins, A. K. Solan, and L. E. Niklason, "Effects of polyglycolic acid on porcine smooth muscle cell growth and differentiation," *J Biomed Mater Res A*, vol. 67A, no. 1, pp. 295–302, 2003.

[76] R. Ross, "The pathogenesis of atherosclerosis: a perspective for the 1990s," *Nature*, vol. 362, pp. 801–809, 1993.

[77] C. B. Weinberg and E. Bell, "A blood vessel model constructed from collagen and cultured vascular cells," *Science*, vol. 231, no. 4736, pp. 397–400, 1986.

[78] L. Buttafoco, N. G. K. P. Engbers-Buijtenhuijs, A. A. Poot, P. J. Dijkstra, I. Vermes, and J. Feijen, "Electrospinning of collagen and elastin for tissue engineering applications," *Biomaterials*, vol. 27, no. 5, pp. 724–734, 2006.

[79] F. L. Nicolas and C. H. Gagnieu, "Denatured thiolated collagen. ii. cross-linking by oxidation," *Biomaterials*, vol. 18, no. 11, pp. 815–821, 1997.

[80] M. Baguneid, D. Murray, H. J. Salacinski, B. Fuller, G. Hamilton, M. Walker, and A. M. Seifalian, "Shear-stress preconditioning and tissue engineering-

based paradigms for generating arterial substitutes," *Biotechnol Appl Biochem*, vol. 39, no. 2, pp. 151–157, 2004.

[81] V. Charulatha and A. Rajaram, "Influence of different crosslinking treatments on the physical properties of collagen membranes," *Biomaterials*, vol. 24, no. 5, pp. 759–767, 2003.

[82] J. Hirai and T. Matsuda, "Self-organized, tubular hybrid vascular tissue composed of vascular cells and collagen for low-pressure-loaded venous system," *Cell Transplant*, vol. 4, no. 6, pp. 597–608, 1995.

[83] E. Uchimura, Y. Sawa, S. Taketani, Y. Yamanaka, M. Hara, H. Matsuda, and J. Miyake, "Novel method of preparing acellular cardiovascular grafts by decellularization with poly(ethylene glycol)," *J Biomed Mater Res A*, vol. 67A, no. 3, pp. 834–837, 2003.

[84] S. L. M. Dahl, J. Koh, V. Prabhakar, and L. E. Niklason, "Decellularized native and engineered arterial scaffolds for transplantation," *Cell Transplant*, vol. 12, pp. 659–666, 2003.

[85] D. W. Courtman, C. A. Pereira, V. K. D. McComb, J. M. Lee, and G. J. Wilson, "Development of a pericardial acellular matrix biomaterial: biochemical and mechanical effects of cell extraction," *J Biomed Mater Res A*, vol. 28, no. 6, pp. 655–666, 1993.

[86] H.-W. Sung, C.-S. Hsu, H. C. Chen, H. L. Hsu, Y. Chang, J. H. Lu, and P. C. Yang, "Fixation of various porcine arteries with an epoxy compound," *Artif Organs*, vol. 21, pp. 50–58, 1997.

[87] S. F. Badylak, R. Record, K. Lindberg, J. Hodde, and K. Park, "Small intestinal submucosa: a substrate for in vitro cell growth," *J Biomater Sci Polym Ed*, vol. 9, no. 8, pp. 863–878, 1998.

[88] S. Nemcova, A. A. Noel, C. J. Jost, P. Gloviczki, V. M. Miller, and K. G. M. Brockbank, "Evaluation of a xenogeneic acellular collagen matrix as a small-diameter vascular graft in dogs-preliminary observations," *J Invest Surg*, vol. 14, no. 6, pp. 321–330, 2001.

[89] L. Gui, A. Muto, S. A. Chan, C. K. Breuer, and L. E. Niklason, "Development of decellularized human umbilical arteries as small-diameter vascular grafts," *Tissue Eng Part A*, vol. 15, no. 9, pp. 2665–2676, 2009.

[90] Y. Zhao, S. Zhang, J. Zhou, J. Wang, M. Zhen, Y. Liu, J. Chen, and Z. Qi, "The development of a tissue-engineered artery using decellularized scaffold

and autologous ovine mesenchymal stem cells," *Biomaterials*, vol. 31, no. 2, pp. 296–307, 2010.

[91] J. Yamashita, H. Itoh, M. Hirashima, M. Ogawa, S. Nishikawa, T. Yurugi, M. Naito, K. Nakao, and S. Nishikawa, "Flk1-positive cells derived from embryonic stem cells serve as vascular progenitors," *Nature*, vol. 408, no. 6808, pp. 92–96, 2000.

[92] Z. Z. Wang, P. Au, T. Chen, Y. Shao, L. M. Daheron, H. Bai, M. Arzigian, D. Fukumura, R. K. Jain, and D. T. Scadden, "Endothelial cells derived from human embryonic stem cells form durable blood vessels in vivo," *Nat Biotechnol*, vol. 25, no. 3, pp. 317–318, 2007.

[93] L. G. Villa-Diaz, H. Nandivada, J. Ding, N. C. N. de Souza, P. H. Krebsbach, K. S. O'Shea, J. Lahann, and G. D. Smith, "Synthetic polymer coatings for long-term growth of human embryonic stem cells," *Nat Biotechnol*, vol. 28, no. 6, pp. 581–583, 2010.

[94] Y. C. Toh and J. V. J, "Fluid shear stress primes mouse embryonic stem cells for differentiation in a self-renewing environment via heparan sulfate proteoglycans transduction," *FASEB J*, vol. 25, no. 4, pp. 1208–1217, 2011.

[95] R. Tatsumi, Y. Suzuki, T. Sumi, M. Sone, H. Suemori, and N. Nakatsuji, "Simple and highly efficient method for production of endothelial cells from human embryonic stem cells," *Cell Transplant*, 2010.

[96] A. Blancas, A. Shih, N. Lauer, and K. E. McCloskey, "Endothelial cells from embryonic stem cells in chemically defined medium," *Stem Cells Dev*, 2011.

[97] K. Schenke-Layland, K. E. Rhodes, E. Angelis, Y. Butylkova, S. Heydarkhan-Hagvall, C. Gekas, R. Zhang, J. I. Goldhaber, H. K. Mikkola, K. Plath, and W. R. MacLellan, "Reprogrammed mouse fibroblasts differentiate into cells of the cardiovascular and hematopoietic lineages," *Stem Cells*, vol. 26, no. 6, pp. 1537–1546, 2008.

[98] A. Haase, R. Olmer, K. Schwanke, S. Wunderlich, S. Merkert, C. Hess, R. Zweigerdt, I. Gruh, J. Meyer, S. Wagner, L. S. Maier, D. W. Han, S. Glage, K. Miller, P. Fischer, H. R. Schler, and U. Martin, "Generation of induced pluripotent stem cells from human cord blood," *Cell Stem Cell*, vol. 5, no. 4, pp. 434–441, 2009.

[99] Q. Lian, Y. Zhang, J. Zhang, H. K. Zhang, X. Wu, Y. Zhang, F. F. Lam, S. Kang, J. C. Xia, W. H. Lai, K. W. Au, Y. Y. Chow, C. W. Siu, C. N.

Lee, and H. F. Tse, "Functional mesenchymal stem cells derived from human induced pluripotent stem cells attenuate limb ischemia in mice," *Circulation*, vol. 121, no. 9, pp. 1113–1123, 2010.

[100] C. Xie, J. Hu, H. Ma, J. Zhang, L. J. Chang, Y. E. Chen, and P. X. Ma, "Three-dimensional growth of ips cell-derived smooth muscle cells on nanofibrous scaffolds," *Biomaterials*, vol. 32, no. 19, pp. 4369–4375, 2011.

[101] R. Quarto, M. Mastrogiacomo, R. Cancedda, S. M. Kutepov, V. Mukhachev, A. Lavroukov, E. Kon, and M. Marcacci, "Repair of large bone defects with the use of autologous bone marrow stromal cells," *N Engl J Med*, vol. 344, no. 5, pp. 385–386, 2001.

[102] F. Colazzo, A. H. Chester, P. M. Taylor, and M. H. Yacoub, "Induction of mesenchymal to endothelial transformation of adipose-derived stem cells," *J Heart Valve Dis*, vol. 19, no. 6, pp. 736–744, 2010.

[103] A. Mirza, J. M. Hyvelin, G. Y. Rochefort, P. Lermusiaux, D. Antier, B. Awede, P. Bonnet, J. Domenech, and V. Eder, "Undifferentiated mesenchymal stem cells seeded on a vascular prosthesis contribute to the restoration of a physiologic vascular wall," *J Vasc Surg*, vol. 47, no. 6, pp. 1313–1321, 2008.

[104] Z. Gong and L. E. Niklason, "Small-diameter human vessel wall engineered from bone marrow-derived mesenchymal stem cells (hmscs)," *FASEB J*, vol. 22, no. 6, pp. 1635–1648, 2008.

[105] P. D. Coppi, G. B. Jr, M. M. Siddiqui, T. Xu, C. C. Santos, L. Perin, G. Mostoslavsky, A. C. Serre, E. Y. Snyder, J. J. Yoo, M. E. Furth, S. Soker, and A. Atala, "Isolation of amniotic stem cell lines with potential for therapy," *Nat Biotechnol*, vol. 25, no. 1, pp. 100–106, 2007.

[106] P. Zhang, J. Baxter, K. Vinod, T. N. Tulenko, and P. J. D. Muzio, "Endothelial differentiation of amniotic fluid-derived stem cells: synergism of biochemical and shear force stimuli.," *Stem Cells Dev*, vol. 118, no. 9, pp. 1299–1308, 2009.

[107] Y. C. Yeh, H. J. Wei, W. Y. Lee, C. L. Yu, Y. Chang, L. W. Hsu, M. F. Chung, M. S. Tsai, S. M. Hwang, and H. W. Sung, "Cellular cardiomyoplasty with human amniotic fluid stem cells: in vitro and in vivo studies," *Tissue Eng Part A*, vol. 16, no. 6, pp. 1925–1936, 2010.

[108] M. Teodelinda, C. Michele, C. Sebastiano, C. Ranieri, and G. Chiara, "Amniotic liquid derived stem cells as reservoir of secreted angiogenic factors capable of stimulating neo-arteriogenesis in an ischemic model," *Biomaterials*, vol. 32, no. 15, pp. 3689–3699, 2011.

[109] T. Takahashi, C. Kalka, H. Masuda, D. Chen, M. Silver, M. Kearney, M. Magner, J. M. Isner, and T. Asahara, "Ischemia and cytokine induced mobilization of bone marrow-derived endothelial progenitor cells for neovascularization," *Nat Med*, vol. 5, pp. 434–438, 1999.

[110] S. C. Pitchford, R. C. Furze, C. P. Jones, A. M. Wengner, and S. M. Rankin, "Differential mobilization of subsets of progenitor cells from the bone marrow," *Cell Stem Cell*, vol. 4, pp. 62–72, 2009.

[111] T. Shirota, H. He, H. Yasui, and T. Matsuda, "Human endothelial progenitor cell-seeded hybrid graft: Proliferative and antithrombogenic potentials in vitro and fabrication processing," *Tissue Eng*, vol. 9, no. 1, pp. 127–136, 2003.

[112] D. Schmidt, C. Breymann, A. Weber, C. I. Guenter, S. Neuenschwander, G. Zund, M. Turina, and S. P. Hoerstrup, "Umbilical cord blood derived endothelial progenitor cells for tissue engineering of vascular grafts," *Ann Thorac Surg*, vol. 78, pp. 2094–2098, 2004.

[113] D. Lu and G. S. Kassab, "Role of shear stress and stretch in vascular mechanobiology," *J R Soc Interface*, vol. 8, no. 63, pp. 1379–1385, 2011.

[114] T. Mammoto and D. E. Ingber, "Mechanical control of tissue and organ development," *Development*, vol. 137, no. 9, pp. 1407–1420, 2010.

[115] B. C. Isenberg, C. Williams, and R. T. Tranquillo, "Small-diameter artificial arteries engineered in vitro," *Circ Res*, vol. 98, pp. 25–35, 2006.

[116] J. D. Kakisis, C. D. Liapis, and B. E. Sumpio, "Effects of cyclic strain on vascular cells,," *Endothelium*, vol. 11, no. 1, pp. 17–28, 2004.

[117] S. Chien, "Mechanotransduction and endothelial cell homeostasis: the wisdom of the cell," *Am J Physiol Heart Circ Physiol*, vol. 292, no. 3, pp. H1209–1224, 2007.

[118] M. J. Levesque, R. M. Nerem, and E. A. Sprague, "Vascular endothelial cell proliferation in culture and the influence of flow," *Biomaterials*, vol. 11, no. 9, pp. 702–707, 1990.

[119] H. Y. Shin, M. E. Gerritsen, and R. Bizios, "Regulation of endothelial cell proliferation and apoptosis by cyclic pressure," *Ann Biomed Eng*, vol. 30, no. 3, pp. 297–304, 2002.

[120] A. G. Vouyouka, R. J. Powell, J. Ricotta, H. Chen, D. J. Dudrick, C. J. Sawmiller, S. J. Dudrick, and B. E. Sumpio, "Ambient pulsatile pressure modulates endothelial cell proliferation," *J Mol Cell Cardiol*, vol. 30, no. 3, pp. 609–615, 1998.

[121] J. Thyberg, "Differentiated properties and proliferation of arterial smooth muscle cells in culture," *Int Rev Cytol*, vol. 169, pp. 183–265, 1996.

[122] A. D. McCulloch, A. B. Harris, C. E. Sarraf, and M. Eastwood, "New multicue bioreactor for tissue engineering of tubular cardiovascular samples under physiological conditions," *Tissue Eng*, vol. 10, pp. 565–573, 2004.

[123] B. C. Isenberg and R. T. Tranquillo, "Long-term cyclic distention enhances the mechanical properties of collagen-based media-equivalents," *Ann Biomed Eng*, vol. 31, p. 937949, 2003.

[124] M. Pei, L. A. Solchaga, J. Seidel, L. Zeng, G. Vunjak-Novakovic, A. I. Caplan, and L. E. Freed, "Bioreactors mediate the effectiveness of tissue engineering scaffolds," *FASEB J*, vol. 16, no. 12, pp. 1691–1694, 2002.

[125] M. Radisic, M. Euloth, L. Yang, R. Langer, L. E. Freed, and G. Vunjak-Novakovic, "High-density seeding of myocyte cells for cardiac tissue engineering," *2003*, vol. 82, no. 4, pp. 403–414, Biotechnol Bioeng.

[126] N. L'Heureux, S. Pquet, R. Labb, L. Germain, and F. A. Auger, "A completely biological tissue-engineered human blood vessel," *FASEB J*, vol. 12, no. 1, pp. 47–56, 1998.

[127] N. L'Heureux, N. Dusserre, G. Konig, B. Victor, P. Keire, T. N. Wight, N. A. Chronos, A. E. Kyles, C. R. Gregory, G. Hoyt, R. C. Robbins, and T. N. M. TN, "Human tissue-engineered blood vessels for adult arterial revascularization," *Nat Med*, vol. 12(3):361-5, no. 3, pp. 361–365, 2006.

[128] T. N. McAllister, M. Maruszewski, S. A. Garrido, W. Wystrychowski, N. Dusserre, A. Marini, K. Zagalski, A. Fiorillo, H. Avila, X. Manglano, J. Antonelli, A. Kocher, M. Zembala, L. Cierpka, L. M. de la Fuente, and N. L'heureux, "Effectiveness of haemodialysis access with an autologous tissue-engineered vascular graft: a multicentre cohort study," *Lancet*, vol. 373, no. 9673, pp. 1440–1446, 2009.

[129] T. Shin'oka, Y. Imai, and Y. Ikada, "Transplantation of a tissue engineered pulmonary artery,," *N Engl J Med*, vol. 344, no. 7, pp. 532–533, 2001.

[130] P. Zilla, R. Fasol, M. Deutsch, T. Fischlein, E. Minar, A. Hammerle, O. Krupicka, and M. Kadletz, "Endothelial cell seeding of polytetrafluoroethylene vascular grafts in humans: a preliminary report," *J Vasc Surg*, vol. 6, pp. 535–541, 1987.

[131] M. Herring, J. Smith, M. Dalsing, J. Glover, R. Compton, K. Etchberger, and T. Zollinger, "Endothelial seeding of polytetrafluoroethylene femoral popliteal bypasses: the failure of low-density seeding to improve patency," *J Vasc Surg*, vol. 20, pp. 650–655, 1994.

[132] L. Bordenave, P. Fernandez, M. Rmy-Zolghadri, S. Villars, R. Daculsi, and D. Midy, "In vitro endothelialized eptfe prostheses: clinical update 20 years after the first realization," *Clin Hemorheol Microcirc*, vol. 33, no. 3, pp. 227–234, 2005.

[133] M. Deutsch, J. Meinhart, T. Fischlein, P. Preiss, and P. Zilla, "Clinical autologous in vitro endothelialization of infrainguinal eptfe grafts in 100 patients: a 9-year experience," *Surgery*, vol. 126, no. 5, pp. 847–855, 1999.

[134] H. R. Laube, J. Duwe, W. Rutsch, and W. Konertz, "Clinical experience with autologous endothelial cell-seeded polytetrafluoroethylene coronary artery bypass grafts," *J Thorac Cardiovasc Surg*, vol. 120, no. 1, pp. 134–141, 2000.

[135] Y. Fujita, M. H. D. Wu, A. Ishida, Q. Shi, M. Walkera, W. P. Hammond, and L. R. Sauvage, "Accelerated healing of dacron grafts seeded by preclotting with autologous bone marrow blood," *Ann Vasc Surg*, vol. 13, no. 4, pp. 402–412, 1999.

[136] M. Pasic, W. Mller-Glauser, B. Odermatt, M. Lachat, B. Seifert, and M. Turina, "Seeding with omental cells prevents late neointimal hyperplasia in small-diameter dacron grafts," *Circulation*, vol. 92, pp. 2605–2616, 1995.

[137] A. Tiwari, A. Kidane, G. Punshon, G. Hamilton, and A. M. Seifalian, "Extraction of cells for single-stage seeding of vascular-bypass grafts," *Biotech App Biochem*, vol. 38, no. 1, pp. 35–41, 2003.

[138] H. J. Salacinski, A. Tiwari, G. Hamilton, and A. M. Seifalian, "Cellular engineering of vascular bypass grafts: Role of chemical coatings for enhancing endothelial cell attachment," *Med Biol Eng Comput*, vol. 39, no. 6, pp. 609–618, 2001.

[139] M. Bosiers, K. Deloose, J. Verbist, H. Schro, G. Lauwers, W. Lansink, and P. Peeters, "Heparin-bonded expanded polytetrafluoroethylene vascular graft

for femoropopliteal and femorocrural bypass grafting: 1-year results," *J Vasc Surg*, vol. 43, no. 2, pp. 313–318, 2006.

[140] M. Kibbe, T. Billiar, and E. Tzeng, "Inducible nitric oxide synthase and vascular injury," *Cardiovasc Res*, vol. 43, no. 3, pp. 650–657, 1999.

[141] L. K. Keefer, "Nitric oxide-and nitroxyl-generating diazeniumdiolates (nonoates): emerging commercial opportunities,," *Curr Top Med Chem*, vol. 5, no. 7, pp. 625–636, 2005.

[142] S. K. Pulfer, D. Ott, and D. J. Smith, "Incorporation of nitric oxide releasing crosslinked polyethyleneimine microspheres into vascular grafts," *J Biomed Mater Res A*, vol. 78, no. 2, pp. 182–189, 1998.

[143] K. A. Mowery, M. H. Schoenffsch, J. E. Saavedra, L. K. Keefer, and M. E. Meyerhoff, "Preparation and characterization of hydrophobic polymeric films that are thromboresistant via nitric oxide release," *Biomaterials*, vol. 21, no. 1, pp. 9–21, 2000.

[144] H. W. Jun, L. J. Taite, and J. L. West, "Nitric oxide-producing polyurethanes," *Biomacromolecules*, vol. 6, no. 2, pp. 838–844, 2005.

[145] M. M. Reynolds, M. C. Frost, and M. E. Meyerhoff, "Nitric oxide-releasing hydrophobic polymers: preparation, characterization, and potential biomedical applications," *Free Radic Biol Med*, vol. 37, no. 7, pp. 926–936, 2004.

[146] H. Gappa-Fahlenkamp, X. Duan, and R. S. Lewis, "Analysis of immobilized l-cysteine on polymers," *J Biomed Mater Res A*, vol. 71A, no. 3, pp. 519–527, 2004.

[147] C. Cagiannos, O. R. A. Abul-Khoudoud, and W. DeRijk, "Rapamycin-coated expanded polytetrafluoroethylene bypass grafts exhibit decreased anastomotic neointimal hyperplasia in a porcine model," *J Vasc Surg*, vol. 42, pp. 980–988, 2005.

[148] B. H. Lee, H. Y. Nam, T. Kwon, S. J. Kim, G. Y. Kwon, H. J. Jeon, H. J. Lim, W. K. Lee, J. S. Park, J. Y. Ko, and D. J. Kim, "Paclitaxel-coated expanded polytetrafluoroethylene haemodialysis grafts inhibit neointimal hyperplasia in porcine model of graft stenosis," *Nephrol Dial Transplant*, vol. 21, no. 9, pp. 2432–2438, 2006.

[149] M. Avci-Adali, A. Paul, G. Ziemer, and H. P. Wendel, "New strategies for in vivo tissue engineering by mimicry of homing factors for self-endothelialisation of blood contacting materials," *Biomaterials*, vol. 29, pp. 3936–3945, 2008.

[150] A. de Mel, G. Jell, M. M. Stevens, and A. M. Seifalian, "Biofunctionalization of biomaterials for accelerated in situ endothelialization: a review," *Biomacromolecules*, vol. 9, pp. 2969–2979, 2008.

[151] N. Alobaid, H. J. Salacinski, K. M. Sales, B. Ramesh, R. Y. Kannan, G. Hamilton, and A. M. Seifalian, "Nanocomposite containing bioactive peptides promote endothelialisation by circulating progenitor cells: an in vitro evaluation," *Eur J Vasc Endovasc Surg. 2006 Jul;32(1):76-83*, vol. 32, no. 1, pp. 76–83, 2006.

[152] J. Li, M. Ding, Q. Fu, H. Tan, X. Xie, and Y. Zhong, "A novel strategy to graft rgd peptide on biomaterials surfaces for endothelization of small-diamater vascular grafts and tissue engineering blood vessel," *J Mater Sci Mater Med*, vol. 19, no. 7, pp. 2595–2603, 2008.

[153] J. I. Rotmans, J. M. M. Heyligers, H. J. M. Verhagen, E. Velema, M. M. Nagtegaal, D. P. V. de Kleijn, F. G. de Groot, E. S. G. Stroes, and G. Pasterkamp, "In vivo cell seeding with anti-cd34 antibodies successfully accelerates endothelialization but stimulates intimal hyperplasia in porcine arteriovenous expanded polytetrafluoroethylene grafts," *Circulation*, vol. 112, pp. 12–18, 2005.

[154] D. C. Miller, A. Thapa, K. M. Haberstroh, and T. J. Webster, "Endothelial and vascular smooth muscle cell function on poly(lactic-co-glycolic acid) with nano-structured surface features," *Nat Biotechnol*, vol. 25, no. 1, pp. 53–61, 2004.

[155] D. C. Miller, K. M. Haberstroh, and T. J. Webster, "Plga nanometer surface features manipulate fibronectin interactions for improved vascular cell adhesion," *J Biomed Mater Res A,*, vol. 81, no. 3, pp. 678–684, 2007.

[156] B. M. Baker, A. M. Handorf, L. C. Ionescu, W. J. Li, and R. L. Mauck, "New directions in nanofibrous scaffolds for soft tissue engineering and regeneration," *Expert Rev Med*, vol. 6, pp. 515–532, 2009.

[157] N. Ashammakhi, A. N. L. Nikkola, I. Wimpenny, and Y. Yang, "Advancing tissue engineering by using electrospun nanofibers," *Regen Med*, vol. 3, pp. 547–574, 2008.

[158] Y. Zhang, C. T. Lim, S. Ramakrishna, and Z. M. Huang, "Recent development of polymer nanofibers for biomedical and biotechnological applications," *J Mater Sci Mater Med*, vol. 16, pp. 933–946, 2005.

[159] A. Thorvaldsson, H. Stenhamre, P. Gatenholm, and P. Walkenstrom, "Electrospinning of highly porous scaffolds for cartilage regeneration," *Biomacromolecules*, vol. 9, no. 3, pp. 1044–1049, 2008.

[160] O. Ishii, M. Shin, T. Sueda, and J. P. Vacanti, "In vitro tissue engineering of a cardiac graft using a degradable scaffold with an extracellular matrix-like topography," *J Thorac Cardiovasc Surg*, vol. 130, no. 5, pp. 1358–1363, 2005.

[161] D. E. Heath, J. J. Lannutti, and S. L. Cooper, "Electrospun scaffold topography affects endothelial cell proliferation, metabolic activity, and morphology," *J Biomed Mater Res A*, vol. 94, no. 4, pp. 1195–204, 2010.

[162] C. Grasl, H. Bergmeister, M. Stoiber, H. Schima, and G. Weigel, "Electrospun polyurethane vascular grafts: in vitro mechanical behavior and endothelial adhesion molecule expression," *J Biomed Mater Res A*, vol. 93, no. 2, pp. 716–723, 2010.

[163] C. Y. Xu, R. Inai, M. Kotaki, and S. Ramakrishna, "Aligned biodegradable nanofibrous structure: a potential scaffold for blood vessel engineering," *Nat Biotechnol*, vol. 25, no. 5, pp. 877–886, 2004.

[164] P. Uttayarat, A. Perets, M. Li, P. Pimton, S. J. Stachelek, I. Alferiev, R. J. Composto, R. J. Levy, and P. I. Lelkes, "Micropatterning of three-dimensional electrospun polyurethane vascular grafts," *Acta Biomater*, vol. 6, no. 11, pp. 4229–4239, 2010.

[165] Z. Ma, M. Kotaki, T. Yong, W. He, and S. Ramakrishna, "Surface engineering of electrospun polyethylene terephthalate (pet) nanofibers towards development of a new material for blood vessel engineering," *Nat Biotechnol*, vol. 26, no. 15, pp. 2527–2536, 2005.

[166] W. He, T. Yong, W. E. Teo, Z. Ma, and S. Ramakrishna, "Fabrication and endothelialization of collagen-blended biodegradable polymer nanofibers: Potential vascular graft for blood vessel tissue engineering," *Tissue Eng*, vol. 11, no. 9-10, p. 1574, 2005.

[167] J. J. Stankus, L. Soletti, K. Fujimoto, Y. Hong, D. A, and W. R. Wagner, "Fabrication of cell microintegrated blood vessel constructs through electrohydrodynamic atomization," *Nat Biotechnol*, vol. 28, no. 17, pp. 2738–2746, 2007.

[168] E. Gazit, "Molecular self-assembly: bioactive nanostructures branch out," *Nat Nanotechnol*, vol. 3, no. 1, pp. 8–9, 2008.

[169] L. C. Palmer and S. I. Stupp, "Molecular self-assembly into one-dimensional nanostructures," *Acc Chem Res*, vol. 41, no. 12, pp. 1674–1684, 2008.

[170] H. Cui, M. J. Webber, and S. I. Stupp, "Self-assembly of peptide amphiphiles: from molecules to nanostructures to biomaterials," *Biopolymers*, vol. 94, no. 1, pp. 1–18, 2010.

[171] F. W. Kotch and R. T. Raines, "Self-assembly of synthetic collagen triple helices," *PNAS*, vol. 103, no. 9, pp. 3028–3033, 2006.

[172] A. Andukuri, W. P. Minor, M. Kushwaha, J. M. Anderson, and H. W. Jun, "Effect of endothelium mimicking self-assembled nanomatrices on cell adhesion and spreading of human endothelial cells and smooth muscle cells," *Nanomedicine*, vol. 6, no. 2, pp. 289–297, 2010.

[173] D. E. Discher, P. Janmey, and L. Y. Wang, "Tissue cells feel and respond to the stiffness of their substrate," *Science*, vol. 310, no. 5751, pp. 1139–1143, 2005.

[174] F. J. Byfield, R. K. Reen, T. P. Shentu, I. Levitan, and K. J. Gooch, "Endothelial actin and cell stiffness is modulated by substrate stiffness in 2d and 3d," *J Biomech*, vol. 42, pp. 1114–1119, 2009.

[175] A. Engler, L. Bacakova, C. Newman, A. Hategan, M. Griffin, and D. Discher, "Substrate compliance versus ligand density in cell on gel responses," *Biophys J*, vol. 86, no. 1, pp. 617–628, 2004.

[176] T. Yeung, P. C. Georges, L. A. Flanagan, B. Marg, M. Ortiz, M. Funaki, N. Zahir, W. Ming, V. Weaver, and P. A. Janmey, "Effects of substrate stiffness on cell morphology, cytoskeletal structure, and adhesion," *Cell Motil Cytoskeleton*, vol. 60, no. 1, pp. 24–34, 2005.

[177] R. McBeath, D. M. Pirone, C. M. Nelson, K. Bhadriraju, and C. S. C. CS, "Cell shape, cytoskeletal tension, and rhoa regulate stem cell lineage commitment," *Dev Cell*, vol. 6, no. 4, pp. 483–495, 2004.

[178] G. Z. Li, L. C. Wang, L. H. Ni, and C. U. Pittman, "Polyhedral oligomeric silsesquioxane (poss) polymers and copolymers: A review," *J Inorg Organomet Polym*, vol. 11, p. 123154, 2001.

[179] J. W, D. S. Schlitzer, and J. D. Lichtenhan, "Low earth orbit resistant siloxane copolymers," *J Appl Polym Sci*, vol. 60, p. 591596, 1996.

[180] A. L. Brunsvold, T. K. Minton, I. Gouzman, E. Grossman, and R. Gonzalez, "An investigation of the resistance of polyhedral oligomeric silsesquioxane

polyimide to atomic-oxygen attack," *High Perform Polym*, vol. 16, p. 303318, 2004.

[181] R. Y. Kannan, H. Salacinski, P. E. Butler, and A. M. Seifalian, "Polyhedral oligomeric silsesquioxane nanocomposites: The next generation material for biomedical applications,," *Acc Chem Res*, vol. 38, pp. 879–884, 2005.

[182] R. Y. Kannan, H. Salacinski, M. Odlyha, P. E. Butler, and A. M. Seifalian, "The degradative resistance of polyhedral oligomeric silsesquioxane nanocore integrated polyurethanes: an in vitro study," *Biomaterials*, vol. 27, no. 9, pp. 1971–1979, 2006.

[183] R. Y. Kannan, H. J. Salacinski, J. E. Ghanavi, A. Narula, M. Odlyha, H. Peirovi, P. E. Butler, and A. M. Seifalian, "Silsesquioxane nanocomposites as tissue implants," *Plast Reconstr Surg*, vol. 119, no. 6, pp. 1653–1662, 2007.

[184] R. Y. Kannan, H. Salacinski, J. D. Groot, I. Clatworthy, L. Bozec, M. Horton, P. E. Butler, and A. M. Seifalian, "The antithrombogenic potential of a polyhedral oligomeric silsesquioxane (poss) nanocomposite," *Biomacromolecules*, vol. 7, pp. 215–223, 2006.

[185] R. Y. Kannan, H. J. Salacinski, K. M. Sales, P. E. Butler, and A. M. Seifalian, "The endothelialisation of polyhedral oligomeric silsequioxane nanocomposite: an in vitro study," *Cell Biochem Biophys*, vol. 45, no. 2, pp. 129–136, 2006.

[186] A. G. Kidane, G. Burriesci, M. Endrisinghe, J. Ghanbari, P. Bonhoeffer, and A. M. Seifalian, "A novel nanocomposite polymer for development of synthetic heart valve leaflets," *Acta Biomater*, vol. 5, no. 7, pp. 2409–2417, 2009.

[187] R. Bakhshi, A. Darbyshire, J. E. Evans, Z. You, J. Lu, and A. M. Seifalian, "Polymeric coating of surface modified nitinol stent with poss-nanocomposite polymer," *Colloids Surf B Biointerfaces*, vol. 86, no. 1, pp. 93–105, 2011.

[188] S. Sarkar, G. Burriesci, A. Wojcik, N. Aresti, G. Hamilton, and A. M. Seifalian, "Manufacture of small calibre quadruple lamina vascular bypass grafts using a novel automated extrusion-phase-inversion method and nanocomposite polymer," *J Biomech*, vol. 42, no. 6, pp. 722–730, 2009.

[189] Z. Zhang, Z. Wang, S. Liu, and M. Kodama, "Pore size, tissue ingrowth, and endothelialization of small-diameter microporous polyurethane vascular prostheses," *Biomaterials*, vol. 25, no. 1, pp. 177–187, 2004.

[190] J. Zeltinger, J. K. Sherwood, D. A. Graham, R. Mueller, and L. G. Griffith, "Effect of pore size and void fraction on cellular adhesion, proliferation, and matrix deposition," *Tissue Eng*, vol. 7, no. 5, pp. 557–572, 2001.

[191] G. Wei and P. Ma, "Nanostructured biomaterials for regeneration," *Adv Funct Mater*, vol. 18, no. 22, pp. 3566–3582, 2008.

[192] Q. Z. Zheng, P. Wang, and Y. N. Yang, "Rheological and thermodynamic variationin polysulfone solution by peg introduction and its effect on kinetics of membrane formation via phase-inversion process," *J Membr Sci*, vol. 279, p. 230, 2006.

[193] M. S. Bazarjani, N. Mohammadi, and S. M. Ghasemi, "Ranking the key parameters of immersion precipitation process and modeling the resultant membrane structural evolution," *J Appl Polym Sci*, vol. 113, no. 3, p. 15291538, 2009.

[194] K. S. Chian, "Factors affecting the morphology and mechanical properties of a coagulated thermoplastic polyurethane," *J Appl Polym Sci*, vol. 65, no. 10, p. 19471954, 1997.

[195] H. Wang, J. Pieper, F. Peters, C. A. van Blitterswijk, and E. N. Lamme, "Synthetic scaffold morphology controls human dermal connective tissue formation,"

[196] D. J. Lin, H. H. Chang, T. C. Chen, Y. C. Lee, and L. P. Cheng, "Formation of porous poly(vinylidene fluoride) membranes with symmetric or asymmetric morphology by immersion precipitation in the water/tep/pvdf system," *Eur Polym J*, vol. 42, p. 15811594, 2006.

[197] P. Aerts, I. Genne, R. Leysen, I. F. J. Vankelecom, and P. A. Jacobs, "polysulfone-aerosil composite membranes: part 2. the influence of the addition of aerosil on the skin characteristics and membrane properties," *J Memb Sci*, vol. 178, no. 1-2, pp. 1–11, 2000.

[198] Y. Yang, W. Jun, Z. Qing-zhu, C. Xue-si, and Z. Hui-xuan, "The research of rheology and thermodynamics of organicinorganic hybrid membrane during the membrane formation," *J Memb Sci*, vol. 311, no. 1-2, pp. 200–207, 2008.

[199] X. D. Zhang, C. W. Macosko, H. T. Davis, A. D. Nikolov, and D. T. Wasan, "Role of silicone surfactant in flexible polyurethane foam," *J Colloid Interface Sci*, vol. 215, no. 2, pp. 270–279, 1999.

[200] L. L. Wong, V. O. Ikem, A. Menner, and A. Bismarck, "Macroporous polymers with hierarchical pore structure from emulsion templates stabilised by both particles and surfactants," *Macromol Rapid Commun*, 2011.

[201] W. RA, "The effect of porosity and biomaterial on the healing and long-term mechanical properties of vascular prostheses," *ASAIO Trans*, vol. 34, no. 2, pp. 95–100, 1988.

[202] A. K. Salem, R. Stevens, R. G. Pearson, M. C. Davies, S. J. Tendler, C. J. Roberts, P. M. Williams, and K. M. Shakesheff, "Interactions of 3t3 fibroblasts and endothelial cells with defined pore features," *J Biomed Mater Res*, vol. 61, no. 2, pp. 212–217, 2002.

[203] E. Claes, J. M. Atienza, G. V. Guinea, F. J. Rojo, J. M. Bernal, J. M. Revuelta, and M. Elices, "Mechanical properties of human coronary arteries," *Conf Proc IEEE Eng Med Biol Soc*, pp. 3792–3795, 2010.

[204] D. P. Sokolis, E. M. Kefaloyannis, M. Kouloukoussa, E. Marinos, H. Boudoulas, and P. E. Karayannacos, "A structural basis for the aortic stress-strain relation in uniaxial tension," *J Biomech*, vol. 39, no. 9, pp. 1651–1662, 2006.

[205] S. Sarkar, H. J. Salacinski, G. Hamilton, and A. M. Seifalian, "The mechanical properties of infrainguinal vascular bypass grafts: their role in influencing patency," *Eur J Vasc Endovasc Surg*, vol. 31, no. 6, pp. 627–636, 2006.

[206] N. R. Tai, H. J. Salacinski, A. Edwards, G. Hamilton, and A. M. Seifalian, "Compliance properties of conduits used in vascular reconstruction," *Br J Surg*, vol. 87, no. 11, pp. 1516–1524, 2000.

[207] W. Zhang, Y. Liu, and G. S. Kassab, "Viscoelasticity reduces the dynamic stresses and strains in the vessel wall: implications for vessel fatigue," *Am J Physiol Heart Circ Physiol*, vol. 293, no. 4, pp. H2355–2360, 2007.

[208] A. Giudiceandrea, H. J. Salacinski, N. R. M. Tai, G. Punshon, G. Hamilton, and A. M. Seifalian, "Development and evaluation of an ideal flow circuit: assessing the dynamic behavior of endothelial cell seeded grafts," *J Artif Organs*, vol. 3, no. 1, pp. 16–24,, 2000.

[209] P. D. Ballyk, C. Walsh, J. Butany, and M. Ojha, "Compliance mismatch may promote graft-artery intimal hyperplasia by altering suture-line stresses," *J Biomech*, vol. 31, no. 3, pp. 229–237, 1998.

[210] R. S. Taylor, R. J. McFarland, and M. I. Cox, "An investigation into the causes of failure of ptfe grafts," *Eur J Vasc Surg*, vol. 1, no. 5, pp. 335–343, 1987.

[211] N. Chakfe, C. Jahn, P. Nicolini, J. G. Kretz, S. Edah-Tally, M. Beaufigeau, Y. Lebras, R. Beaujeux, B. Durand, and B. E. B, "The impact of knee joint

flexion on infrainguinal vascular grafts: an angiographic study," *Eur J Vasc Endovasc Surg*, vol. 13, no. 1, pp. 23–30, 1997.

[212] R. L. Armentano, J. G. Barra, F. M. Pessana, D. O. Craiem, S. Graf, D. B. Santana, and R. A. Sanchez, "Smart smooth muscle spring-dampers. smooth muscle smart filtering helps to more efficiently protect the arterial wall," *IEEE Eng Med Biol Mag*, vol. 26, no. 2, pp. 62–70, 2007.

[213] R. R. Thakrar, V. P. Patel, G. Hamilton, B. J. Fuller, and A. M. Seifalian, "Vitreous cryopreservation maintains the viscoelastic property of human vascular grafts," *FASEB J*, vol. 20, no. 7, pp. 874–881, 2006.

[214] J. T. Butcher, B. C. Barrett, and R. M. Nerem, "Equibiaxial strain stimulates fibroblastic phenotype shift in smooth muscle cells in an engineered tissue model of the aortic wall," *Biomaterials*, vol. 27, no. 30, pp. 5252–5258, 2006.

[215] A. T. Halka, N. J. Turner, A. Carter, J. Ghosh, M. O. Murphy, J. P. Kirton, C. M. Kielty, and M. G. Walker, "The effects of stretch on vascular smooth muscle cell phenotype in vitro," *Cardiovasc Pathol*, vol. 17, no. 2, pp. 98–102, 2008.

[216] L. W. Longest and C. Kleinstreuer, "Numerical simulation of wall shear stress conditions and platelet localization in realistic end-to-side arterial anastomoses," *J Biomech Eng*, vol. 125, no. 5, pp. 671–681, 2003.

[217] S. F. Stewart and D. J. Lyman, "Effects of an artery/vascular graft compliance mismatch on protein transport: a numerical study," *Ann Biomed Eng*, vol. 32, no. 7, pp. 991–1006, 2004.

[218] K. Rhee and S. M. Lee, "Effects of radial wall motion and flow waveform on the wall shear rate distribution in the divergent vascular graft," *Ann Biomed Eng*, vol. 26, pp. 955–964, 1998.

[219] I. Surovtsova, "Effects of compliance mismatch on blood flow in an artery with endovascular prosthesis," *J Biomech*, vol. 38, no. 10, pp. 2078–2086, 2005.

[220] A. B. Brochu, S. L. Craig, and W. M. Reichert, "Self-healing biomaterials," *J Biomed Mater Res A*, vol. 96, no. 2, pp. 492–506, 2011.

[221] Y. X. Wang, J. L. Robertson, W. B. Spillman, and R. O. Claus, "Effects of the chemical structure and the surface properties of polymeric biomaterials on their biocompatibility," *Pharm Res*, vol. 21, no. 8, pp. 1362–1373, 2004.

[222] K. L. Menzies and L. Jones, "The impact of contact angle on the biocompatibility of biomaterials," *Optom Vis Sci*, vol. 87, no. 6, pp. 387–399, 2010.

[223] F. Guilak, D. M. Cohen, B. T. Estes, J. M. Gimble, W. Liedtke, and C. S. Chen, "Control of stem cell fate by physical interactions with the extracellular matrix," *Cell Stem Cell*, vol. 5, no. 1, pp. 17–26, 2009.

[224] Y. W. Chun, D. Khang, K. M. Haberstroh, and T. J. Webster, "The role of polymer nanosurface roughness and submicron pores in improving bladder urothelial cell density and inhibiting calcium oxalate stone formation," *Nanotechnology*, vol. 20, no. 8, p. 085104, 2009.

[225] A. I. Teixeira, G. A. Abrams, P. J. Bertics, C. J. Murphy, and P. F. Nealey, "Epithelial contact guidance on well-defined micro- and nanostructured substrates," *J Cell Sci*, vol. 116, no. 10, pp. 1881–1892, 2003.

[226] D. H. Kim, E. A. Lipke, P. Kim, R. Cheong, S. Thompson, M. Delannoy, K. Y. Suh, L. Tung, and A. Levchenko, "Nanoscale cues regulate the structure and function of macroscopic cardiac tissue constructs," *Proc Natl Acad Sci USA*, vol. 107, no. 2, pp. 565–570, 2010.

[227] M. J. Biggs, R. G. Richards, and M. J. Dalby, "Nanotopographical modification: a regulator of cellular function through focal adhesions," *Nanomedicine*, vol. 6, no. 5, pp. 619–633, 2010.

[228] C. S. Chen, "Mechanotransduction - a field pulling together?," *J Cell Sci*, vol. 121, no. 20, pp. 3285–3292, 2008.

[229] A. J. Engler, S. Sen, H. L. Sweeney, and D. E. Discher, "Matrix elasticity directs stem cell lineage specification," *Cell*, vol. 126, no. 4, pp. 677–689, 2006.

[230] B. Hinz, "Formation and function of the myofibroblast during tissue repair," *J Invest Dermatol*, vol. 127, no. 3, pp. 526–537, 2007.

[231] R. G. Wells, "The role of matrix stiffness in regulating cell behavior," *Hepatology*, vol. 47, no. 4, pp. 1394–1400, 2008.

[232] W. C. Oliver and G. M. Pharr, "Measurement of hardness and elastic modulus by instrumented indentation: Advances in understanding and refinements to methodology," *J Mater Res*, vol. 19, pp. 3–20, 2004.

[233] T. A. Thorstenson, J. B. Huang, M. W. Urban, and K. Haubennestel, "Mobility and distribution of silicone additives in coatings; a spectroscopic study," *Prog Org Coat*, vol. 24, pp. 341–358, 1994.

[234] C. W. Chung, j Y Kang, I. S. Yoon, H. D. Hwang, P. Balakrishnan, H. J. Cho, K. D. Chung, D. H. Kang, and D. D. Kim, "Interpenetrating polymer network (ipn) scaffolds of sodium hyaluronate and sodium alginate for chondrocyte culture," *Colloids Surf B Biointerfaces*, vol. 83, no. 2, pp. 204–213, 2011.

[235] G. Sun and S. Gerecht, "Vascular regenration: engineering the stem cell microenvironment," *Regen Med*, vol. 4, no. 3, pp. 435–447, 2009.

[236] P. Schon, K. Bagdi, K. Molnr, P. Markus, B. Puknszky, and J. Vancso, "Quantitative mapping of elastic moduli at the nanoscale in phase separated polyurethanes by afm," *Eur Polym J*, vol. 47, pp. 692–698, 2011.

[237] F. N. Jones, W. Shen, S. M. Smith, Z. H. Huang, and R. A. Ryntz, "Studies of microhardness and mar resistance using a scanning probe microscope," *Prog Org Coat*, vol. 34, no. 1-4, pp. 119–129, 1998.

[238] E. Amitay-Sadovsky, B. Ward, G. A. Somorjai, and K. Komvopoulos, "Nanomechanical properties and morphology of thick polyurethane films under contact pressure and stretching," *J Appl Phys*, vol. 91, no. 1, pp. 375–385, 2002.

[239] G. Huang and H. Lu, "Measurement of youngs relaxation modulus using nanoindentation," *Mech Time-Depend Mater*, vol. 10, pp. 229–243, 2006.

[240] L. Xu, P. Soman, J. Runt, and C. A. Siedlecki, "Characterization of surface microphase structures of poly(urethane urea) biomaterials by nanoscale indentation with afm," *J Biomater Sci Polymer Edn*, vol. 18, no. 4, p. 353368, 2007.

[241] B. Xu, Y. Q. Fu, W. M. Huang, Y. T. Pei, Z. G. Chen, J. T. M. D. Hosson, A. Kraft, and R. L. Reuben, "Thermal-mechanical properties of polyurethane-clay shape memory polymer nanocomposites," *Polymers*, vol. 2, pp. 31–39, 2010.

[242] C. E. Foerster, F. C. Serbena, I. T. S. Garcia, C. M. Lepienski, L. S. Roman, J. R. Galvao, and F. C. Zawislak, "Mechanical properties of polyhedral oligomeric silsesquioxane (poss) thin films submitted to si irradiation," *Nucl Instr and Meth in Phys Res B*, vol. 218, p. 375380, 2004.

[243] M. Yaseen, H. J. Salacinski, A. M. Seifalian, and J. R. Lu, "Dynamic protein adsorption at the polyurethane copolymer/water interface," *Biomed Mater*, vol. 3, no. 3, p. 034123, 2008.

[244] M. Yaseen, X. Zhao, A. Freund, A. M. Seifalian, and J. R. Lu, "Surface structural conformations of fibrinogen polypeptides for improved biocompatibility," *Biomaterials*, vol. 31, no. 14, pp. 3781–3792, 2010.

[245] J. M. Anderson, A. Rodriguez, and D. T. Chang, "Foreign body reaction to biomaterials," *Seminars in Immunology*, vol. 20, no. 2, pp. 86–100, 2008.

[246] Z. Xia and J. T. Triffitt, "A review on macrophage response to biomaterials," *Biomedical Materials*, vol. 1, pp. R1–R9, 2006.

[247] W. G. Brodbeck and J. M. Anderson, "Giant cell formation and function," *Current Opinions in Hematology*, vol. 16, no. 1, pp. 53–57, 2009.

[248] H. P. Greisler, "Interactions at the blood/material interface," *Annals of Vascular Surgery*, vol. 4, no. 1, pp. 98–103, 1990.

[249] J. H. Silver, J.-C. Lin, F. Lim, V. A. Tegoulia, M. K. Chaudhury, and S. L. Cooper, "Surface properties and hemocompatibility of alkyl-siloxane monolayers supported on silicone rubber: effect of alkyl chain length and ionic functionality," *Biomaterials*, vol. 20, pp. 1533–1543, 1999.

[250] L. Poussard, F. Burel, J. Couvercelle, O. Lesouhaitier, Y. Merthi, M. Tabrizian, and C. Bunel, "*In vitro* throbogenicty investigation of new water dispersible polyurethane anionomers bearing carboxylate groups," *Journal of Biomaterials Science: Polymer Edition*, vol. 16, no. 3, pp. 335–351, 2005.

[251] N. Tsunoda, K. Kokubo, K. Sakai, M. Fukuda, M. Miyazaki, and T. Hiyoshi, "Surface roughness of cellulose hollow fiber dialysis membranes and platelet adhesion," *ASAIO Journal*, vol. 45, no. 5, pp. 418–423, 1999.

[252] K. R. Milner, A. J. Snyder, and C. A. Siedlecki, "Sub-micron texturing for reducing platelet adhesion to polyurethane biomaterials," *Journal of Biomedical Materials Research Part A*, vol. 76, no. 3, pp. 561–570, 2006.

[253] W. G. Brodbeck, Y. Nakayama, T. Matsuda, E. Colton, N. P. Ziats, and J. M. Anderson, "Biomaterial surface chemistry dictates adherent monocyte/macrophage cytokine expression *in vitro*," *Cytokine*, vol. 18, no. 6, pp. 311–319, 2002.

[254] A. K. Refai, M. Textor, D. M. Brunette, and J. D. Waterfield, "Effect of titanium surface topography on macrophage activation and secretion of proinflammatory cytokines and chemokines," *Journal of Biomedical Materials Research Part A*, vol. 70A, no. 2, pp. 194–205, 2004.

[255] A. Rosengren, L. M. Bjursten, N. Danielsen, H. Persson, and M. Kober, "Tissue reactions to polyethylene implants with different surface topography," *Journal of Materials Science: Materials in Medicine*, vol. 10, no. 2, pp. 75–82, 1999.

[256] R. I. Mehta, A. K. Mukherjee, T. D. Patterson, and M. C. Fishbein, "Pathology of explanted polytetrafluoroethylene vascular grafts," *Cardiovasc Pathol*, vol. 20, no. 4, pp. 213–221, 2011.

[257] C. Sperling, M. Fischer, M. F. Maitz, and C. Werner, "Blood coagulation on biomaterials requires the combination of distinct activation processes," *Biomaterials*, vol. 30, no. 27, pp. 4447–4456, 2009.

[258] L. Soletti, A. Nieponice, Y. Hong, S. H. Ye, J. J. Stankus, W. R. Wagner, and D. A. Vorp, "In vivo performance of a phospholipid-coated bioerodable elastomeric graft for small-diameter vascular applications," *J Biomed Mater Res A*, vol. 96, no. 2, pp. 436–448, 2011.

[259] T. Groth, J. Synowitz, G. Malsch, K. Richau, W. Albrecht, K. P. Lange, and D. Paul, "Contact activation of plasmatic coagulation on polymeric membranes measured by the activity of kallikrein in heparinized plasma," *J Biomed Sci Polymer Ed*, vol. 8, no. 10, pp. 797–807, 1997.

[260] L. Chen, D. Han, and L. Jianga, "On improving blood compatibility: From bioinspired to synthetic design and fabrication of biointerfacial topography at micro/nano scales," *Colloids Surf B Biointerfaces*, vol. 85, pp. 5–7, 2011.

[261] P. C. Georges and P. A. Janmey, "Cell type-specific response to growth on soft materials.," *J Appl Physiol*, vol. 98, no. 4, pp. 1547–1553, 2005.

[262] L. B. Koh, I. Rodriquez, and S. S. Venkatraman, "The effect of topography of polymer surfaces on platelet adhesion," *Biomaterials*, vol. 31, no. 7, pp. 1533–1545, 2010.

[263] P. Lauzurica, D. Sancho, M. Torres, B. Albella, M. Marazuela, T. Merino, J. A. Bueren, A. C. Martnez, and F. Snchez-Madrid, "Phenotypic and functional characteristics of hematopoietic cell lineages in cd69-deficient mice," *Blood*, vol. 95, no. 7, pp. 2312–2320, 2000.

[264] P. J. Murray, "The primary mechanism of the il-10-regulated antiinflammatory response is to selectively inhibit transcription," *Proc Natl Acad Sci USA*, vol. 102, no. 24, pp. 8686–8691, 2005.

[265] S. J. Leibovich, P. J. Polverini, H. M. Shepard, D. M. Wiseman, V. Shively, and N. Nuseir, "Macrophage-induced angiogenesis is mediated by tumour necrosis factor-alpha," *Nature*, vol. 328, no. 6140, pp. 630–632, 1987.

[266] S. Chen, J. A. Jones, Y. Xu, H. Y. Low, J. M. Anderson, and K. W. Leong, "Characterization of topographical effects on macrophage behavior in a foreign body response model," *Biomaterials*, vol. 31, no. 13, pp. 3479–3491, 2010.

[267] J. A. Jones, M. Dadsetan, T. O. Collier, M. Ebert, K. S. Stokes, R. S. W. andd P A Hiltner, and J. M. Anderson, "Macrophage behavior on surface-modified polyurethanes," *J Biomater Sci Polym Ed*, vol. 15, no. 5, pp. 567–584, 2004.

[268] R. O. Darouiche, "Treatment of infections associated with surgical implants," *N Engl J Med*, vol. 350, no. 14, pp. 1422–1429, 2004.

[269] A. Nagpal and M. R. Sohail, "Prosthetic vascular graft infections: A contemporary approach to diagnosis and management," *Curr Infect Dis Rep*, vol. DOI 10.1007/s11908-011-0191-y, 2011.

[270] L. M. Baddour, M. A. Bettmann, A. F. Bolger, A. E. Epstein, P. Ferrieri, M. A. Gerber, M. H. Gewitz, A. K. Jacobs, M. E. Levison, J. W. Newburger, T. J. Pallasch, W. R. Wilson, R. S. Baltimore, D. A. Falace, S. T. Shulman, L. Y. Tani, and K. A. Taubert, "Nonvalvular cardiovascular device-related infections," *Clin Infect Dis*, vol. 38, no. 8, pp. 1128–1130, 2004.

[271] Y. Z. Zhang, L. M. Bjursten, C. Freij-Larsson, M. Kober, and B. W. B, "Tissue response to commercial silicone and polyurethane elastomers after different sterilization procedures," *Biomaterials*, vol. 17, no. 23, pp. 2265–2272, 1996.

[272] H. J. Haugen, M. Brunner, F. Pellkofer, J. Aigner, J. Will, and E. Wintermantel, "Effect of different gamma-irradiation doses on cytotoxicity and material properties of porous polyether-urethane polymer," *J Biomed Mater Res B Appl Biomater*, vol. 80, no. 2, pp. 415–423, 2007.

[273] H. Shearer, M. J. Ellis, S. P. Perera, and J. B. Chaudhuri, "Effects of common sterilization methods on the structure and properties of poly(d,l lactic-co-glycolic acid) scaffolds," *Tissue Eng*, vol. 12, no. 10, pp. 2717–2727, 2006.

[274] C. E. Holy, C. Cheng, J. E. Davies, and M. S. Shoichet, "Optimizing the sterilization of plga scaffolds for use in tissue engineering," *Biomaterials*, vol. 22, no. 1, pp. 25–31, 2001.

[275] S. Simmons, J. Hyvarinen, and L. Poole-Warren, "The effect of sterilisation on a poly(dimethylsiloxane)/poly(hexamethylene oxide) mixed macrodiol-based polyurethane elastomer," *Biomaterials*, vol. 27, no. 25, pp. 4484–4497, 2006.

[276] K. Gorna and S. Gogolewski, "The effect of gamma radiation on molecular stability and mechanical properties of biodegradable polyurethanes for medical applications," *Polym Degrad Stab*, vol. 79, no. 3, pp. 465–474, 2003.

[277] E. Briganti, K. T. Al, S. Kull, P. Losi, D. Spiller, S. Tonlorenzi, D. Berti, and G. Soldani, "The effect of gamma irradiation on physical-mechanical properties and cytotoxicity of polyurethane-polydimethylsiloxane microfibrillar vascular grafts," *J Mater Sci Mater Med*, vol. 21, no. 4, pp. 1311–1319, 2010.

[278] Y. W. Tang, R. S. Labow, and J. P. Santerre, "Isolation of methylene dianiline and aqueous-soluble biodegradation products from polycarbonate-polyurethanes," *Biomaterials*, vol. 24, no. 17, pp. 2805–2819, 2003.

[279] C. V. Santa, T. R. Dugas, and M. F. K. MF, "Mitochondrial dysfunction occurs before transport or tight junction deficits in biliary epithelial cells exposed to bile from methylenedianiline-treated rats," *Toxicol Sci*, vol. 84, no. 1, pp. 129–138, 2005.

[280] H. Shintani, "Formation and elution of toxic compounds from sterilized medical products: methylenedianiline formation in polyurethane.," *J Biomater Appl*, vol. 10, no. 1, pp. 23–58, 1995.

[281] E. E. Golli-Bennour, B. Kouidhi, M. Dey, R. Younes, C. Bouaziz, C. Zaied, H. Bacha, and A. Achour, "Cytotoxic effects exerted by polyarylsulfone dialyser membranes depend on different sterilization processes," *Int Urol Nephrol*, vol. 43, no. 2, pp. 483–490, 2011.

[282] S. L. M. Dahl, A. P. Kypson, J. H. Lawson, J. L. Blum, J. T. Strader, Y. Li, R. J. Manson, W. E. Tente, L. DiBernardo, M. T. Hensley, R. Carter, T. P. Williams, H. L. Prichard, M. S. Dey, K. G. Begelman, and L. E. Niklason, "Readily available tissue-engineered vascular grafts," *Sci Transl Med*, vol. 3, no. 68, pp. 1–11, 2011.

[283] S. Wolfensohn and M. Lloyd, *Handbook of laboratory animalmanagement and welfare*. Oxford: Blackwell Science, 1998.

[284] T. R. Kohler and T. R. Kirkman, "Dialysis access failure: a sheep model of rapid stenosis," *J Vasc Surg*, vol. 30, p. 74451, 1999.

[285] S. T. Rashid, H. J. Salacinski, G. Hamilton, and A. M. Seifalian, "The use of animal models in developing the discipline of cardiovascular tissue engineering: a review," *Biomaterials*, vol. 25, no. 9, pp. 1627–1637, 2004.

[286] L. L. Stept, W. R. Flinn, W. J. McCarthy, S. T. Bartlett, J. J. Bergan, and J. S. T. Yao, "Technical defects as a cause of early graft failure after femorodistal bypass," *Arch Surg*, vol. 122, no. 5, pp. 599–604, 1987.

[287] N. Singh, A. N. Sidawy, K. J. DeZee, R. F. Neville, C. Akbari, and W. Henderson, "Factors associated with early failure of infrainguinal lower extremity arterial bypass," *J Vasc Surg*, vol. 47, no. 3, pp. 556–561, 2006.

[288] N. Singh, A. N. Sidawy, K. J. DeZee, R. F. Neville, J. Weiswasser, G. Aidinian, C. Akbari, and W. Henderson, "The effect of the type of anesthesia on outcomes of lower extremity infrainguinal bypass," *J Vasc Surg*, vol. 44, no. 3, pp. 964–970, 2006.

[289] A. Rosengren and L. M. Bjursten, "Pore size in implanted polypropylene filters is critical for tissue organisation.," *J Biomed Mater Res A*, vol. 67, p. 918926, 2003.

[290] S. Grad, L. Kupcsik, K. Gorna, S. Gogolewski, and M. Alini, "The use of biodegradable polyurethane scaffolds for cartilage tissue engineering: potential and limitations," *Biomaterials*, vol. 24, p. 51635171, 2003.

[291] F. J. Schoen, H. Harasaki, K. M. Kim, H. C. Anderson, and R. J. Levy, "Biomaterial-associated calcification: pathology, mechanism, and strategies for prevention," *J Biomed Mater Res*, vol. 22, no. (Suppl. A1), pp. 11–36, 1988.

[292] P. Zilla, D. Bezuidenhout, and P. Human, "Prosthetic vascular grafts: Wrong models, wrong questions and no healing," *Biomaterials*, vol. 28, p. 50095027, 2007.

[293] J. D. Roh, R. Swah-Martinez, M. P. Brennan, S. M. Jay, L. Devine, D. A. Rao, T. Yi, T. L. Mirensky, A. Nalbandian, B. Udelsman, N. Hibino, T. Shinoka, W. M. Saltzman, E. Snyder, T. R. Kyriakides, J. S. Pober, and C. K. Breuer, "Tissue-engineered vascular grafts transform into mature blood vessels via an inflammation-mediated process of vascular remodeling," *Proc Natl Acad Sci USA*, vol. 107, no. 10, pp. 4669–4674, 2010.

[294] N. Hibino, T. Yi, D. R. Duncan, A. Rathore, E. Dean, Y. Naito, A. Dardik, T. Kyriakides, J. Madri, J. S. Pober, T. Shinoka, and C. K. Breuer, "A critical role for macrophages in neovessel formation and the development of stenosis in tissue-engineered vascular grafts," *FASEB J*, 2011.

[295] N. Hibino, G. Villalona, N. Pietris, T. Yi, D. R. Duncan, A. Rathore, E. Dean, Y. Naito, R. Sawh-Martinez, J. K. Harrington, A. Sinusas, D. S. Krause, T. Kyr-

iakides, W. M. Saltzman, J. S. Pober, T. Shinoka, and C. K. Breuer, "Tissue-engineered vascular grafts from neovessels that arise from regeneration of the adjacent blood vessel," *FASEB J*, vol. 25, no. 8, pp. 2731–2739, 2011.